



# WASTEBRICK

Improvement in bricks production by the  
addition of conventional waste as a  
breakthrough in the construction  
industry

Laura Crespo-López López

Doctoral Thesis

2024

Supervisor: Giuseppe Cultrone



UNIVERSIDAD  
DE GRANADA

Departamento de Mineralogía y Petrología



Programa Doctorado  
Ciencias de la Tierra



# UNIVERSIDAD DE GRANADA

Departamento de Mineralogía y Petrología

***WASTEBRICK: Improvement in bricks production by the addition of conventional waste as a breakthrough in the construction industry***

Laura Crespo-López

Editor: Universidad de Granada. Tesis Doctorales  
Autor: Laura Crespo López  
ISBN: 978-84-1195-306-1  
URI: <https://hdl.handle.net/10481/92351>



# Universidad de Granada

Programa de Doctorado-Ciencias de la Tierra

Departamento de Mineralogía y Petrología

---

## **WASTEBRICK: Improvement in bricks production by the addition of conventional waste as a breakthrough in the construction industry**

### PhD THESIS

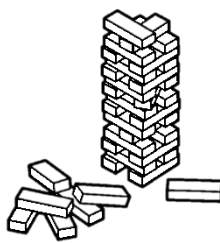
Dr. Giuseppe Cultrone, catedrático de la Universidad de Granada, adscrito al Departamento de Mineralogía y Petrología, hace constar que la presente memoria de Tesis Doctoral presentada por Dña. Laura Crespo-López López ha sido realizada bajo su dirección y cumple todos los requisitos necesarios para poder optar al Grado de Doctor por la Universidad de Granada.

VºBº del director

Fdo. Laura Crespo-López López

Fdo. Giuseppe Cultrone





The best way to predict the future is to ***invent it.***

Alan Kay

# AGRADECIMIENTOS

En primer lugar, deseo agradecer a mi director de Tesis, Giuseppe Cultrone, por su orientación experta, su paciencia infinita y su compromiso inquebrantable a lo largo de este viaje. Sus observaciones y su apoyo constante han sido fundamentales para dar forma a este trabajo. Sin duda, estar donde hoy me encuentro se lo debo en gran parte a él. *Grazie mille, Giuseppe.*

También debo agradecer al grupo de investigación RNM-179 y a los profesores que componen el Departamento de Mineralogía y Petrología de la Universidad de Granada, en especial a su directora Concha Lázaro y a mi tutor Carlos Rodríguez Navarro por su ayuda científica y personal siempre que la he necesitado. Agradecer igualmente a Encarni y Alejandro Rodríguez Navarro, su cercanía, entereza y calidad humana. Gracias también a los técnicos de laboratorio que componen el Departamento: Eva, Jesús y Sonia, por su disponibilidad y dedicación. Y a Esther, cuya ayuda ha sido fundamental en cada momento que la he necesitado.

Quiero expresar un profundo agradecimiento a Eduardo Sebastián y Anna Arizzi. Fuisteis vosotros quienes me introdujeron en el mundo de la investigación, guiándome en mis primeros pasos y encendiendo en mí la pasión por el conocimiento. Agradezco sinceramente vuestra confianza y apoyo desde mis días como estudiante de grado. Sin vuestra influencia y creencia en mí, no estaría donde estoy hoy. Gracias por todo.

Agradezco sinceramente a todo el *Ministerio de Becarios*, a los de siempre y a los de ahora, mis colegas y amigos, quienes han compartido este viaje conmigo. En especial a Luis, Igor, Pedro, Jorge, Cristina, Nazaret, Paco y Christian, vosotros me habéis brindado vuestra amistad, vuestro ánimo y vuestros valiosos consejos siempre. Gracias también a Aurelia, amiga y confidente, por tu apoyo incondicional. Y a todos los que han caminado conmigo fugazmente en este camino: Alberto, Jacopo, Claudio, Maura y Maphole.

Asimismo, agradecer también a David Benavente del Departamento de Ciencias de la Tierra y del Medio Ambiente de la Universidad de Alicante, quien me ha acogido con generosidad y dedicado innumerables horas de su tiempo. Por ser mi *salvavidas*

ante cualquier problema y por estar siempre presente. Muchas gracias, David, de todo corazón.

Gracias a mis *bellezze* del Departamento de Geociencias de la Universidad de Padova, quienes me recibieron con los brazos abiertos y me acogieron como una más. Chiara, Elena, Manu, Federica, Eirini, *grazie infinite ragazze*. Vuestra calidez y amabilidad hicieron que me sintiera como en casa en una ciudad nueva. Mi estancia en Italia fue un verdadero regalo gracias a vosotras. También quiero agradecer a Lara Maritan, Claudio Mazzoli, Luca Valentini, Alessandro Fontanari, Chiara Dalconi y Giampaolo Girardi por su valiosa ayuda y disposición. Su apoyo fue fundamental para mí.

Gracias a mis amigos de toda la vida, Javi y Juan Carlos, quienes han estado a mi lado durante más de dos décadas. Sus consejos siempre han sido invaluable; nadie me conoce ni me quiere como vosotros. También quiero agradecer a mis compañeros de la carrera, Fede, Alex, Nico, Carlos, Víctor, Emilio y Ricardo, con quienes he sudado en el campo y compartido risas y lágrimas. Su amistad ha sido un pilar fundamental en mi vida.

Quiero expresar mi profundo agradecimiento a todas las empresas colaboradoras que fueron cómplices en esta investigación, cuya participación fue fundamental en este trabajo. Gracias a la empresa *Cerámica Castillo Siles (Viznar, Granada)*, quienes proporcionaron las materias primas arcillosas de Viznar, Jun y Guadix para poder elaborar parte de los ladrillos estudiados. Gracias a la *Clínica Veterinaria Plaza de Toros (Almería)*, por brindarme la oportunidad de utilizar su unidad de Rayos-X como método no destructivo para caracterizar los ladrillos. En especial a Kuki y a Rocío, por su dedicación y tiempo invertido. Gracias a *Tesela, Centro de Innovación, construcción y Patrimonio (Granada)*, quienes, además de proporcionarme la fibra de carbono utilizada como residuo, me dieron la oportunidad de trabajar con ellos durante más de 3 años. Sin vosotros, no hubiese comenzado esta Tesis Doctoral con los conocimientos que vosotros me aportasteis, científicos y humanos. Gracias Eugenio y gracias Jordi, por vuestra generosidad y disponibilidad siempre. Gracias a *Bodegas Navarro Racimo de Oro (Valdepeñas)*, y en especial a Vicente, por facilitarme el orujo del vino utilizado y por abrirme las puertas de su casa.

También expresar mi más sincero agradecimiento a todo el personal del Centro de Instrumentación Científica por su amabilidad y valiosa ayuda. En particular, quiero reconocer a Alicia, Bendi e Isabel por su dedicación y disposición en todo momento. Asimismo, quiero agradecer a Begoña Toledo, de la Escuela Internacional de Posgrado de la Universidad de Granada, por su paciencia y asistencia constante siempre que la he necesitado. Sin ella todavía estaría perdida entre algún documento referente al depósito de esta Tesis.

Cómo olvidar el agradecimiento a Nigel Walkington, cuya valiosa ayuda a lo largo de toda la tesis ha sido fundamental. Su apoyo ha sido crucial para mejorar mi dominio del inglés y ha tenido un impacto significativo en mi desarrollo académico. Sin él, mi habilidad en el idioma no sería la misma.

Asimismo, deseo reconocer el respaldo financiero otorgado por la Universidad de Granada a través de la concesión de un proyecto precompetitivo, cuyo apoyo ha sido crucial para llevar a cabo parte de esta investigación. Además, quiero agradecer el financiamiento proporcionado por los proyectos de investigación B-RNM-188-UGR20 y PID2020-119838RA-I00, los cuales han sido esenciales para el desarrollo de este trabajo.

Quiero expresar mi más profundo agradecimiento a mi familia, en especial a mis padres y mi hermano, quienes han sido los pilares de mi vida. Su amor ilimitado, su apoyo constante y su sacrificio han sido la fuerza motriz que me ha llevado a alcanzar este logro. Sin su aliento y comprensión, nada de esto habría sido posible.

Finalmente, dedico este logro a Ángel, quien siempre ha creído en mí y me ha brindado un apoyo incondicional, cuyo constante esfuerzo y dedicación continúan inspirándome día tras día. Y a nuestros hijos, Ángel y Darío.

**Gracias a todos los que habéis sido parte de este viaje, vuestro granito de arena ha dejado una marca indeleble en mí.**

Laura

Febrero, 2024.

# CONTENTS

Summary .....	9
Resumen .....	15
Figures.....	21
Tables.....	31
<b>1. Introduction.....</b>	<b>35</b>
1.1. <i>The invention of bricks</i> .....	36
1.2. <i>Building standards applicable to bricks</i> .....	43
1.2.1. <i>Building standards in Europe</i> .....	43
1.2.2. <i>Building standards in Spain</i> .....	44
1.3. <i>Background: clay depletion and the accumulation of waste</i> .....	45
1.4. <i>Eco-friendly bricks</i> .....	46
<b>2. Objectives of this research .....</b>	<b>48</b>
<b>3. Materials .....</b>	<b>51</b>
3.1. <i>Raw materials</i> .....	52
3.1.1. <i>Clayey materials</i> .....	52
3.1.1.1. Geological context of the clayey materials .....	53
3.1.1.1.1. The Betic Cordillera.....	53
3.1.1.1.2. The Iberian Chain.....	61
3.1.2. <i>Wastes</i> .....	64
3.1.2.1. Household glass (Chapter I).....	64
3.1.2.2. Carbon fibre from the wind-power industry (Chapter II).....	65
3.1.2.3. Waste pomace (Chapter III) .....	66
3.1.2.4. Tea residue (Chapter IV).....	66
3.2. <i>Brick making</i> .....	67
3.2.1. <i>Traditional brick-making</i> .....	67
3.2.2. <i>Extrusion method</i> .....	69
<b>4. Analytical techniques and methods .....</b>	<b>73</b>
4.1. <i>Granulometry</i> .....	76
4.2. <i>Shrinkage and weight changes</i> .....	76
4.3. <i>Chemistry, mineralogy and texture</i> .....	76
4.3.1. <i>Attenuated Total Reflectance Fourier Transform Infrared Spectroscopy (FTIR)</i> .....	76

4.3.2. <i>Elemental analysis</i> .....	77
4.3.3. <i>X-ray fluorescence (XRF)</i> .....	77
4.3.4. <i>Powder X-ray diffraction (PXRD)</i> .....	77
4.3.5. <i>Thermal Decomposition and differential scanning calorimetry (TG-DSC)</i> ...	78
4.3.6. <i>Thermal conductivity Scanner (TCS)</i> .....	78
4.3.7. <i>High-resolution field emission scanning electron microscope (HR-FESEM)</i>	79
4.3.8. <i>Digital image analysis (DIA)</i> .....	80
4.4. <i>Determination of the pore system</i> .....	80
4.4.1. <i>Hydric test</i> .....	80
4.4.2. <i>Mercury intrusion porosimetry (MIP)</i> .....	84
4.4.3. <i>Environmental chamber</i> .....	84
4.5. <i>Compressive strength (Cs)</i> .....	85
4.6. <i>Non-destructive testing</i> .....	85
4.6.1. <i>Ultrasound propagation velocity (UPV)</i> .....	85
4.6.2. <i>Videomicroscopy</i> .....	87
4.6.3. <i>Spectrophotometry</i> .....	87
4.6.4. <i>Radiographic images</i> .....	87
4.6.5. <i>Leeb hardness microdurometer (LH)</i> .....	88
4.7. <i>Accelerated ageing test</i> .....	88
4.7.1. <i>Freeze-thaw test</i> .....	88
4.7.2. <i>Salt crystallization test</i> .....	89
4.7.3. <i>Wet-dry test</i> .....	90
4.8. <i>The analysis of variance technique (ANOVA)</i> .....	90
<b>5. Results and discussion</b> .....	91
Summaries.....	92
Chapter I. Bricks with household glass added .....	97
Chapter II. Carbon fibre from wind-power industry for making porous bricks .....	152
Chapter III. Waste pomace from wine industry as additive for making bricks.....	190
Chapter IV. Effect of tea waste as additive to solid bricks .....	216
<b>6. Conclusions</b> .....	248
<b>7. References</b> .....	262

# SUMMARY

From the earliest unfired mudbricks dating back 9,000 years to the most modern, most innovative products made from less traditional components, bricks have played a fundamental part in human history, in the construction of houses and countless other types of buildings and monuments. Today, they continue to play a crucial role in modern society as one of the most widely used, most versatile building materials on the market. However, over-exploitation of the main raw material, clay, over a long period of time has had a negative impact on the environment and is leading to the depletion of reserves.

The demand for bricks is increasing with the growth of urban areas and the construction of infrastructures. As a result, societal interest in sustainable construction has led to the development and production of 'greener' bricks made from partially recycled, recyclable or environmentally-friendly materials, thus promoting a circular economy. This has been combined with more energy-efficient production techniques. Within this field, research is being conducted into the use of conventional organic and inorganic wastes as additives in brick production. This reduces the amount of natural clay resources required to produce the bricks and, in many cases, enables energy savings in the production process. The addition of waste can also improve the physical properties of the bricks, such as their mechanical strength or thermal insulation. In addition to improving the sustainability of the construction business and reducing its dependence on clay, the use of waste materials in brick production can bring other important socioeconomic benefits in terms of jobs and income for local communities and could encourage innovation and entrepreneurship. The use of additives could also improve the aesthetic appeal of brick buildings by offering a wider variety of textures, colours and finishes, so stimulating architectural creativity in the design of visually striking structures that comply with sustainable design principles.

For this reason, a detailed, accurate characterization of these new types of brick, exploring a range of issues, from chemical-mineralogical to macro-textural and durability aspects, is of great importance so as to ensure that these waste-based building materials have the technical quality required for their use in the building industry.

The aim of this Doctoral Thesis is to produce technically high-quality, high-performance durable bricks, which can be used in both modern buildings and in the restoration of architectural heritage using a mixture of clay additives in the form of inorganic (household glass dust and carbon fibre from the wind-power industry) and organic (wine pomace and tea residues) waste products. Brick manufacture is highly dependent on the chemical and mineralogical characteristics of the clayey soils used as raw materials, which directly influence the physical properties of the fired bricks. The clay used in this research came from various different quarries in Granada and Teruel (Spain). The bricks were prepared by hand or by extrusion in a local factory and were then fired in an electric kiln with an oxidising atmosphere at temperatures of 800, 950 and 1100 °C. Within the general framework of providing a complete characterization of these bricks, our specific objectives include the study of the mineralogical and textural changes that take place during firing and the relationship between these changes and the physical and mechanical properties of the bricks. The alterations in the porous system were also analysed and the durability and technical quality of brick samples made with and without additives was assessed.

The use of additives in the brick manufacturing process has created new properties and potential applications of bricks that need to be studied in detail. Understanding the characteristics of bricks, including their composition, microstructure, mechanical properties and performance under different conditions, is therefore fundamental to ensuring the quality, reliability and durability of the buildings in which they are used. In this thesis, a comprehensive characterization of the chemical, mineralogical, textural, physical and mechanical properties of these bricks is conducted using a variety of techniques and tests.

The particle size of the clayey materials, household glass, carbon fibre and wine pomace was determined by laser particle size measurement. The particles in the tea residue were too large for laser measurement and their size was determined by sieving. Identification of the major elements of the clayey soils and the inorganic residues (household glass and carbon fibre) was carried out by X-ray fluorescence. The composition of the clayey materials and residues was determined by analysing their molecular vibrations using attenuated total reflectance Fourier transform infrared spectroscopy. X-ray diffraction was used to identify the mineral phases of the clayey soils and the new phases formed during the firing of the bricks. Thermal decomposition and differential scanning



calorimetry were used to determine the temperatures at which changes take place. In the bricks made with added tea residue, their thermal conductivity was also tested. The petrographic characteristics (mineralogy and texture) of the bricks made with and without residues were observed using polarized optical microscopy.

Detailed observations of the morphology and texture of the bricks, the morphology of the pores and the degree of vitrification were made using a high-resolution field emission scanning electron microscope (FESEM). The FESEM images of the bricks made with and without tea residue were analysed using a digital image analyser to estimate the percentage of pores of over 4  $\mu\text{m}$  in size.

In addition to microscopic observation, the pore system of the bricks made with and without residues was also assessed using hydric (water and climatic chamber) and porosimetric tests (mercury intrusion porosimetry). The porosity of a brick can directly affect its compactness. In order to determine the compactness of the bricks, first were evaluated their compressive strength and UV propagation velocity. In both these tests, three measurements were made for each type of brick. At the same time, it is also essential to understand how the different types of brick react to different environmental conditions in order to ensure the longevity and structural integrity of the buildings in which they are used. To this end, the brick samples were subjected to accelerated aging tests involving thirty freeze-thaw cycles, fifteen salt crystallization cycles and thirty dry-wet cycles and the resulting deterioration was observed.

In most cases, the addition of residues affected the colour of the fired bricks. The decision was made to assess the difference in color between the samples produced with and without residues using a spectrophotometer. Other non-destructive techniques, such as radiography and Leeb surface microhardness, provided a wealth of relevant data on how the addition of residues to the clayey mix affected different aspects of the fired bricks.

One of the additives tested was household glass. The results indicated that the strength of the bricks was increased by the addition of 20% by weight of household glass. In this research, one set of samples was prepared with a clayey material rich in carbonates (Jun) and the other with a clay that was rich in silicates (Guadix). The bricks were made by hand and by extrusion and fired at 800, 950 and 1100  $^{\circ}\text{C}$ . The different mineralogy of the clayey materials meant that the bricks underwent different mineralogical changes during firing. In those made with clay from Jun, new Ca-(Mg-) silicates such as gehlenite,

diopside, wollastonite and anorthite developed, while mullite appeared in those made with clay from Guadix. The addition of glass caused substantial changes in the porous system. These bricks absorbed less water and dried faster than the bricks without residue. The extruded bricks were also less porous. The addition of glass led to a reduction in pore interconnection and increased vitrification, which could enable energy savings. This new type of brick with added glass was more resistant to compression than those made solely with clay. This was more evident in the bricks made with the silicate-rich clay. These results were confirmed by ultrasound, which showed that the compactness of the bricks increased in line with the firing temperature and in line with the amount of glass added. In terms of colour, the Jun bricks ranged from yellow to orange, while the Guadix bricks had a dark reddish hue. The Jun bricks were more resistant than the Guadix bricks in accelerated ageing tests, perhaps due to the fluxing effect of carbonates at low firing temperatures.

The use of non-destructive techniques to characterize the bricks showed that the addition of glass increased vitrification and improved compressive strength. The X-ray technique proved to be a very useful tool for observing the anisotropic density distribution in the fired samples. According to statistical analyses, the bricks made with clay from Jun tended to have higher mean values for all the variables (luminosity, chromatic values and petrophysical parameters) than the bricks made with clay from Guadix, regardless of whether or not they contained added glass. Furthermore, the ANOVA analysis showed that the Jun bricks had better technical properties than those made with Guadix clay. However, the Jun bricks with added glass fired at 1100 °C showed the greatest variations in colour, which could make them less suitable for Architectural Heritage restoration purposes.

This investigation also explored the potential use of carbon fiber from dismantled wind turbine blades as an additive in brick production. The use of 5 and 10% by weight of this additive resulted in an increase in the microporosity of the matrix due to the partial disintegration of this residue and its associated compounds (mainly resins), so improving its thermal insulation properties. The addition of carbon fibre partially modified the mineralogical composition of the bricks, reducing the concentration of hematite and causing the orientation of the fibres inside the bricks. Despite the reduction in mechanical strength due to the increase in porosity, the bricks made with carbon fibre had higher surface hardness. In terms of durability, the carbon fibre bricks were more resistant to

salt crystallisation. The colour changes caused by the addition of carbon fibre were not significant, which means that these bricks could offer a more sustainable alternative to traditional materials.

In another set of experiments, the possibility of using wine pomace as an additive (at 2.5, 5, and 10% by weight) in the production of lightweight bricks was evaluated by assessing their physical-mechanical behaviour. The clayey material used was a mixture of 3/5 of clay rich in quartz and phyllosilicates (Guadix) and 2/5 of clay rich in carbonates (Viznar). The addition of wine pomace reduced the linear shrinkage of the unfired samples and created new pores, making the fired bricks lighter. The mineralogy of the bricks was not affected by the addition of pomace. However, the mechanical strength of the bricks was impaired, especially at 800 °C. Nevertheless, most of the tested bricks met the strength specifications set out in EN standards for use in construction as lightweight bricks. The addition of wine pomace also affected the brightness and chromaticity of the bricks and increased the water absorption and open porosity values, so making the fired bricks less durable against salt crystallization. The study highlighted several economic and environmental advantages of using wine pomace in brick production, emphasizing in particular that it would reduce the amount of clay required and offer a useful means of disposing of this waste.

As happened with wine pomace, the addition of 5 and 10% by weight of tea residue did not modify the mineralogy of the bricks, which in this case were made with clayey material from Teruel. Tea residues increased the porosity and water vapor absorption of the bricks, and this increase was greater with higher amounts of residue. This is because the residue is consumed during firing, creating more empty spaces inside the brick, as observed and quantified using digital image analysis and mercury intrusion porosimetry. The addition of this residue reduced the thermal conductivity and the diffusion of heat in the bricks. Although the bricks made solely with clay were mechanically stronger than those made with tea residues, both met construction industry specifications. The bricks with added tea residues were a dark red colour, with reduced brightness and chromatic parameters. In terms of durability, bricks manufactured with 10% by weight of tea residues experienced the greatest change in weight due to salt crystallization in the pores and fissures, regardless of the firing temperature. Bricks without added residues or with 5% by weight of tea residues showed similar levels of deterioration, indicating that the

addition of this percentage of residues does not affect the durability of the bricks when subjected to salt crystallization.

The addition of various types of waste, both organic and inorganic, in brick manufacturing can offer, depending on the type of waste, significant improvements in terms of durability and thermal properties, but it also presents challenges in terms of porosity and mechanical strength. Careful selection of additives and their optimization in the manufacturing process are therefore key to maximizing the benefits and minimizing the detrimental impacts on brick performance.

# RESUMEN

Desde los primeros ladrillos de barro sin cocer datados hace 9000 años hasta los ladrillos más modernos e innovadores desarrollados a partir de otros componentes menos tradicionales, los ladrillos han sido y siguen siendo un material fundamental en la historia de la humanidad, tanto en la construcción de viviendas como en el levantamiento de monumentos. Su importancia perdura en la sociedad como uno de los materiales de construcción más utilizados y versátiles. Sin embargo, la extracción excesiva de tierras arcillosas durante periodos prolongados de tiempo afecta negativamente al medioambiente y lleva al agotamiento de las reservas.

La demanda de ladrillos se incrementa conforme crecen las áreas urbanas y la construcción de infraestructuras. A raíz de esto, el interés social en la construcción sostenible ha impulsado el desarrollo y producción de ladrillos más “ecológicos”, es decir fabricados utilizando en parte materiales reciclados, reciclables o de bajo impacto ambiental, favoreciendo así una economía circular, y utilizando técnicas de producción más energéticamente eficientes. La incorporación de residuos convencionales, orgánicos e inorgánicos, reduce la cantidad necesaria de recursos naturales arcillosos y, en muchos casos, disminuye la energía requerida para la producción de ladrillos. La adición de residuos puede también mejorar las propiedades físicas de los ladrillos, como la resistencia mecánica o el aislamiento térmico, haciéndolos aún más adecuados para su uso en construcción. La integración de residuos convencionales en la producción de ladrillos ofrece numerosos beneficios más allá de la sostenibilidad. Por un lado, al reducir la dependencia de materiales arcillosos se ayuda a preservar el medio ambiente. Por otro lado, el uso de materiales de desecho en la producción de ladrillos puede tener un impacto socioeconómico positivo, generando empleo e ingresos en las comunidades locales y fomentando la innovación y el emprendimiento. Incluso, se puede mejorar el atractivo estético de los edificios al ofrecer una mayor variedad de texturas, colores y acabados, fomentando la creatividad y permitiendo la creación de estructuras visualmente llamativas que reflejen los principios de un diseño sostenible.

Por este motivo, llevar a cabo una correcta y precisa caracterización de los ladrillos desde aspectos los químico-mineralógicos hasta los macro-texturales y de durabilidad

es de gran relevancia para otorgar a estos materiales de construcción con residuos, la calidad técnica necesaria para su uso constructivo.

Esta Tesis Doctoral tiene como objetivo producir ladrillos de alta calidad técnica, eficientes y duraderos en los que parte de las materias primas arcillosas se han reemplazado por residuos inorgánicos (polvo de vidrio doméstico y fibra de carbono procedente de la industria eólica) y orgánicos (orujo del vino y residuo del té) y que puedan utilizarse tanto en obras de intervención del Patrimonio Arquitectónico como en la construcción moderna. La fabricación de cerámica para construcción depende en gran medida de las características químicas y mineralógicas de las tierras arcillosas utilizadas como materia prima, lo que influye directamente en las propiedades físicas de los productos cocidos. En esta investigación, la materia prima arcillosa utilizada para la elaboración de ladrillos macizos proviene de diversas canteras ubicadas en Granada y Teruel. Se ha procesado utilizando métodos de fabricación manual y extrusión y se ha cocido en horno eléctrico y atmósfera oxidante a temperaturas de 800, 950 y 1100 °C. Los objetivos específicos abarcan el estudio de los cambios mineralógicos y texturales que tienen lugar tras la cocción, la relación entre estos cambios y las propiedades físicas y mecánicas de los ladrillos, la modificación del sistema poroso y la evaluación de la durabilidad y calidad técnica de las muestras elaboradas con y sin residuos.

La integración de aditivos en los procesos de fabricación de ladrillos ha añadido nuevos aspectos a sus propiedades y aplicaciones potenciales y estos deben de ser examinados en detalle. La comprensión de las características de los ladrillos, incluyendo su composición, microestructura, propiedades mecánicas y rendimiento bajo diferentes condiciones, es fundamental para garantizar la calidad, confiabilidad y durabilidad de las estructuras construidas con ellos. En esta tesis se llevó a cabo una caracterización exhaustiva de las propiedades químicas, mineralógicas, texturales, físicas y mecánicas mediante el uso de diferentes técnicas y ensayos.

El tamaño de partículas de las tierras arcillosas y del vidrio doméstico, fibra de carbono y orujo del vino se llevó a cabo mediante granulometría laser. El residuo del té, al presentar un tamaño de partícula mayor al rango de análisis, se determinó mediante tamizado. La identificación de los elementos mayores de las tierras arcillosas y los residuos inorgánicos (vidrio doméstico y fibra de carbono) se realizó por fluorescencia de Rayos X. La determinación cualitativa de las vibraciones composicionales de las

tierras arcillosas y los residuos se analizaron mediante espectroscopia infrarroja por transformada de Fourier de reflectancia total atenuada. La difracción de Rayos X permitió identificar las fases minerales de las tierras arcillosas y las de neo formación que se desarrollaron tras la cocción de los ladrillos. A partir de la descomposición térmica y calorimetría diferencial de barrido se determinó la afectación térmica por rangos de las tierras arcillosas. Asimismo, se comprobó la conductividad térmica de los ladrillos con residuo del té. Las características petrográficas (mineralogía y textura) de los ladrillos con y sin residuos se observaron mediante microscopía óptica polarizada. Se realizaron observaciones detalladas de la morfología y la textura de los ladrillos, la morfología de los poros y el grado de vitrificación utilizando un microscopio electrónico de barrido de emisión de campo de alta resolución, cuyas imágenes obtenidas de los ladrillos con y sin residuos del té fueron analizadas utilizando un analizador digital de imagen para estimar el porcentaje de poros de más de 4  $\mu\text{m}$  de tamaño.

A parte de la observación mediante microscopía, el sistema poroso también se determinó mediante métodos de saturación de líquido o vapor. Se realizaron pruebas hídricas (ensayos hídricos y cámara climática) y porosimétricas (porosimetría de intrusión de mercurio) para esclarecer el sistema poroso de los ladrillos con y sin residuos. La porosidad es un factor directamente correlacionado con la compacidad de las piezas. Para determinar compacidad de los ladrillos se llevaron a cabo la determinación de la resistencia a la compresión y la velocidad de la propagación de las ondas ultrasónicas. En ambos tipos de ensayos, se llevaron a cabo tres mediciones por tipo de ladrillo estudiado. Paralelamente, comprender cómo responden a distintas condiciones ambientales los distintos tipos de ladrillos analizados, es crucial para garantizar la longevidad y la integridad estructural de los edificios. Con este fin, se realizaron treinta ciclos de congelación-descongelación, quince de cristalización de sales y treinta de secado-humedad para observar una degradación teórica.

La adición de residuos, en la mayoría de los casos, afectó al color de las piezas tras su cocción, por este motivo, se determinó la diferencia de color entre las piezas con y sin residuos mediante un espectrofotómetro. Otras técnicas no destructivas, como las imágenes radiográficas o la determinación de la microdureza superficial Leeb, aportaron numerosos datos relevantes sobre cómo afectaron estos residuos tras su mezcla para conformar los ladrillos.

La adición del 20% en peso de vidrio doméstico incrementó la resistencia de los ladrillos. Estos se elaboraron utilizando dos tierras arcillosas, una rica en carbonatos (Jun), y otra silicatada (Guadix). Los ladrillos macizos se fabricaron a mano y por extrusión y se cocieron a 800, 950 y 1100 °C. La diferencia en la mineralogía de las materias primas arcillosas dio lugar a diferencias en la evolución mineralógica de los ladrillos después de la cocción, es decir, el desarrollo de nuevos silicatos de Ca-(Mg-) como gehlenita, dióxido, wollastonita y anortita cuando se utilizó la materia prima de Jun, mientras que apareció mullita con la tierra de Guadix. La adición de vidrio modificó el sistema poroso. En efecto estos ladrillos absorbían menos agua y se secaban más rápido que los ladrillos sin residuo. También se demostró que los ladrillos extruidos eran menos porosos. La adición de vidrio condujo a una disminución en la interconexión de poros y aumentó la vitrificación, lo que puede suponer un ahorro energético. Este nuevo tipo de ladrillo con vidrio añadido era más resistente a la resistencia a compresión que aquel hecho solo con arcilla. Esto fue más evidente en los ladrillos elaborados con la materia prima arcillosa de naturaleza silicatada. Estos resultados se confirmaron mediante ultrasonidos que revelaron que la compacidad de los ladrillos aumentaba junto con la temperatura de cocción y la adición de vidrio. En cuanto al color, los ladrillos de Jun variaban de amarillo a naranja, mientras que los de Guadix tendían a un rojo oscuro. Los ladrillos de Jun fueron más resistentes que los de Guadix en pruebas de envejecimiento acelerado, quizás debido a la acción fundente de los carbonatos a bajas temperaturas de cocción.

El uso de técnicas no destructivas en la caracterización de los ladrillos revelaron que la adición de vidrio efectivamente aumentaba la vitrificación y mejoraba la resistencia a compresión. La técnica de radiografía resultó ser una herramienta muy útil para observar la distribución anisotrópica de la densidad en las muestras cocidas. Según las predicciones estadísticas, los ladrillos hechos con material arcilloso procedente de Jun tendieron hacia valores medios más altos para todas las variables estadísticas establecidas (luminosidad, valores cromáticos, y parámetros petrofísicos) que los ladrillos hechos con material arcilloso procedente de Guadix, independientemente de si fueron cocidos añadiendo o no polvo de vidrio común. Además, el análisis ANOVA reveló que la arcilla de Jun dio lugar a ladrillos con mejores propiedades técnicas que la de Guadix. Sin embargo, los ladrillos de Jun cocidos a 1100 °C y con vidrio sufrieron las mayores variaciones de color, lo que podría hacerlos menos adecuados en obras de restauración del Patrimonio Arquitectónico.



La adición del 5 y 10% en peso de fibra de carbono procedente de las palas de turbinas eólicas desmanteladas en la producción de ladrillos determinaron un incremento de la microporosidad en la matriz debido a la parcial desintegración de este residuo y sus compuestos asociados (sobre todo resinas) mejorando su aislamiento térmico. Esta adición modificó parcialmente la composición mineralógica de los ladrillos, disminuyendo la concentración de hematites y causó la orientación de las fibras dentro del ladrillo. A pesar de empeorar la resistencia mecánica debido a la porosidad generada, los ladrillos con fibra de carbono mostraron una mayor dureza superficial. En cuanto a la durabilidad, los ladrillos con fibra de carbono fueron más resistentes frente a la cristalización de sal. Los cambios de color causados por la adicción de fibra de carbono no fueron significativas, por lo que estos ladrillos podrían ser una alternativa sostenible a los materiales tradicionales.

Se evaluó la efectividad del uso del orujo del vino como aditivo al 2,5, 5 y 10% en peso en el comportamiento físico-mecánico de ladrillos ligeros. La materia prima arcillosa utilizada fue una mezcla compuesta por 3/5 de material arcilloso rico en cuarzo y filosilicatos (Guadix) y 2/5 de otro con carbonatos (Víznar). El orujo de vino redujo la contracción lineal de las muestras sin cocer y aumentó su ligereza tras la cocción, generando nuevos poros. La mineralogía de los ladrillos no se vio afectada por la adicción de orujo. Sin embargo, los ladrillos redujeron su resistencia mecánica, especialmente a 800 °C. A pesar de ello, la mayoría de los ladrillos ensayados cumplieron con los estándares de resistencia recomendados por las normas EN para su uso en construcción como ladrillos ligeros. La adición de orujo de vino influyó en la luminosidad y el cromatismo de los ladrillos e incrementó los valores de absorción de agua y porosidad abierta, empeorando la durabilidad de las piezas cocidas frente a la cristalización de sal. Se destacó la ventaja económica y ambiental de usar el orujo de vino en la producción de ladrillos, lo que podría reducir la cantidad de arcilla requerida y ofrecer una disposición útil de este residuo.

La adición del 5 y 10% en peso de residuo del té, al igual que el orujo del vino, no modificó la mineralogía de los ladrillos que en este caso se fabricaron con un material arcilloso procedente de Teruel. Los residuos de té aumentaron la porosidad y la absorción de vapor de agua de los ladrillos y este aumento era mayor incrementando la cantidad de

residuo. Esto se debe a que el residuo se consume durante la cocción, creando más espacios vacíos que se observaron y cuantificaron mediante análisis digital de imagen y porosimetría de inyección de mercurio. La adición de este residuo redujo la conductividad térmica y la difusión de calor en los ladrillos. Por otra parte, los ladrillos sin residuo añadido fueron mecánicamente más fuertes que los fabricados con residuos de té, pero ambos cumplen con las especificaciones requeridas por la industria de la construcción. La adición de residuos de té dio lugar a ladrillos de color rojo oscuro, disminuyendo la luminosidad y los parámetros cromáticos. En términos de durabilidad, los ladrillos fabricados con 10% en peso de residuos de té sufrieron la mayor variación de peso debido a la cristalización de la sal en los poros y fisuras de las piezas, independientemente de la temperatura de cocción. Los ladrillos sin residuos añadidos o con el 5% en peso de residuos de té mostraron un deterioro similar. Por lo tanto, la adición de este porcentaje de residuos no merma la durabilidad de los ladrillos cuando están sujetos a cristalización de la sal.

La adición de diferentes tipos de residuos, orgánicos e inorgánicos, en la fabricación de ladrillos puede ofrecer, dependiendo del tipo de residuo, mejoras significativas en términos de durabilidad y propiedades térmicas, pero también presenta desafíos en cuanto a porosidad y resistencia mecánica. La selección cuidadosa de los aditivos y su optimización en el proceso de fabricación son clave para maximizar los beneficios y minimizar los impactos perjudiciales en el rendimiento de los ladrillos.

# FIGURES

**Figure 1.** The earliest unfired bricks in history were handmade eight thousand years ago on the Iranian Plateau in ancient Persia. Image obtained and adapted from: <https://nationalgeographic.com> (accessed January, 2024).

**Figure 2.** Before and after the excavation and restoration of the Great Ziggurat of Ur, built approximately 4000 years ago by King Ur-Nammu of the Neo-Sumerian Empire and dedicated to the Moon God, Nanna. Image obtained and modified from: <https://reddit.com> (accessed January, 2024).

**Figure 3.** An Egyptian hieroglyph from the tomb of Rekhmire showing Hebrews making bricks. Image obtained and modified from: <https://lacorriente.com> (accessed January, 2024).

**Figure 4.** Detail of the Great Wall of China. Photograph: Sergio Rademacher. Image obtained and modified from: <https://researchgate.net/> (accessed January, 2024).

**Figure 5.** Roman bricks with Legio XXII stamp (Saalburg Museum, Germany) (Linge, 2016). Image obtained from: <https://worldhistory.org> (accessed January, 2024).

**Figure 6.** Lübeck old town. Image obtained and adapted from: <https://visit-luebeck.com> (accessed January, 2024).

**Figure 7.** A) Ramp-loaded brickmaking machine by Henry Clayton, c.1860 (obtained and adapted by Woodforde, 1976); B) brick and tile machine patented by John Ainslie, British Patent No.8965, 1841. (obtained and adapted by the Civil Engineer and Architect's Journal Vol. V 1842, p.427); C) brickmaking and pressing machine, John Whitehead, manufacturer (obtained and adapted from John Whitehead's Trade Catalogue, 1851).

**Figure 8.** A) Ceramica Castillo Siles factory; B) drying of extruded bricks; C) stack of bricks ready for firing in the oven; D) clayey material piled up outside the factory; E) moulds used for the production of handmade bricks.

**Figure 9.** A) Simplified geological map of the Betic Cordillera showing the main geological domains and Neogene-Quaternary basins. Insets show the location of the study basins (Granada and Guadix) located in the central sector of the Cordillera; B)

simplified geological map of the Granada Basin (from Sanz de Galdeano et al., 2012). The location of the sampling sites of the Jun and Víznar clayey materials at the northeastern margin of the basin is indicated; C) simplified geological map of the Guadix Basin showing the location of the sampling site of the Guadix clayey materials used in this Thesis (modified from Altoaguirre et al., 2021).

**Figure 10.** A) Neogene to Quaternary stratigraphy of the Granada Basin (adapted from Braga et al., 1990). The clay samples from Jun and Viznar come from late Messinian (Turolian) continental sediments; B) palaeoenvironmental reconstruction of the Granada Basin during the Messinian (middle-late Turolian) (from García-Alix, 2008) (see basin boundary in Fig.10B). The approximate location of the Jun and Víznar sampling sites is indicated.

**Figure 11.** A) Neogene to Quaternary stratigraphy of the Guadix Basin (based on data from Rodríguez-Fernández, 1982; García-Aguilar and Martín, 2000; Betzler et al., 2006). Guadix clayey materials (red star) were collected from the most recent unit; B) palaeoenvironmental reconstruction of the Guadix Basin during the Plio-Pleistocene (Villanian- Pleistocene Turolian) (from Pla-Pueyo, 2009). The site from which the Guadix clay was obtained is indicated with a red star.

**Figure 12.** A) Main mountain ranges (made up of Palaeozoic and Mesozoic rocks) and sedimentary basins in the Iberian Peninsula; B) simplified geological map of the central and southeastern sector of the Iberian Chain ('Cordillera Ibética'). Inset shows the location of the Teruel Basin ('Cuenca de Teruel'), also known as Teruel Graben; C) simplified geological map of the Teruel Basin/Graben (northern sector) and adjacent Jiloca Graben (adapted from Simón et al., 2012). The red star marks the site where the Teruel clay was sampled; D) Miocene to Pliocene stratigraphy of the Teruel Basin (units in Roman numbers) (from Ezquerro, 2017, based on Alonso-Zarza et al., 2012). The Teruel clay was collected from distal alluvial lutites of Unit 1.

**Figure 13.** Brick production process. A) The clay is mixed with water and waste product (when applicable) until a paste with a uniform consistency suitable for brickmaking is obtained; B) the paste is placed in wooden moulds; C) the bricks are removed from their moulds, cut into cubes and left to dry; D) the bricks were fired in a Herotec CR-35 electric

oven in the laboratory of the Department of Mineralogy and Petrology at the University of Granada.

**Figure 14.** A, B and C) Part of the machinery used by the Castillo de Siles brick factory in the production of extruded bricks; D) extruded bricks being dried prior to firing at the factory.

**Figure 15.** Extruded bricks supplied by the Castillo de Siles brick factory. The bricks on the left, with rectangular shapes and brighter colours, were made with clay from Guadix and household glass powder. The bricks on the right, with square shapes and less luminous colours, were made with clay from Jun and household glass powder.

**Figure 16.** Summary table of all the raw materials used (clayey materials and wastes), firing temperatures used and elaboration process (extrusion or by hands) carried out. The nomenclature of the assigned samples and the organization that has been followed in this PhD Thesis by chapters are also described.

**Figure 17.** Conceptual summary of the techniques and methodologies employed in this Thesis. Acronyms: FTIR: Attenuated Total Reflectance Fourier Transform Infrared Spectroscopy; TG-DSC: Thermal Decomposition and differential scanning calorimetry; HR-FESEM: High-resolution field emission scanning electron microscope; UPV: Ultrasound propagation velocity.

**Figure 18.** Thermal behaviour of the bricks with tea residue added analysed in the Department of Geosciences at the University of Padua.

**Figure 19.** A) Image of the capillarity test carried out on the handmade bricks of Chapter I (bricks from Jun and Guadix with and without added household glass powder); B) capillarity rise in the handmade bricks made with raw material from Guadix with household glass added.

**Figure IA-1.** Grain size distribution of the clayey raw materials from Jun and Guadix and of household glass.

**Figure IA-2.** X-ray diffraction patterns of the raw materials from Jun and Guadix. Legend according to Whitney and Evans (2010): Qz = quartz; Cal = calcite; Dol = dolomite; Illt = illite; Pg = paragonite; Kln= kaolinite; Chl = chlorite; Hem = hematite; Mc = microcline.

**Figure IA-3.** TG-DSC analysis of the raw materials from Jun and Guadix. The abscissa represents the temperature (in °C) and the two ordinates represent the weight loss (in %) (TG blue curve) and the differential scanning calorimetry (in mW) (DSC green curve).

**Figure IA-4.** X-ray diffraction patterns for bricks made with the raw material from Jun (by hand and by extrusion) and fired at 800, 950 and 1100 °C. Legend according to Whitney and Evans (2010): Qz = quartz; Cal = calcite; Ill = illite; Hem = hematite; Or = orthoclase; Sa = sanidine; An = anorthite; Gh = gehlenite; Di = diopside; Wo = wollastonite.

**Figure IA-5.** X-ray diffraction patterns for bricks made with the raw material from Guadix (by hand and by extrusion) and fired at 800, 950 and 1100 °C. Legend according to Whitney and Evans (2010): Qz = quartz; Ill = illite; Hem = hematite; Or = orthoclase; SA = sanidine; Mul = mullite.

**Figure IA-6.** Bricks made with clay from Jun with and without household glass fired at 800, 950 and 1100 °C. Abbreviation: PPL = plane-polarized light; PPX = cross-polarized light. A) fragments of quartz and gneiss fragments in the matrix of J800 (PPX); B) carbonate grain partially decomposed in J800 (PPX); C) general view of the matrix of Jg800 made with added glass (PPL); D) detailed image of a glass fragment in Jg800 which is starting to decompose (PPX); E) pores with different morphology in J950 (PPL); F) extended vitrification in the matrix of Jg1100 produced by the addition of glass (PPL).

**Figure IA-7.** Bricks made with clay from Guadix with and without household glass fired at 800, 950 and 1100 °C. Abbreviation: PPL = plane-polarized light; PPX = cross-polarized light. A) detailed image of the G800 sample showing fragments of quartz (PPX); B) matrix of Gg800 sample in which glass fragments with angular morphology are visible (PPX); C) glass fragments in the matrix of Gg800 sample (PPX); D) glass fragment in the Gg950 sample with acicular crystals intergrowth (PPX); E) detailed image of the matrix of the G1100 sample showing pores with varying shapes (PPX); F) porosity, melted glass and vitrification in the Gg1100 sample (PPX).

**Figure IA-8.** A) Dehydroxylation of phyllosilicates along (001) planes in G800; B) view of J800 showing the partial decomposition of a dolomite grain with a depletion of Ca at the core; C) detail of a glass fragment from Jg800 showing the change in the composition along the edge of the grain due to devitrification or the formation of a pseudowollastonite; D) detail of small hematite crystal growth within the phyllosilicate sheets; E) rounded

pores and small hematite crystals in Gg1100; F) detail of elongated crystals that have developed inside a glass fragment in Jg1100.

**Figure IA-9.** Free (a) and forced water absorption (b) and drying curves (c) for handmade bricks made with and without household glass and fired at 800, 950 and 1100 °C using the raw material from Jun and from Guadix.

**Figure IA-10.** Free (a) and forced water absorption (b) and drying curves (c) for extruded bricks made with household glass and fired at 800, 950 and 1100 °C using the raw material from Jun and from Guadix.

**Figure IA-11.** MIP cumulative (dashed line) and pore size distribution (continuous line) curves for handmade bricks made with clay from Jun with and without added household glass fired at 800, 950 and 1100 °C.

**Figure IA-12.** MIP cumulative (dashed line) and pore size distribution (continuous line) curves for handmade bricks made with clay from Guadix with and without added household glass fired at 800, 950 and 1100 °C.

**Figure IA-13.** Mean ultrasound velocities (in m/s) in fired Jun and Guadix bricks made with and without added glass. The table on the right shows the structural anisotropy ( $\Delta M$ ) of the bricks.

**Figure IA-14.** A) Chromatic values ( $a^*$  and  $b^*$ ) for handmade and extruded Jun and Guadix bricks with and without added glass.

**Figure IA-15.** Freeze-thaw diagrams for handmade and extruded bricks made with clay from Jun or Guadix fired at 800, 950 and 1100 °C with and without the addition of household glass.

**Figure IA-16.** A) Salt crystallization diagrams for handmade and extruded bricks made with clay from Jun and Guadix fired at 800, 950 and 1100 °C with and without added household glass; B) wet-dry diagrams of handmade and extruded bricks made with clay from Jun and Guadix fired at 800, 950 and 1100 °C with and without added household glass.

**Figure IB-1.** Photograph of the bricks studied in this work. A) Unfired bricks made from raw materials from Jun and Guadix with and without household glass; B-C) general view of fired bricks with and without household glass.

**Figure IB-2.** Infrared absorption spectroscopy carried out on the raw materials from Guadix and Jun and on the household glass.

**Figure IB-3.** Mineralogy of the raw materials (Jun and Guadix). Legend according to Warr (2020): Illt = illite; Pg = paragonite; Kln= kaolinite; Chl = chlorite; Qz = quartz; Cal = calcite; Dol = dolomite; Mc = microcline; Hem = hematite.

**Figure IB-4.** Mineralogy of the bricks made with clay from Jun (left) and Guadix (right) with and without glass added and fired at different temperatures. Legend according to Warr (2020): Qz = quartz; Cal = calcite; Illt = illite; Hem = hematite; Sa = sanidine; Or = orthoclase; An = anorthite; Mul = mullite; Gh = gehlenite; Di = diopside; Wo = wollastonite.

**Figure IB-5.** Macroscopic features of the bricks from Jun (J, first and second columns) and Guadix (G, third and fourth columns) fired at 800, 950 and 1100 °C, with or without added glass (g).

**Figure IB-6.** Volume chart showing the lightness ( $L^*$ ) and  $a^*$  values for bricks made with or without glass and fired at 800, 950 and 1100 °C.

**Figure IB-7.** X-rays of the bricks made with clay from Jun and Guadix with or without added glass and fired at 800, 950 and 1100 °C.

**Figure IB-8.** Hardness (LH) of bricks made with raw materials from Jun and Guadix with or without added glass and fired at 800, 950 and 1100 °C.

**Figure IB-9.** Volume chart showing the LH, UPV and CS values for bricks made with or without added glass and fired at 800, 950 and 1100 °C.

**Figure II-1.** Grain size distribution of the raw materials (clayey material and carbon fibre, CF) (A) and TG-DSC analysis of the clayey material (B). A) Particle size (in  $\mu\text{m}$ ) vs. volume (in %); B) temperature (in °C) vs. weight loss (right ordinate, in %) and differential scanning calorimetry (left ordinate, in mW).

**Figure II-2.** Infrared spectrum of the carbon fibre used in this study. The range of the spectrum from 2000 to 1000  $\text{cm}^{-1}$  has been marked to highlight the presence of other components in the carbon fibre sample.

**Figure II-3.** Optical microscopy images of bricks with or without added carbon fibres fired at 800, 950 and 1100 °C, as observed in plane-polarized light. A) Orange matrix of sample FC0/800; B) and C) brown matrix of the samples fired at 800 °C with added CF



(CF5/800 and CF10/800, respectively); D) phyllosilicate grains with a preferential orientation in the FC0/950 sample; E) and F) the matrix is slightly darker due to the gradual vitrification and the presence of imprints of CF; G) dark matrix in the CF0/1100 sample; H) and I) rounded pores in the samples fired at 1100 °C with added CF (CF5/1100 and CF10/1100).

**Figure II-4.** Left – Optical microscopy images in plane-polarized light. The fibres and their imprints are highlighted in yellow. Right – Schematic view of a thin section of the CF10/1100 brick. Moving inwards from the outside to the core of the brick, three quite distinct zones can be observed: Zone A, the outermost zone, corresponds to MOP image A, zone B to image B and zone C, the innermost area, to image C.

**Figure II-5.** FESEM secondary electron images of carbon fibres added to the clayey material to make the bricks. A) General view of carbon fibres and other particulate matter from wind turbines; B) unidentified aggregates with irregular morphology together with fibres; C) detailed image of the cylindrical morphology of the carbon fibres; D) detail of the surface morphology of a carbon fibre highlighting the presence of striae on the surface.

**Figure II-6.** FESEM secondary electron images. A) General view of the texture and porosity of the sample CF0/800; B) dehydroxylation of a phyllosilicate grain along (001) planes in CF0/800 (the EDS of the phyllosilicate can be seen in the inset); C) general view of the texture and porosity of the sample CF10/800; D) imprints left by carbon fibres in sample CF10/800.

**Figure II-7.** Influence of temperature on the reorientation of carbon fibres.

**Figure II-8.** MIP curves for bricks fired at 800, 950 and 1100 °C without additive (black continuous line) and with added CF (red and blue dashed lines, respectively). The pore diameter at the maximum peak in each porosimetric curve is indicated.

**Figure II-9.** Mechanical behaviour of the bricks fired at 800, 950 and 1100 °C made without additives (control group, CF0) and with added CF (CF5 and CF10). The standard deviation appears in brackets. The lines connecting the different brick types (CF0, CF5 and CF10) correspond to trend lines and the black lines at 10 and 5 MPa show minimum thresholds for solid and lightweight bricks respectively, according to the official specifications of the Spanish Ministry of Public Works (Pliego RL-88, 1988).

**Figure II-10.** Surface hardness of the bricks as determined by the Leeb Hardness Test (LH).

**Figure II-11.** Chromatic ( $a^*$  and  $b^*$ ) and lightness ( $L^*$ ) values for bricks with and without added CF. The visual appearance of the nine types of bricks is shown.

**Figure II-S1.** Brick making process. A) Raw materials are kneaded with water; B) the kneaded clayey mass is placed in the wooden mould; C) cut samples are left to dry in the laboratory; D) fired bricks: control group (bricks with no added carbon fibre) in the top row, bricks with 5 wt.% carbon fibre in the middle row, and bricks with 10 wt.% carbon fibre in the bottom row.

**Figure III-1.** Grain size distribution of the raw material and waste pomace.

**Figure III-2.** X-ray diffraction pattern of the raw material. Legend according to Whitney and Evans (2010): Qz = quartz; Cal = calcite; Gp: Gypsum; Dol = dolomite; Ill = illite; Pg = paragonite; Kln= kaolinite; Chl = chlorite; Sme = smectite; Mc = microcline.

**Figure III-3.** TG-DSC analysis of the raw material. The abscissa represents the temperature (in °C) and the two ordinates represent the weight loss (right ordinate, in %) and the differential scanning calorimetry (left ordinate, in mW).

**Figure III-4.** PDRX patterns for control bricks (Mi) and bricks with added wine pomace (W) fired at 800, 950 and 1100 °C. Legend according to Whitney and Evans (2010): Qz = quartz; Cal = calcite; Ill = illite; Hem = hematite; Or = orthoclase; Sa = sanidine; An = anorthite; Gh = gehlenite; Di = diopside; Wo = wollastonite; Mul = mullite.

**Figure III-5.** Bricks with and without added wine pomace fired at 800 and 1100 °C. Abbreviation: PPL = plane-polarized light; PPX = cross-polarized light. A) matrix of sample Mi800 (PPX); B) detailed image of extended vitrification in the matrix of Mi1100 (PPL); C) phyllosilicate grains with a preferential orientation (PPX); D) muscovite-type crystals with a whitish colour (red arrows, sample W1100/2.5, PPX); E) unaltered phyllosilicates in W800/2.5 sample (PPX); F) ellipsoidal-to-rounded pores and darker matrix in W1100/5(PPL);G) decomposed carbonate grain in W10/800 sample (PPL); H) very large and rounded pores in W10/1100 sample (PPL).

**Figure III-6.** FESEM images of bricks fired at 800 °C without additives (A and C) and with wine pomace (B, D and E). EDS spectra of some of the mineral phases have been included.

**Figure III-7.** FESEM images of bricks fired at 1100 °C made without (A and C) and with wine pomace (B, D and E).

**Figure III-8.** Free (a) and forced water absorption (b) and drying curves (c) for bricks made without (Mi) and with wine pomace (W) fired at 800, 950 and 1100 °C.

**Figure III-9.** MIP curves for bricks fired at 800, 950 and 1100 °C without additive (Mi, continuous line) and with added wine pomace (W, dashed line).

**Figure III-10.** Salt crystallization diagram for bricks made with and without wine pomace added and fired at 800, 950 and 1100 °C. Weight variation ( $\Delta M/M$ ) vs. time (in hours).

**Figure III-S1.** Relationship between weight difference (%) and linear shrinkage (mm) between unfired and fired bricks based on firing temperature (800, 950 and 1100 °C) and the amount of residue added (no residue, 2.5, 5 and 10 wt.%).

**Figure III-S2.** Macroscopic view of control bricks and bricks made with added wine pomace fired at 800, 950 and 1100 °C.

**Figure IV-1.** Amount of clay (kg) and water (L) used in relation to the amount of tea residue added (g).

**Figure IV-2.** Bricks with and without added tea residue fired at 800 and 1100 °C. All photographs were taken with plane-polarized light (PPL).

**Figure IV-3.** High resolution SEM-BSE images of bricks made with and without added tea residue fired at 800 and 1100 °C.

**Figure IV-4.** A) SEM-EDS elemental maps and B) a linear chemical analysis along a reaction rim between quartz and calcite grains.

**Figure IV-5.** Interaction of the bricks with water vapour and their behaviour in relation to RH variations (mass increase versus relative humidity both in %), hydric behaviour of the bricks (weight variation in % versus time in hours) and MIP curves (frequency in % versus pore diameter in  $\mu\text{m}$ ) for bricks fired at 800, 950 and 1100 °C with no additive (continuous line) and with added tea residue (dashed lines).

**Figure IV-6.** Mechanical behaviour for bricks fired at 800, 950 and 1100 °C made without additives (control group, T0) and with added tea residue (T5 and T10).

**Figure IV-7.** A) Weight variation in the bricks made without additives (T0) and with added tea residue (T5 and T10) over 15 salt crystallization test cycles. Each curve represents

the mean of three measurements. B)  $V_P$  velocities during the salt crystallization test for bricks fired at 800, 950 and 1100 °C without additives and with added tea residue.

**Figure IV-S1.** Geological mapping of the Teruel area from where the raw material was obtained (red point). Map obtained and modified from IGME (<https://igme.es>).

**Figure IV-S2.** Mineralogy of the bricks with and without tea residue added and fired at different temperatures. Legend according to Warr (2020): Qz = quartz; Cal = calcite; Ill = illite; Hem = hematite; Mc = microcline; Or = orthoclase; Sa = sanidine; An = anorthite; Aug = augite; Gh = gehlenite; Wo = wollastonite.

**Figure IV-S3:** Correlation between thermal conductivity and porosity measured by hydric test (orange spot,  $R^2 = 0.9552$ ), MIP (blue circles,  $R^2 = 0.8061$ ) and DIA (grey triangles,  $R^2 = 0.8864$ ).

**Figure IV-S4.** Surface hardness as determined from the Leeb Hardness Test (LH) on the bricks studied.

**Figure IV-S5.** Lightness (up) and chromaticity (down) of fired bricks with and without tea residue added.

# TABLES

**Table I-1.** Acronyms assigned to the bricks according to the raw material used, the addition of 20 wt.% household glass, the production process and the firing temperature.

**Table I-2.** XRF (in %) results for the raw materials from Jun and Guadix and the household glass used to manufacture the bricks.

**Table IA-3.** XRF results (in %) for the handmade and extruded (e) Jun bricks (J) and Guadix (G) bricks fired at 800, 950 and 1100 °C.

**Table IA-4.** Hydric parameters of handmade and extruded bricks. Ab: free water absorption (%); Af: forced water absorption (%); Ax: degree of pore interconnection (%); S: saturation coefficient (%); Di: drying index; P<sub>o</sub>: open porosity (%); C: capillarity coefficient (g/m<sup>2</sup>s<sup>0.5</sup>); ρ<sub>a</sub>: apparent density (g cm<sup>-3</sup>); ρ<sub>r</sub>: real density (g cm<sup>-3</sup>).

**Table IA-5.** Compressive strength (R<sub>c</sub>, MPa) and standard deviation (σ) values for handmade bricks made with raw materials from Jun and Guadix with and without added glass.

**Table IA-6.** Lightness (L\*), chromatic values (a\* and b\*), chroma (C\*) hue angle (h°) and colour difference (ΔE) values caused by the addition of household glass with respect to the bricks made without additive. Each value indicated is the average of nine values. Standard deviation is indicated in brackets.

**Table IB-1.** Acronym assigned to each brick according to the raw material used, the addition of 20 wt.% household glass and the firing temperature

**Table IB-2.** Average lightness values (L\*), chromatic values (a\* and b\*) and standard deviation (σ) for handmade bricks made with clay from Jun and Guadix with or without added glass.

**Table IB-3.** Summary of average values ( $\bar{x}$ ) for LH, UPV (m/s) and CS (R<sub>c</sub>, MPa) and standard deviation (σ) values for handmade bricks made with raw materials from Jun and Guadix with or without added glass.

**Table IB-4.** Classification of subsets (a, b and c) for aesthetic ( $L^*$ ,  $a^*$  and  $b^*$ ) and physical (UPV, LH and CS) properties according to the tests proposed by Tukey and by Ducan and the ANOVA method.

**Table II-1.** FTIR bands identified for CF, their attribution and references.

**Table II-2.** Chemical analysis of mayor oxides (in wt.%) in the raw material and CF.

**Table II-3.** Mineralogical characterization by PXRD of the clayey material and the fired bricks with or without added CF. Data is provided in weight %. Abbreviations of minerals according to Warr (2020): Sme = smectite; Ill = illite; Pg = paragonite; Kln = kaolinite; Chl = chlorite; Mc = microcline; Qz = quartz; Cal = calcite; Dol = dolomite; Hem = hematite; Or = orthoclase; Sa = sanidine; Gh = gehlenite; An = anorthite; Mul = mullite; Wo = wollastonite; Di = diopside; Amph = amorphous phase.

**Table II-4.** Hydric parameters of bricks: Ab: free water absorption (%); Af: forced water absorption (%); Ax: degree of pore interconnection (%); S: saturation coefficient (%); Di: drying index; Po: open porosity (%); C: capillarity coefficient ( $\text{g}/\text{m}^2\text{s}^{0.5}$ );  $\rho_a$ : apparent density ( $\text{g cm}^{-3}$ );  $\rho_r$ : real density ( $\text{g cm}^{-3}$ ); MIP:  $P_{\text{MIP}}$ : open porosity (%), determined by MIP); SSA: specific surface area ( $\text{m}^2 \text{g}^{-1}$ , determined by MIP). The standard deviation of each result is indicated in brackets.

**Table II-5.** Average velocities (V) for the propagation of ultrasonic P and S pulses (m/s).  $\bar{x}$ : average values;  $\sigma$ : standard deviation;  $\Delta M$  total anisotropy (in %);  $\nu$ : Poisson's ratio; E: Young's modulus (GPa); G: shear modulus (GPa); K: bulk modulus (GPa).

**Table II-S1.** Amount of clayey material, carbon fibre (CF) and water (in wt.%) used to produce the brick samples.

**Table II-S2.** Abbreviations used to identify the brick samples according to the firing temperatures and the amount of carbon fibre added (CF).

**Table II-S3.** Equations used to calculate the parameters from test data. Abbreviations:  $M_0$  = mass of dried sample;  $M_l$  = mass of sample saturated with water at atmospheric pressure;  $M_s$  = mass of sample saturated under vacuum;  $M_H$  = hydrostatic weight of sample saturated under vacuum;  $M_t$  = decreasing water weight content as a function of time;  $t_0$  and  $t_f$  = start and finish times of the drying test;  $M_c$  = amount of water absorbed;  $t$  = time;  $h$  = height of water reached by capillary;  $F$  = is the breaking load (in N);  $A$  = cross-sectional area (in  $\text{m}^2$ );  $V_p$  = compressional pulse;  $V_s$  = shear pulse;  $V_{p1}$  = mean

maximum velocity;  $V_{p2}$  = mean intermediate velocity;  $V_{p3}$  = mean minimum velocity in any of the three orthogonal directions;  $\Delta L$  = variation of the lightness parameter between control samples and those with carbon fibre;  $\Delta a^*$  and  $\Delta b^*$  = variation of the chromatic values ( $a^*$  and  $b^*$ ) between control samples and those with carbon fibre.

**Table III-1.** Reference and firing temperatures of brick samples made with (W samples) and without (Mi samples) added wine pomace.

**Table III-2.** Elemental analysis (in %) of wine pomace.

**Table III-3.** XRF results (in %) for the raw material used to manufacture the bricks.

**Table III-4.** Lightness ( $L^*$ ), chromatic coordinates ( $a^*$ ,  $b^*$ ) and colour change ( $\Delta E$ ) values in fired bricks.  $\sigma$  is the standard deviation of nine measurements per brick.

**Table III-6.** MIP parameters for bricks without additive (Mi) and with added wine pomace (W) fired at 800 and 1100 °C. SSA = specific surface area ( $m^2/g$ );  $\rho_{aMIP}$  = apparent density ( $g \cdot cm^{-3}$ );  $\rho_{rMIP}$  = real density ( $g \cdot cm^{-3}$ );  $P_{oMIP}$  = open porosity (%).

**Table III-7.** Average UPV ( $\bar{x}V_p$ , in m/s) and compressive strength (CS, in MPa) values for handmade bricks made without (Mi) additive and with added wine pomace (W).  $\sigma$  is the standard deviation of  $\bar{x}V_p$  and CS values.

**Table IV-1.** Acronyms assigned to the bricks according to the addition of 0, 5 or 10 wt.% of tea residue and the firing temperature (800, 950 or 1100 °C)

**Table IV-2.** XRF results (in %) for the raw material and for the fired bricks.

**Table IV-3.** Mineralogical characterization by XRD of the clayey material and the fired bricks with or without tea residue. Data is provided in weight %. Abbreviations of minerals according to Warr (2020): Qz = quartz; Kln = kaolinite; Cal = calcite; Ill = illite; Hem = hematite; Mc = microcline; Or = orthoclase; Sa = sanidine; An = anorthite; Aug = augite; Gh = gehlenite; Wo = wollastonite; AM = amorphous phase.

**Table IV-4.** Hydric, MIP and DIA parameters for bricks with and without tea residue. Ab: free water absorption (%); Af: forced water absorption (%); Ax: degree of pore interconnection (%); S: saturation coefficient (%); Di: drying index.  $P_o$ : open porosity by hydric test (%); C: capillarity coefficient ( $g/m^2s^{0.5}$ );  $\rho_a$ : apparent density ( $g \cdot cm^{-3}$ );  $\rho_r$ : real density ( $g \cdot cm^{-3}$ ).  $P_{oMIP}$  = open porosity by MIP (%);  $\rho_{aMIP}$  = apparent density ( $g \cdot cm^{-3}$ );

$\rho_{\text{MIP}}$  = real density ( $\text{g cm}^{-3}$ ); SSA = specific surface area ( $\text{m}^2/\text{g}$ );  $\text{Po}_{\text{DIA}}$  = open porosity by DIA (%); MinFerret = the largest MinFerret diameter measured by DIA.

**Table IV-5.** Thermal behaviour:  $\lambda(a)$ ,  $\lambda(b)$  and  $\lambda(c)$  = thermal conductivity measured normal to the sides a (perpendicular to the pressure exerted), b and c (parallel to the pressure exerted) of the sample ( $\text{W}/(\text{m}\cdot\text{K})$ );  $\lambda_{\text{mean}}$  = mean thermal conductivity ( $\text{W}/(\text{m}\cdot\text{K})$ ) calculated on the three sides  $\lambda(a)$ ,  $\lambda(b)$  and  $\lambda(c)$ ;  $\alpha$  = thermal diffusivity calculated by  $\lambda_{\text{mean}}$  ( $\text{mm}^2/\text{s}$ ).

**Table IV-6.** Average velocities for the propagation of ultrasonic  $V_P$  and  $V_S$  (in  $\text{m}/\text{s}$ ).  $\nu$ : Poisson's ratio; E: Young's modulus (in  $\text{GPa}$ ); G: shear modulus (in  $\text{GPa}$ ); K: bulk modulus (in  $\text{GPa}$ ).

**Table IV-S1.** Weight difference average and standard deviation of fired bricks with and without tea residues added

**Table IV-S2.** Colour difference ( $\Delta E$ ) due to the addition of tea residue to the brick samples as compared to those made without additive.



# 1. INTRODUCTION

### 1.1. The invention of bricks

Bricks have a fascinating history spanning thousands of years and many highly diverse civilizations around the world. The earliest recorded mudbricks date back some 9,000 years to the regions of Mesopotamia and the Indus Valley in modern-day Iraq, Iran and Pakistan (Fig.1) (Heathcote, 1995; Pollock, 1999; Minke, 2006). The discovery of mudbricks changed the way communities built their homes and fortifications (Richardson, 2015; Momčilović-Petronijević et al., 2018).

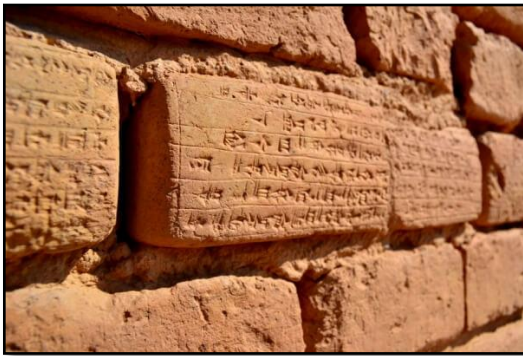


**Figure 1.** The earliest unfired bricks in history were handmade eight thousand years ago on the Iranian Plateau in ancient Persia. Image obtained and adapted from: <https://nationalgeographic.com> (accessed January, 2024).

These bricks were important to the development of stable agricultural communities and the first villages and towns (Berge, 2007). These early bricks were made by mixing clays with water and straw or other fibrous materials, such as reeds, to increase their strength and prevent them from shrinking and forming cracks as they dried out (Parisi et al., 2015; Calatan et al., 2016; Waters et al., 2016). Once the clay mix had been kneaded to the right consistency, it was placed inside rectangular moulds to give it the desired

shape. Later, the moulds were removed and the bricks were left to dry outside in the sun or indoors in ventilated rooms for variable periods of time (Gallipoli, 2017). Although they were relatively fragile, mudbricks played a key role in the development of stronger, more durable structures than earlier constructions, which were often made of flimsy, more temporary materials such as branches, tree leaves and animal skins (McHenry, 1989; Almsad et al., 2022). Although useful, these first mudbricks had important limitations. Mudbrick houses were vulnerable to water and erosion, which meant that in areas of heavy rainfall they often had to be rebuilt. Likewise, their fragility made them unsuitable for high-rise structures (Silveira et al., 2012 and 2013).

Around 3500 BC, the Sumerians, an ancient civilization in Mesopotamia, started firing their mudbricks, making them more resistant and durable (Crawford, 1972). The manufacturing process was very similar to that of mudbricks, except that they were fired in ovens at high temperatures, often exceeding 600°C (Tay, 1987). Firing transformed

the clayey raw material into a more solid, more resistant product. These bricks were widely used in the construction of houses, temples, walls and other architectural structures in Mesopotamia and brick-firing technology was soon acquired by other nearby peoples, such as the Babylonians and Assyrians (Bertman, 2005; Oppenheim, 2013). One of the most notable architectural achievements of the Sumerians were the *ziggurats* (Kramer, 1963; Crawford, 2004; Mohsen and Hameed, 2021). These were stepped terrace structures, built mainly of mudbricks, which often had a temple on top. One of the best-known examples is the *Ziggurat of Ur* (Fig.2).

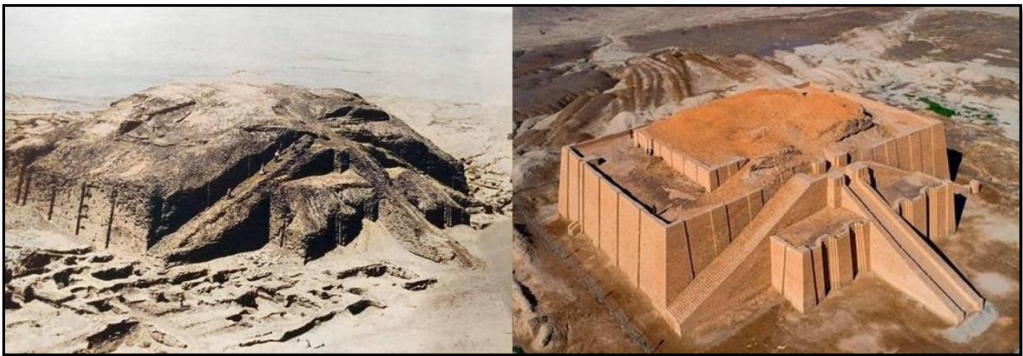


**Figure 2.** Before and after the excavation and restoration of the Great Ziggurat of Ur, built approximately 4000 years ago by King Ur-Nammu of the Neo-Sumerian Empire and dedicated to the Moon God, Nanna. Image obtained and modified from: <https://reddit.com> (accessed January, 2024).

The Ancient Egyptians (c.3100 BC to 30 BC) also used fired bricks in their architecture (Fig.3) (Almssad et al., 2022). There was an abundant supply of clay on the banks of the River Nile, so making brick production economically viable (Massoud, 2007). The clay was mixed with water and moulded into a rectangular shape, in much the same way as the Sumerians had done. The fact that the bricks had the same size and shape facilitated the construction of impressive structures (Spencer, 2023). The Egyptians also developed special ovens to produce fired bricks on a larger, more industrial scale. These ovens allowed a large number of bricks to be fired at the same time, so making production more efficient. Firing was carried out at relatively low temperatures compared to modern bricks, giving them a distinctive red or yellow appearance (Fernandes et al., 2010). Fired bricks like these were used in a variety of structures, including temples, tombs, houses, walls and other important buildings and were often adorned with hieroglyphs and decorative reliefs. The step pyramid of *Djoser* at Saqqara is one of the earliest-known examples of

the use of fired bricks in a monumental structure (Massoud, 2007; Spencer, 2023). Although this pyramid was later clad with limestone, its core was mainly composed of fired bricks (Davidovits, 2008). Another notable example is the *Temple of Karnak* at Luxor, where fired bricks were used in various parts of the structure (El-Badry, 2019). In addition to religious and funerary structures, fired and mudbricks were also used in the construction of simple dwellings for the general population, so helping insulate them from Egypt's desert climate.

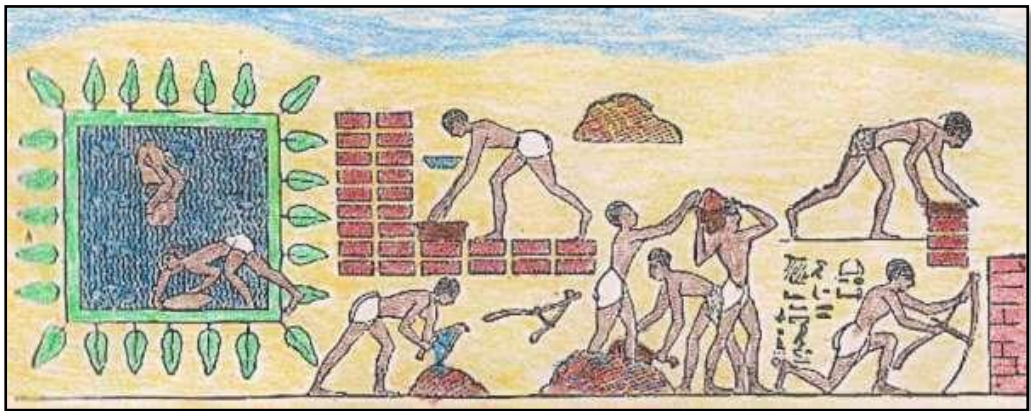


**Figure 3.** An Egyptian hieroglyph from the tomb of Rekhmire showing Hebrews making bricks. Image obtained and modified from: <https://lacorriente.com> (accessed January, 2024).

The earliest bricks used in China were found in 2009 at the Xi'an archaeological site and are estimated to be about 3800 years old. The first descriptions of the brick production process appear in the Song dynasty, in a manual by the carpenter Yingzao Fashi, published in 1103. China is also home to the world's largest brick structure: the Great Wall (Fig.4). More than twice as long as originally thought, it stretched over 21,000 kilometres from the Korean border to the Gobi Desert. Although brick was the main building material used, it also contains sections built of stone, granite and clay, depending on the period of history and the available materials (Dalín, 1984; Di Cosmo, 1993).

The fired-brick technology developed by the Egyptians was also adopted by neighbouring civilisations, such as the Greeks and Romans. This helped to spread the knowledge and practice of fired brick construction throughout the ancient world.





**Figure 4.** Detail of the Great Wall of China. Photograph: Sergio Rademacher. Image obtained and modified from: <https://researchgate.net/> (accessed January, 2024).

The Romans were pioneers in the production and widespread use of fired bricks in construction and left behind a long-lasting legacy in architecture and civil engineering (Fig.5) (Artioli et al., 2019; Mogetta, 2021; Almssad et al., 2022). They used fired bricks, known as “Roman bricks”, in a wide variety of building projects throughout their vast empire, so bringing about significant advances in architecture and construction (Wilson, 2006). The Romans inherited the idea of making bricks from fired clay from previous civilizations, such as the Egyptians, but refined and systematized their methods to enable large-scale production. The Romans also established standard measurements for their bricks, which allowed them to produce bricks of specific uniform dimensions, known as “*modulorum*” (Wilson, 2006). The most common sizes were approximately 30 x 15 x 7.5 cm, which made them easy to use in construction. They also perfected the manufacturing process by developing efficient ovens for firing the bricks (Pérez-Monserrat et al., 2022a).



**Figure 5.** Roman bricks with Legio XXII stamp (Saalburg Museum, Germany). Imagen obtained from: <https://worldhistory.org> (accessed January, 2024).

These were often installed close to construction sites, so as to reduce transport costs and ensure that bricks were available in sufficient quantities. Fired bricks played a key role in the construction of aqueducts and sewage systems. *The Flavian Amphitheatre* (or *Colosseum*) in Rome (Italy) was built with travertine quarried near the ancient city of Tibur,

tuff, lime mortar (the famous *opus caementicium*) and bricks. Other examples include the *Pantheon* in Rome, with its impressive brick-lined concrete dome, and the *Pont du Gard* aqueduct in Gaul (France), which featured brick arches.

In the 1<sup>st</sup> century BC, Vitruvius mentioned the “floating” bricks made in Hispania (Spain), which were so light that once dry, they did not sink when placed in water. It seems likely that pumice stone played an important part in the production of these bricks, which also caught the attention of the Greek philosopher Posidonius around the same time.

During the early Middle Ages, after the fall of the Roman Empire, in the architectural period known as 'Romanesque' (11<sup>th</sup>-13<sup>th</sup> centuries), the use of fired bricks declined sharply in Western Europe (Rush, 2022). This was due to a number of factors, such as the disappearance of the Roman brick-making technology and a preference for other building materials, such as wood and stone (Heywood, 1985; Fernie, 2006). However, thanks to Byzantine influences, the tradition of using fired bricks persisted in Eastern Europe (Stoianovich, 1971), where churches and other religious buildings continued to be built with fired bricks. As the Middle Ages progressed, the use of fired bricks experienced a renaissance in Western Europe (Smith, 1896; Fernie, 2006) due in part to the increasing availability of brick-making technology, as well as the need to build strong, durable structures. Bricks were used for the construction of churches, monasteries and castles. In Italy in particular, bricks were used widely in the construction of Romanesque churches, often combined with stone (Burgini and Folli, 2021). With the transition to the Gothic style (12<sup>th</sup>-15<sup>th</sup> centuries), bricks became more important in medieval architecture (McClendon, 2005; Fernandes et al., 2010). The Gothic style was characterized by high walls and large stained-glass windows. By using bricks it was possible to build taller and thinner structures than with stone. The Hanseatic League, a powerful trading alliance between cities in northern Europe, promoted the use of brick in the construction of churches, houses and defensive walls (Clark, 2009). Cities such as Lübeck in Germany are famous for their Gothic brick architecture (Fig.6) (Nesbitt, 1863).

During the Renaissance, architects rediscovered the beauty and versatility of bricks, using them in iconic buildings such as the *Pitti Palace* and the *Church of Santa Maria del Fiore* in Florence. A distinctive feature of the Renaissance was the creation of 'Roman front' (Mazzanti, 2016), a building technique in which the front of the bricks was left

exposed, often with intricate decorative details, such as geometric patterns or sculptural motifs using coloured bricks in red, yellow or brown.



**Figure 6.** Lübeck old town. Image obtained and adapted from: <https://visit-luebeck.com> (accessed January, 2024).

As the influence of the Italian Renaissance spread, so did the use of bricks in Renaissance architecture across Europe, as can be seen in buildings in countries such as France, the Netherlands, Germany and Spain (Anderson, 2013).

The Industrial Revolution, which began in the 18<sup>th</sup> century in the United Kingdom and then spread across the world, brought significant advances in brick production (Shannon, 1934; Wilkinson; 1988). The invention of the brick-making machine (extruder) in the 19<sup>th</sup> century enabled the mass production and standardization of bricks (Fig.7) (Adeloye, 2017). During the Industrial Revolution, cities underwent rapid growth and bricks became the material of choice for the cladding of residential, commercial and industrial buildings. Bricks were also used in the construction of bridges and aqueducts, where solid structural strength was required (Dale et al., 2021). Brick arches became a common feature in bridge construction at the time.

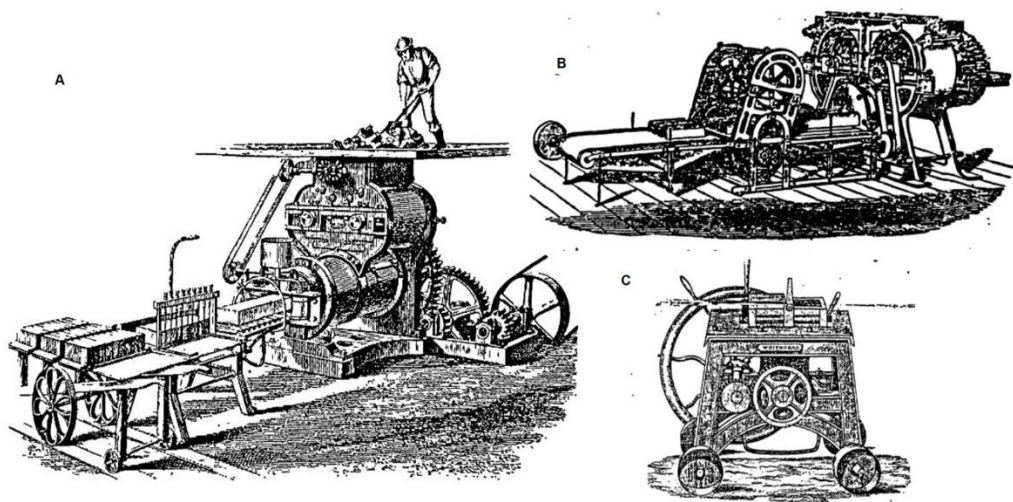


**Figure 7.** A) Ramp-loaded brickmaking machine by Henry Clayton, c.1860 (obtained and adapted by Woodforde, 1976); B) Brick and tile machine patented by John Ainslie, British Patent No.8965, 1841. (obtained and adapted by the Civil Engineer and Architect's Journal Vol. V 1842, p.427); C) Brickmaking and pressing machine, John Whitehead, manufacturer (obtained and adapted from John Whitehead's Trade Catalogue, 1851).

In the early 20<sup>th</sup> century, in the United States of America, various brick skyscrapers were built in the Beaux-Arts architectural style above all in New York and Chicago, (Moudry, 2005; Garric, 2017). These buildings often featured ornate brick fronts and elaborate architectural details. During the 1920s and 1930s, the Art Deco style also entered architecture, and some buildings from this period incorporated brick cladding in their façades, often combined with terracotta and metalwork details (Allwright, 1997). In the 1950s, the Brutalist architectural movement emerged. Although Brutalist buildings could be clad in a variety of materials, some featured exposed brick as part of their blunt, unadorned construction aesthetic (Mould, 2017). As the 20<sup>th</sup> century progressed, new types of brick were developed, such as hollow and concrete bricks (Thorat et al., 2015). These new materials expanded the architectural possibilities of bricks and improved building efficiency. Bricks remain a prominent feature in modern architecture and were used in innovative designs by architects such as Frank Lloyd Wright and Louis Kahn (Kroger, 2005; Higgott, 2018).



## 1.2. Building standards applicable to bricks

The standards affecting the brick industry vary depending on the country and region where they are used, although they are generally designed to ensure the safety, durability and sustainability of brick-built structures. These standards may include specifications governing brick size and quality, installation techniques, structural and compressive strength, water absorption, moisture content, and other physical and chemical properties. In earthquake-prone areas, building standards often include specific guidelines for the design of seismic-resistant brick structures (Arya et al., 2014; Khan and Ali, 2020) that can help protect life and property in the event of an earthquake.

Some building standards provide detailed guidelines on how bricks should be laid and joined together. These include specific techniques for building walls, arches, columns and other brick elements. Depending on the thermal and acoustic insulation needs of a building, building standards may also establish specific requirements for the installation of insulation materials in brick walls. Standards may also address the resistance of brick structures to local weather conditions, such as wind, rain, extreme cold and heat. However, there are some general standards and guidelines governing construction with bricks that are common to most countries in Europe.

### *1.2.1. Building standards in Europe*

In the European Union (EU), many construction products, including bricks and other fired clay products, must be labelled with the CE (*Conformité Européenne*) marking to demonstrate that they comply with applicable European safety and performance standards. This facilitates the marketing of products throughout the EU, as they are recognized as complying with established standards. The Construction Products Directive is a European directive that sets out the conditions for the marketing of construction products in the EU. It defines essential performance requirements for construction products, including bricks, and establishes procedures for conformity assessment. Sustainability has become an increasingly important aspect of brick regulation in Europe. Building regulations and standards can address the energy efficiency of buildings, the management of construction and demolition waste, and the use of sustainable materials in brick manufacturing. Waste management and responsible disposal of bricks and other building materials at the end of their useful life are regulated

in many European countries. This may include the reuse, recycling and proper disposal of bricks and other building materials.

### 1.2.2. Building standards in Spain

In addition to European regulations, each EU country may have its own national regulations and standards covering the brick and construction industry. The Technical Building Code (CTE, Código Técnico de Edificación, in Spanish) is a set of technical documents that establish the basic requirements for quality and safety in the construction of buildings in Spain. It contains detailed information on various aspects of construction, including building materials, and standards for the use of bricks and other materials in construction projects. In addition to national regulations, the regions (known as autonomous communities) and municipalities in Spain may have their own specific regulations and standards in relation to construction materials. These regulations may vary from one place to another and may be influenced by local climate conditions and construction practices.

In June 1977, Royal Decree 1650/1977 established that basic building regulations (NBE, in Spanish) are compulsory for all building projects and works, their purpose being to defend the safety of people and establish the minimum conditions to meet human needs and protect the economy and society. In 2004, the NBE FL-90 "Resistant brick masonry walls" standard was introduced, updating the earlier Royal Decree 1324/1972. The updated standard included the acoustic, thermal and fire protection conditions covered in more specific standards (NBE CA-88, NBE CT-79 and NBE-CPI-82 respectively). It also specified that the manufacturers of wall bricks must comply with the General Specifications (*Pliego General*) for the reception of ceramic bricks in construction works RL-88, regarding the designation of their products and must guarantee that the material they supply meets all the conditions applicable to the designated class, i.e. common brick for buildings with cladding, or facing brick for buildings without cladding. RL-88 specifies that the compressive strength of solid and lightweight bricks must not be less than 10 MPa or 5 MPa, respectively.

In Spain, as in other EU countries, regulations have been implemented to improve the energy efficiency of buildings. These regulations may affect the choice of construction materials, including bricks.

### 1.3. Background: clay depletion and the accumulation of waste

Clay depletion is an environmental problem that can arise when large amounts of clay are quarried from a specific location over an extended period of time (Drew et al., 2002). Clay is a valuable natural resource used in the manufacture of brick, stoneware, porcelain and other ceramic products, and is therefore intensively quarried in certain regions (Aboudi Mana et al., 2017). Brick manufacturing has traditionally relied heavily on clay as the main raw material. Demand for bricks can be high in expanding urban areas and in infrastructure construction (Fernandez et al., 2010), which can put pressure on local clay reserves, in some cases leading to their exhaustion. When this happens, brickmaking companies have to seek new sources of clay, which can increase production costs due to transportation and logistics (Youssef et al., 2020). Intensive exploitation of clays can have a negative impact on the local environment. Once a clay quarry is exhausted, it can be difficult and expensive to restore the area to its original natural state (Grilli et al., 2021). This can leave wasteland or disturbed landscapes that are unsuitable for agriculture, recreation or conservation.

The depletion of natural resources and the accumulation of waste have caused the scientific world to search for new alternative, sustainable building materials. In many countries, the most fertile soils are being depleted due to their extensive use in the manufacture of ceramic products, particularly bricks. The environment is also being polluted by the increasing accumulation of waste and pollutants in landfills. The possibility of incorporating a wide range of waste products into the production of efficient building materials that are also more economical would encourage the development of a circular economy (Priyadarshini et al., 2021). The economic and cultural importance of bricks, in both the construction of new buildings and the restoration of architectural heritage, and the concern for environmental protection, means that we must continue research into the development of new brick products made with organic and inorganic additives from domestic and industrial waste. It is vital that these new products have good physical-mechanical performance and durability, so as to increase their commercial value and make them a viable alternative to traditional bricks.

#### 1.4. Eco-friendly bricks

The need for sustainable construction has led to increasing interest in the development of “eco-friendly bricks”, made from recycled or low environmental impact materials, and using more energy-efficient production techniques (Hafez et al., 2022). The incorporation of conventional waste reduces the extraction of natural resources, the waste being sent to landfills and in many cases, the energy required for production, all of which help mitigate the negative environmental impacts (Cultrone et al., 2020; Crespo-López et al., 2022; Simão et al., 2022). However, this process has traditionally required large amounts of natural resources and energy, resulting in a considerable ecological footprint. In fact, the disposal of conventional waste has become a growing challenge due to environmental concerns and increasingly stringent regulations. The use of conventional waste as an additive in brick production has emerged as an innovative solution to address these challenges. By using locally available waste, companies can reduce their raw material procurement costs (Crespo-López et al., 2023b and c). This practice promotes the circular economy by reusing materials that would otherwise be discarded, thus contributing to a longer and more sustainable life cycle for building materials. In addition, production efficiencies and the reduction in the energy required to fire the bricks can result in significant long-term savings. Using a careful mixing and kneading process, the waste is safely incorporated into the mix from which the bricks are formed. This not only reduces the demand for natural resources, but also minimizes the amount of waste that ends up in landfills (Antico et al., 2017). The addition of waste can also improve the physical properties of the bricks, such as strength and thermal insulation (Coletti et al., 2023), making them even more suitable for use in construction.

The integration of conventional waste into brick production offers many benefits for the environment. For example, by reducing reliance on natural, previously unused raw materials, it reduces the pressure on ecosystems and habitats, preserving biodiversity and ecosystem services (Edike et al., 2020). In addition to these environmental benefits, the use of waste as an additive also contributes to a more resilient, more resource-efficient construction sector that is less vulnerable to fluctuations in the availability and price of clay (Sohling et al., 2009).

The use of waste materials in brick production can have a positive socio-economic impact. By creating opportunities for waste collection, sorting and processing, this

approach can generate employment and income in local communities. It also encourages innovation and entrepreneurship as companies and researchers explore new ways to make effective use of different waste streams (Caro et al., 2024).

In turn, the use of waste bricks can enhance the aesthetic appeal of buildings by offering architects and designers a wider range of textures, colours and finishes to work with (Coletti et al., 2016; Crespo-López et al., 2023c). This encourages creativity and allows for the creation of visually striking and unique structures that reflect sustainable design principles.

Definitely, the viability and success of this technique is highly dependent on proper waste selection, research and development to optimise mixes, and collaboration between industry and the scientific community. As awareness of sustainability continues to grow in the construction industry, the addition of conventional waste in brick production is emerging as a significant and promising development that has the potential to positively transform the way we build the world.

## 2. OBJECTIVES OF THIS RESEARCH

This Doctoral Thesis aims to provide both builders and restorers, as well as society in general, with a series of objective data about innovative brick products of high technical quality in which part of the raw material has been replaced by waste.

The general objectives of this Doctoral Thesis are:

- To make highly efficient, durable bricks using a mixture of clay and organic or inorganic wastes fired at 800, 950 and 1100 °C.
- To create economic savings by reducing the amount of clay required in brick production.
- To obtain environmental benefits by reusing waste that would otherwise end up in landfills.
- To optimize the firing temperature, so saving energy without affecting the quality of the final products.

The specific objectives of this thesis are:

1. To obtain a detailed understanding of the mineralogical changes affecting the mineral phases present in the clay, and find out how these reactions are influenced by the presence of waste products.
2. To understand the textural changes that occur in the bricks after firing them at different temperatures and the extent to which these changes are affected by the type of preparation (by hand or by extrusion), the mineralogy and the waste products.
3. To relate the mineralogical and textural changes in the bricks with their physical and mechanical properties and find out whether the addition of wastes affects the petrophysical parameters of the fired samples.
4. To use additives to modify the porous system in an attempt to reduce the density of the brick samples in order to obtain lighter bricks with a higher degree of thermal insulation, without harming their technical quality.
5. To use ageing tests to find out more about the decay mechanisms in bricks and their relationship with their textural and physical characteristics. To evaluate the durability and

technical quality of our handmade and extruded bricks made with different raw materials, wastes and firing temperatures.

The overall aim is to perform a comprehensive systematization of this question, so as to create a model that not only provides a better, more detailed understanding of the intricacies involved in this innovative approach to brick production, but also serves as a valuable resource for researchers interested in conducting future investigations in diverse fields such as geology, engineering, chemistry and materials science. We hope that the comprehensive nature of the data presented in this thesis will inspire and support future exploration and research, encouraging interdisciplinary collaboration and the promotion of sustainable practices within the wider scientific community.



### 3. MATERIALS

### 3.1. Raw materials

#### 3.1.1. *Clayey materials*

Clays are the main raw material used in the manufacture of bricks. This group of minerals is found in all types of rock formations, from the oldest to the most recent, and in all types of sedimentary formations (Barnhisel and Rich, 1967; Blight, 1997; Ugidos et al., 1997). As a result, their physical, chemical and mineralogical characteristics vary widely, sometimes even between different layers in the same clay deposit (Righi and Meunier, 1995). Therefore, as happens in all ceramic industries, quality control of the end product must begin with the analysis and characterization of the clays.

A thorough evaluation of clays must include an analysis of both their chemical composition and mineralogy, as these characteristics directly influence the properties of the fired bricks (Montana, 2017; Eramo, 2020; Pérez-Monserrat et al., 2024). For example, clays with a high kaolinite content have a crystalline structure that makes the bricks remarkably resistant to heat, making them ideal for refractory applications (Chakraborty, 2014; Silva et al., 2021). They normally have a light colour and excellent mechanical strength (Prasad et al., 1991). For their part, clays with high concentrations of illite have great plasticity, which makes them easy to mould into a particular shape (El Idrissi, 2021). However, this plasticity can lead to shrinkage during drying and sintering (Vieira et al., 2008), which increases the risk of cracks appearing in the fired bricks (Pérez-Monserrat et al., 2022b). To counteract this effect, a tempering agent such as sand is added to control the plasticity of the body and reduce the probability of unwanted deformation (Cultrone, 2001).

The clayey materials used in the production of three of the four types of bricks studied in this Doctoral Thesis come from the province of Granada, Spain. The clayey materials from Guadix, Jun and Viznar were supplied by the brick factory “Ceramica Castillo Siles”, known also as “Ceramica San Francisco” (Fig.8). This company is located in Víznar (Granada) and is a four-generation family company that opened in 1992. They also supplied us with the extruded bricks. The company offers a wide range of ceramic products, including roof tiles, wall tiles and bricks. In their production, the clay, which is sourced from various quarries (described below, see section 3.1.1.2. *Geological context of clayey materials*), is first ground up in a ball mill to a particle size of up to 80 µm and then mixed with about 10-15% of water. The amount of water varies according to the

desired end-product. The ceramics are then fired in electric or, more frequently, gas ovens at temperatures of between 920 and 960°C, depending on the end product and the type of clay used. The samples are then left to cool for 30 hours, before being completely soaked in water to prevent possible “lime blowing” due to the presence of lime grains (Laird and Worchester, 1956).

The fourth type of clayey material used in the research for this thesis (Chapter IV) comes from the province of Teruel, where there is a long brickmaking tradition (Meseguer et al., 2009; Sánchez-Jiménez et al., 2012). It was extracted near the city of Teruel, from a site close to old quarries that were not in use at the time, but are now in operation again.



**Figure 8.** A) Ceramica Castillo Siles factory; B) Drying of extruded bricks; C) Stack of bricks ready for firing in the oven; D) Clayey material piled up outside the factory; E) Moulds used for the production of handmade bricks.

### 3.1.1.1. Geological context of the clayey materials

#### 3.1.1.1.1. The Betic Cordillera

The Betic Cordillera in southern Spain forms the westernmost segment of the peri-Mediterranean Alpine Orogen, extending in a WSW-ENE direction from Gibraltar to Alicante before continuing under the sea to the Balearic Islands (Fig.9A). It forms the northern branch of the orogenic belt and appeared as a result of the convergence

between the African and Eurasian plates during the Cenozoic (Platt et al., 2013). The Betic Cordillera has traditionally been subdivided into three major geological domains (Sanz de Galdeano and Vera, 1992): the Internal Zones to the north and the External Zones to the south, which collided in the early Burdigalian, and the Flysch Trough Units (Campo de Gibraltar Complex), located between the External and Internal zones (Fig.9A).

The Internal Zones are intensely deformed and consist of three tectonically stacked complexes, in ascending stratigraphic order, the Nevado-Filábride Complex, the Alpujárride Complex and the Maláguide Complex (Egeler and Simon, 1969). The Nevado-Filábride Complex includes Palaeozoic or older, high-pressure metamorphic rocks (Gómez-Pugnaire et al., 2000). The Alpujárride Complex also includes Permo-Triassic or older, high-pressure metamorphic rocks and sedimentary rocks (carbonates). From bottom to top, it comprises a mica schist formation, a phyllite formation and a carbonate formation (Sanz de Galdeano and López-Garrido, 2003). The Maláguide Complex has not undergone significant metamorphism and includes Ordovician to Lower Miocene sediments deposited in a suite of continental, shallow-water and deep-water environments (Martín-Algarra et al., 2009; Critelli et al., 2021). The Maláguide Complex is linked to the 'Dorsal' Complex (Durand-Delga and Foucault, 1967) or Frontal Units (Vera, 2004), and it also shares some affinities with the Triassic part of the Alpujárride Complex.

The External Zone of the Betic Cordillera corresponds to the Mesozoic and Cenozoic sedimentary cover of the Palaeozoic south Iberian Massif and is subdivided into two tectono-stratigraphic zones, the Prebetic and the Subbetic (Vera, 2004). The Prebetic zone includes continental to shallow-marine deposits laid down between the Triassic and the Upper Miocene over the Iberian continental margin, while the Subbetic is in a more distal position and includes, above all, pelagic sediments (García-Hernández et al., 1980).

The Flysch Trough Units include Cretaceous to Aquitanian deep-water deposits (calcareous and siliciclastic turbidites, marls and clays) accumulated in a narrow basin (Pendon, 1978; Stromberg and Bluck, 1998).

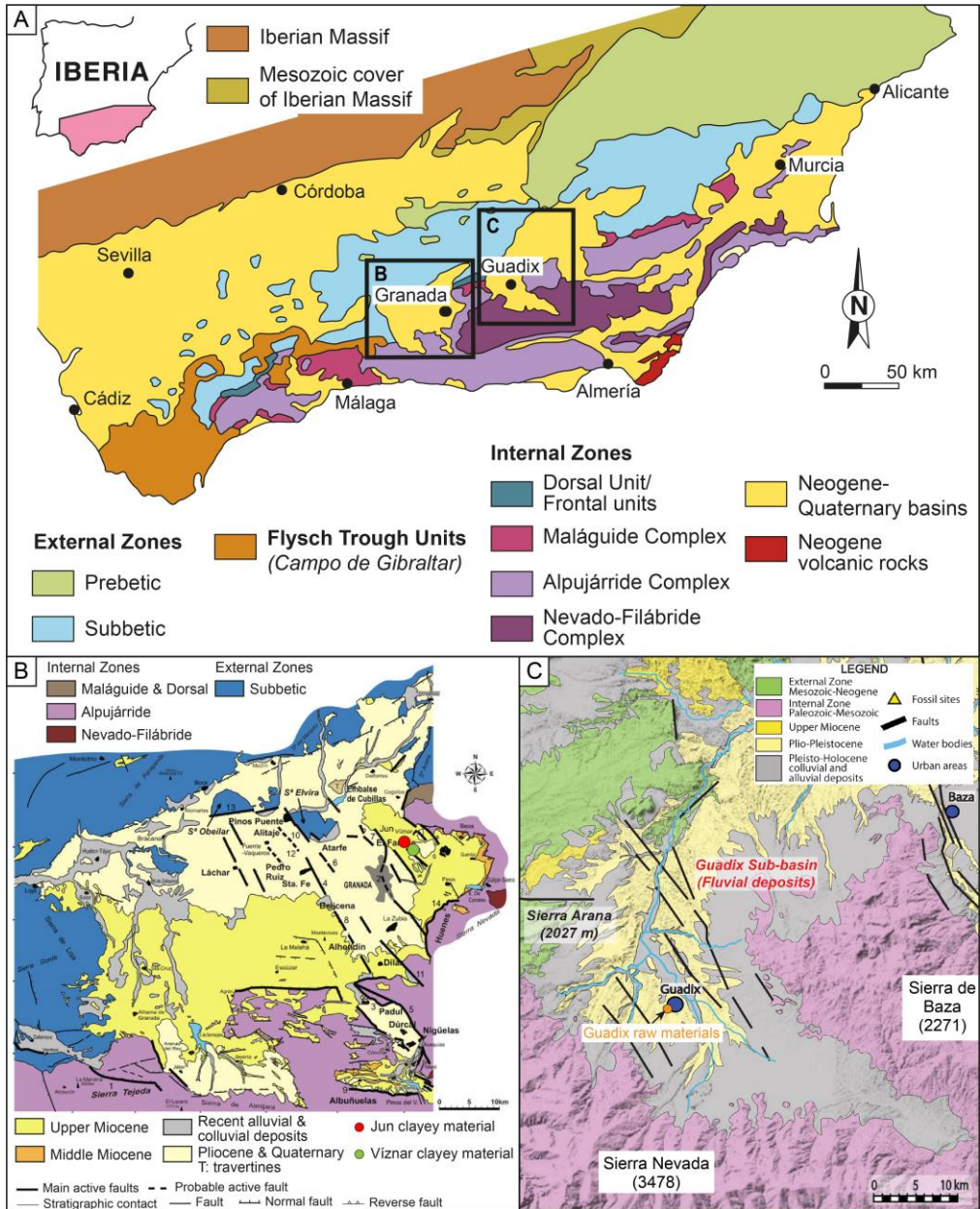


**Figure 9.** A) Simplified geological map of the Betic Cordillera showing the main geological domains and Neogene-Quaternary basins. Insets show the location of the Granada and Guadix basins in the central sector of the Cordillera; B) simplified geological map of the Granada Basin (from Sanz de Galdeano et al., 2012). The sampling sites for the clay from Jun and Viznar are indicated at the northeastern edge of the basin; C) simplified geological map of the Guadix Basin showing the site where the Guadix clay was sampled (modified from Altoaguirre et al., 2021).

### The Neogene-Quaternary basins

The Neogene-Quaternary basins in the Betic Cordillera are intermontane basins (Fig.9A) which evolved since the late Miocene driven by tectonic deformations and uplift of the basement reliefs (Galindo-Zaldivar et al., 2019). The ongoing Eurasian-African convergence caused the uplift of these reliefs in relation to regional E-W to NE-SW folds (Braga et al., 2003; Galindo-Zaldivar et al., 2019). The sedimentary record of the Neogene basins is the result of a combination of tectonically controlled local processes and regional processes driven by relative sea level and climate, and reflects the uplift of the cordillera and the progressive closure of the connections between the Atlantic Ocean and the Mediterranean Sea through the present-day Iberian Peninsula. As a consequence, the sedimentary record in many of the Betic Neogene-Quaternary basins shares common depositional traits at coeval intervals (Galindo-Zaldivar et al., 2019). In the specific case of the inner Granada and Guadix basins (Fig.9A), the stratigraphic successions record a comparable sequence of events leading to the continentalization of the basins, although their records correspond to different sedimentary environments.

#### Granada Basin

The Granada Basin is a relatively (~60 x 50 km) intermontane basin located in the central Betic Cordillera at the contact between the Internal and External zones of the cordillera (Fig.9). Its Neogene-Quaternary sedimentary infilling unconformably overlies an irregular, fault-controlled (E-W and NW-SE oriented systems) basement palaeorelief with the main depocentres in the central and eastern part of the basin (Braga et al., 1990; Morales et al., 1990, Rodríguez-Fernández and Sanz de Galdeano, 2006; Sanz de Galdeano, 2008). The sedimentary infill comprises several units separated by unconformities (Braga et al., 1990; Galindo-Zaldivar et al., 2019) (Fig.10A). The oldest units are previous to the individualization of the basin as such, which took place in the late Tortonian around 8.3 Ma (Braga et al., 2003; Rodríguez-Fernández and Sanz de Galdeano, 2006). Lower Miocene units overlie the Alpujarride basement at the eastern and southern margins of the basin and both are unconformably overlain by a Serravallian fluvatile (red conglomerates, silts and clays) continental unit (Braga et al., 1996; Martín-Suárez et al., 1993), which in turn is covered by a shallow-marine reefal unit (Rivas et al., 1999) (Fig.10A).

After the configuration of the Granada Basin and major basin reflooding, temperate-water bioclastic marine deposition took place on narrow carbonate platforms surrounding the emergent Betic highs and punctuated by terrigenous sediments accumulated in deltaic systems (Braga et al., 1990; Puga-Bernabéu et al., 2008) (Fig.10A). During the late Tortonian, tectonic uplift along the eastern and north-eastern margins promoted the accumulation at the base of the uplifted areas of thick successions of coarse-grained sedimentary bodies formed in deltas and fan deltas at the mouth of rivers draining the emergent reliefs of Sierra Nevada and Sierra Arana (Braga et al., 1990). Patch reefs grew on top of the deltaic deposits in periods and areas of reduced terrigenous supply (Braga et al., 1990). Continued uplift of southern and western margins led to the progressive isolation of the basin, with stromatolites developing (now replaced by celestine) at the margins and progressive evaporite deposition (selenite gypsum and halite) towards the basin centre (Martín et al., 1984; García-Veigas et al., 2015), and its final desiccation in the latest Tortonian (7.3-7.2 Ma) (Corbí et al., 2012).

Continental deposition continued in the basin during the earliest Messinian (middle-late Turolian) (Fig. 9a) (García-Alix et al., 2008). Terrigenous sediments (mainly sands and lutites) and reworked gypsum accumulated in a lacustrine basin. Delta deposition, including local lignite formation, took place at the northeastern and southwestern margins of the basin (Fig.10). The clayey materials from Jun and Víznar (Fig.10) were mainly composed of fine-grained sediments, silts and clays that had accumulated in these environments. Lacustrine limestones accumulated in the latest Messinian (latest Turolian). Pliocene (Ruscianian) sedimentation includes detrital materials accumulated in two main depocentres at the eastern and western edges (Fig.10A). In the eastern part, alluvial fans formed at the foot of Sierra Nevada and Sierra Arana, converting further north into a fluvial system that ends in a lake (Fernández and Soria, 1986-87). A similar depositional setting developed in the western part of the basin, with alluvial fans at the foot of Sierra Tejada moving to a fluvial system that flowed out of the basin towards the northwest (Dabrio and Fernández, 1986). Fluvial sedimentation related to the palaeo-Cacín and palaeo-Genil rivers continued during the Pleistocene (Fernández and Soria, 1986-87).



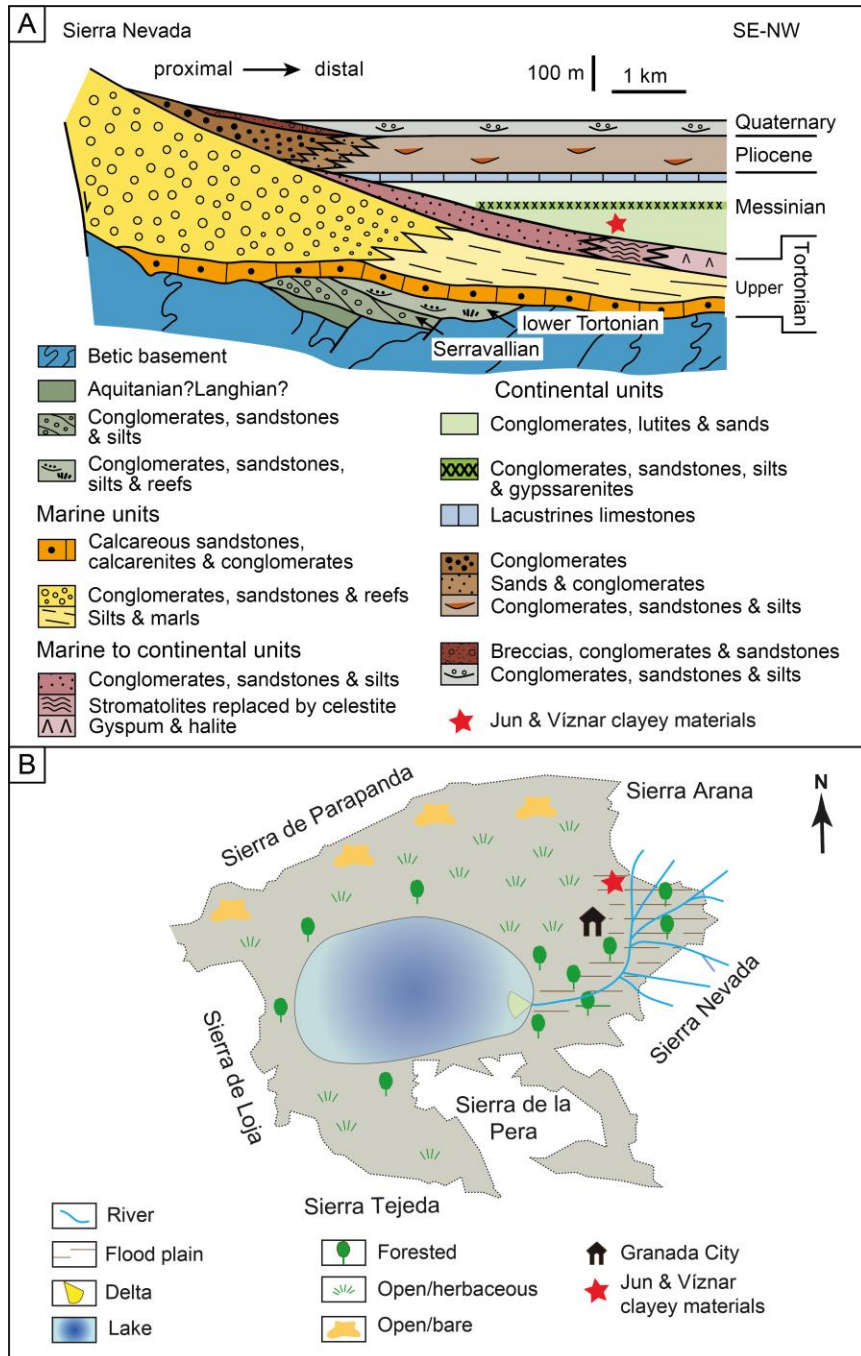


**Figure 10.** A) Neogene to Quaternary stratigraphy of the Granada Basin (adapted from Braga et al., 1990). The clay samples from Jun and Viznar come from late Messinian (Turolian) continental sediments; B) palaeoenvironmental reconstruction of the Granada Basin during the Messinian (middle-late Turolian) (from García-Alix, 2008) (see basin boundary in Fig. 10B). The approximate location of the Jun and Viznar sampling sites is indicated.



## Guadix Basin

The Guadix Basin is a small NW-SE elongated (~ 55 x 25 km) intermontane basin located in the central sector of the Betic Cordillera at the contact between the Internal and External zones (Fig.9A and C). Its Neogene-Quaternary sedimentary infill comprises several units, ranging from the Lower Miocene to the Pleistocene (Fig.11A). The oldest unit only outcrops at the southern margin of the basin and corresponds to marine conglomerates and sands in the lower part and marls with olistoliths from the External Zones embedded in clays at the top (Rodríguez-Fernández, 1982). This basal unit is unconformably overlain by Serravallian to lower Tortonian continental deposits (conglomerates, sands, lacustrine limestones, travertine limestones and nodular gypsum) at the southern margin and shallow- to deep-marine deposits (bioclastic limestones, conglomerates, sands and marls) at the northern margin (Rodríguez-Fernández, 1982; Betzler et al., 2006). The configuration of the basin took place during major tectonic activity at the southwestern and northeastern margins at the beginning of the Late Miocene (Braga et al., 2003). The lowest deposits recording the individualization of the Guadix Basin comprise upper Tortonian shallow-water temperate-water carbonates and deep-water marls, locally punctuated by deltaic terrigenous inputs (Soria et al., 2003; Betzler et al., 2006; Puga-Bernabéu et al., 2010) (Fig.11A). The disconnection of the basin with the Atlantic Ocean is recorded by the change in the late Tortonian (~7.4 Ma) of a mixed carbonate-siliciclastic unit exhibiting large-scale cross-bedding accumulated in the Dehesas de Guadix Strait to a tropical coral-reef unit and fan delta and delta sediments (Braga and Martín, 1988; Betzler et al., 2006) (Fig.11A).

Continued regional uplift led to basin isolation and continental deposition began in an endorheic basin in the latest Messinian (late Turolian) (~ 6.25 Ma) (Minwer-Barakat et al., 2012). The first continental record corresponds to alluvial fan and fan delta conglomerates and sands from the External Zones interfingering with lacustrine lutites (Fernández et al., 1993, García-Aguilar and Martín, 2000) (Fig.11A). In the Early Pliocene (Alfambrian), alluvial sedimentation continued and widespread lacustrine sedimentation took place, especially towards the adjacent Baza Basin in the northeast (Fig.11A). The Late Pliocene (Villanian) to Pleistocene record comprises detrital alluvial and fluvial sediments sourced from the Internal Zones and associated carbonate lacustrine-palustrine deposits (Viseras, 1991, Viseras and Fernández, 1995; García-Aguilar and Martín, 2000, Pla-Pueyo, 2009) (Fig.11A). Lutites that accumulated in small lakes and

swamps of the river systems are the source of the clayey material used to make the Guadix bricks (Fig.11B). Finally, the Guadix Basin changed from an endorheic to an exorheic watershed in the Late Pleistocene after the capture of the Guadix drainage by headward erosion of a tributary of the River Guadalquivir (Calvache and Viseras, 1997).

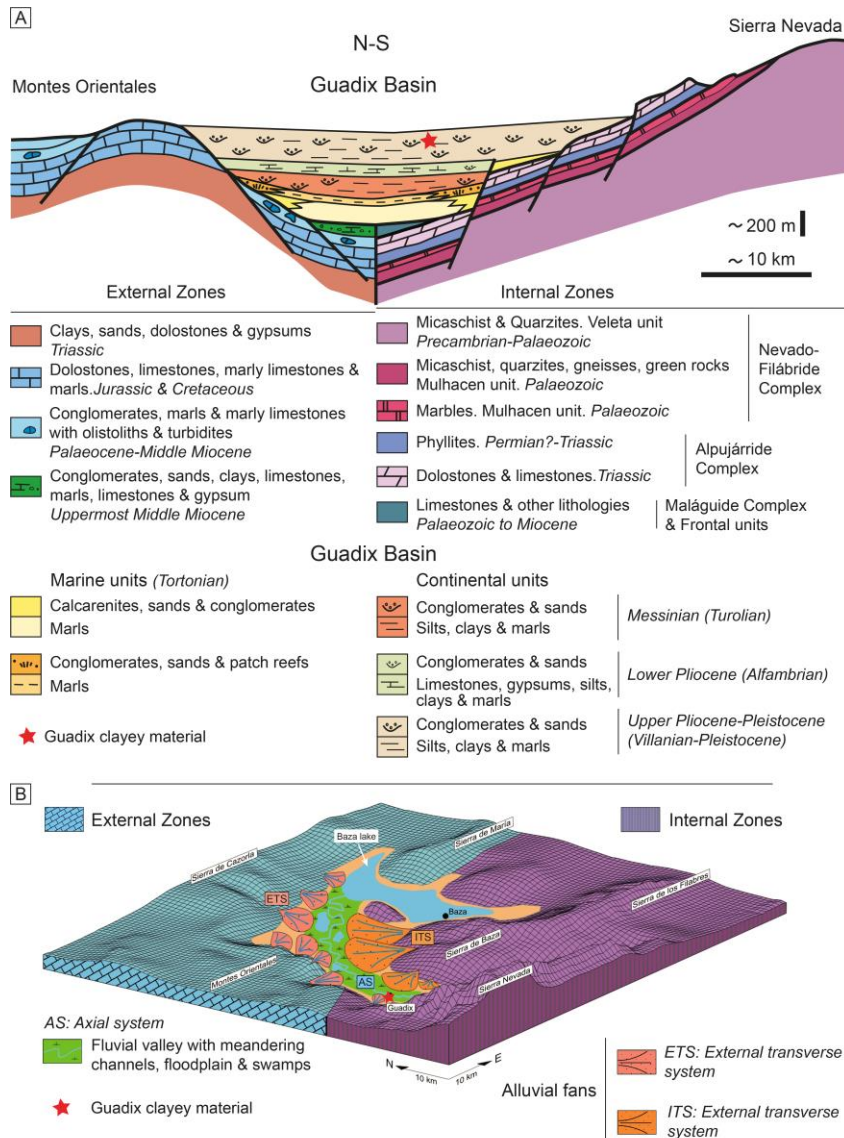


**Figure 11.** A) Neogene to Quaternary stratigraphy of the Guadix Basin (based on data from Rodríguez-Fernández, 1982; García-Aguilar and Martín, 2000; Betzler et al., 2006). Guadix clayey materials (red star) were collected from the most recent unit; B) palaeoenvironmental reconstruction of the Guadix Basin during the Plio-Pleistocene (Villanian- Pleistocene Turolian) (from Pla-Pueyo, 2009). The site from which the Guadix clay was obtained is indicated with a red star.

### 3.1.1.1.2. The Iberian Chain

The Iberian Chain is an NW-SE elongated (~400 x 100 km) intraplate mountain range extending from the Duero Basin to the Mediterranean coast of Valencia (Fig.12A). It developed between the Pyrenean (north) and Betic (south) cordilleras by positive inversion of the intracratonic Iberian Basin and pre-Mesozoic successions (De Vicente et al., 2009). The Iberian Basin experienced two major rifting cycles, the first during the Permian and Triassic and the second from Late Jurassic to Early Cretaceous, which was coeval with the rifting tectonics in the western Tethys and Atlantic (Rosembaum et al., 2002; Liesa et al., 2019). Between the two rifting phases, the basin was dominated by shallow-water carbonate sedimentation. The extensional structures that developed during the Palaeozoic and Mesozoic strongly controlled the present-day geometry of the Iberian Chain.

The onset of the basin inversion and the formation of the fold-and-thrust belt started in the late Eocene due to the convergence between the Eurasian, Iberian and African plates (Guimera, 2018). Uplifted reliefs were partially eroded and derived detrital sediments accumulated in the adjacent basins in alluvial fans at the margins, which towards the centre of the basin became carbonate and evaporite lakes (González et al., 1984; Ortí et al., 2003). Extensional tectonics resumed progressively during the Early Miocene and extended until the Pleistocene in the central and eastern part of the Iberian Chain (Capote et al., 2002), although depositional environments did not change substantially. In the Plio-Quaternary, the extensional tectonics generated the Gallocanta, Munabrega, and Jiloca basins (Gutiérrez et al., 2008), while others, such as the Teruel Basin, were reactivated.

#### The Teruel Basin

The Teruel Basin (also known as Teruel Graben) is a NNE-SSW elongated (~100 x 15 km) half-graben basin located in the central Iberian Chain (Fig.12B and C). The basin is bounded by echelon NNE-SSW normal faults formed in an extensional regime during the Miocene (Anadón and Moissenet, 1996). The ~500 m sedimentary infill comprises Lower Miocene to Pliocene coarse-grained detrital sediments deposited in alluvial fans in the proximal areas that change laterally to carbonates and gypsum associated with lacustrine sedimentation in the central part of the basin (Moissenet, 1983; Ezquerro, 2017).

The Teruel Basin can be divided into three sectors: the northern sector (Alfambra-Tortajada-Teruel), the central sector (Castralvo-Libros) and the southern sector (Ademuz). In the northern sector, where the raw material for the Teruel bricks was obtained, the Neogene succession comprises five units from Tortonian (Vallesian) (units 1-3) to Pliocene in age (units 4-5) unconformably overlying the Mesozoic and Palaeogene substrate (Fig.12D) (Alonso-Zarza and Calvo, 2000; Alonso-Zarza et al., 2012). Unit 1 (lower Tortonian; Vallesian) comprises red conglomerates at the eastern and western basin margins, which change at the base to finer-grained sediments with palaeosoils and lacustrine limestones at the top. Teruel raw materials were collected from red silts and clays at the base of this unit (Fig.12D). Unit 2 (upper Tortonian-lowermost Messinian; Vallesian to middle Turolian) unconformably overlies unit 1 and includes similar deposits, although coarse-grained sediments are much restricted to the proximal areas. Unit 3 (Messinian-Lower Pliocene; lower Turolian-Ruscinian) is mainly composed of a thick evaporite succession (up to 140 m thick) of gypsum bed with terrigenous sedimentation in more proximal locations than in unit 2. Unit 4 (Lower Pliocene; Ruscinian) comprises red conglomerates and sands, lacustrine limestones and local gypsum. Finally, unit 5 (Upper Pliocene; Villanian) has a fluvial character and includes gravels, red lutites, calcretes and local limestones.

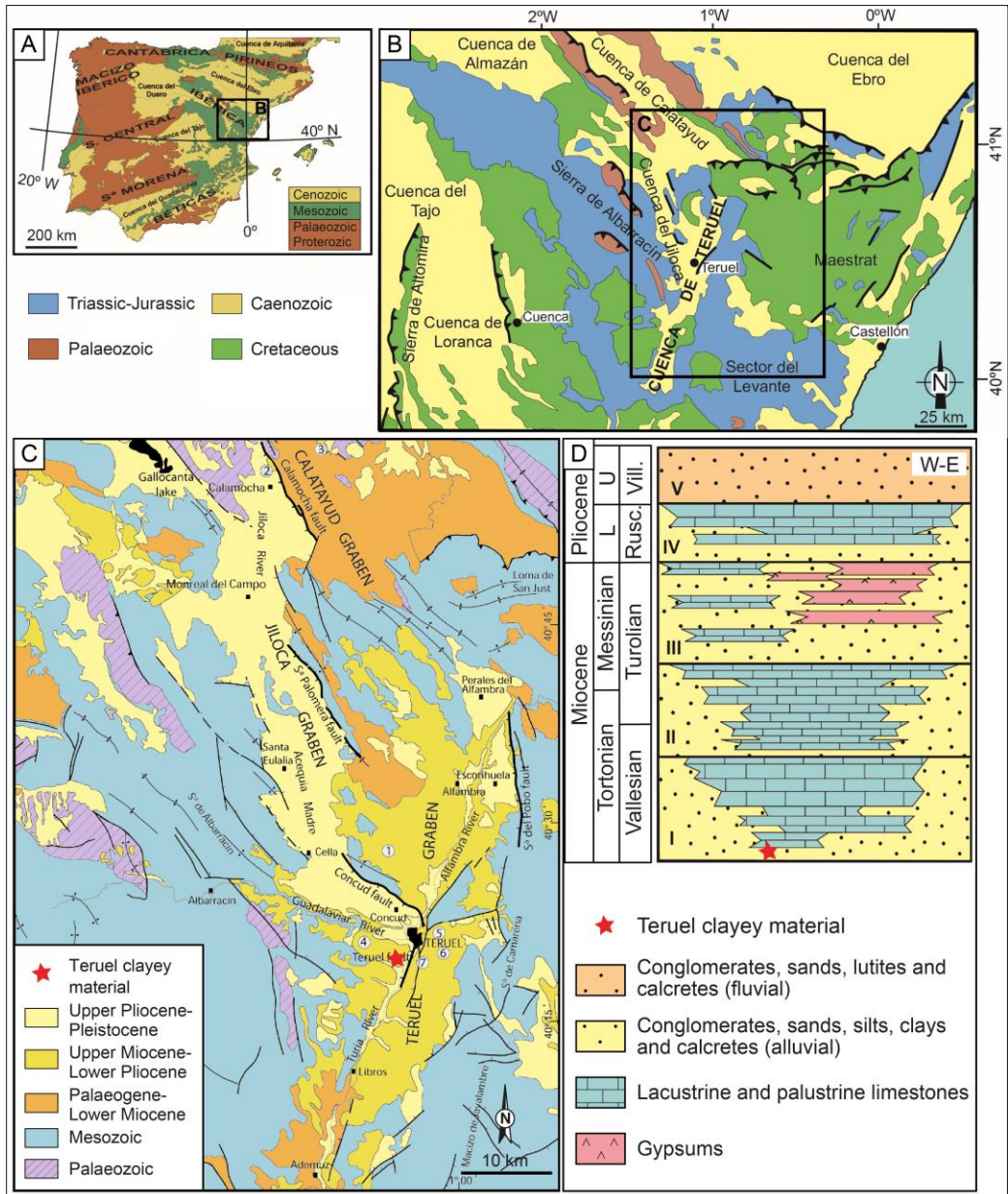


**Figure 12.** A) Main mountain ranges (made up of Palaeozoic and Mesozoic rocks) and sedimentary basins in the Iberian Peninsula; B) simplified geological map of the central and southeastern sector of the Iberian Chain ('Cordillera Ibérica'). Inset shows the location of the Teruel Basin ('Cuenca de Teruel'), also known as Teruel Graben; C) simplified geological map of the Teruel Basin/Graben (northern sector) and adjacent Jiloca Graben (adapted from Simón et al., 2012). The red star marks the site where the Teruel clay was sampled; D) Miocene to Pliocene stratigraphy of the Teruel Basin (units in Roman numerals) (from Ezquerro, 2017, based on Alonso-Zarza et al., 2012). The Teruel clay was collected from distal alluvial lutites of Unit 1.

### 3.1.2. Wastes

Care should be taken not to damage the environment when quarrying clayey material, as governments want to reduce the number of large-scale quarries and are concerned about protecting the environment. In this regard, China, among other countries, has restricted the use of clay by brick manufacturers (Yang et al., 2014). These restrictions are pushing manufacturers to find a solution. The amount of solid waste generated per capita is increasing every day as a result of changing consumption habits. Within the context of global sustainable development, a new waste management strategy is being adopted in which waste becomes an input for the economy. The use of wastes in the manufacture of bricks is increasingly widespread and depends on the particular characteristics required (Cultrone et al., 2005). The main factors in brick production are the type of raw material used and the firing temperature, both of which affect the quality of the final product (Saenz et al., 2019; Crespo-López et al., 2022; Crespo-López et al., 2023a). The addition of wastes will alter certain physical parameters of the bricks.

#### 3.1.2.1. Household glass (Chapter I)

Glass is an amorphous material, usually transparent or translucent, which is formed by melting and then cooling silica sand (silicon dioxide, about 70-75%), sodium oxide ( $\text{Na}_2\text{O}$ , about 12-15%) and calcium oxide ( $\text{CaO}$ , about 10-15%). Other compounds, such as aluminium or magnesium oxides, may also be present in small amounts, to bestow specific properties on the glass. Glass is durable, corrosion resistant, non-porous, electrically and thermally insulating (for the most part), and can be moulded into various shapes and sizes. However, it is fragile and can break easily depending on its composition and processing. The glass manufacturing process involves melting the ingredients at high temperatures (around 1700-2000 °C) in an oven, followed by controlled cooling (Willhauk and Harikantha, 2005; Mandal and Sen, 2017). This process produces a glassy material that hardens without crystallising.

In this chapter, the use of crushed household glass as an additive in brick production was analysed, focusing particularly on any changes it may have caused in the petrophysical properties of the fired bricks, as compared to other bricks made solely with clay. The glass was collected from household containers and bottles over a period of time. As regards the decision as to how much waste should be added to the bricks, Dondi et al. (2009) demonstrated that the addition of up to 2 wt.% glass did not produce any

significant changes in the fired bricks, but when 5 wt.% glass was added, an improvement in mechanical properties was observed. Phonphuak et al. (2016) found that the addition of up to 10 wt.% glass enhanced the physical properties of the bricks. Our decision to add a larger quantity of waste, i.e. 20 wt.%, was based on recent investigations which seemed to show that these bricks performed better (Tyrrell and Goode, 1972; Tyrrell et al., 1972; Leshina et al., 2002; Loryuenyong et al., 2009; Lin et al., 2013; Kazmi et al., 2017).

### 3.1.2.2. Carbon fibre from the wind-power industry (Chapter II)

Due to the increasing installation of wind farms worldwide and the replacement of outdated turbines with more modern systems, the wind-power industry is investing in research and development to find more sustainable and efficient solutions for recycling turbine blades. These blades are generally made of composite materials, such as carbon fibre (CF), which has exceptional properties that make the blades lighter, stronger and more durable (Brøndstedet al., 2005; Hayman et al., 2008). At the end of their useful lives, these blades must be removed and properly managed so as to avoid negative environmental impacts (Saidur et al., 2011).

Despite its low weight, carbon fibre is exceptionally strong and rigid. This means that the blades can withstand significant aerodynamic and mechanical forces, which is crucial for their safe and reliable operation in variable wind conditions. Some companies are developing mechanical recycling methods that break down the blades into their basic components for later reuse (Jensen and Skelton, 2018; Joustra et al., 2021). This process may include shredding the blades into small particles. Another option is chemical recycling, in which chemicals are used to break down composite materials into their original components, which can then be reused in other products (Chen et al., 2019; Mattsson et al., 2020). In some cases, used blades can be reused in construction projects, for example as a filler in infrastructure development, or as an input in the manufacture of products of different kinds (Jensen and Skelton, 2018). Several countries and regions are implementing regulations and specific legislation to address the recycling and management of wind turbine blades at the end of their useful lives instead of disposing of them in landfills.

This chapter investigates the effects on fired bricks when carbon fibre is used as an additive. A maximum of 10 wt.% of CF was added. Given that CF is a very lightweight

material in relation to its volume, the addition of over 10 wt.% could have prevented the residue from mixing properly with the clayey materials.

#### 3.1.2.3. Waste pomace (Chapter III)

Using pomace as an additive in brick production could reduce the accumulation of waste and improve some of the properties of the fired bricks such as, for example, increased porosity and thermal insulation. It could also reduce the density of the bricks, making them lighter and potentially easier to handle during construction (Coletti et al., 2023). Pomace is normally the by-product left over after processing fruits, such as the grapes used in winemaking. It usually consists of skins, seeds and other organic materials. The use of waste pomace in brick production can reduce environmental impacts by reusing organic waste that would otherwise end up in landfill or incineration. However, achieving consistent brick properties can be a challenge when using this waste material, as the composition of the pomace can also vary. Another problem is that organic materials tend to absorb more moisture, which could affect the durability of the bricks, especially in humid environments.

In this chapter, in a bid to reduce clay consumption and recycle a waste product, wine pomace (grape skins, seeds, stems and wine lees) in three different concentrations (2.5, 5 and 10 wt.%) was added to two clayey soils from Granada (Guadix and Víznar, Spain) to manufacture and investigate handmade bricks.

#### 3.1.2.4. Tea residue (Chapter IV)

Tea is the second most consumed non-alcoholic beverage in the world after coffee, with an average of 85 litres per person per year (<https://es.statista.com/>). Originating in China around 1500 BC, it first became popular in the West in the 16<sup>th</sup> century and its use skyrocketed in the 20<sup>th</sup> century with the introduction of tea bags (Macfarlane and Macfarlane, 2009). In 2020, global tea production was over seven million tonnes, with Asia contributing 83% (<https://www.fao.org>). According to Tea Statistics, the global Tea Market is expected to grow at a Compound Annual Growth Rate (CAGR) of 42% per year from 2023 to 2025. This surge in tea consumption is creating a significant environmental challenge in the form of an escalating volume of tea waste. Known to be rich in organic compounds such as lignin and holocellulose, tea waste could potentially be used to produce biochar or biofuel (Hussain et al., 2018a; Basumatary et al., 2018) as a pollutant



adsorbent (Hussain et al., 2018b; Nigam et al., 2019; Debnath et al., 2021), although more research is required in this field and other alternatives must be proposed. A brief review of previous research on the use of tea residues as an additive in brick manufacturing reveals an evolving field, in which important knowledge gaps persist. This innovative approach focuses on crucial aspects for assessing the technical quality of bricks, such as the impact of additives on colour, compactness and porous structure. Through comparisons with previous studies (Saman, 2017; Ozturk et al., 2019, Anjum et al., 2021), a number of differences were identified in the methodology and results, so highlighting the need for a more complete understanding of the effects of tea residue on physical and mechanical properties of bricks.

In this chapter the use of tea waste as an additive in brick production was investigated. This could potentially provide various environmental and economic benefits, as well as improving the thermal insulation of the buildings in which these bricks are used. To this end, we produced brick samples with 0, 5 and 10wt.% of tea waste mixed with a clayey material from Teruel (Spain). The tea residue came from the tea bags discarded by local households.

### 3.2. Brick making

The brick-manufacturing process has a considerable environmental impact in that 0.41 kg of carbon dioxide is generated for each brick produced (Reddy and Jagadish 2003). In this PhD Thesis, the brick samples we studied were made either by extrusion (chapter I) or by hand (chapters I to IV) (Fig.16). The process used to make them is described below.

#### *3.2.1. Traditional brick-making*

The traditional handmade brickmaking process has been applied for thousands of years on a smaller scale than industrial brick production. The first step in making handmade bricks is to quarry the clayey materials, which are then sieved and large fragments are discarded. These raw materials must be mixed in appropriate proportions to produce a clay paste that is suitable for brickmaking. In the case of the bricks made with added household glass powder (Chapter IA and IB) or tea residue (Chapter IV), only one type of clayey material was used to make the bricks (Guadix in Chapter IA and Jun in IB,

respectively, and Teruel in Chapter IV). However, for the bricks made with added carbon fibre or wine pomace (chapters II and III), two types of clay (Viznar and Guadix) were mixed together in a proportion of 3/5 and 2/5 respectively, according to the mixing procedure used by the brick factory that supplied the clay (Ceramica Castillo Siles).

The clay, with or without added waste, was mixed with water until a uniform consistency was achieved (Fig.13A). The clayey paste was then placed in moistened wooden moulds of 15 × 20 × 4 cm (Fig.13B) and pressed down by hand to remove any excess air and create a solid shape. Once the moulds had been filled, the top surface was smoothed off with a plastic ruler. After one hour, the moulds were removed, forming paste blocks that were cut into 4 cm edge cubes using a stretched cotton thread (Fig.13C). These were left to dry for several days in the open air.

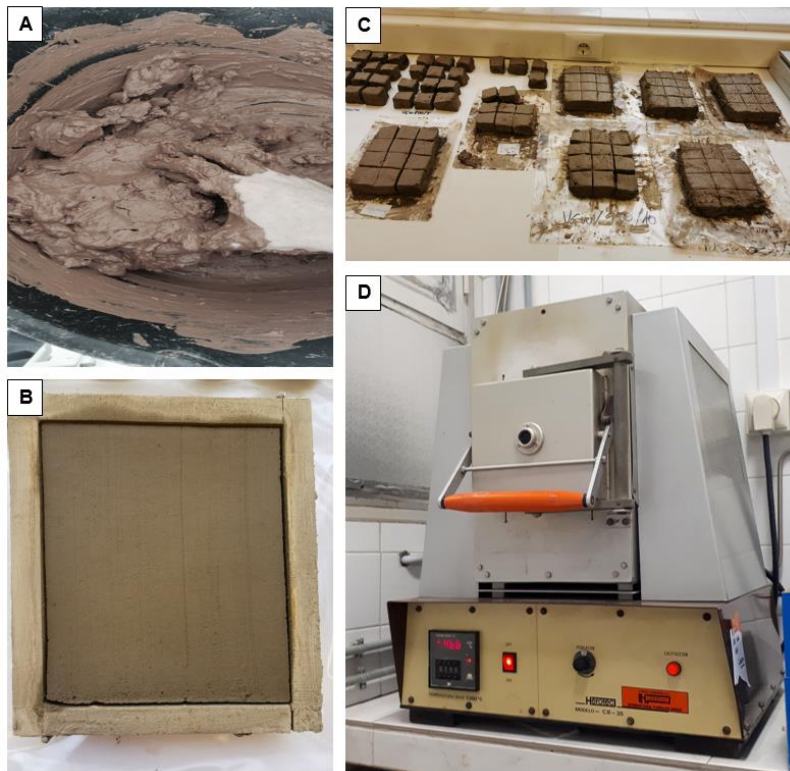


**Figure 13.** Brick production process. A) The clay is mixed with water and waste product (when applicable) until a paste with a uniform consistency suitable for brickmaking is obtained; B) the paste is placed in wooden moulds; C) the bricks are removed from their moulds, cut into cubes and left to dry; D) the bricks were fired in a Herotec CR-35 electric oven in the laboratory of the Department of Mineralogy and Petrology at the University of Granada.

Once they were dry, the bricks were fired in an oxidizing atmosphere in an electric oven Herotec CR-35 at the laboratory of the Department of Mineralogy and Petrology of the University of Granada (UGR) (Fig.13D). The firing temperatures chosen were 800, 950 and 1100 °C, so as to enable us to study the mineralogical and physical changes that occur over a 300 °C range. The temperature inside the oven was initially kept constant for 1 hour at 100 °C so as to eliminate any residual moisture in the samples. It was then increased at a rate of 2 °C/min. Once the desired temperature had been reached, the oven was maintained at a constant temperature for 3 hours. Finally, it was turned off and the samples were left to cool slowly. They were not removed from the oven until the next day. This is because slow cooling prevents the development of fissures due to  $\beta$ -to- $\alpha$  quartz transition. After removal from the oven, the bricks were immersed in water for about 1 hour so as to prevent possible “lime blowing” due to the presence of lime grains (Laird and Worcester, 1956).

### 3.2.2. *Extrusion method*

Extrusion is an industrial brick-manufacturing process in which advanced machinery is used to produce standardized bricks in large quantities. The same raw materials are used as in the production of handmade bricks, i.e. clay, water and (when present) additives. However, in this case, less water is used. The mixture is fed into an extruder machine, which resembles a large worm drive (Fig.14A-C). The machine applies pressure and forces the clay mixture through a nozzle to form the desired brick shape. After extrusion, the bricks are cut into individual units of predetermined lengths using blades or wire strands (Fig.14D). Markings or patterns can also be applied to the surface of the bricks if a specific design is required. Freshly cut bricks are then dried, either in dryers using hot air or in drying tunnels where the humidity and temperature conditions are controlled. The dried bricks are then fired in an oven usually at temperatures of between 920 and 960 °C. The temperature and firing time vary depending on the composition of the raw material and the type of ceramic being produced. After firing, the bricks are left to cool in the oven before being inspected and graded. The bricks are then packed and distributed to construction sites, building material stores etc. Extrusion is a highly efficient process in which large quantities of bricks of consistent shape and size can be produced in a short period of time. This makes it suitable for large building projects. In addition,

characteristics such as the strength, texture and colour of the bricks can be controlled during the manufacturing process to meet customer-specific standards.

The extruded bricks used in this research were made with clay (from Guadix or Jun) plus 20 wt.% household glass powder as an additive. They were then compared with the handmade samples. The extruded bricks were supplied by the brick factory that supplied the clay from Guadix and Jun (Ceramica Castillo de Siles, Víznar, Spain). The extruded bricks measured approximately 1 × 2 × 5 cm (Guadix) and 1 × 4 × 5 cm (Jun) (Fig.15).

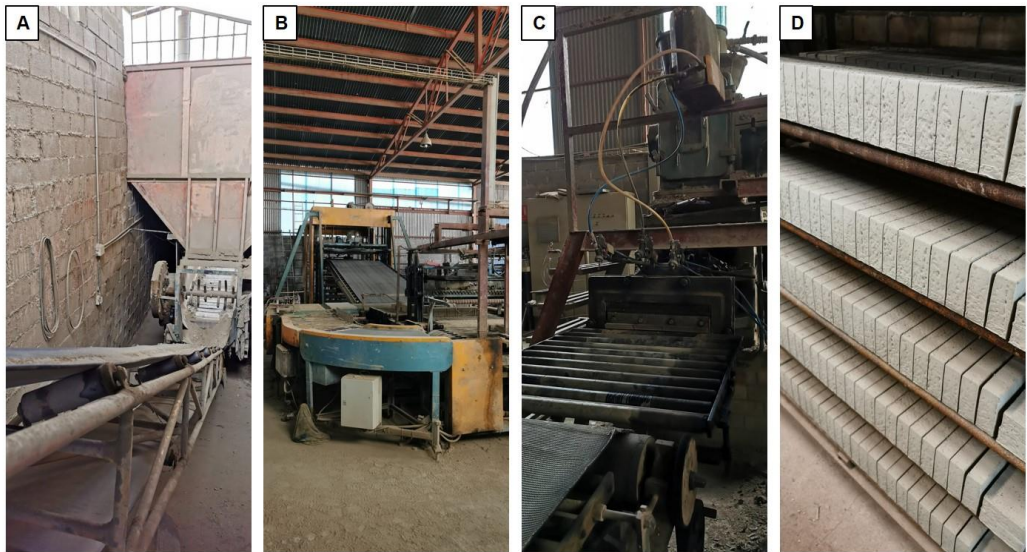


**Figure 14.** A, B and C) Part of the machinery used by the Castillo de Siles brick factory in the production of extruded bricks; D) extruded bricks being dried prior to firing at the factory.



**Figure 15.** Extruded bricks supplied by the Castillo de Siles brick factory. The bricks on the left, with rectangular shapes and brighter colours, were made with clay from Guadix and household glass powder. The bricks on the right, with square shapes and less luminous colours, were made with clay from Jun and household glass powder.

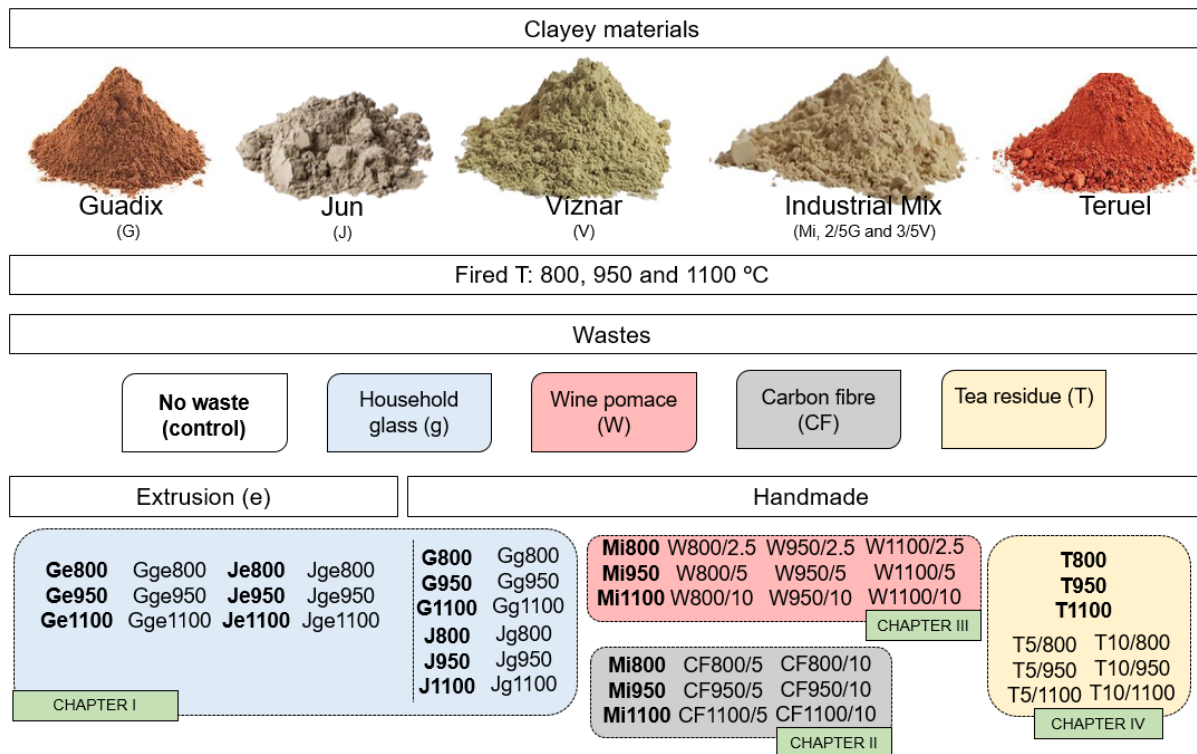


**Figure 16.** Summary table of all the raw materials used (clayey materials and wastes), firing temperatures used and elaboration process (extrusion or by hands) carried out. The nomenclature of the assigned samples and the organization that has been followed in this PhD Thesis by chapters are also described.

# 4. ANALYTICAL TECHNIQUES AND METHODS

The correct characterisation of bricks, both with and without the addition of waste products, is very important because it helps determine whether or not a brick is suitable for use in construction and/or restoration work.

Understanding the characteristics of bricks, including their composition, microstructure, mechanical properties and performance under different conditions, is critical to ensuring the quality, reliability and longevity of the structures built with them. In addition, the incorporation of organic and inorganic residues into the brickmaking process aims to improve specific properties such as strength or thermal insulation.

Accurate characterisation methods are essential for a full assessment of the effects of waste addition on brick properties. The knowledge acquired will enable the development of innovative brick formulations tailored to meet different performance requirements in a variety of research and construction applications.

Proper characterisation of the bricks is also essential to ensure compliance with regulatory standards and promote sustainable building practices. It could also encourage construction companies to work with new materials and technologies. Figure 17 provides a conceptual summary of the analytical techniques and methodologies applied in this Thesis in a bid to characterise the raw materials and bricks as completely and accurately as possible.



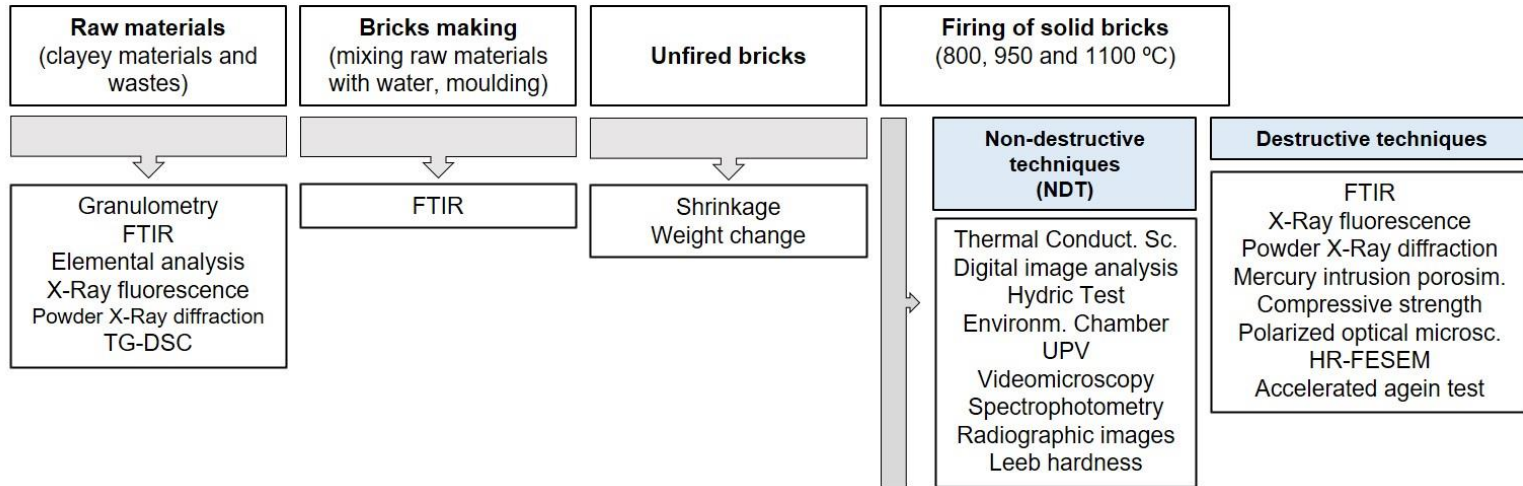


**Figure 17.** Conceptual summary of the techniques and methodologies employed in this Thesis. Acronyms: FTIR: Attenuated Total Reflectance Fourier Transform Infrared Spectroscopy; TG-DSC: Thermal Decomposition and differential scanning calorimetry; HR-FESEM: High-resolution field emission scanning electron microscope; UPV: Ultrasound propagation velocity

#### 4.1. Granulometry

The particle size distribution of the clayey materials and several residues (household glass, carbon fibre and wine pomace) was analysed using a Galai CIS-1 laser gauge that uses laser diffraction to measure the range of the particles after 10 s sonication in water in the range 0.02-1500  $\mu\text{m}$  available at the Centro de Instrumentación Científica (CIC) of the University of Granada (UGR). For fractions above the range of this technique, e.g. tea residues, particle size was determined by sieving, using sieves with diameters ranging from 50  $\mu\text{m}$  to 1 mm mesh. These are available at the Department of Mineralogy and Petrology of the UGR.

#### 4.2. Shrinkage and weight changes

The shrinkage and weight change that occur in bricks as a result of the loss of water during drying and the loss of organic matter in the brick structure due to combustion is a factor to be assessed. The organic matter present in the clay mixture can come from two sources: either because it is naturally present in the raw material or because an organic residue has been added to it. This characterization contributes to the selection of appropriate raw materials and additives, thereby promoting sustainability and efficiency in the construction industries.

#### 4.3. Chemistry, mineralogy and texture

##### *4.3.1. Attenuated Total Reflectance Fourier Transform Infrared Spectroscopy (FTIR)*

Infrared spectroscopy is a technique based on the study of the interaction between matter and infrared radiation. The infrared spectrum is obtained by passing infrared radiation through a sample and determining what fraction of the incident radiation is absorbed at a given energy. The energy at which a peak appears in an absorption spectrum corresponds to the frequency of vibration of part of a sample molecule (Stuart, 2004). Fourier transform infrared spectroscopy improves the quality of the spectra and minimises the time required for data collection. In this PhD Thesis, clayey materials and wastes were measured by reflection (attenuated total reflection mode ATR) with a FTIR spectrometer (Jasco, Model 6600) at the Department of Mineralogy and Petrology of the UGR. This spectrometer is equipped with a diamond crystal ATR accessory (Pro One, Jasco) and works within a frequency range of 4000-400  $\text{cm}^{-1}$  and a step size of 0.50  $\text{cm}^{-1}$ . The spectra obtained were processed with Spectra Maganer 2.0 software.

#### 4.3.2. *Elemental analysis*

Elemental analysis provides the total content of C, H, N and S elements present in a wide range of samples of organic and inorganic nature both solid and liquid. The technique is based on the complete and immediate oxidation of the sample by combustion with pure oxygen at a temperature of approximately 1000 °C. The different combustion products CO<sub>2</sub>, H<sub>2</sub>O and N<sub>2</sub>, are transported by the carrier gas (He) through a reduction tube and then selectively separated to be thermally desorbed. Thermal conductivity detector provides a signal proportional to the concentration of each element. The elemental analysis of the wine pomace was carried out using a CHSN TM FlashSmart (Thermo Scientific) elemental analyser and the calorific value was determined using an IKA Werke model C5003 calorimetric pump, available at the technical research services of the University of Alicante.

#### 4.3.3. *X-ray fluorescence (XRF)*

X-ray fluorescence (XRF) was used to analyse the spectrum of X-rays emitted by the different elements present in the clayey material, the fired bricks and inorganic wastes (household glass and carbon fibre) to quantify their chemical composition, and to determine the major elements (SiO<sub>2</sub>, Al<sub>2</sub>O<sub>3</sub>, Fe<sub>2</sub>O<sub>3</sub>, MnO, MgO, CaO, Na<sub>2</sub>O, K<sub>2</sub>O, TiO<sub>2</sub> and P<sub>2</sub>O<sub>5</sub>, expressed in %) with a PANalytical Zetium spectrometer with a Rh anode and a 4 kV X-ray generator available at the CIC of the UGR. 3 g of each sample were milled to powder in an agate mortar and then analysed. The Loss On Ignition (LOI) was determined by burning the samples at 1000 °C for one hour.

#### 4.3.4. *Powder X-ray diffraction (PXRD)*

The mineralogical composition of the clayey materials and the fired bricks was determined by powder X-ray diffraction (PXRD) using a PANalytical X'Pert PRO diffractometer available at the Department of Mineralogy and Petrology of the UGR. The working conditions were as follows: CuK $\alpha$  radiation ( $\lambda = 1.5405 \text{ \AA}$ ), 45 kV voltage, 40 mA current, 3 to 70° 2 $\theta$  exploration range, and 0.1 2 $\theta \text{ s}^{-1}$  goniometer speed. As regards as the clay fraction of the clayey materials, the following oriented aggregates were prepared according to the recommendations of Moore and Reynolds (1989): air dried (OA), solvated with ethylene glycol (OA+EG), solvated with dimethyl sulfoxide (OA+DMSO) and heated at 550 °C (OA+550).

A qualitative mineral phase identification was performed using the PANalytical X'pert Highscore Plus 3.0 software matching the experimental diffraction peaks with those included in the *Joint Committee for Powder Diffraction Standards* (JCPDS) PDF-2 database. A semi-quantitative phase analysis was carried out by using open-source Profex-BGMN software with dedicated fitting functions (Tsipursky and Drits, 1984; Taut et al., 1998; Ufer et al., 2004; Dobelin and Kleeberg, 2015) and 10 wt.% internal standard  $\alpha$ -Al<sub>2</sub>O<sub>3</sub> was added to the powder samples to comply with the Rietveld refinements (Rietveld, 1969).

#### 4.3.5. *Thermal Decomposition and differential scanning calorimetry (TG-DSC)*

Thermogravimetric analysis measures the change in weight (loss or gain) of a material when heated in a controlled atmosphere. This change is due to the loss of water, combustion of organic matter and decomposition of minerals as well as to the formation of new phases. The resulting graph of weight loss (or gain) versus temperature is known as a thermogram. In it, the ordinate axis represents the change in mass of the material and the abscissa axis reflects the increase in temperature.

The thermal decomposition of the clayey materials was determined using a METTLER-TOLEDO TGA/DSC1 thermogravimetric analyser coupled with differential scanning calorimetry available at the Department of Mineralogy and Petrology of the UGR and at the Centro de Instrumentación Científica (CIC) of the UGR. The samples were deposited on an Al crucibles and analysed in a flowing air atmosphere (50 ml/min) at a heating rate of 20 °C/min up to 950 °C.

#### 4.3.6. *Thermal conductivity Scanner (TCS)*

A Thermal Conductivity Scanner (TCS) was used to assess the thermal behaviour of the bricks with tea residue added. This high precision noncontact method uses an optical scanning technology (OSI) based on scanning a sample surface with a focused, mobile, continuously operated heat source in combination with infrared temperature sensors (Fig.18). The thermal conductivity range varied from 0.2 to 25 W/m·K, with an accuracy of 3%. The standards used for calibration were glass (Standard 1) and fused quartz (Standard 2), in line with the components of the bricks. The bricks were painted with acrylic black paint, with a stripe width of approximately 30 mm for each orthogonal side, so as to ensure proper infrared absorption to heat the sample. The thermal diffusivity ( $\alpha$ ,

mm<sup>2</sup>/s) of the samples was determined indirectly on the basis of the apparent density ( $\rho_a$ ) values measured by hydric test or mercury intrusion porosimetry (MIP) and a mean heat capacity ( $C_p$ ) value of 800 kJ/g·K established in previous research (Bwayo and Obwoya, 2014; Kubiś et al., 2020). This analysis was carried out at the Department of Geosciences of the University of Padua (Italy).



**Figure 18.** Thermal behaviour of the bricks with tea residue added analysed in the Department of Geosciences at the University of Padua.

#### 4.3.7. Polarized optical microscopy (POM)

The petrographic features (mineralogy and texture) of the bricks with and without residues were observed under plane- and cross-polarized light by means of polarized optical microscopy (POM) using two different microscopes: a Carl Zeiss Jenapol-U microscope equipped with a Nikon D7000 digital camera at the Department of Mineralogy and Petrology of the UGR and a Zeiss AXIO Scope A1 microscope equipped with a Canon EOS 550D digital camera at the University of Padua.

#### 4.3.7. High-resolution field emission scanning electron microscope (HR-FESEM)

Detailed observations of the mineralogy and texture of the bricks, pore morphology and the degree of vitrification of the matrix were made using an high-resolution field emission scanning electron microscope (HR-FESEM) Carl Zeiss SMT (AURIGA series) coupled with energy dispersive X-ray spectroscopy (EDS) available at the Centro de Instrumentación Científica of the UGR. Polished thin sections and brick fragments were carbon coated before the observation under the microscope. Another HR-FESEM, a

TESCAN SOLARIS coupled with EDS available at the Department of Geosciences of the University of Padua (Italy) was used to study the bricks with tea waste.

#### 4.3.8. *Digital image analysis (DIA)*

Digital image analysis (DIA) on HR-FESEM images was performed to estimate the percentage of pores of over 4  $\mu\text{m}$  in size in the bricks with and without tea waste fired at 800 and 1100  $^{\circ}\text{C}$ . For each sample, a total of 250 images overlapped by 10% were acquired by the HR-FESEM using the same working conditions mentioned above and then automatically stitched together to cover as much of the thin section as possible, so increasing its representativeness (Coletti et al., 2016; Salvini et al., 2023). ImageJ software was used to calculate the pore ratio by segmenting and binarizing the BSE images and calculating the ratio of the pixels corresponding to pores to the total area of interest (Schneider et al., 2012). The resolution limit was 4  $\mu\text{m}$ , the size of one pixel. This technique was carried out at the Department of Geosciences of the University of Padua (Italy).

#### 4.4. Determination of the pore system

In addition to microscopic observation, the porous system was also studied by liquid or vapour saturation methods. Hydric and porosimetric tests were carried out to shed light on the porous system of the bricks with and without residues.

##### 4.4.1. *Hydric test*

Hydric tests provide information on the movement of fluids through the pore system. This movement of fluids through the samples is of great importance because the alteration processes depend largely on the circulation of fluid in the pores and fissures of the samples, thus assessing their durability. These tests were carried out in accordance with UNE-EN, NORMAL and RILEM standards, mainly using cubic-shaped bricks, but also those extruded supplied by the brick factory. In addition, the temperature and relative humidity of the laboratory where the tests were performed were controlled at all times. The temperature ( $T^{\circ}$ ) was 20  $^{\circ}\text{C}$  and the relative humidity between 30 and 50%. Three samples of each type of brick were used for each test.

- *Free water absorption ( $A_b$ )*: this test determines the amount of water absorbed by a sample per unit of time at atmospheric pressure, in accordance with UNE-

EN-13755 (2008) standard. Prior to the test, the bricks were placed in a ventilated oven at 90 °C for 24 hours to eliminate any internal moisture and weighed ( $M_0$ ). Then, after total immersion in deionised water, the weight of the sample ( $M_t$ ) was determined at fixed time intervals in order to construct the free water absorption curves according to the following formula:

$$Ab = \left( \frac{M_t - M_0}{M_0} \right) \cdot 100$$

The submerged samples were placed on a grid to promote uniform absorption of all surfaces. This test ended once the difference between two consecutive weighing was less than or equal to 0.1 wt.%.

- *Forced water absorption ( $A_f$ ):* after the free water absorption test, the samples were placed in a laboratory glass desiccator filled with deionised water. A vacuum pump was used to create a vacuum for 8 hours. After this period, the samples were weighed (RILEM, 1980).  $A_f$  was calculated using the following formula:

$$A_f = \left( \frac{M_s - M_0}{M_0} \right) \cdot 100$$

where  $M_s$  represents the saturated mass under vacuum (in g).

- *Drying ( $D_i$ ):* during desorption, it was possible to calculate the drying index ( $D_i$ ). This test measures the speed and therefore the ability of each sample to facilitate the escape of fluids from its interior. The samples with high  $D_i$  are those that dry fast. According to NORMAL 29/88 (1988), the samples were placed on a grid to favour homogeneous desorption and measurements were taken at defined time intervals. The drying index ( $D_i$ ) is defined by the following formula:

$$D_i = \frac{\int_{t_0}^{t_f} f(M_t) dt}{M_s \cdot t_f}$$

where  $t_0$  is the initial time (zero);  $t_f$  is the final time of the test (expressed in hours);  $f(M_t)$  is the water content expressed as a percentage of the final dry mass and as a function of time and  $M_s$  is the initial water content (the saturated mass) expressed as a percentage of the final dry mass.

- *Capillarity coefficient (C)*: the rise of water depends on the pore system of the material with which it is in contact. Therefore, the height to which water (with or without soluble salts) could rise is strictly dependent on the porous system of the brick and could cause significant deterioration. In accordance with UNE-EN-1926 (2007) standard, the samples were dried in an oven at 60 °C for 48 hours prior to the test. After measuring their dry weight ( $M_0$ ), they were placed in a container containing a grid, absorbent paper and a sheet of approximately 5 mm of water (Fig.19). The base in contact with the water was the side opposite to that on which the pressure was exerted during brick molding. Capillarity was expressed in  $g/m^2s^{0.5}$  and calculated using the following formula:

$$C = \frac{M_t - M_0}{A \cdot \sqrt{t}}$$

where  $M_t$  is the weight of the samples during the test (in g);  $A$  is the area of the face immersed in water (in  $m^2$ );  $t$  is the time (in s) from the beginning to the end of the test.



**Figure 19.** A) Image of the capillarity test carried out on the handmade bricks of Chapter I (bricks from Jun and Guadix with and without added household glass powder); B) capillarity rise in the handmade bricks made with raw material from Guadix with household glass added.



- *Degree of pore interconnection ( $A_x$ ):* this parameter compares the values of free ( $A_b$ ) and forced ( $A_f$ ) water absorption and indicates the degree of interconnection between the pores as a result of the tortuosity of the pore network (Cultrone et al., 2003). If  $A_x$  values are low, the interconnection between the pores is good and therefore water easy circulate inside the material. This parameter has been calculated using the following formula:

$$A_x = \left( \frac{A_f - A_b}{A_f} \right) \cdot 100$$

- *Saturation coefficient (S):* the saturation coefficient has been calculated to determine the amount of water absorbed after 48 hours of total immersion ( $M_{48}$ ) in relation to the maximum saturation water content (RILEM, 1980). The value obtained corresponds to the maximum water content and would be reached by taking into account the accessibility of all pores, discarding closed pores and those so small that no water penetrates. The higher the S, the higher amount of connected pores are filled by water and more likely it is that the bricks will be altered. This parameter was calculated using the following formula:

$$S = \left( \frac{M_{48} - M_0}{M_S - M_0} \right) \cdot 100$$

- *Apparent ( $\rho_a$ ) and real ( $\rho_r$ ) densities.* Apparent density ( $\rho_a$ ) is defined as the ratio of dry mass to apparent volume and, real density ( $\rho_r$ ) is defined as the ratio of dry mass to impermeable volume (RILEM, 1980). These values are calculated using the following formulae:

$$\rho_a = \left( \frac{M_0}{M_S - M_H} \right) \cdot 100; \rho_r = \left( \frac{M_0}{M_S - M_H} \right) \cdot 100$$

where  $M_H$  is the hydrostatic weight (in g) of the saturated sample.

- *Open porosity* ( $P_o$ ) (UNE-EN 1936, 2007). Open porosity is defined as the ratio of the pore volume accessible to water divided by the apparent volume.  $P_o$  can be calculated from the following formulae:

$$P_o = \left( \frac{M_S - M_0}{M_S - M_H} \right) \cdot 100$$

$P_o$  represents the quotient of the volume of pores accessible to water divided by the apparent volume.

#### 4.4.2. Mercury intrusion porosimetry (MIP)

The physical principle of this technique for measuring the pore size distribution of a solid is based on the fact that Hg is a liquid that does not wet the majority of natural substances because its contact angle overcomes  $90^\circ$ . Therefore, when Hg is in contact with a porous material, it is subjected to a confining pressure that, as it increases, enters through the porous core of the material, so that at higher pressures it penetrates into each pore ever smaller. In this process, the capillary forces between the Hg and the porous solid play an active role.

The samples analysed (with a mass between 0.8-1.2 g) were previously dried at  $60^\circ\text{C}$  for at least 24 hours. They were then analysed using two different porosimeters: a) a Micromeritics Autopore IV 9600 porosimeter able of measuring pores between 0.002 to  $750\ \mu\text{m}$  available in the Department of Mineralogy and Petrology of the UGR. The maximum pressure exerted by this porosimeter is 227.5 MPa, and b) a Micromeritics Autopore IV 9500 porosimeter able of measuring pores between 0.002 to  $200\ \mu\text{m}$  available in the Department of Earth and Environmental Sciences of the University of Alicante. Open porosity ( $P_{oMIP}$ , %), specific surface area (SSA,  $\text{m}^2/\text{g}$ ) and apparent and real densities ( $\rho_{aMIP}$  and  $\rho_{rMIP}$ ,  $\text{g}/\text{cm}^3$ ) were determined.

#### 4.4.3. Environmental chamber

Hygroscopic water adsorption and desorption were measured on three cubic samples according to the EN 12571 (2000) standard. Brick samples were oven-dried and then placed in an environmental chamber, available at the Department of Geosciences of the University of Padova (Italy) at a constant temperature of  $23^\circ\text{C}$  and with relative humidity (RH) increasing according to the following sequence 30-50-70-75-80-85-90-95% and

then decreasing through the same steps in reverse order. The mass of each sample was measured at each step after equilibration at constant RH.

#### 4.5. Compressive strength (Cs)

The compressive strength (Cs) was determined using two different pressing machines: a) a Matest E181 hydraulic press with double frame 25 kN/300 kN according to the UNE-EN1926 (2007) standard, provided by the company Tesela, Materiales, Innovación y Patrimonio S.L. (Spain); and b) a Controls Uniframe T1192 electromechanical universal tester, equipped with 100 kN and 25 kN load cells, available in the rock mechanics laboratory at the Department of Geosciences of the University of Padova (Italy). Three samples of each brick type were analysed to obtain correct standard deviation values. The dimensions of the samples were mostly cubic of 4 cm-edge. However, samples with dimensions of 1.5 x 1.5 x 6 cm<sup>3</sup> were also analysed using a specifically designed device mounted in the press according to the requirements of the UNE-EN 196-1 (2005) standard. Cs was calculated in MPa according to the formula:

$$Cs = \frac{F}{A}$$

where F is the breaking load (in N) and A is the cross-sectional area (in m<sup>2</sup>).

#### 4.6. Non-destructive testing

##### *4.6.1. Ultrasound propagation velocity (UPV)*

Ultrasound gives a measure of the degree of compactness and was used to determine the elastic-dynamic properties of the bricks, properties that affect their mechanical resistance (Gomez-Heras et al., 2020). UPV is increasingly mentioned in the literature, especially in Europe, due to the possibility of establishing a correlation with CS (Mesquita et al., 2018; Rosa et al., 2019).

The wave propagation velocity was measured with three different instruments: a) a Control 58-E4800 ultrasonic pulse velocity tester with transducers of 54 kHz and a circular surface of 27 mm in diameter and available at the Department of Mineralogy and Petrology of the UGR was used to measure the P-wave velocity ( $V_p$ ); b) a Paranetrics

HV Pulser/Receiver 5058PR coupled to a Tektronic TDS 3012b oscilloscope available at the University of Alicante was used to measure the P- and S-waves velocity ( $V_p$  and  $V_s$ ) using transducers of with transducers of 1 or 0.5 MHz depending on the type of waves to be determined; and c) an EPOCH650® Ultrasonic Flaw Detector (Olympus) with transducers of 1 MHz or 0.5 MHz and a circular contact surface of 30 mm in diameter, available at the Department of Geosciences of the University of Padova, was used to measure  $V_p$  and  $V_s$ .

For the three instruments, gels were used to allow a homogeneous contact between the transducers and the brick to determine P and S waves' propagation. The measurements were carried out on three samples per brick type in the three perpendicular directions on cubic samples in m/s according to the ASTM D2845 (2000) standard. Once the ultrasound velocities had been determined, total anisotropy ( $\Delta M$ ), relative anisotropy ( $\Delta m$ ), the Poisson coefficient ( $\nu$ ), and the Young (E), Shear (G) and Bulk (K) moduli were calculated.

$$\Delta M = \left[ 1 - \frac{2V_{\min}}{V_{\max} + V_{\text{mean}}} \right] \cdot 100$$

$$\Delta m = \left[ \frac{2 \cdot (V_{\max} - V_{\text{mean}})}{(V_{\max} + V_{\text{mean}})} \right] \cdot 100$$

where  $V_{\min}$ , is the minimum speed;  $V_{\max}$  is the maximum speed and  $V_{\text{mean}}$  is the average speed. The three values have been measured in the three orthogonal directions.

Poisson coefficient ( $\nu$ ):

$$\nu = \frac{\left(\frac{V_p}{V_s}\right)^2 - 2}{2 \cdot \left[\left(\frac{V_p}{V_s}\right)^2 - 1\right]}$$

Young modulus (E):

$$E = 2\rho V_s^2 (1 + \nu)$$

where  $\rho$  is the apparent density ( $\text{g/cm}^3$ ) of the bricks at each time.

Shear modulus (G):

$$G = \frac{E}{2(1-2\nu)}$$

Bulk modulus (B):

$$K = \frac{E}{3(1-2\nu)}$$

#### 4.6.2. Videomicroscopy

A Leica DVM 2000 digital videomicroscope, using the Leica Application Suite V.3.8.0 for photo acquisition available at the Department of Mineralogy and Petrology of the UGR, was used as a preliminary tool to identify textural differences and relevant features on the surface of the samples with a higher magnification than the naked eye.

#### 4.6.3. Spectrophotometry

Colour measurements were performed to quantify the lightness and chromaticity of the fired bricks with and without residues. A Konica Minolta CM-700d spectrophotometer was used to quantify the colour of the bricks according to the UNE-EN 15886 (2011) standard. Illuminant D65, 10° observer and 8 mm measurement area were used. Nine measurements per sample were performed to determine their lightness ( $L^*$ ) and chromatic values ( $a^*$  and  $b^*$ ). The total colour variation ( $\Delta E$ ) between bricks without and wastes was calculated as follows:

$$\Delta E = \sqrt{(L_1 - L_2)^2 + (a_1 - a_2)^2 + (b_1 - b_2)^2}$$

where  $L_1$ ,  $a_1$  and  $b_1$  are the lightness and chromaticity values for the control bricks made with no added residue and  $L_2$ ,  $a_2$  and  $b_2$  for those made with waste.

#### 4.6.4. Radiographic images

Radiography is a useful NDT for detecting possible non-visible defects in the bricks as its shortwave elementary particles can penetrate the bricks without causing any damage.

In particular, X-rays were used to detect significant differences in the degree of vitrification (i.e., differences in apparent density) of the bricks made with or without glass. X-rays were generated using a TROPHY radiologic VETOX 11ST with 95 kV and 50 mA working conditions. A Micro Computer with METRON-DVM software was used to process the radiographic images.

#### *4.6.5. Leeb hardness microdurometer (LH)*

The LH tester PCE-2500N was used for the non-destructive measurement of the surface hardness of bricks using a rebound hammer. The brick cubes were cut in half and 5-10 linear measurements per brick were made from the left outer edge through the core to the right outer edge. The harder the surface of the material, the higher the rebound speed. This analysis was carried out at the laboratory of the Department of Mineralogy and Petrology (UGR).

#### *4.7. Accelerated ageing test*

The alterability of a construction material refers to its ability to withstand the deterioration once set on a building, especially under certain environmental conditions. This concept is inversely proportional to the durability of the material and is influenced by several factors, including its porous structure. The porosity of the material plays a crucial role in its alterability, as more porous bricks tend to be more susceptible to penetration by external decay agents (Hughes and Bargh, 1982; Manohar et al., 2019).

Understanding how the different types of brick studied in this thesis respond to environmental conditions is crucial to ensuring the longevity and structural integrity of buildings. This can guide the selection of appropriate materials for specific projects and promote more sustainable and resilient building practices in the long term. To this end, thirty freeze-thaw, fifteen salt crystallization and thirty wet-dry cycles were performed to observe a theoretical degradation that could affect the lifetime of the handmade and extruded bricks according to the UNE-EN 12371 (2011), UNE-EN 12370 (2002) and ASTM D 5313, (2004) standards, respectively.

##### *4.7.1. Freeze-thaw test*

The freeze-thaw test assesses the resistance of materials to extreme climatic conditions, particularly in areas where frosts occur. This process mimics the effects of water entering the pores and fissures of the material, freezing and causing internal stresses due to

water-to-ice increase volume that can weaken the structure. When the water thaws, the stresses are released, which can lead to cracking and fragmentation of the material. The freeze-thaw test studies the fatigue caused in pores and fissures by the increase in the volume of water due to freezing at temperatures below 0 °C.

Brick decay during these ageing tests was monitored daily by weighing the bricks (wt.%) and observing possible loss of fragments on their surface during 30 cycles.

#### *4.7.2. Salt crystallization test*

Construction materials can contain soluble salts absorbed from the ground water. Water can be present and migrates both as liquid and vapour moving the soluble salts in pores and fissures. When the water evaporates, the dissolved salts remain behind and crystallise. The cycles of dissolution and reprecipitation of salts cause damage on materials.

Three methods of salt contamination have been identified (Lubelli et al., 2018; Alves et al. 2017; Lubelli et al., 2014) in the available standards and recommendations, i.e. salt spraying (EN 14147 (2004)), partial immersion (RILEM MS-A1, 1998a); (RILEM MS-A2, 1998b), and total immersion (UNE-EN 12370, 2020). Among them, total immersion exposure is the most aggressive and gives results in a relatively shorter duration (Lubelli et al., 2018; Manohar et al., 2019). Sodium sulphate ( $\text{Na}_2\text{SO}_4$ ) is a highly harmful salt due to its nature (Manohar et al., 2019). A sodium sulphate-water system has two stable crystalline phases of the salt (Rodríguez-Navarro et al., 2000; Benavente et al., 2004; Benavente et al., 2015), the anhydrous form, tenardite, and the decahydrate form, mirabilite. At temperatures above 32.4 °C, only tenardite is stable and can precipitate directly in a saturated sodium sulphate solution (Rodríguez-Navarro et al., 2000). Below this temperature, the crystallising phase also depends on the relative humidity (Rodríguez-Navarro et al., 2000).

The durability of the bricks was evaluated with salt crystallization test throughout 15 cycles (UNE-EN 12370, 2020). The salt crystallization test reproduces the decay that the bricks may undergo due to the dissolution and recrystallization of soluble salts within their porous systems. One cycle of salt crystallization test consisted of the immersion of bricks in oversaturated solution (14%) of  $\text{Na}_2\text{SO}_4 \cdot 10\text{H}_2\text{O}$  for two hours and successive drying in an oven at 105 °C for at least 16 hours and cooling at room temperature (25 °C).

#### 4.7.3. *Wet-dry test*

This test is designed to reproduce the cyclical conditions of wet and dry days, mimicking the natural variations in temperature and relative humidity that occur between day and night. By subjecting the bricks to these alternating environmental conditions, the test aims to give an idea of how bricks will behave in real-life situations where they are exposed to different levels of humidity and temperature fluctuations. For this purpose, each 24-hour cycle starts with a 16 hour immersion in water at 20 °C, followed by a forced drying in an oven at 100 °C for the next 6 hours, to end the cycle with a 2 hour cooling at ambient temperature (20 °C). A total of 30 cycles were performed.

#### 4.8. *The analysis of variance technique (ANOVA)*

ANOVA is a statistical test used to compare the means of two or more groups of variables or factors, such as firing temperature (800, 950 and 1100 °C) and the type of clay material used. It can also be used to evaluate how the addition of a certain residue affects the samples. This analysis was carried out in Chapter IB, where the effect of different factors such as the type of clay used (from Jun or Guadix) on the number of variables (firing temperature, colour variations, etc.) and the possible interaction between the variables were analysed. Statistically different groups were identified using the Tukey and Duncan tests ( $P < 5\%$ ). The experiment and procedure were checked for significant errors that could invalidate the study.



## 5. RESULTS AND DISCUSSION

# SUMMARIES

## Chapter IA and IB: Household glass brickmaking

### **A) Improvement in the petrophysical properties of solid bricks by adding household glass waste.**

Laura Crespo-López, Giuseppe Cultrone

Published in *Journal of Building Engineering*

Vol. 59, 105039 (2022)

DOI: 10.1016/j.job.2022.105039

The extensive consumption of clayey soils to manufacture bricks has caused the depletion of these non-renewable natural resources. In this paper, in a bid to reduce clay consumption and recycle waste glass, 20 wt.% crushed household glass was added to clayey soils from Jun and Guadix (Granada, Spain) to manufacture handmade and extruded bricks fired at 800, 950 and 1100 °C. The presence of carbonates in the soil from Jun favored the development of new Ca-(Mg) silicates such as gehlenite, diopside, wollastonite and anorthite, while mullite developed in the bricks made with clay from Guadix. The addition of glass altered the porous system of the bricks, which absorbed less water and dried more quickly than conventional bricks. As regards the manufacturing procedure, extruded bricks turned out to be less porous than handmade ones. The porosity of both handmade and extruded bricks fell as the firing temperature increased. Bricks with added glass were more resistant to compressive strength tests than those made exclusively with clay. These results were confirmed by ultrasound measurements from which we observed that the compactness of bricks increases in line with the increase in the firing temperature and by adding glass. Accelerated ageing tests (freeze-thaw, salt crystallization and wet-dry) revealed that the addition of glass provides the bricks with more compactness, strength and durability than those without glass fired at the same temperature. 20 wt.% proved to be the ideal proportion for waste glass added to the clay used in the production of high-quality compact bricks.

## **B) Non-destructive techniques (NDT) and statistical analysis for the characterization of bricks made with added glass**

L. Crespo-López, D. Benavente, S. Morales-Ruano, M. Vázquez-Vílchez, G. Cultrone

Published in *Construction and Building Materials*

Vol. 408, 133583 (2023)

DOI: 10.1016/j.conbuildmat.2023.133583

The aim of this paper was to assess how adding crushed household glass to the clay mix affects the properties of handmade bricks. To this end, non-destructive techniques (NDT) were used to characterize solid bricks made with two mineralogically different clays with or without the glass additive. One of the clays (Jun) was rich in carbonates, while the other (Guadix) was richer in silicates and had no carbonates. The use of NDT combined with statistical analysis of the initial hypotheses proved to be a very useful method for evaluating whether these handmade bricks are suitable and efficient for use in heritage restoration and the construction industry in general. A second objective was to assess whether the firing temperature influenced the aesthetic (tested using videomicroscopy, colour measurement and radiography) and physical-mechanical (Leeb hardness test, ultrasonic pulse velocity and compressive strength) properties of the bricks. The addition of glass increased the vitrification and compressive strength of the bricks. The colour varied according to the raw materials used and the firing temperature. Radiography proved to be a very useful tool for observing the heterogeneous distribution of the density. In terms of physical-mechanical properties, the bricks from Jun performed better than those from Guadix, as confirmed by ANOVA analysis. However, the more pronounced variation in the colour of the bricks from Jun fired at 1100 °C made with added household glass could make them less suitable for heritage restoration work, where matching colours are a crucial factor.

**Use of recycled carbon fibre as an additive in the manufacture of porous bricks more durable against salt crystallization**

Laura Crespo-López, Chiara Coletti, Salvador Morales-Ruano, Giuseppe Cultrone

Published in *Ceramics International*

Vol. 50, 9681-9696 (2024)

DOI: 10.1016/j.ceramint.2023.12.287

Within the framework of the Sustainable Development Goals of the Agenda 2030, the circular economy is being promoted as a means of ensuring a sustainable use of resources and a reduction in the amount of waste produced. The aim is to reduce the demand for often scarce raw materials through the continuous reuse, recycling and regeneration of materials and products. This paper explores the use of carbon fibre from wind turbine blades as an additive in the production of new efficient bricks. Clay mixes with 0, 5 and 10 wt.% additive were fired at three temperatures (800, 950 and 1100 °C) and the fired bricks were analysed from mineralogical and physical points of view to determine their suitability for use in the construction industry. The results show that carbon fibre improves the durability of the bricks, which became 16% more porous as the firing temperature increased. However, the compressive strength of the bricks with 10 wt.% carbon fibre was about 50 % lower than that of the control bricks made without additive. It is interesting to note that the distribution of the carbon fibres within the brick varies considerably and that they are shorter and wider in the core of the samples. These results could offer an alternative line for new product development in the brick industry. The bricks tested here are an example of a circular economy in which waste from one industrial process (wind turbine blades) is reused as an input in another (brick manufacture). The environmental benefits achieved are twofold: reduced demand for clay and recycling of decommissioned turbine blades, which are currently amassed in wind turbine graveyards.

**Pomace from the wine industry as an additive in the production of traditional sustainable lightweight eco-bricks**

Laura Crespo-López, Alberto Martínez-Ramírez, Eduardo Sebastián, Giuseppe Cultrone

Published in *Applied Clay Science*

Vol. 243, 107084 (2023)

DOI: 10.1016/j.clay.2023.107084

This research examines fired clay bricks made with waste pomace from the wine industry as an additive in brick production. To this end, we analyse and discuss the chemical, mineralogical, textural and physical-mechanical behaviour of fired bricks made with three concentrations of wine pomace (2.5, 5 and 10 wt.%) and at three different firing temperatures (800, 950 and 1100 °C) and evaluate their durability to salt crystallization. Variations in colour were also examined. The firing process resulted in the decomposition of phyllosilicates and carbonates, the crystallization of Fe oxides and the appearance of high-temperature Ca- (and Mg-) silicates phases such as gehlenite, wollastonite, anorthite and diopside. The bricks made with added wine pomace had very similar mineralogy to the control samples made without it. The bricks made with added wine pomace were lighter than the control samples and underwent less linear shrinkage during the drying process. Particles in the wine pomace were consumed during firing, leading to the appearance of voids. The bricks made with this additive had higher levels of water absorption and poorer mechanical strength. The greatest colour differences were detected after increasing the amount of waste, which generally resulted in yellower bricks. The increase in firing temperature resulted in an improvement in mechanical resistance regardless of the composition of the bricks. However, bricks fired at 1100 °C made without additive are more resistant to damage caused by salts than those made with wine pomace.

**Effects of using tea waste as an additive in the production of solid bricks in terms of their porosity, thermal conductivity, strength and durability**

Laura Crespo-López, Chiara Coletti, Anna Arizzi, Giuseppe Cultrone

Published in *Sustainable Materials and Technology*

Vol. 39, e00859 (2024)

DOI: 10.1016/j.susmat.2024.e00859

In this paper, we investigated the use of tea waste as an additive in the production of traditional bricks. This could provide several environmental and economic benefits, as well as improving thermal insulation in construction. To this end, we produced brick samples with 0, 5 and 10 wt.% of tea waste mixed with a clayey material from Teruel (Spain) that was rich in quartz and phyllosilicates and had smaller amounts of carbonates. These samples were fired at 800, 950 and 1100 °C in an electric oven. We then analysed and discussed their chemical, mineralogical, textural and physical-mechanical behaviour and evaluated their durability in response to salt crystallization. The pore system of the bricks was examined using a combination of different analytical techniques (hydric tests, mercury intrusion porosimetry and digital image analysis). We also evaluated their thermal conductivity and observed that an increase in the firing temperature and the amount of tea waste altered the texture of the bricks, increasing their porosity. This happened above all at 1100 °C, where it led to the appearance of a new family of pores and increased the porosity to about 39% for bricks made with 10 wt.% added tea waste. The increased porosity made the bricks lighter. The bricks made with tea waste showed higher levels of water absorption and poorer mechanical strength. Our results suggest that the addition of tea residues strongly decreases the thermal conductivity and heat diffusion capacity of the bricks. They could therefore be used as lightweight bricks for the thermal insulation of buildings.

# CHAPTER I

*Bricks with household glass added*

**Laura Crespo-López, Giuseppe Cultrone**

Published in *Journal of Building Engineering*

Vol. 59, 105039 (2022)

DOI: 10.1016/j.job.2022.105039

*Impact Factor: 6.4*

*Position 13/139 (Q1)*

*Category: Engineering, Civil (JCR 2022)*



Journal of Building Engineering




Volume 59, 1 November 2022, 105039




# Improvement in the petrophysical properties of solid bricks by adding household glass waste

[Laura Crespo-López](#)   [Giuseppe Cultrone](#)

Show more 

 Add to Mendeley  Share  Cite

<https://doi.org/10.1016/j.job.2022.105039>

[Get rights and content](#) 

**Keywords:** solid bricks; household glass; mineralogy; petrophysical properties; manufacturing processes; compactness.

## 1. Introduction

Bricks are the most common ceramic products and are widely used in both historic and modern buildings (Drysdale et al., 1994). Together with stone and concrete, they are amongst the most frequently used materials in construction. Unfortunately, in the last 20 years the market for these products within the construction industry has reached saturation point (Bolden et al., 2013; Dachowski and Kostrzewa, 2016; Sudharsan and Sivalingam, 2019; Małek, 2022). This has led the brick industry to diversify towards less standard, more competitive products (Gulghane and Khandve, 2015). In addition, the



extensive consumption of clayey soils to manufacture bricks has caused the depletion of these non-renewable natural resources (Dabaieh et al., 2020). If we could replace at least part of these soils with other (preferably cheap) products, large savings could be made in raw materials, which together with the use of waste products, can generate a direct benefit for the environment. Therefore, the use of waste products as an additional material in brick manufacture could provide a solution to this problem (Trotti et al., 1996; Vu et al., 2012; Monteiro et al., 2014; Dabaieh et al., 2020). It could also help reduce the accumulation of waste in landfills.

The waste products that could potentially be used in this way include household glass, an inert, amorphous, nonporous, fragile material (Chindaprasirt et al., 2021) that has been part of our lives for thousands of years (Palaniyappan et al., 2022). Much of the common bottle glass produced is difficult to recycle due to the colouring additives and lead content and may therefore end up in landfills. As an additive for bricks, the glass acts as a flux due to its  $\text{Na}_2\text{O}$  content and amorphous composition, which reduces the temperature required for brick sintering (Trotti et al., 1996; Leshina and Pivnev, 2002). Although recycling waste glass for the production of new glass products has many advantages in terms of the conservation of raw materials, a considerable amount of this waste cannot be recycled and is dumped into landfills, producing pollution due to lead accumulation (Trevelyan and Haslam, 2001; Whitehouse, 2012; Lin et al., 2013). In this regard, the European Union generates around 0.9 million tons of waste glass each year (<https://ec.europa.eu/eurostat/>) and, according to the Environmental Protection Agency (EPA, <https://www.epa.ie/>), glass represents 5.1% of the total solid waste collected. Therefore, the use of household glass waste as an additive in brick manufacture could provide a way to “store” this waste product, so reducing landfill and the associated environmental burden.

The first research into the possible use of glass in brick manufacture was conducted in the 1970's. In these initial investigations varying amounts of between 5 and 94 wt.% of glass was added (Tyrrell and Goode (1972); Tyrrell et al. (1972); Leshina and Pivnev (2002), and references therein). The conclusion was that the ideal amount of glass to add to the clay mixture was between 15 and 30 wt.%. The effects of using this waste as an additive in brick production were further explored by Loryuenyong et al. 2009, Kazmi et al. 2017, Saenz et al. 2019 and Hasan et al. 2021, who studied the effects of added glass on the physical properties of bricks obtaining promising results, such as a decrease in porosity or an increase in compactness compared to other added wastes. Other

authors added waste glass in brick production in an attempt to immobilize heavy metals (Mao et al., 2019) or to improve the intrinsic material properties and environmental development from the production of bricks with electroplating sludge (Mao et al., 2020). In this study, we investigate a novel aspect of bricks made with added waste glass by comparing handmade and extruded samples from a petrophysical point of view. The most commonly used brick production method today is extrusion, which has advantages in terms of the speed of manufacture and the homogeneity of the final product. Nevertheless, in handmade brick production, it is easier to control the number actually required by the market, so reducing the consumption of raw materials (Dachowski and Kostrzewa, 2016; Sudharsan and Sivalingam, 2019; Dabaieh et al., 2020; Palaniyappan et al., 2022). This is why in this research we considered both manufacturing processes (handmade and extrusion) and analysed samples of both types of brick. To this end, crushed household glass was added to two clayey materials with a different mineralogical composition so as to assess how this waste product affects the petrophysical properties and durability of the bricks. Samples were made at three different firing temperatures in order to find out how the bond between the waste and the clayey matrix is affected by temperature.

## **2. Materials and Methods**

### ***2.1. Preparation of the brick samples***

Solid bricks were made using raw materials quarried in Guadix and Jun (both in Andalusia, Spain). Both raw materials are post-orogenic continental sediments deposited in the intermontane basins of Guadix-Baza and Granada. The raw material from Guadix was deposited in the middle-late Pleistocene during the last stages of the infilling of the basin (Viseras, 1991; García-Aquilar and Martín, 2000), above all in small lakes and swamps that developed temporarily on the banks of braided rivers that drained from the nearby Sierra Nevada mountains (García-Aquilar and Martín, 2000). The raw material from Jun was deposited during the late Turolian in a lacustrine environment with nearby fan deltas that drained carbonate sediments eroded from Sierra Arana (García-Alix et al., 2008).

The extruded and handmade bricks used in this research were made with the raw materials (from Guadix or Jun) plus 20 wt.% household glass waste. These were then

compared with handmade samples made without glass, which served as the control group (Table IA-1). As regards the decision as to how much waste should be added to the bricks, Dondi et al. (2009) demonstrated that the addition of up to 2 wt.% glass did not produce any significant change in the fired ceramics, but with 5 wt.% glass addition, an improvement in mechanical properties was observed. Phonphuak et al., 2016 found that the addition of up to 10 wt.% glass enhanced the physical properties of the bricks. The decision to add a larger quantity of waste, i.e. 20 wt.%, was based on recent investigations which seemed to show that this resulted in better performance (Tyrrell and Goode, 1972; Tyrrell et al., 1972; Leshina and Pivnev, 2002; Loryuenyong et al., 2009 ; Lin et al., 2013; Kazmi et al., 2017). It was also a way of reusing more waste. Household glass was milled into powder before being mixed with the raw materials, so as to increase its specific surface area and improve possible reactivity with the brick matrix. Extruded bricks made with clay from Guadix and Jun were provided by the brick factory that supplied the two raw materials (Cerámica Castillo Siles, S.L., Víznar, Spain). The extruded bricks measured approximately 1 × 2 × 5 cm.

As for the handmade bricks, the raw materials were sieved and fragments of over 1.5 mm in size were discarded. They were then mixed with the glass (when applicable) and with water. 308 ml/kg and 333 ml/kg of kneading water were required to knead the raw materials from Guadix and Jun, respectively. Once enough plasticity had been achieved, the clayey paste was placed in moistened wooden moulds of 15 × 20 × 4 cm. After one hour, the moulds were removed and the clayey pastes were cut into 4 cm edge cubes using a stretched cotton thread and left to dry.

Once the extruded and handmade samples were dry, they were fired in a Herotec CR-35 electric oven at 800 °C, 950 °C and 1100 °C. The temperature inside the oven was initially kept constant for 1 hour at 100 °C so as to eliminate any residual moisture in the samples. Then, the temperature was increased at a rate of 2 °C/min. Once the desired temperature was reached, the oven was kept at a constant temperature for 3 hours. Finally, it was turned off and the samples were left to cool slowly. They were not removed from the oven until the next day. Slow cooling prevents the development of fissures due to  $\beta$ -to- $\alpha$  quartz transition. After removal from the oven, the bricks were immersed in water for about 1 hour so as to prevent possible "lime blowing" due to the presence of lime grains (Laird and Worcester, 1956). Glass bubbles with a diameter of up to 1 mm

developed in the bricks made with the clay from Guadix and fired at 1100 °C (samples Gg1100 and Gge1100, Table IA-1).

**Table IA-1.** Acronyms assigned to the bricks according to the raw material used, the addition of 20 wt.% household glass, the production process and the firing temperature.

Raw material	Production process			Firing temperature (°C)
	Handmade	Handmade + glass	Extrusion + glass	
Jun (J) and Guadix (G)	J800	Jg800	Jge800	800
	G800	Gg800	Gge800	
	J950	Jg950	Jge950	950
	G950	Gg950	Gge950	
	J1100	Jg1100	Jge1100	1100
	G1100	Gg1100	Gge1100	

## 2.2. Analytical techniques

### 2.2.1. Chemistry, mineralogy and texture

The granulometry of the raw materials from Guadix and Jun and that of the household glass was measured using a Galai CIS-1 laser gauge. X-ray fluorescence (XRF) was used to determine the major elements in the two raw materials, the fired bricks and the household glass with a PANalytical Zetium compact spectrometer. 3 g of each sample was ground to powder prior to its analysis. The mineralogical composition of the raw samples, clay fraction and fired bricks was determined by powder X-ray diffraction (PXRD) using a PANalytical X'Pert PRO diffractometer. The working conditions were as follows: CuK $\alpha$  radiation, 45 kV voltage, 40 mA current, 3 to 70° 2 $\theta$  exploration range, 0.1 2 $\theta$  s<sup>-1</sup> goniometer speed. The mineral phases were identified using the PANalytical X'pert Highscore Plus 3.0 software. As regards the clay fraction, the following oriented aggregates were prepared according to the recommendations of Moore and Reynolds (1989): air dried (OA), solvated with ethylene glycol (OA+EG), solvated with dimethyl sulfoxide (OA+DMSO) and heated at 550 °C (OA+550).

The thermal decomposition of the two raw materials up to 950 °C was determined by a thermogravimetric analysis coupled with differential scanning calorimetry (TG/DSC) using a METTLER-TOLEDO TGA/DSC1 apparatus. The petrographic features (mineralogy and texture) of the fired samples were observed by means of polarized

optical microscopy (POM). Observations under plane- and cross-polarized light were carried out on polished thin sections using a Carl Zeiss Jenapol-U microscope equipped with a Nikon D7000 digital camera. Detailed observations of reaction rims among phases and of the development of sintering and vitrification of the matrix were performed on the same thin sections using a high-resolution field emission scanning electron microscope (FESEM) Carl Zeiss SMT (AURIGA series) coupled with energy dispersive X-ray spectroscopy (EDS).

### 2.2.2. Determination of the pore system

Hydric and porosimetric tests were carried out in order to shed light on the pore system of the bricks. Free (Ab, at atmospheric pressure) and forced (Af, under vacuum) water absorption, drying (Di) and capillarity tests (C) were carried out according to UNE-EN 13755 (2008), NORMAL 29/88 (1988) and UNE-EN 1925 (1999) standards, respectively. These tests enabled us to determine the degree of pore interconnectivity ( $A_x$ ) (Cultrone et al., 2003), the saturation coefficient (S), the apparent ( $\rho_a$ ) and real ( $\rho_r$ ) densities and the open porosity ( $P_o$ ) (RILEM, 1980). Hydric tests were performed under controlled thermo-hygrometric conditions (20 °C and 60% relative humidity) using deionized water. Three samples per brick group were analysed.

The pore system of the bricks within a range of 0.002 to 200  $\mu\text{m}$  was analysed by mercury intrusion porosimetry (MIP) using a Micromeritics Autopore IV 9500 porosimeter. Open porosity ( $P_{oMIP}$ , %), specific surface area (SSA,  $\text{m}^2/\text{g}$ ) and apparent and real densities ( $\rho_{aMIP}$  and  $\rho_{rMIP}$ ,  $\text{g}/\text{cm}^3$ ) were calculated.

### 2.2.3. Mechanical behaviour

The compressive strength ( $R_c$ ) was measured using a Matest E181 hydraulic press with double frame 25 kN/300 kN according to the UNE-EN1926 (2007) standard. This analysis was only carried out on the cubic-shaped handmade samples, as the extruded bricks had a different shape and did not fit into the press properly.  $R_c$  was calculated in MPa on three samples of each brick according to the following Eq. 1:

$$R_c = \frac{F}{A} \quad (1)$$

Where F is the breaking load (in N) and A is the cross-sectional area (in  $\text{m}^2$ ).

#### 2.2.4. Non-destructive testing

Ultrasound gives a measure of the degree of compactness and was used to determine the elastic-dynamic properties of the bricks, properties that affect their mechanical resistance. Measurements were performed using a Control 58-E4800 ultrasonic pulse velocity tester with transducers of 54 kHz and a circular surface of 27 mm in diameter. A water-based eco-gel was used to allow a homogeneous contact between the transducers and the brick. The measurements were carried out on three samples per brick type. P-wave propagation was measured in m/s according to the ASTM D2845 (2000) standard. The structural anisotropy ( $\Delta M$ ) was also calculated using the following Eq. 2 (Guyader and Denis, 1986):

$$\Delta M = 1 - \frac{2VP_1}{VP_2 + VP_3} \cdot 100 \quad (2)$$

where  $VP_1$ ,  $VP_2$  and  $VP_3$  are the propagation velocities of the P-waves in the three orthogonal directions.

Colour measurements were performed to quantify the lightness and chromaticity of the fired bricks. A Konica Minolta CM-700d spectrophotometer was used following the UNE-EN 15886 (2011) standard. Illuminant D65, 10° observer angle and 8 mm measurement area were used. Nine measurements per sample were performed. Once the lightness ( $L^*$ ) and chromatic values ( $a^*$  and  $b^*$ ) had been determined, the total colour variation ( $\Delta E$ ) between bricks without additive and with added household glass was calculated as follows (Eq. 3):

$$\Delta E = \sqrt{(L_1 - L_2)^2 + (a_1 - a_2)^2 + (b_1 - b_2)^2} \quad (3)$$

where  $L_1$ ,  $a_1$  and  $b_1$  are the lightness and chromaticity values for the control bricks made with no added household glass and  $L_2$ ,  $a_2$  and  $b_2$  for those made with glass.

#### 2.2.5. Accelerated ageing tests

Thirty freeze-thaw, fifteen salt crystallization and thirty wet-dry cycles were performed to observe a theoretical degradation that could affect the lifetime of the handmade and extruded bricks according to the UNE-EN 12371 (2011), UNE-EN 12370 (2020) and ASTM D 5313 (2004) standards, respectively. The freeze-thaw test studies the fatigue caused in pores and fissures by the increase in the volume of water due to freezing at temperatures below 0 °C. The salt crystallization test reproduces the decay that the bricks

may undergo due to the dissolution and recrystallization of soluble salts within their porous systems. The wet-dry test simulates the disintegrating and dissolving action of water when enhanced by temperature. Brick decay during these ageing tests was monitored daily by weighing the bricks and observing possible loss of fragments on their surface.

### 3. Results and discussion

#### 3.1. Granulometry, chemistry and mineralogy of raw materials and waste

##### 3.1.1. Grain size distribution

The granulometric analysis shows that the raw materials from Jun and Guadix have unimodal particle size distribution although they differ in terms of maximum peak size and curve shape (Fig.IA-1). While the Guadix curve is quite symmetric with a maximum at 25  $\mu\text{m}$ , the Jun curve shows a maximum at 100  $\mu\text{m}$  and has a marked asymmetry at lower granulometric values. The powdered glass shows three maxima at 7  $\mu\text{m}$ , at around 40  $\mu\text{m}$  and at 300  $\mu\text{m}$ .

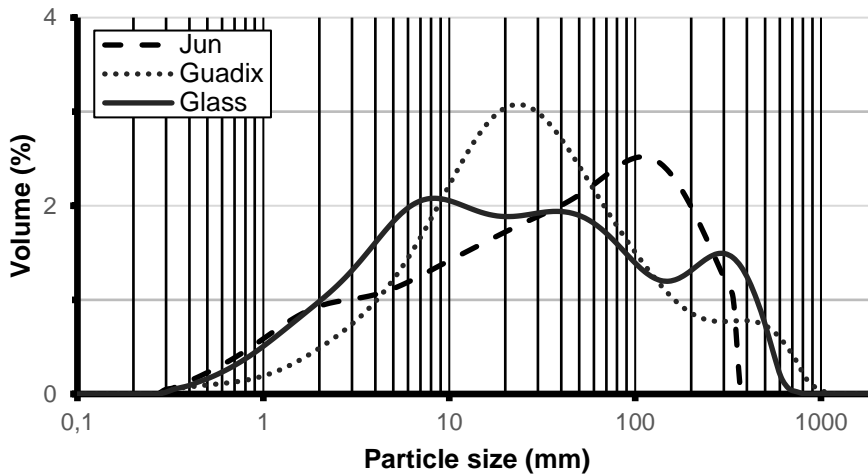


**Figure IA-1.** Grain size distribution of the clayey raw materials from Jun and Guadix and of household glass.

##### 3.1.2. X-ray fluorescence (XRF)

Table I-2 shows the chemistry of the two clayey samples and the household glass. The raw materials from Jun and Guadix have different compositions (Table IA-2). The presence of CaO (11.2%) and MgO (4.1%) in the clay from Jun is a sign of its carbonate content, while the clay from Guadix is carbonate-free (CaO is 0.6 and MgO is 0.9%).

According to Maniatis and Tite, 1981, the raw material from Jun can be classified as calcareous, while the Guadix clay has higher SiO<sub>2</sub>, Al<sub>2</sub>O<sub>3</sub> and Fe<sub>2</sub>O<sub>3</sub> contents.

The household glass is mainly composed of SiO<sub>2</sub> (71.7%), Na<sub>2</sub>O (12.3%) and CaO (12.3%), i.e., the typical compounds of common glass: silica sand, calcium carbonate and sodium carbonate and can be classified as soda-lime glass (Djangang et al., 2014). The considerable amounts of Na<sub>2</sub>O + K<sub>2</sub>O (13.2%) and CaO + MgO (11.7%) in the household glass could act as an energetic fluxing agent in the production of ceramics (Tiffo et al., 2015; Chidiac and Federico, 2007). In addition, the presence of alkali oxides ensures that the glass will have a low softening point during firing. This could help reduce the firing temperature of the bricks (Cultrone, 2001).

**Table IA-2.** XRF (in %) results for the raw materials from Jun and Guadix and the household glass used to manufacture the bricks.

	SiO <sub>2</sub>	Al <sub>2</sub> O <sub>3</sub>	Fe <sub>2</sub> O <sub>3</sub>	MnO	MgO	CaO	Na <sub>2</sub> O	K <sub>2</sub> O	TiO <sub>2</sub>	P <sub>2</sub> O <sub>5</sub>	LOI	Total
Jun	44.63	14.76	5.21	0.06	4.10	11.28	0.84	2.84	0.72	0.12	15.19	99.75
Guadix	63.13	17.79	7.13	0.07	0.96	0.63	0.85	2.67	1.26	0.13	5.34	99.96
Glass	71.71	1.90	0.40	0.01	1.35	10.34	12.33	0.90	0.11	0.03	0.88	99.96

### 3.1.3. Powder X-ray diffraction (PXRD)

PXRD analysis reveals the presence of phyllosilicates (illite, paragonite, chlorite and kaolinite), quartz and k-feldspar (microcline) in the raw materials from Jun and Guadix (Fig.IA-2). Carbonates (calcite and dolomite) and hematite were only detected in the sample from Jun. The presence of chlorite, a mineral that is commonly masked by smectite and kaolinite, is revealed in the clay fraction of both samples by heating the OA at 550 °C (Cultrone, 2001). The raw material from Jun has a slightly higher concentration of kaolinite, illite and paragonite than that from Guadix.

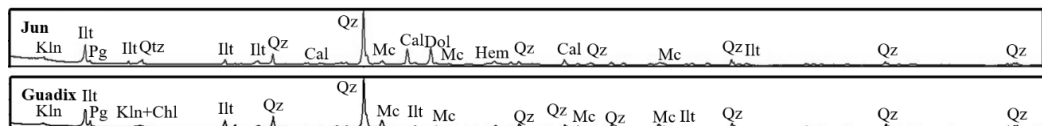


**Figure IA-2.** X-ray diffraction patterns of the raw materials from Jun and Guadix. Legend according to Whitney and Evans (2010): Qz = quartz; Cal = calcite; Dol = dolomite; Illt = illite; Pg = paragonite; Kln= kaolinite; Chl = chlorite; Hem = hematite; Mc = microcline.



### 3.1.4. Thermogravimetry (TG-DSC)

TG-DSC analysis highlighted that at around 100 °C both raw materials suffer a slight weight loss due to the presence of moisture or hygroscopic water (Fig.I-3). At 300 or 340 °C there is an inflection in the DSC curves, which corresponds to the combustion of labile organic matter present in the raw materials (Vieira et al., 2008; Guo et al., 2016). Other endothermic peaks, corresponding to the dehydroxylation of phyllosilicates, can be identified at about 540 °C (Brindley and Nakahira, 1959; Eberhart, 1963; Guo et al., 2016). Dehydroxylation of these minerals is complete at 600 °C (Barlow and Manning, 1999) and therefore does not contribute significantly to the weight loss that takes place at higher temperatures. According to Velde (1966), the equilibrium temperature for dehydroxylation of muscovite and its complete decomposition at 1 atm is approximately 560 °C. Therefore, as in other previous research (Eberhart, 1963; Sánchez-Navas, 1999; Rodríguez-Navarro et al., 2003), the dehydroxylation of the phyllosilicates in the raw materials from Jun and Guadix is not an equilibrium process.

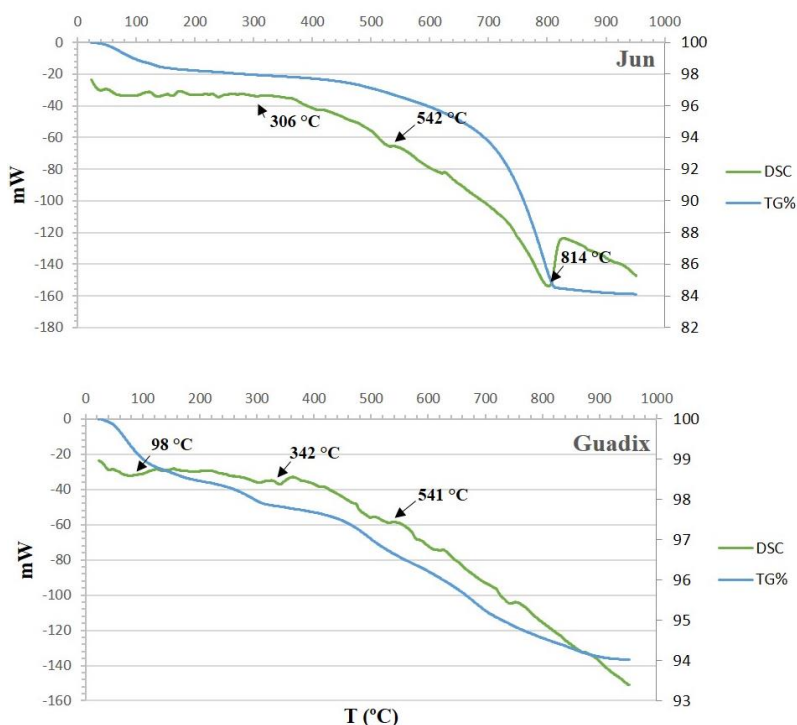


**Figure IA-3.** TG-DSC analysis of the raw materials from Jun and Guadix. The abscissa represents the temperature (in °C) and the two ordinates represent the weight loss (in %) (TG blue curve) and the differential scanning calorimetry (in mW) (DSC green curve).

The clay from Jun undergoes a much more pronounced weight loss, which is clearly visible in the TG curve with a minimum endothermic peak at around 800 °C and a 13% mass loss. This is due to the decomposition of carbonates and the release of CO<sub>2</sub> (Tyrrell et al., 1972; Rodríguez-Navarro et al., 2003; Cultrone et al., 2020). Above 800 °C, both samples show a further small weight loss, which is attributed to the further dehydroxylation of illite-type phyllosilicates (Eberhart, 1963; Barlow and Manning, 1999; Cultrone, 2001; Eliche-Quesada et al., 2017). The clay from Jun suffered a total weight loss of 16%, while the clay from Guadix lost 6%, values that were very similar to those measured by XRF (LOI, Table IA-2).

### 3.2. Chemistry, mineralogy and texture of the fired bricks

#### 3.2.1. X-ray fluorescence (XRF)

Table IA-3 shows the chemistry of the fired bricks. They have the same chemistry as the raw materials. The only difference is the lower loss on ignition (LOI) values, given that the fired samples have lost any organic matter that may have been present in the raw material. The Jun samples have also lost almost all their carbonate content (Rodríguez-Navarro et al., 2009). LOI values decrease as firing temperature increases due to the gradual dehydroxylation of phyllosilicates and, in the Jun samples, due to the decomposition of any remaining carbonates. LOI values are lower in bricks with added household glass because 20 wt.% of the raw material is replaced by this additive. These samples are therefore less rich in phyllosilicates and carbonates.

#### 3.2.2. Powder X-ray diffraction (PXRD)

All the phyllosilicates have disappeared in brick groups fired at 800 °C, with the exception of a dehydroxylated illite, although the reflection (001) at 10 Å is lower compared to that observed in the raw materials, suggesting that there is a lower concentration of this phase. The most abundant phase is quartz. As regards the presence of carbonates in Jun samples, at 800 °C dolomite has already disappeared while calcite content has fallen considerably (J800, Fig.IA-4). According to Rodríguez-Navarro et al. (2009 and 2012), dolomite starts to decompose at 500 °C and disappears completely at around 900 °C, while calcite starts to decompose at 600 °C and disappears completely at around 850 °C. At 800 °C, hematite starts to appear in the Guadix samples (G800, Fig.IA-4). At this temperature, the bricks with and without glass are mineralogically identical, although

higher background noise can be observed in the samples with added glass due to the presence of this increasingly amorphous waste (Parras et al., 1996).

**Table IA-3.** XRF results (in %) for the handmade and extruded (e) Jun bricks (J) and Guadix (G) bricks fired at 800, 950 and 1100 °C.

	SiO <sub>2</sub>	Al <sub>2</sub> O <sub>3</sub>	Fe <sub>2</sub> O <sub>3</sub>	MnO	MgO	CaO	Na <sub>2</sub> O	K <sub>2</sub> O	TiO <sub>2</sub>	P <sub>2</sub> O <sub>5</sub>	LOI	Total
J800	50.98	16.97	5.82	0.07	4.46	12.27	0.74	3.23	0.80	0.14	3.34	99.22
Jg800	56.27	13.49	4.58	0.06	3.63	11.86	3.40	2.68	0.65	0.11	2.75	99.48
Jge800	54.15	13.87	4.85	0.06	4.01	13.47	2.68	2.73	0.66	0.12	2.69	99.29
J950	52.86	17.40	5.92	0.07	4.33	12.20	0.77	3.31	0.81	0.14	1.65	99.46
Jg950	50.61	16.66	7.09	0.07	4.63	13.87	0.87	3.18	0.88	0.14	1.17	99.17
Jge950	54.91	14.01	4.93	0.06	4.09	13.86	2.71	2.74	0.65	0.12	1.10	99.18
J1100	55.13	14.52	6.54	0.09	3.58	11.83	3.14	2.86	0.75	0.12	0.82	99.38
Jg1100	54.38	13.75	6.67	0.07	3.55	12.51	3.74	2.91	0.80	0.11	0.84	99.33
Jge1100	52.94	13.83	6.67	0.07	4.07	13.93	3.27	2.91	0.80	0.12	0.57	99.13
G800	65.62	18.58	7.47	0.08	1.01	0.65	0.88	2.78	1.31	0.13	1.46	99.97
Gg800	66.37	15.14	5.92	0.06	0.96	2.80	3.32	2.37	1.01	0.11	1.92	99.98
Gge800	66.44	15.78	6.27	0.07	1.23	2.80	2.58	2.45	0.99	0.12	1.02	99.75
G950	65.86	18.89	7.54	0.08	1.01	0.64	0.89	2.83	1.28	0.14	0.83	99.99
Gg950	66.80	15.57	6.19	0.07	0.99	2.54	3.07	2.43	1.07	0.12	0.73	99.58
Gge950	66.25	15.84	6.30	0.06	1.20	2.89	2.61	2.47	1.01	0.12	0.68	99.43
G1100	65.86	18.82	7.61	0.08	1.03	0.66	0.90	2.81	1.30	0.13	0.41	99.61
Gg1100	66.26	15.58	6.25	0.07	1.17	2.83	3.31	2.42	0.96	0.12	1.01	99.98
Gge1100	66.61	15.91	6.40	0.07	1.43	2.82	2.61	2.47	1.00	0.12	0.51	99.95

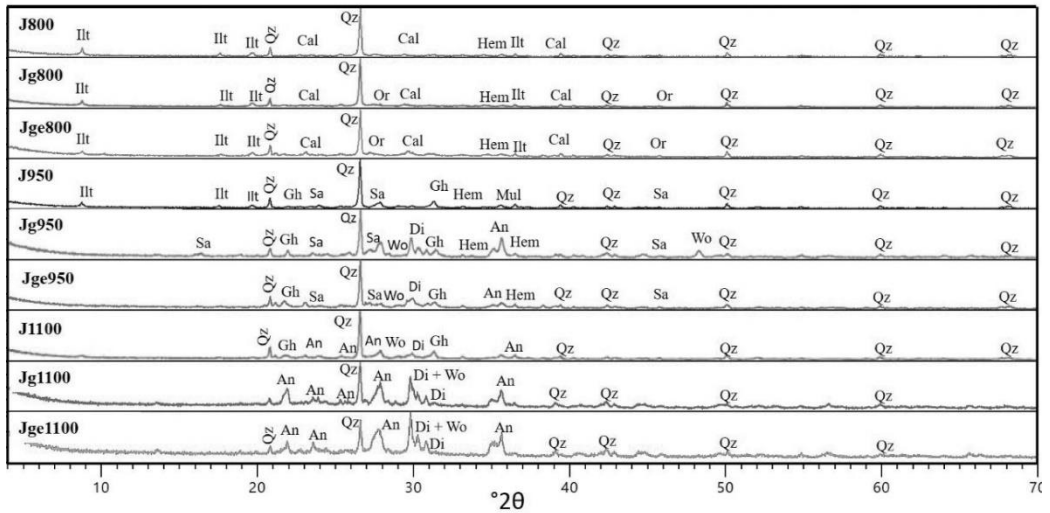


**Figure IA-4.** X-ray diffraction patterns for bricks made with the raw material from Jun (by hand and by extrusion) and fired at 800, 950 and 1100 °C. Legend according to Whitney and Evans (2010): Qz = quartz; Cal = calcite; Ilt = illite; Hem = hematite; Or = orthoclase; Sa = sanidine; An = anorthite; Gh = gehlenite; Di = diopside; Wo = wollastonite.

At 950 °C, the differences between the samples with and without glass are more pronounced than at 800 °C. In both brick groups, orthoclase transforms into a higher temperature polymorph phase, sanidine (Figs.IA-4 and 5). Hematite increases in concentration, mainly in Guadix samples, probably due to the decomposition of phyllosilicates, which favour Fe recrystallization (Eliche-Quesada et al., 2017). In the Jun samples (Fig.IA-4) calcite has disappeared while new mineral phases - gehlenite, wollastonite and diopside - are detected. Rathossi and Pontikes, 2010 pointed out that gehlenite is formed by the reaction between illite, calcite and quartz. Wollastonite and diopside can be formed by the reaction between quartz and carbonates (Capel et al., 1985; Cultrone and Rosua, 2020). The addition of glass brings about further mineralogical changes in that it seems to act as a flux agent accelerating the reactions or increasing the formation of new mineral phases. This is evident for example in the fact that illite has disappeared in the Jg950 and Jge950 samples, while a new phase, anorthite, has appeared. These bricks also seem to have higher concentrations of gehlenite, wollastonite, diopside and hematite than J950. The samples from Guadix fired at 950 °C had a lower illite content than at 800 °C, but there was almost no difference in the mineralogy between the bricks made with and without glass (G950, Gg950 and Gge950, Fig.IA-5).

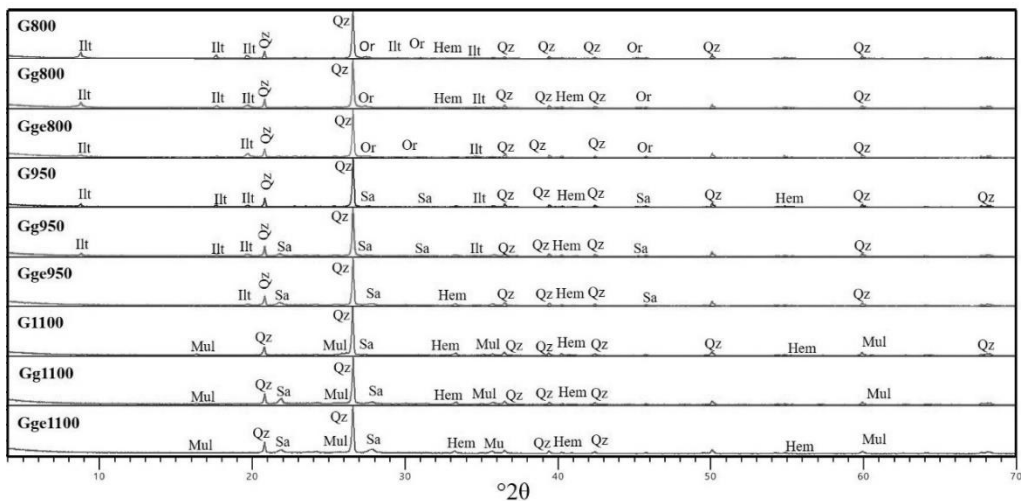


**Figure IA-5.** X-ray diffraction patterns for bricks made with the raw material from Guadix (by hand and by extrusion) and fired at 800, 950 and 1100 °C. Legend according to Whitney and Evans (2010): Qz = quartz; Ilt= illite; Hem = hematite; Or = orthoclase; SA = sanidine; Mul = mullite.

The mineralogical changes produced by the addition of glass become more obvious at 1100 °C (Figs.IA-4 and IA-5). In both brick groups (Jun and Guadix), there is an increase in the amorphous component, which suggests that the vitrification of the matrix is more advanced. The amount of hematite remains almost unchanged. In Jun bricks, the gehlenite content is lower in J1100 and disappears in Jg1100 and Jge1100 because it is involved in the formation of anorthite and wollastonite + diopside (Capel et al., 1985; Cultrone and Carrillo Rosua, 2020). Another new phase, mullite, was identified in the Guadix bricks. According to Rodriguez Navarro et al. (2003) this phase replaces the illite/muscovite inheriting specific crystallographic orientations of the phyllosilicate. The sanidine peaks are higher in the bricks with added glass.

### 3.2.3. Polarized optical microscopy (POM)

#### 3.2.3.1. Jun

The observations under the microscope of the samples from Jun fired at 800 °C revealed the presence of fragments of metamorphic rocks (mica-schists and gneiss) of about 1 mm in length. These fragments are scattered in an orange matrix (Fig.IA-6A) that forms the main skeleton of the bricks. The carbonate grains are partially decomposed (Fig.IA-6B). For their part, the muscovite crystals appear unaltered and reach 2<sup>nd</sup> order interference colour. Phyllosilicates and elongated fragments often show a preferential orientation due to the pressure exerted on the raw material during kneading. This is also evident with the porosity as elongated pores follow the same orientation as planar minerals (Fig.IA-6C). Glass fragments start to decompose in Jg800, as manifested in the development of fan-shaped structures (Fig.IA-6D). At 950 °C, the matrix is slightly darker due to the gradual vitrification of the bricks (De Bornis et al., 2017).

The carbonates are completely decomposed and the phyllosilicates start to lose their birefringence, above all in bricks with added glass. At 1100 °C, due to the high firing temperature, the pores turn ellipsoidal-to-rounded in morphology and the matrix becomes dark (Fig.IA-6E). This phenomenon is again more noticeable in the samples made with glass (Fig.IA-6F), so confirming that the addition of glass accelerates textural changes.

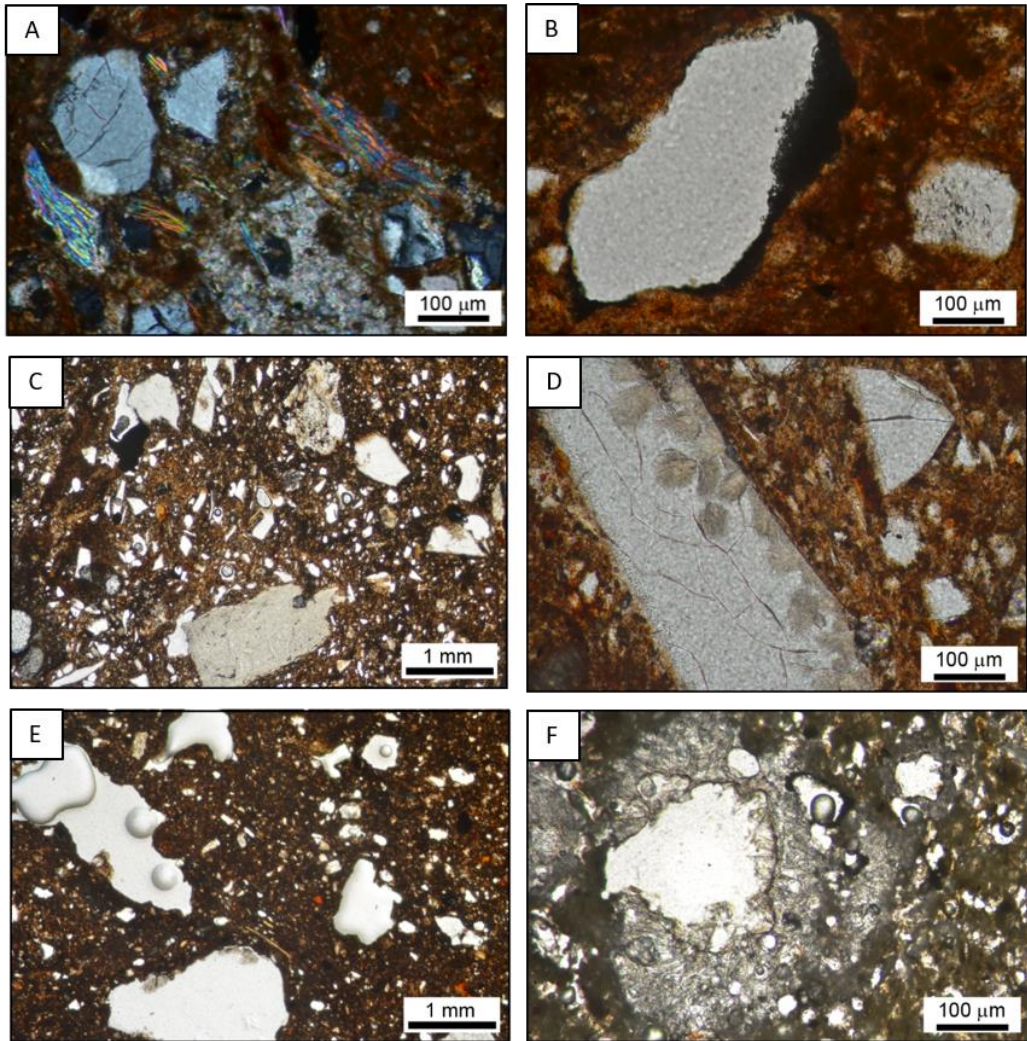


**Figure IA-6.** Bricks made with clay from Jun with and without household glass fired at 800, 950 and 1100 °C. Abbreviation: PPL = plane-polarized light; PPX = cross-polarized light. A) Fragments of quartz and gneiss fragments in the matrix of J800 (PPX); B) carbonate grain partially decomposed in J800 (PPX); C) general view of the matrix of Jg800 made with added glass (PPL); D) detailed image of a glass fragment in Jg800 which is starting to decompose (PPX); E) pores with different morphology in J950 (PPL); F) extended vitrification in the matrix of Jg1100 produced by the addition of glass (PPL).

### 3.2.3.2. Guadix

The bricks made with clay from Guadix fired at 800 °C (G800, Fig.IA-7A) have more quartz grains than those from Jun (Fig.IA-6C) and fragments of gneiss in an orange matrix (Fig.IA-7B). As in the Jun samples, phyllosilicates and elongated fragments



(gneiss) often have a preferential orientation due to the pressure exerted during kneading. At 950 °C, the matrix becomes darker and the phyllosilicates become less birefringent. Glass fragments start to decompose in a similar way to that observed in Jun samples with the development of finger-type structures (Figs.IA-7C and 7D). At 1100 °C, muscovite-type phyllosilicates have lost their birefringence and have a whitish colour. According to Rodríguez Navarro et al. (2003) and the PXRD results (Fig.IA-4), these phyllosilicates have probably been replaced by mullite. The pores acquire a rounded shape when the glass melts (Fig.IA-7F).

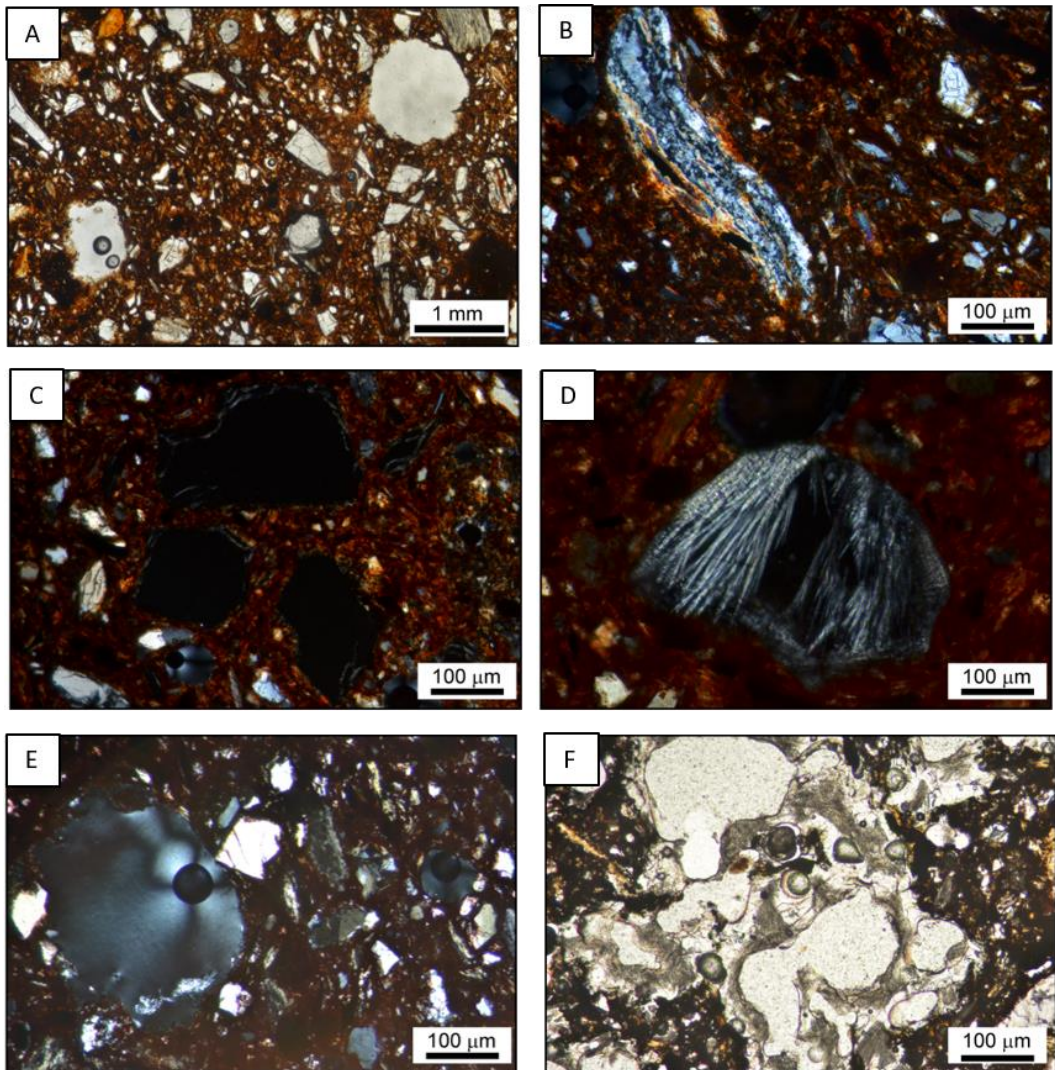


**Figure IA-7.** Bricks made with clay from Guadix with and without household glass fired at 800, 950 and 1100 °C. Abbreviation: PPL = plane-polarized light; PPX = cross-polarized light. A) Detailed image of the G800

sample showing fragments of quartz (PPX); B) matrix of Gg800 sample in which glass fragments with angular morphology are visible (PPX); C) glass fragments in the matrix of Gg800 sample (PPX); D) glass fragment in the Gg950 sample with acicular crystals intergrowth (PPX); E) detailed image of the matrix of the G1100 sample showing pores with varying shapes (PPX); F) porosity, melted glass and vitrification in the Gg1100 sample (PPX).

#### 3.2.4. *Field emission scanning electron microscopy (FESEM)*

FESEM observations were only carried out on the bricks fired at 800 °C and 1100 °C, where any textural differences would be more significant (Fig.IA-8). At 800 °C, in both brick groups the phyllosilicates maintain their laminar habit, although the lamellae tend to separate along the basal plane due to dehydroxylation (Fig.IA-8A) (Capel et al., 1985). In the Jun bricks, the carbonate grains start to decompose, so confirming MOP observation. In some dolomite grains, a depletion of Ca at the core of these crystals could be observed (see EDS analysis in Fig. IA-8B). This is probably due to the higher mobility of Ca ions with respect to Mg, which gives rise to the formation of new phases such as gehlenite, so causing Ca content to fall. The addition of glass to the Jun bricks (Jg800) seems to favour the formation of reaction rims and the development of new phases. At 800 °C, a partial decomposition of glass fragments can be seen along the edge of these grains in the form of fan-shaped structures (Fig.IA-8C), as observed earlier under MOP (see Fig.IA-6D). These structures show depletion in Al and Na and a slight enrichment in Si. This could be due to an increase in  $\beta$ -wollastonite (pseudowollastonite), which forms at a lower temperature than  $\alpha$ -wollastonite (wollastonite) (Vichaphund et al., 2011; De Bornis et al., 2017; Coletti et al., 2018). Otherwise, these structures only indicate glass devitrification. Hematite crystals begin to nucleate in the matrix and within the phyllosilicate sheets (Fig.IA-8E). The addition of glass to the Guadix bricks fired at 800 °C (Gg800) does not accelerate the reactions between phases. At 1100 °C, the matrix of both brick groups was more vitrified and vitrification was more pronounced in the bricks made with glass. The pores become increasingly rounded and hematite crystals can be seen (Figs. IA-8D and 8E). The phyllosilicates lose their planar morphology and a secondary porosity can be detected inside these crystals. In the samples with added household glass (Gg1100 and Jg1100), the phyllosilicates have almost completely disappeared. Accessory minerals such as ilmenite and rutile have been identified. At this temperature, new phases such as gehlenite and diopside can be identified in the Jun bricks, and elongated crystals with a composition similar to that of wollastonite are clearly



distinguishable inside the glass fragments (Fig.IA-8F). These findings confirm MOP observations and the data provided by PXRD results.

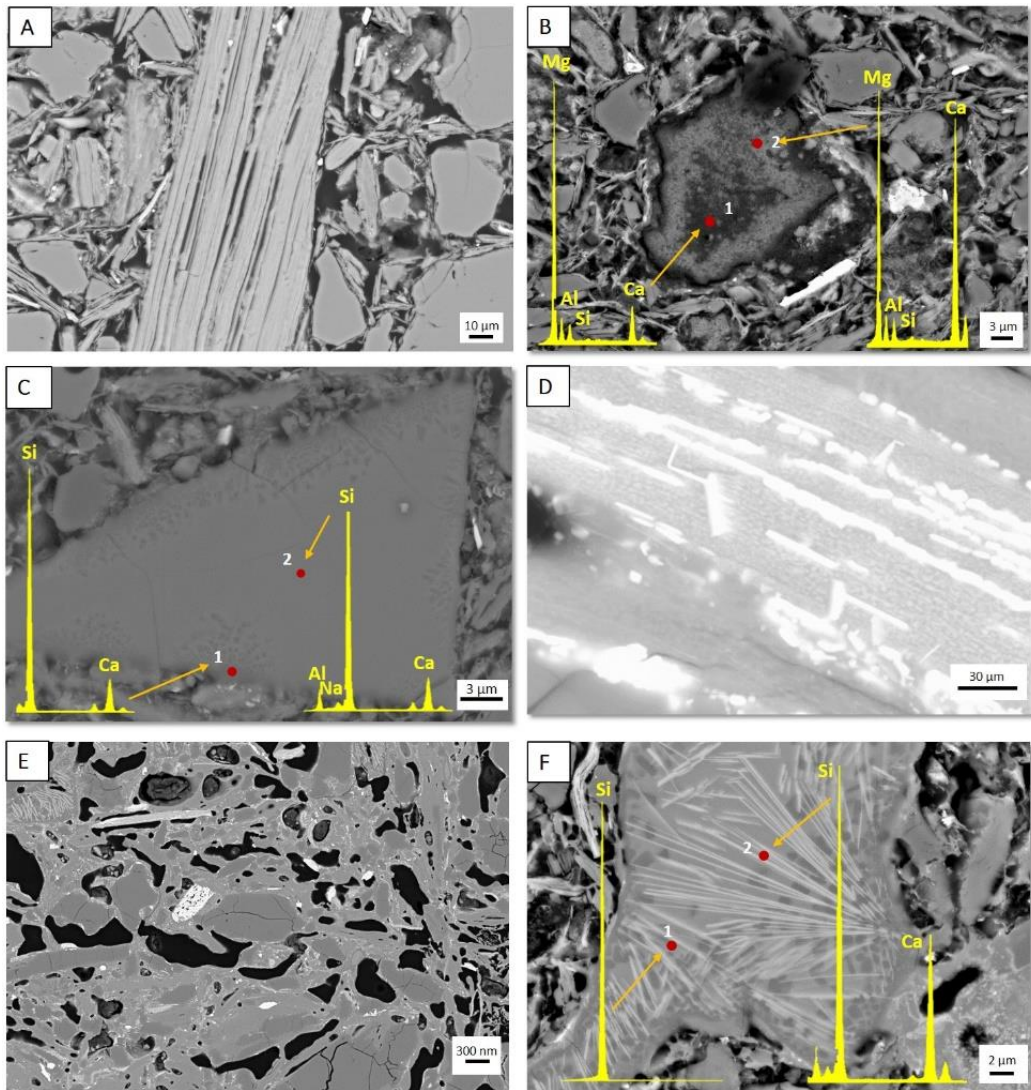


**Figure IA-8.** A) Dehydroxylation of phyllosilicates along (001) planes in G800; B) view of J800 showing the partial decomposition of a dolomite grain with a depletion of Ca at the core; C) detail of a glass fragment from Jg800 showing the change in the composition along the edge of the grain due to devitrification or the formation of a pseudowollastonite; D) detail of small hematite crystal growth within the phyllosilicate sheets; E) rounded pores and small hematite crystals in Gg1100; F) detail of elongated crystals that have developed inside a glass fragment in Jg1100.

### 3.3. Hydric tests

The results of the absorption, drying and capillarity tests are shown in Table IA-4 and Figs. IA-9 and 10. In general, the behaviour of handmade and extruded bricks varies in line with the raw materials used and the presence or not of glass. All the samples absorb less water as firing temperature increases and with the addition of glass (Ab and Af, Table IA-4). Between the two groups, the Jun bricks absorb more water than those from Guadix. The least absorbent of all were those made with glass and fired at 1100 °C (Gg1100 and Gge1100). The interconnection between the pores worsens (i.e.,  $A_x$  values augment) as the firing temperature increases. This is because the gradual vitrification of the matrix worsens the interconnection between the pores (Wang et al., 2008), so making the bricks less absorbent (S, Table IA-4). As for the drying, the bricks fired at the lowest temperature dry faster (Di, Table IA-4), which is logical given that they have the best pore interconnection and water can flow out (i.e. dry) more easily.

The Guadix bricks always dry faster than the Jun bricks (Figs. IA-9 and 10). The increase in the firing temperature (and the vitrification of samples) leads to a decrease in open porosity ( $P_o$ , Table IA-4). This decrease is more pronounced between 950 and 1100 °C, suggesting that the vitrification of the bricks occurs particularly in this firing range. It is interesting to note that the addition of household glass always reduces the porosity of the bricks, amongst which those manufactured by extrusion show the least porosity. Water absorption by capillarity decreases as the temperature increases (C, Table IA-4). This tendency is accentuated by the addition of glass, above all, in extruded bricks.

As regards density, there is no clear tendency between the two groups and the firing temperatures. In general, the addition of glass seems to increase real density ( $\rho_r$ ).

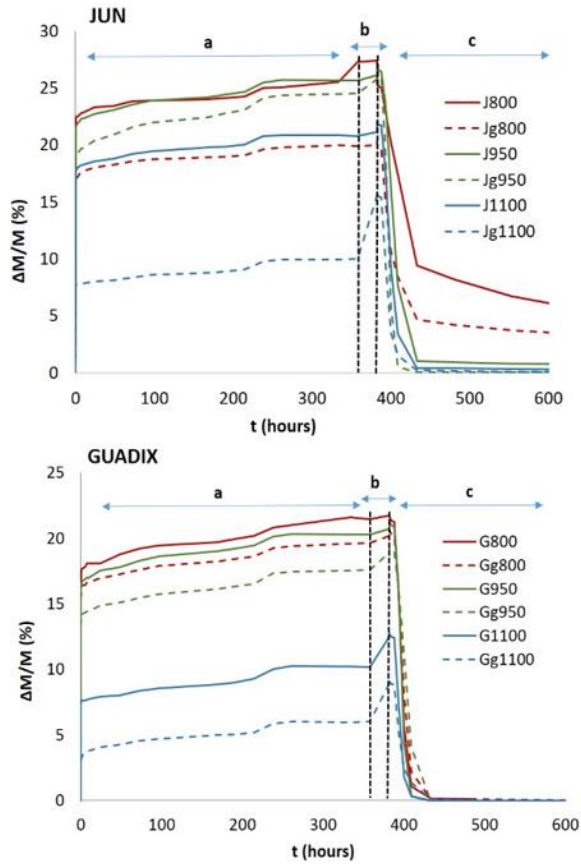


**Figure IA-9.** Free (a) and forced water absorption (b) and drying curves (c) for handmade bricks made with and without household glass and fired at 800, 950 and 1100 °C using the raw material from Jun and from Guadix.

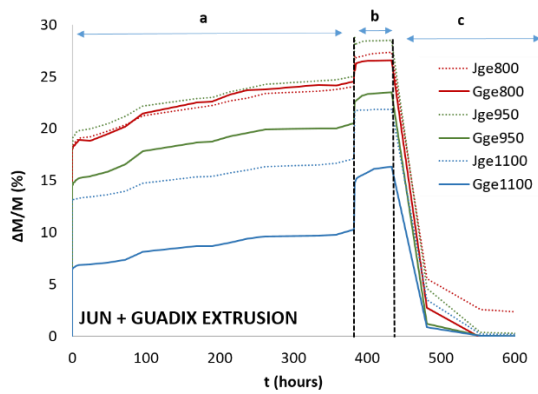


**Figure IA-10.** Free (a) and forced water absorption (b) and drying curves (c) for extruded bricks made with household glass and fired at 800, 950 and 1100 °C using the raw material from Jun and from Guadix.

**Table IA-4.** Hydric parameters of handmade and extruded bricks. Ab: free water absorption (%); Af: forced water absorption (%); Ax: degree of pore interconnection (%); S: saturation coefficient (%); Di: drying index; P<sub>o</sub>: open porosity (%); C: capillarity coefficient (g/m<sup>2</sup>s<sup>0.5</sup>); ρ<sub>a</sub>: apparent density (g cm<sup>-3</sup>); ρ<sub>r</sub>: real density (g cm<sup>-3</sup>).

	Ab	Af	Ax	S	Di	P <sub>o</sub>	C	ρ <sub>a</sub>	ρ <sub>r</sub>
J800	27.32	27.43	0.40	85.39	1.08	40.96	3.09	1.96	3.23
Jg800	19.93	19.95	0.10	91.61	1.34	27.14	1.27	1.53	2.20
Jge800	22.65	26.97	16.02	93.20	1.39	25.64	0.57	1.17	2.37
J950	25.65	26.14	1.87	89.30	1.16	37.64	1.36	1.29	1.94
Jg950	21.52	25.80	16.59	81.23	1.47	26.48	1.06	1.48	2.39
Jge950	20.88	28.75	27.37	81.06	1.50	24.19	0.52	1.42	2.39
J1100	20.80	21.14	1.61	78.07	1.58	30.74	2.32	1.53	2.63
Jg1100	9.99	15.51	35.59	77.18	1.66	22.11	0.68	1.99	2.69
Jge1100	8.74	9.97	12.34	77.79	1.71	21.74	0.37	1.60	2.45
G800	21.44	21.75	1.43	86.25	0.91	39.24	3.26	1.69	2.68
Gg800	19.62	20.15	2.63	85.48	1.28	31.04	1.30	1.33	1.95
Gge800	20.95	22.18	5.55	74.35	1.30	30.27	0.36	1.55	2.62
G950	20.28	20.72	2.12	95.10	0.92	37.32	3.06	1.42	2.01
Gg900	17.59	18.92	7.03	79.71	1.34	24.15	1.09	1.59	2.28
Gge950	19.98	22.58	11.51	75.23	1.37	24.06	0.32	1.66	2.65
G1100	10.16	12.52	18.85	64.34	0.93	19.40	1.53	1.49	1.83
Gg1100	6.03	8.91	32.32	77.48	1.59	16.74	0.35	1.64	1.92
Gge1100	7.74	8.80	12.05	76.02	1.63	15.12	0.19	1.68	2.23

### 3.4. Mercury intrusion porosimetry (MIP)

The handmade Jun bricks (Fig.IA-11) with no added glass show a unimodal pore size distribution with a maximum peak at 0.4 μm (J800), 0.5 μm (J950) and 0.6 μm (J1100). This means that the increase in temperature causes larger maximum peaks. The addition of glass causes the maximum peak to shift to the right (towards larger pores) and leads to the formation of a second family of pores around 70 μm at 800 and 950 °C. At 1100 °C the curve turns trimodal with the appearance of two new families at around 1 and 100 μm (Fig.IA-11).

The Guadix samples (Fig.IA-12) follow the same trend as those from Jun, with a unimodal pore size distribution in the bricks without added glass and a maximum peak at 1 μm (G800), 1.9 μm (G950) and 2.1 μm (G1100). In the samples with added glass, a bimodal or polymodal distribution was detected. It is interesting to note that the specific surface area (SSA, in m<sup>2</sup>/g, Figs. IA-11 and 12) generally drops as the firing temperature increases. This is due to the gradual coalescence of the smaller pores into larger ones

at 950 and 1100 °C. If we compare bricks with and without the addition of household glass, the results show that those made with added glass have slightly lower SSA values at 800 °C, while significant drops are observed at 950 and 1100 °C. This suggests that the glass acts as a flux in the matrix of the bricks within this firing range (950 – 1100 °C).

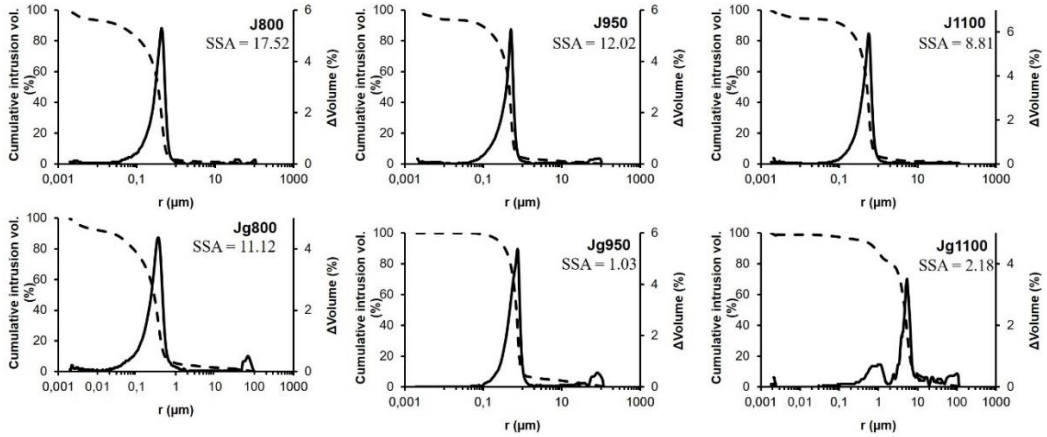


**Figure IA-11.** MIP cumulative (dashed line) and pore size distribution (continuous line) curves for handmade bricks made with clay from Jun with and without added household glass fired at 800, 950 and 1100 °C.

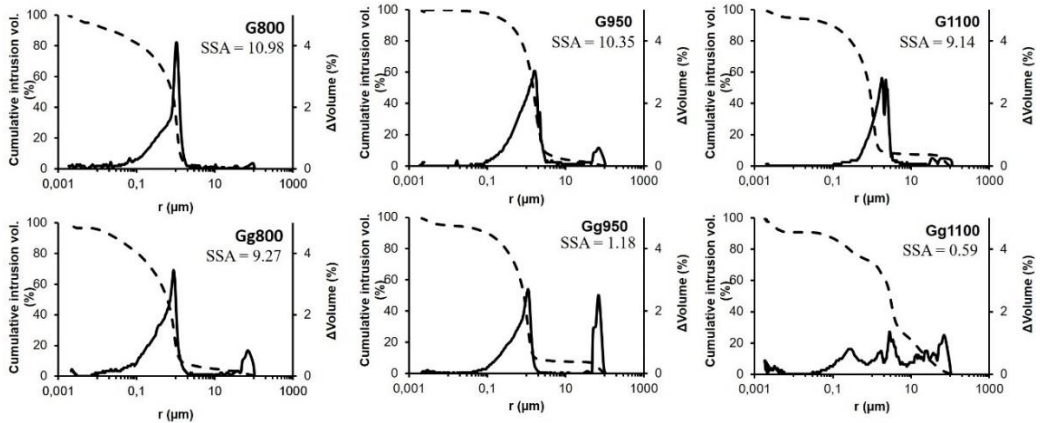


**Figure IA-12.** MIP cumulative (dashed line) and pore size distribution (continuous line) curves for handmade bricks made with clay from Guadix with and without added household glass fired at 800, 950 and 1100 °C.

### 3.5. Mechanical properties

The Jun bricks, with and without added glass, showed higher compressive strength than the Guadix bricks. The addition of glass always increases the strength (Table IA-5). This increase is related to textural and microstructural changes in the bricks. As mentioned before, glass acts as a flux agent bonding the particles together and reducing the porosity. The highest values were found in the bricks fired at 1100 °C, due to the high level of vitrification. The sample with the highest compressive strength (78.6 N/mm<sup>2</sup>) was Jg1100.

Several authors have found that compressive strength is more closely related with porosity and the degree of vitrification than with the mineralogy of the clay (Elert et al., 2003; Saravanapavan and Hench, 2003; Cultrone et al., 2004; Dondi et al., 2009). Tite and Maniatis (1975) found that in bricks made with carbonate-rich clays the structure formed at low temperatures (840-960 °C) remains almost unchanged until about 1080 °C. This is why Jun samples (without added glass) fired at 800 and 950 °C show very similar compressive strength. According to official specifications from the Spanish Ministry of Public Works (Pliego RL-88, 1988), all the samples, with the exception of G800, have enough compressive strength to be used for construction purposes.

**Table IA-5.** Compressive strength (Rc, MPa) and standard deviation ( $\sigma$ ) values for handmade bricks made with raw materials from Jun and Guadix with and without added glass.

Sample	Rc	$\sigma$	Sample	Rc	$\sigma$
J800	21.8	0.7	G800	6.4	0.3
Jg800	33.2	1.8	Gg800	10.3	2.1
J950	24.4	1.1	G950	13.4	1.1
Jg950	36.8	2.0	Gg950	17.3	0.8
J1100	26.4	2.7	G1100	23.8	1.4
Jg1100	78.6	0.6	Gg1100	45.9	0.6

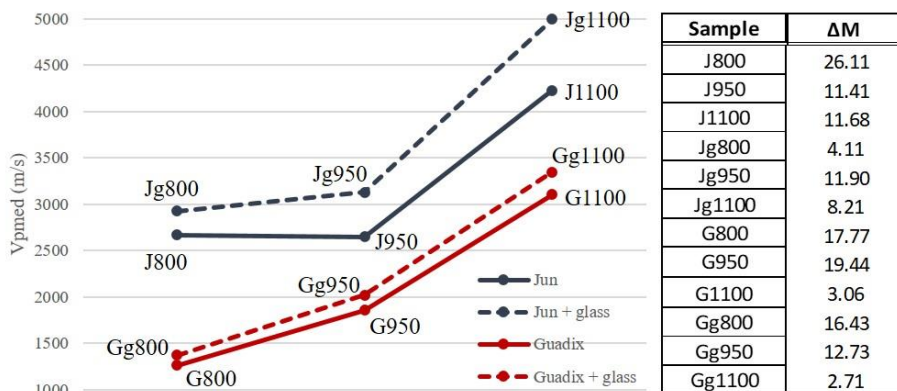
### 3.6. Ultrasounds

Fig.IA-13 shows the ultrasonic wave velocities propagation measured in handmade bricks with and without added glass. In general, the Jun bricks show higher Vp values than the Guadix bricks and the addition of glass tends to increase velocity values. This is because the bricks begin to vitrify and the internal structure becomes more homogeneous and loses the marked orientation provided by the phyllosilicates due to the addition of irregular, non-planar particles (glass). Ultrasound velocity increases not only with the addition of glass but also due to the increase in the firing temperature. It is

interesting to note that the samples made with clay from Guadix show a gradual increase in velocity in line with increasing firing temperature, while those from Jun show similar values at 800 and 950 °C and a sharp increase at 1100 °C, especially in those made with added glass (Jg1100) This may be because the glass grains in the body of the brick cause the ultrasonic waves to scatter, so delaying their propagation (Martínez-Martínez et al., 2011; Martínez et al., 2011).

The different behaviour between the two brick groups is due to their different mineralogical composition. In fact, even if the calcite and dolomite present in the raw material from Jun act as flux agents at low firing temperatures (800 °C), they do not promote vitrification at higher temperatures, in that the structure remains quite stable between 800 and 950 °C (Cultrone et al., 2004). The formation of new Ca-(Mg-) silicate phases (gehlenite, wollastonite, diopside and anorthite) hinders the development of an alumina-silicate melt (Tite and Maniatis, 1975).

At 1100 °C the firing temperature is so high that both brick groups undergo extensive vitrification regardless of the composition of the raw material. Ultrasound tests indicate that as the firing temperature increases, bricks become more compact and tend to be more homogeneous as the structural anisotropy decreases (Cultrone, 2001).



**Figure IA-13.** Mean ultrasound velocities (in m/s) in fired Jun and Guadix bricks made with and without added glass. The table on the right shows the structural anisotropy ( $\Delta M$ ) of the bricks.

### 3.7. Colour measurements

In Fig.IA-14, the bricks are grouped into three main groups based on their chromaticity. One group is made up of Jun bricks fired at 950 and 1100 °C with added glass (Jg950,

Jge950, Jg1100 and Jge1100). These bricks have the lowest  $a^*$  value and tend to be greyish/yellowish in colour. They also have the highest lightness values ( $L^*$ , Table IA-6). The second group is also made up of Jun bricks, mainly without added glass (J800, Jg800, J950 and J1100). The  $a^*$  value is around 16 and the samples tend to be red/orange in colour. The third group is the largest. Most of the samples are made with the raw material from Guadix fired at different temperatures with and without added glass (Fig.IA-14). The  $a^*$  value is over 19, and the samples have dark red tones, which is also because they have the lowest  $L^*$  values (Table IA-6). The Guadix samples show a more reddish colour with higher  $a^*$  and  $b^*$  values than the Jun samples. This is due to the crystallization of iron oxides from the decomposition of Fe-containing minerals within illitic-chloritic clays, while in the Jun samples, Fe is partly involved in the formation of new Ca-silicates such as gehlenite (Alia et al., 1999; Chindaprasirt et al., 2021). On this question, Nodari et al. (2007) observed that colour changes are related with the microstructural location and grain size of hematite particles as well as with the presence of iron in the glass rather than in the calcium silicate phases. This may explain why, as the firing temperature rises, the hematite content increases and a reddish colouration becomes more noticeable in the fired samples. Gg1100 bucks the general trend observed in the other samples (Fig.IA-14). This is due to the development of small glass bubbles on the surface (as described above in Section 2), which alter the colour values. In the Jun bricks, the samples that showed the greatest variation in colour due to the addition of glass were those fired at 950 °C, while the greatest variation in the Guadix bricks was observed in those fired at 1100 °C ( $\Delta E$ , Table IA-6). According to Grossi et al. (2007), colour variations of over 3 are perceptible to the human eye. This means that the variations in colour due to the addition of glass are visible in all the bricks except for those fired at the lowest temperature (800 °C).



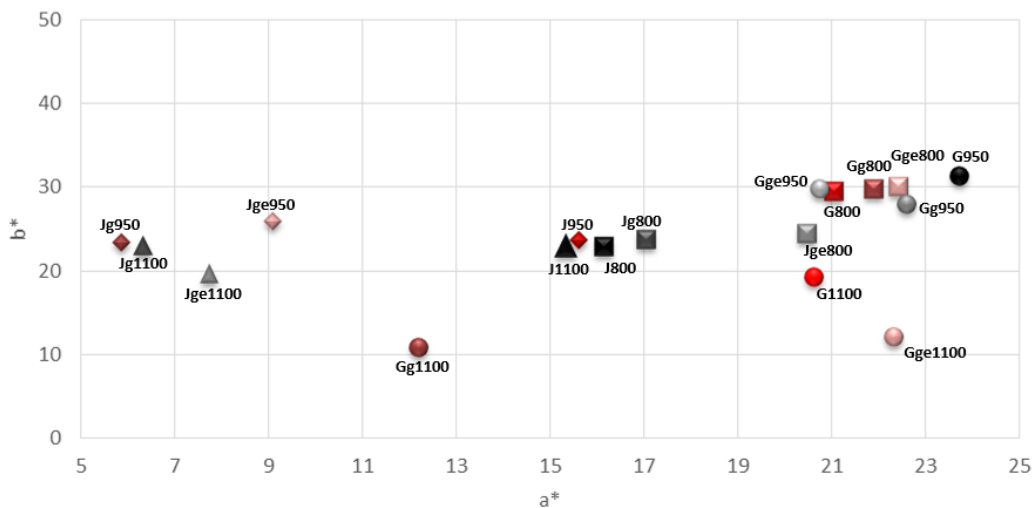


**Figure IA-14.** A) Chromatic values ( $a^*$  and  $b^*$ ) for handmade and extruded Jun and Guadix bricks with and without added glass.

**Table IA-6.** Lightness ( $L^*$ ), chromatic values ( $a^*$  and  $b^*$ ), chroma ( $C^*$ ) hue angle ( $h^\circ$ ) and colour difference ( $\Delta E$ ) values caused by the addition of household glass with respect to the bricks made without additive. Each value indicated is the average of nine values. Standard deviation is indicated in brackets.

	$L^*$	$a^*$	$b^*$	$C^*$	$h^\circ$	$\Delta E$
J800	58.49 (2.93)	16.13 (0.59)	22.90 (0.79)	28.02 (0.86)	55 (1.03)	
Jg800	59.75 (0.99)	17.03 (0.82)	23.83 (1.60)	29.30 (1.74)	54 (0.89)	1.29
Jge800	61.49 (1.02)	20.46 (0.61)	24.56 (0.84)	28.35 (1.11)	55 (0.95)	
J950	62.96 (1.43)	15.61 (1.15)	23.69 (1.98)	28.38 (2.13)	57 (1.75)	
Jg950	73.55 (2.36)	5.87 (0.89)	23.35 (0.85)	24.10 (0.81)	76 (2.22)	14.39
Jge950	75.62 (0.91)	9.09 (0.29)	25.98 (1.06)	23.47 (1.24)	79 (1.14)	
J1100	62.75 (1.35)	15.35 (1.15)	23.02 (0.72)	27.68 (1.13)	56 (1.60)	
Jg1100	63.01 (1.73)	6.33 (0.97)	22.83 (1.34)	23.72 (1.21)	74 (2.68)	9.02
Jge1100	63.16 (1.41)	7.74 (0.77)	19.55 (1.21)	22.78 (1.04)	72 (1.66)	
G800	55.01 (1.25)	21.04 (0.90)	29.56 (1.24)	36.28 (1.53)	55 (0.24)	
Gg800	53.26 (1.55)	21.88 (0.87)	29.83 (1.15)	36.99 (1.41)	54 (0.45)	1.96
Gge800	52.65 (0.89)	22.41 (0.68)	30.19 (1.13)	36.89 (1.25)	52 (0.30)	
G950	55.18 (2.69)	23.70 (0.97)	31.38 (1.09)	39.33 (1.30)	53 (0.99)	
Gg950	52.01 (2.42)	22.59 (0.92)	28.00 (2.02)	35.99 (1.91)	51 (1.83)	4.77
Gge950	51.82 (2.04)	20.74 (0.61)	29.84 (0.84)	37.12 (1.04)	50 (0.12)	
G1100	44.12 (1.41)	20.61 (1.57)	19.24 (2.05)	28.20 (2.50)	43 (1.26)	
Gg1100	45.14 (1.63)	12.18 (1.89)	10.83 (1.16)	16.31 (1.97)	42 (1.46)	11.91
Gge1100	42.13 (0.97)	22.32 (1.24)	12.14 (1.04)	15.46 (1.46)	43 (1.64)	

### 3.8. Accelerated ageing tests

#### 3.8.1. *Freeze-thaw*

All the bricks fired at 800 °C suffered more decay than those fired at higher temperatures, as might be expected given that they are less vitrified. The bricks fired at 1100 °C are generally the most resistant to ice and gain the least weight (Fig.IA-15). The addition of glass reduces the decay. The bricks with added glass show less porosity and less water absorption capacity (see Table IA-4). When comparing the manufacturing processes (handmade or extruded) of the bricks made with glass, the handmade bricks seem to perform better than the extruded ones. This may be due to the different anisotropy ( $\Delta M$ , Table IA-6) in that handmade bricks are more homogeneous and therefore more resistant to the crystallization pressures exerted by the water-ice phase change. If we compare the two brick groups, the Guadix bricks fired at 800 °C and the Jun bricks without glass fired at the same temperature suffered the most ice crystallization. In the Guadix samples, this took the form of a gradual loss of fragments over the course of the test, while in the case of Jun more abrupt jumps were observed (Fig.IA-15).

#### 3.8.2. *Salt crystallization*

The handmade and extruded bricks behave differently depending on the type of raw material used and the presence or not of household glass. However, as we observed with the freeze-thaw test, the handmade bricks seem to perform better than the extruded ones. Leshina and Pivnev (2002), who used sodium sulphate to simulate freeze-thaw tests, reported that samples containing 20 wt.% glass residue were resistant to at least 70 freeze-thaw cycles. The general trend in all the bricks involves an increase in weight at the beginning of the decay test, due to the presence of sodium sulphate in brick pores and fissures, followed by a sharp or more gradual descent in the following cycles (Fig.IA-16A).

The Jun bricks show a rapid weight gain above all at 800 °C until they reach cycle 5, which is when they start to break up and gradually lose fragments. At 950 °C, the bricks generally gain less weight or, as in the case of J950, lose less weight. However, in this case the weight of the brick fluctuates over the 15 cycles. This fluctuation indicates that after the initial crystallization of salts in the pore system (weight gain), these salts start to break the brick down, causing fissures to develop and fragments to fall off (weight loss). Then the salts crystallize again in the new fissures (new weight gain).

These weight gains and losses can be observed in various samples over the 15 test cycles. Bricks fired at 1100 °C are more resistant. Resistance also increases when household glass is added, as manifested by the fact that Jg1100 and Jge1100 are the samples that gain least weight and undergo least weight variation.

Guadix bricks fired at 800 °C show a smaller weight gain compared to the Jun bricks and a pronounced, constant weight loss just after the second cycle due to powdering. These bricks do not withstand the 15 test cycles and disintegrate before the end of the test (Fig.IA-16a). In a similar way, the Guadix bricks proved more resistant to salt attack as the firing temperature increased and when glass was added (Fig. IA-16A).

### 3.8.3. *Wet-dry*

The wet-dry test shows higher weight variations between cycles in the Jun samples than in those from Guadix (Fig.IA-16B). At higher firing temperatures, these variations are reduced due to the sintering and vitrification of the bricks. It should be noted that extruded bricks made with clay from both Jun and Guadix generally undergo higher weight variations than the handmade bricks. This could be due to the fact that the extruded samples retain more moisture within their pore systems than the handmade ones.

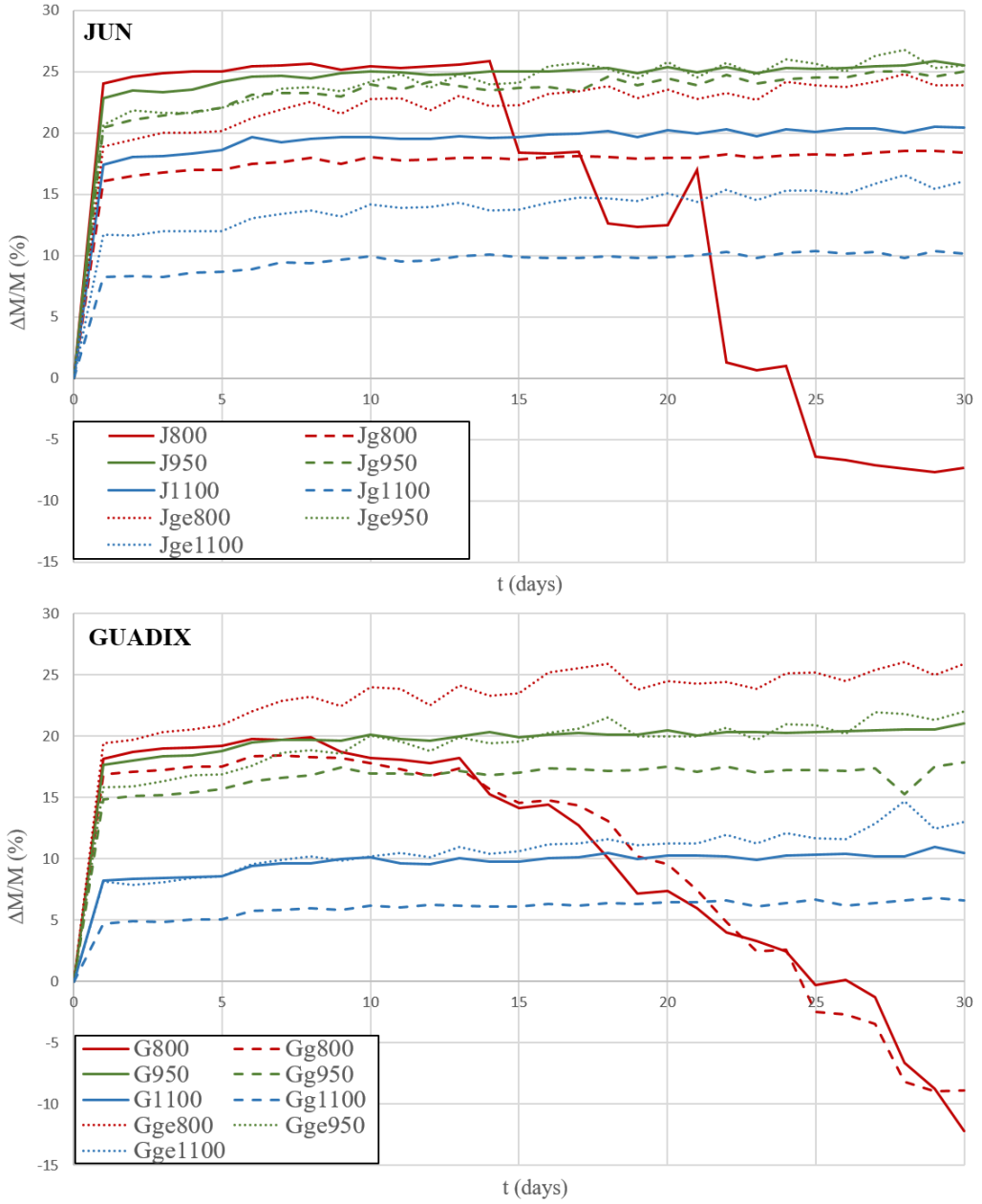


**Figure IA-15.** Freeze-thaw diagrams for handmade and extruded bricks made with clay from Jun or Guadix fired at 800, 950 and 1100 °C with and without the addition of household glass.

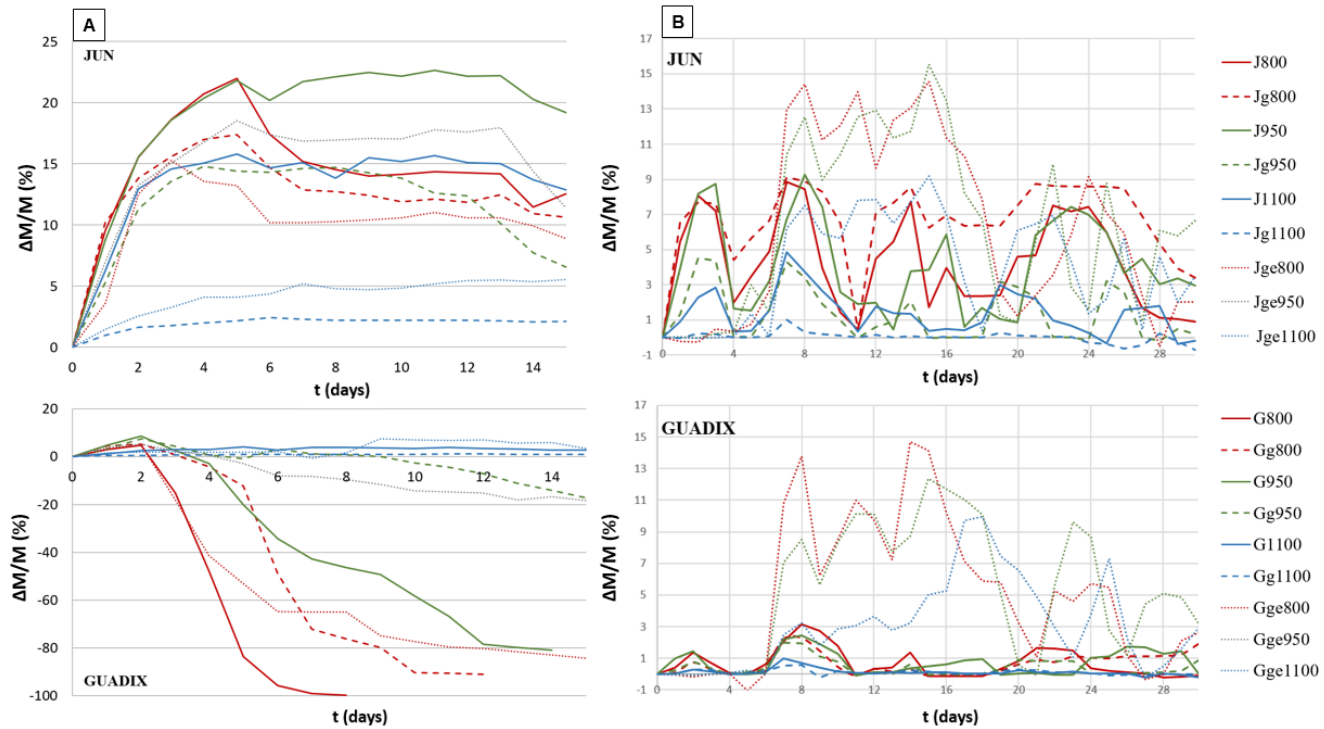


**Figure IA-16.** A )Salt crystallization diagrams for handmade and extruded bricks made with clay from Jun and Guadix fired at 800, 950 and 1100 °C with and without added household glass; B) wet-dry diagrams of handmade and extruded bricks made with clay from Jun and Guadix fired at 800, 950 and 1100 °C with and without added household glass

#### 4. Conclusions

This paper evaluated how the addition of 20 wt.% household glass improves the strength of solid bricks by comparing samples made with two different raw materials (Jun and Guadix), two different manufacturing methods (handmade and extrusion) and three different firing temperatures, 800, 950 and 1100 °C. The clayey soils used as raw materials have different mineralogies. The soil from Jun contains carbonates, while that from Guadix is rich in quartz and phyllosilicates. This leads to differences in the mineralogical evolution of bricks after firing, i.e. the development of new Ca-(Mg-) silicates such as gehlenite, diopside, wollastonite and anorthite when the raw material from Jun was used, while mullite appeared with the raw material from Guadix. The increase in firing temperature also leads to an increase in the amount of amorphous phase due to the vitrification of the bricks. The addition of glass modifies the porous system. In fact, bricks with added household glass fired at high temperature absorb less water and dry more quickly than conventional bricks. It has also been shown that extruded bricks are less porous. The addition of glass leads to a decrease in pore interconnection and augments vitrification. The porosity of both handmade and extruded bricks diminishes as the firing temperature increases.

Bricks with added glass are more resistant to compressive strength tests than those made with just clay. This is more evident in the bricks made with the clay from Jun. These results are confirmed by ultrasound measurements which revealed that the compactness of bricks increases in line with the firing temperature and by adding glass.

The colour of the bricks reflects the composition of the two raw materials (with or without carbonates) and the mineralogical and textural changes that take place during firing. The Jun bricks vary from yellow to orange in colour, while those made with clay from Guadix tend to be dark red. Colour does not seem to be linked with the durability and the physical properties of the bricks.

The Jun bricks perform better than those from Guadix in accelerated ageing tests, perhaps due to the melting action of carbonates at low firing temperatures.

In general, the use of household glass as an additive in the production of bricks provides benefits for the environment and for the brick industry. It also improves certain physical properties of the bricks, for example by making them less porous and reducing their water absorption capacity. It also provides greater resistance and durability. These improvements represent a step forward in the production of more efficient, more environmentally friendly products for use in the construction industry.

L. Crespo-López, D. Benavente, S. Morales-Ruano, M. Vázquez-Vílchez, G. Cultrone

Published in *Construction and Building Materials*

Vol. 408, 133583 (2023)

DOI: 10.1016/j.conbuildmat.2023.133583

Impact Factor: 7.4

Position 6/139 (Q1)

Category: Engineering, Civil (JCR 2022)



Construction and Building Materials

Volume 408, 8 December 2023, 133583



Review

# Non-destructive techniques (NDT) and statistical analysis for the characterization of bricks made with added glass

L. Crespo-López<sup>a</sup>, D. Benavente<sup>b</sup>, S. Morales-Ruano<sup>a, c</sup>, M. Vázquez-Vílchez<sup>d</sup>, G. Cultrone<sup>a</sup>

Show more

+ Add to Mendeley Share Cite

<https://doi.org/10.1016/j.conbuildmat.2023.133583>

[Get rights and content](#)

**Keywords:** Physical-mechanical properties, handmade bricks, ANOVA, Characterisation, Building materials, Environmental savings.

## 1. Introduction

Handmade bricks are used throughout the world, often in combination with stone masonry and timber roofs or floors. This is because bricks are easy to produce, easy to shape and in most cases are lighter than stone, forming fire-resistant, durable walls. Bricks are made of clay, a natural, non-renewable resource. One option to help reduce the continuous depletion of this resource would be to use waste products that would

otherwise accumulate in landfills as additives in the brick production process, so reducing the amount of clay required (Zhang, 2013). This in turn would reduce the need for clay extraction, a process that causes environmental disturbances, through soil erosion, and produces pollutants such as particulate matter. It also results in the emission of gases such as carbon monoxide, carbon dioxide, nitrogen oxides and sulphur oxides (Mukherjee, 2013). This is why some governments, such as the Chinese, are discouraging the use of clay bricks and promoting eco-friendly construction materials after an annual loss of 66.7 million square meters of fertile land due to the extraction of clay for brick production (Al-Fakih et al., 2019). In research into these materials, it has been observed for example that bricks made exclusively with water treatment sludge or with sludge and other residues proved highly weather-resistant (Al-Fakih et al., 2019). Various studies have been conducted recently to investigate the reuse of wastes in the production of building materials in general (Preethi et al., 2019; Soni et al., 2022) and of bricks in particular (Eliche-Quesada et al., 2012a; Cultrone et al., 2020; D'Angelo et al., 2021; Karslioglu et al., 2021; Crespo-López and Cultrone, 2022; Cultrone, 2022; Santhosh et al., 2022; Simão et al., 2022; Coletti et al., 2023; Crespo-López et al., 2023b and C; López Gomez and Cultrone, 2023; Crespo-López et al., 2024). Promising, yet contrasting, results have been obtained in terms of the porosity of fired samples, as in the case of Fe-rich metallurgical wastes (Simão et al., 2022). The use of certain waste products as additives in brick manufacture can improve the properties of the bricks (porosity, strength, durability, etc.) and promote sustainability through recycling (Eliche-Quesada et al., 2011 and 2012b). This study goes beyond the interesting, descriptive analysis typically provided by these previous studies, and uses statistical techniques such as analysis of variance or factorial analysis to assess the influence of using additives on the physical properties of the bricks. In this case, it was decided to investigate the use of household glass as an additive in brick production to enable, on the one hand, the reuse of domestic glass waste, so promoting the circular economy, and on the other to reduce the amount of clay required to produce the bricks. The reuse of waste glass in this way would also produce energy savings and environmental benefits by reducing the need for landfill. The final aim was to produce highly efficient handmade bricks for use in heritage restoration and new buildings, of higher quality than those currently available.

The petrophysical properties of handmade bricks are very important for the structural behaviour of both modern and historic buildings in that they are the main factor influencing the compressive strength of the masonry (Crespo-López and Cultrone, 2022).



Recent studies have proposed new approaches in the characterization of historic building materials (Mesquita et al., 2018; Rosa et al., 2019; Teschemacher et al., 2022). When carrying out an exhaustive characterization of the materials used in a building, a series of precautions must be taken, so as to avoid compromising the stability of the structure. Whenever possible, non-destructive techniques (NDT) should be used. Researchers analysing the petrophysical characteristics of bricks have used NDT to explore their physical properties and interpret them on the basis of their petrographic characteristics, assessing the pores, fissures, anisotropies, hardness, chemistry and mineralogy of the fired samples (Ramos et al., 2010; Mesquita et al., 2016). NDT are easier to use in bricks than in other materials such as stone. This is because bricks are almost homogeneous materials. They have no internal discontinuities and are fairly isotropic, which makes it much easier to interpret the results obtained and to apply the basic principles of elementary physics, which are based on assumptions regarding the behaviour of homogeneous, isotropic materials with no discontinuities (Miranda et al., 2012). For these reasons, in this paper, NDT were combined with statistical analysis to create a useful method for the safe assessment of the state of both historic buildings and modern constructions. Some of these NDT, such as ultrasonic pulse velocity (UPV) or the Leeb hardness (LH) test, can be applied in situ, an important consideration in heritage restoration. This methodology enabled the accurate characterization of the components of the building materials and provided information about their physical and mechanical properties.

The main objective of this paper was to use non-destructive and statistical techniques to determine whether handmade bricks were suitable and efficient for use in building restoration and in the construction industry in general. An attempt was also made to assess whether the addition of crushed household glass improved the properties of the bricks, and whether the firing temperature affected their aesthetic and physical-mechanical properties.

## **2. Materials and methods**

### **2.1. Production of bricks**

The bricks used in this research were made of clay from two localities, Guadix (G) and Jun (J) (Granada, Spain), about 50 km apart. Both these clays are post-orogenic, continental sediments deposited in the intermontane basins of Guadix-Baza and

Granada. The clay from Guadix was deposited in the middle-late Pleistocene during the last stages of the infilling of the basin (Viseras, 1991; García-Aguilar and Martín, 2000; Granados et al., 2021), above all in small lakes and swamps that developed temporarily on the banks of braided rivers that drained from the nearby Sierra Nevada mountains (Viseras, 1991). The clay from Jun was deposited during the late Turolian in a lacustrine environment with nearby fan deltas that drained carbonate sediments eroded from Sierra Arana (García-Alix et al., 2008).

In order to test the possible use of glass as an additive, 20 wt.% crushed household glass was added to clay mixes from Guadix and Jun. The bricks were fired and then compared with other bricks made without glass, which served as the control group. Both brick types, with or without waste glass, were handmade. The decision as to how much glass to add (20 wt.%) was based on recent investigations with promising results (Loryuenyong et al., 2009; Mao et al., 2020; Zhang et al., 2022). The clay (from Guadix and Jun) was sieved, so as to remove fragments of over 1.5 mm in size prior to mixing with glass (when present) and water. The mixture was then kneaded until sufficient plasticity was achieved. 308 ml/kg and 333 ml/kg of kneading water were needed for bricks with or without glass, respectively. The clayey paste was then placed in moistened wooden moulds of 15 × 20 × 4 cm. After one hour, the moulds were removed from the clayey paste and cut into 4 cm edge cubes using a stretched cotton thread (Fig.IB-1A).



**Figure IB-1.** Photograph of the bricks studied in this work. A) Unfired bricks made from raw materials from Jun and Guadix with and without household glass; B-C) general view of fired bricks with and without household glass.

When the bricks were totally dry, they were fired in a Herotec CR-35 electric oven at 800, 950 and 1100 °C (Fig.IB-1B and C). Once the desired temperature was reached, it was kept constant for 3 hours. Then the oven was turned off and the samples were left inside to cool until the next day. Slow cooling in this way prevents the development of fissures due to  $\beta$ -to- $\alpha$  quartz transition at 573 °C. Finally, the fired samples were removed from the oven and immersed in water for about 1 hour so as to avoid “lime blowing” due to the presence of lime grains (Laird and Worcester, 1956). Table IB-1 shows the acronyms assigned to the 12 types of bricks studied in this research.

**Table IB-1.** Acronym assigned to each brick according to the raw material used, the addition of 20 wt.% household glass and the firing temperature.

Raw materials	Firing temperature (°C)	Additive	
		without glass	with glass
Jun (J) and Guadix (G)	800	J800	Jg800
		G800	Gg800
	950	J950	Jg950
		G950	Gg950
	1100	J1100	Jg1100
		G1100	Gg1100

## 2.2. Methods

The following methodology was used to study the raw materials and the fired bricks. The first step was to characterize the two raw materials and the fired bricks in order to determine their chemical-mineralogical composition. To this end, a Fourier transform infrared spectroscopy using an attenuated total reflectance sample holder (ATR-FTIR) was used and the mineralogical information was obtained by powder X-ray diffraction (PXRD) using a PANalytical X'Pert PRO diffractometer. The working conditions were: CuK $\alpha$  radiation, 45 kV voltage, 40 mA current, 3 to 70° 2 $\theta$  exploration range, 0.1 2 $\theta$  s<sup>-1</sup> goniometer speed. The mineral phases were identified using the PANalytical X'pert Highscore Plus 3.0 software. In order to identify the clay fraction more accurately, the following oriented aggregates were prepared according to the recommendations of Moore and Reynolds (1989): air dried, solvated with ethylene glycol, solvated with dimethyl sulfoxide and heated at 550 °C. The qualitative determination of the

compositional vibrations of the raw materials and the household glass was analysed by ATR-FTIR, within a frequency range of 4000-400  $\text{cm}^{-1}$  and with a step size of 0.50  $\text{cm}^{-1}$ .

Videomicroscopy, radiography and spectrophotometry were used to assess the appearance of the fired bricks. A Leica DVM 2000 digital videomicroscope, using the Leica Application Suite V.3.8.0 for photo acquisition, was used as a preliminary tool to identify textural differences and relevant features on the surface of the samples with a higher magnification than the naked eye. A Konica Minolta CM-700d spectrophotometer was used to quantify the colour of the bricks according to the UNE-EN 15886 (2011) standard. Illuminant D65, 10° observer and 8 mm measurement area were used. Nine measurements per sample were performed to determine their lightness ( $L^*$ ) and chromatic values ( $a^*$  and  $b^*$ ).

Radiography is a useful NDT for detecting possible non-visible defects in the bricks as its shortwave elementary particles can penetrate the bricks without causing any damage. In particular, X-rays were used to detect significant differences in the degree of vitrification of the bricks made with or without glass. X-rays were carried out using a TROPHY radiologic VETOX 11ST with 95 kV and 50 mA working conditions. A Micro Computer with METRON-DVM software was used to process the radiographic images.

Finally, the physical-mechanical properties of the bricks were evaluated using the LH and UPV tests. The uniaxial compression (CS) test, which causes the samples to break and become unusable, was used to confirm the results obtained with LH and UPV. The LH tester PCE-2500N was used for the non-destructive measurement of the surface hardness of bricks using a rebound hammer. The brick cubes were cut in half and 5 linear measurements per brick were made from the left outer edge through the core to the right outer edge. The harder the surface of the material, the higher the rebound speed. UPV is increasingly mentioned in the literature, especially in Europe, due to the possibility of establishing a correlation between CS and UPV (Mesquita et al., 2018; Rosa et al., 2019).

UPV measures the degree of compactness and was used to determine the elastic-dynamic properties of the bricks, properties that affect their mechanical resistance (Gomez-Heras et al., 2020). Measurements were performed using a Control 58-E4800 ultrasonic pulse velocity tester with transducers of 54 kHz and a circular surface of 27 mm in diameter. A water-based eco-gel was used to enable homogeneous contact between the transducers and the brick surfaces. The measurements were carried out on

three samples per brick type. P-wave propagation was measured in m/s according to the ASTM D2845 (2000) standard.

The compressive strength ( $R_c$ ) was measured using a Matest E181 hydraulic press with double frame 25 kN/300 kN according to the UNE-EN 772-1 (2000) standard.  $R_c$  was calculated in MPa on three samples of each brick according to the following Eq. 1:

$$R_c = \frac{F}{A} \quad (1)$$

where  $F$  is the breaking load (in N) and  $A$  is the cross-sectional area in  $m^2$ .

The analysis of variance technique (ANOVA) is a statistical test used to compare the means of two or more groups of variables or factors, such as the firing temperature (800, 950 and 1100 °C) and the type of raw material used. It can also be used to assess how adding the glass affects the samples. In this analysis, both the effect of each factor on the various parameters studied and the possible interaction between the variables were analysed. Statistically different groups were identified using Tukey's and Duncan's tests ( $P < 5\%$ ). In addition, the experiment and the procedure were checked to ensure that there were no significant errors that would invalidate the study.

### **3. Results and discussion**

#### **3.1. Raw materials**

##### **3.1.1. ATR-FTIR**

The analysis carried out on the clays from Guadix and Jun and the household glass showed that the bands related to the asymmetric stretching of the Si-O of quartz or free silica ( $SiO_4$ ) in the region between  $\sim 900$  and  $\sim 1050$   $cm^{-1}$  and between  $\sim 400$  and  $\sim 500$   $cm^{-1}$  (Saravanapavan and Hensch, 2003; Nesbitt et al., 2018; Jollands et al., 2020) are well defined in all the samples (Fig.IB-2). The peak at  $1046$   $cm^{-1}$  corresponded to the intense Si-O and Si-O-Al stretching frequencies, characteristic of the aluminium silicates (Dan and Raman, 1986; Lavat et al., 2007) present in the clayey materials. Peaks were also detected in the region near  $475$   $cm^{-1}$ , which could correspond to the typical peak of the Fe-O bond of hematite (Liu et al., 2007). Another peak appeared near  $795$   $cm^{-1}$ , which could be attributed to maghemite (Darezereshki, 2010), a polymorphic form of  $Fe_2O_3$  called  $\gamma$ - $Fe_2O_3$  with an inverse spinel structure, which differentiates it from  $\alpha$ - $Fe_2O_3$  (hematite), which has a corundum structure.

The shoulders observed between 3000  $\text{cm}^{-1}$  and 3400  $\text{cm}^{-1}$  correspond to the moisture (Ameitphale et al., 1992) present in the clayey samples (Fig.IB-2, green and blue lines), while the bands located at  $\sim 3600 \text{ cm}^{-1}$  ( $\nu_1$ , symmetric stretching) and  $\sim 3700 \text{ cm}^{-1}$  ( $\nu_3$ , anti-symmetric stretching (Shimanouchi, 1973)) correspond to the vibration of the molecules in the O-H group and in Al-OH, which are probably associated with the presence of phyllosilicates (Mukhopadhyay et al., 2010). Illite/muscovite may be characterized by OH-stretching around  $3620 \text{ cm}^{-1}$  (Post and Borer, 2002; Lavat et al., 2007). The peaks at  $\sim 800$  and  $\sim 750 \text{ cm}^{-1}$  confirm the presence of a Si-O-Al stretching frequency where Al is in tetrahedral coordination and support the possible presence of illite or muscovite (Mukhopadhyay et al., 2010). The absorption band at  $3694\text{--}3620 \text{ cm}^{-1}$  indicates the stretching vibrations of -OH groups from the kaolinite network (Elimbi et al., 2011).

The two clayey samples can be differentiated by the fact that in the raw material from Jun (Fig.IB-1, green line), the presence of carbonates is corroborated by the appearance of characteristic  $\text{CO}_3^-$  group ( $\nu_2$ ) ( $\sim 874 \text{ cm}^{-1}$ ) and  $\text{CO}_3^-$  group ( $\nu_3$ ) ( $\sim 1430$  and  $\sim 1460 \text{ cm}^{-1}$ ) vibrations (Hellwege et al., 1970; Panda et al., 2003; Choudhary et al., 2015; Balan et al., 2019).

When characterizing the household glass, the shoulder observed between 800 and 1200  $\text{cm}^{-1}$  was taken into account (Fig.IB-2, orange line). This range houses the Si-O-Ca bonds (980 and 905  $\text{cm}^{-1}$ ) containing non-bridging oxygen, the O-Si-O bonds (819  $\text{cm}^{-1}$ ) and symmetric stretching of the Si-O-Si bonds (1090, 503 and 464  $\text{cm}^{-1}$ ) (Barde et al., 2015; Mukherjee and Das, 2013).

MacDonald et al., 2000 determined that the presence of alkali ions, such as sodium, adds new vibrational modes, Si-O-[alkali] bending and stretching. These break up the original network, altering the modes associated only with the silica network. The characteristic ranges of these modes (Si-O-[alkali] stretching) are in line with those observed by previous authors (Zellmer and White, 1984; Husung and Doremus, 1990).

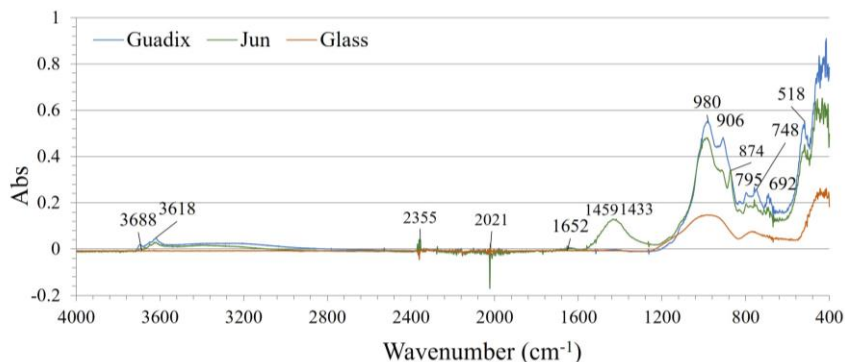


**Figure IB-2.** Infrared absorption spectroscopy carried out on the raw materials from Guadix and Jun and on the household glass.

### 3.1.2. PXRD

PXRD analysis of the clays from Jun and Guadix has highlighted the presence in both samples of quartz, k-feldspars and phyllosilicates (illite, paragonite, chlorite and kaolinite) (Fig. IB-3). The clay from Jun has a slightly higher concentration of kaolinite, illite and paragonite than the clay from Guadix and the presence of chlorite, a mineral that is commonly masked by smectite ( $\sim 14 \text{ \AA}$ ) and kaolinite ( $\sim 7 \text{ \AA}$ ), has been confirmed by heating the oriented aggregates to  $550 \text{ }^\circ\text{C}$  (Cultrone et al., 2001). Carbonates (calcite and dolomite) and hematite were only detected in the clay from Jun.

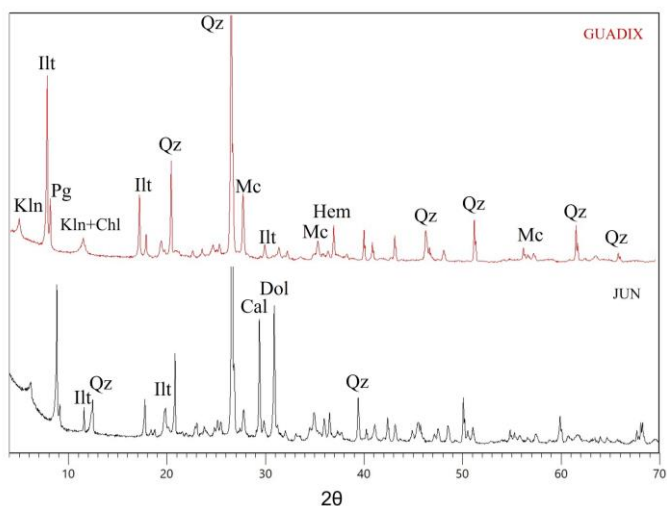


**Figure IB-3.** Mineralogy of the raw materials (Jun and Guadix). Legend according to Warr (2020): Ilt = illite; Pg = paragonite; Kln= kaolinite; Chl = chlorite; Qz = quartz; Cal = calcite; Dol = dolomite; Mc = microcline; Hem = hematite.

## 3.2. Fired bricks

### 3.2.1. Mineralogical properties

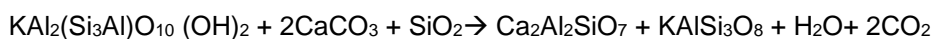
#### 3.2.1.1. PXRD

PXRD analysis of the bricks from Jun (J) and Guadix (G) fired at 800 °C shows that all the phyllosilicates had disappeared with the exception of dehydroxylated illite, which can still be detected, although the reflection (001) at 10 Å is lower compared to the raw materials, which suggests a lower concentration (Fig.IB-4). Quartz is the most abundant phase and hematite is beginning to be detected.

In J800, the dolomite has disappeared while calcite is present in smaller concentrations. An increase in the amorphous phase can be detected in samples with added glass (Jg800 and Gg800).

At 950 °C the differences in the samples with or without added glass are more evident than at 800 °C (Fig.IB-4). In both brick groups, orthoclase is transformed into a higher temperature polymorph phase, sanidine. They also have a higher hematite content probably due to the decomposition of phyllosilicates, which favours Fe recrystallization (Parras et al., 1996). In J950, calcite disappeared and new mineral phases, such as gehlenite, wollastonite and diopside, were formed (Fig.IB-4). According to Rathossi and Pontikes, 2010, gehlenite is formed by the reaction between illite, calcite and quartz as follows:

Illite                      calcite      quartz      gehlenite      sanidine



In Jg950, other phases such as anorthite appear, while illite disappears. The quartz concentration decreases and high temperature phases (gehlenite, wollastonite, diopside, hematite) are detected in larger amounts than in J950. The addition of glass seems to cause the reactions between the mineral phases to happen earlier. As a result, phases typical of higher firing temperatures begin to appear earlier in the samples with added glass than in the samples made without it (Crespo-López and Cultrone, 2022). In G950, the illite and quartz content is lower. There is a negligible difference in the mineralogy between the bricks made with added glass (Gg950) and those made without it (G950). Mullite diffraction peaks are more intense in phyllosilicate-rich samples (Guadix) than in carbonate-rich samples (Jun).



At 1100 °C, the changes in the mineralogy produced by the addition of glass are even more distinguishable (Fig.IB-4). In the bricks made with clay from Jun, the sample fired at 1100 °C without glass (J1000) is mineralogically very similar to the sample fired at 950 °C with glass (Jg950). The two samples have very similar hematite content. The amount of gehlenite decreases in J1100 and disappears completely in Jg1100, as it is involved in the formation of anorthite and wollastonite + diopside (Capel et al., 1985; Cultrone and Carrillo Rosua, 2020). In Jg1100, the increase in background noise indicates a larger amount of amorphous phase due to the vitrification of the bricks. This could be due to the fact that, with an increase in firing temperature and vitrification, the silica content of the quartz starts converting into amorphous silica, so adding to the amorphous silica already present in the glass (Galvao et al., 2015). However, in the samples in which household glass, an amorphous material, is present, the background noise is more noticeable. In the samples made with clay from Guadix fired at 1100 °C, there is little difference in mineralogical terms between the samples made with (Gg1100) or without added glass (G1100) and there is less background noise than in the Jun samples fired at the same temperature.

### 3.2.2. *Assessment of aesthetic properties*

#### 3.2.2.1. Videomicroscopy and colour measurement

The colour of the bricks after firing will depend on the composition of the raw materials and the degree of transformation of the bricks during the firing process, which in turn is mainly dependent on the temperature, time and oxidant-redox environment inside the oven (Rathossi and Pontikes, 2010; Bautista- Marín et al., 2021).

The bricks fired at low temperatures (800 °C), with or without added glass, had a reddish appearance (Fig.IB-5). However, as the firing temperature increased, the difference in colour between the bricks made with clay from Jun and Guadix became more evident. In the bricks fired at 950 °C, a considerable difference in colour can be observed between those made with added glass and those made without it. This may also be due to an apparently higher porosity in the samples fired at higher temperatures. In addition, from 950 °C onwards, “glass bubbles” began to form on the surface of the bricks. These were more evident in the samples made with clay from Guadix (Fig.IB-5).

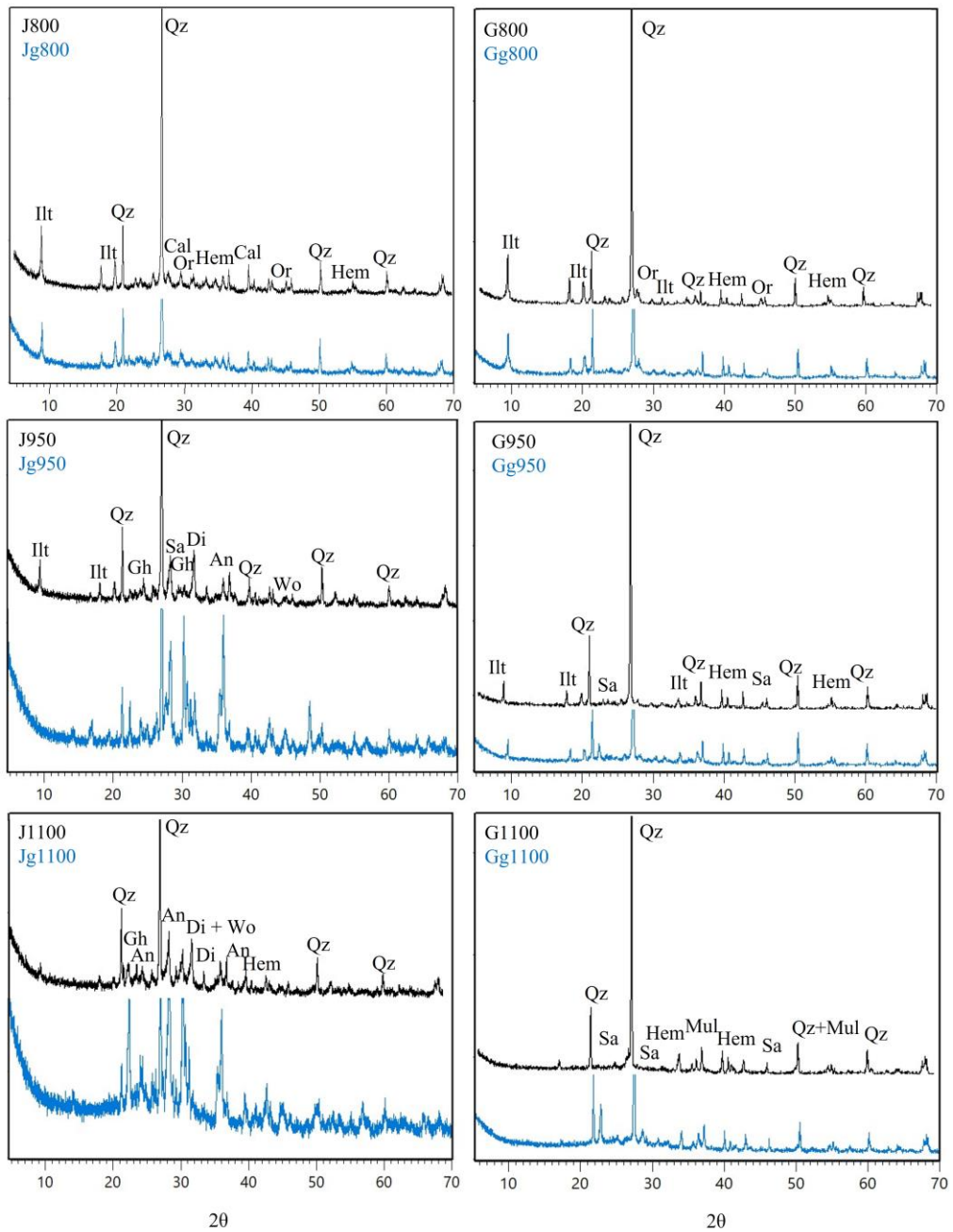


**Figure IB-4.** Mineralogy of the bricks made with clay from Jun (left) and Guadix (right) with and without glass added and fired at different temperatures. Legend according to Warr (2020): Qz = quartz; Cal = calcite; Ilt = illite; Hem = hematite; Sa = sanidine; Or = orthoclase; An = anorthite; Mul = mullite; Gh = gehlenite; Di = diopside; Wo = wollastonite.

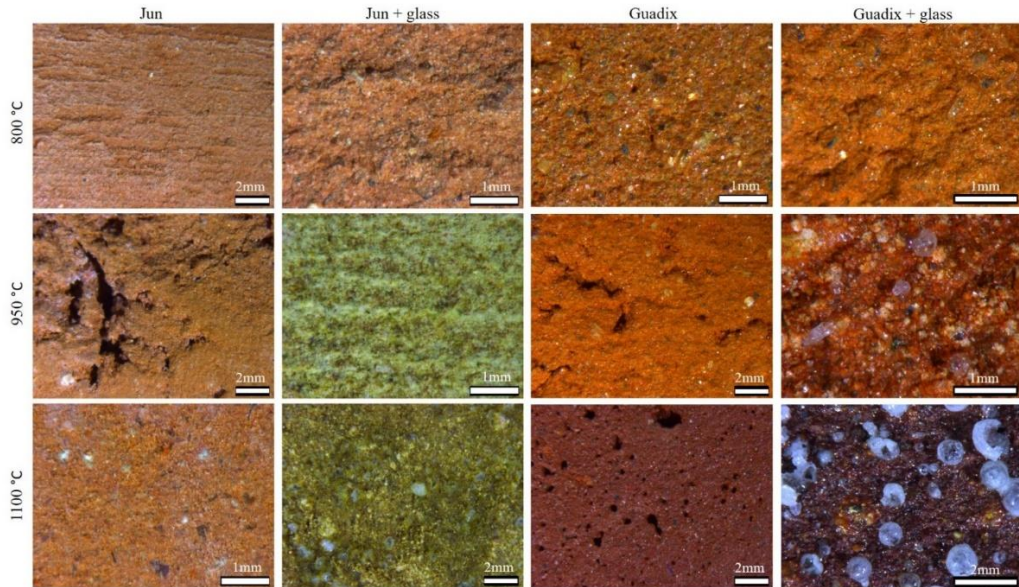


**Figure IB-5.** Macroscopic features of the bricks from Jun (J, first and second columns) and Guadix (G, third and fourth columns) fired at 800, 950 and 1100 °C, with or without added glass (g).

The lightness in the bricks from Jun increases in line with the firing temperature ( $L^*$ , table IB-2). The opposite occurs in the Guadix bricks, where a decreasing trend can be observed in average lightness values as the firing temperature increases ( $L^*$ , Table IB-2). The average lightness values for the samples with added glass follow a similar pattern to those for the samples without additive, with Jun bricks showing increasing  $L^*$  values and Guadix bricks showing the opposite tendency. This is probably due to the fact that there are more glass bubbles on the surface of the Guadix bricks, which makes them slightly darker (Fig. IB-5).

The  $a^*$  values show a similar trend for both types of bricks. The average values fall as temperature increases, more steeply in the samples with added glass than in those without it, which show a gentler decline. The samples with the lowest  $b^*$  values are those fired at high temperature with added glass (Gg1100). The samples from Guadix have a more reddish colour than those from Jun with higher  $a^*$  and  $b^*$  values. This is due to the crystallisation of iron oxides from the decomposition of phyllosilicates, whereas in the Jun samples, Fe is partly involved in the formation of new Ca-silicates such as gehlenite (Maniatis et al., 1983; De Bornis et al., 2017).

**Table IB-2.** Average lightness values ( $L^*$ ), chromatic values ( $a^*$  and  $b^*$ ) and standard deviation ( $\sigma$ ) for handmade bricks made with clay from Jun and Guadix with or without added glass.

		$L^*$		$a^*$		$b^*$	
		$\bar{x}$	$\sigma$	$\bar{x}$	$\sigma$	$\bar{x}$	$\sigma$
JUN	J800	58.49	3.11	16.13	0.63	22.90	0.84
	J950	62.96	1.51	15.06	1.22	23.69	2.10
	J1100	62.74	1.43	15.34	1.22	23.02	0.76
	Jg800	59.75	1.05	17.03	0.86	23.83	1.69
	Jg950	73.55	2.50	5.87	0.95	23.35	0.90
	Jg1100	63.01	8.20	6.33	1.03	22.83	1.41
GUADIX	G800	55.01	1.32	21.04	0.95	29.55	1.31
	G950	55.18	2.85	23.70	1.03	31.38	1.16
	G1100	44.12	1.49	20.61	1.66	19.23	2.17
	Gg800	53.26	1.64	21.87	0.93	29.82	1.21
	Gg950	52.00	2.57	22.59	0.97	27.99	2.14
	Gg1100	45.14	1.73	12.17	4.12	10.82	3.35

Figure IB-6 shows a volume chart diagram for the  $L^*$  and  $a^*$  parameters. The  $b^*$  parameter was not included in Figure IB-6 because the  $a^*$  values indicate the red/green coordinates (+a indicates red, -a indicates green), the most important parameters in the colour analysis of bricks, which normally have a reddish hue.

Bricks made with both types of clay fired at 800 °C have similar mean  $L$  and  $a^*$  values and a similarly low standard deviation, regardless of whether or not they have added glass. From 950 °C onwards, the samples follow similar trends depending on the composition of the raw material. While the bricks from Jun show greater dispersion, those from Guadix are more homogeneous. This difference in the dispersion values continues at 1100 °C, where the samples from Jun with added glass (Jg1100) have very high (and dispersed) lightness values compared to those from Guadix. This could be related to the fact that the addition of glass gives the Jun bricks fired at 1100 °C a more yellowish colour than the Guadix bricks, which have an intense red tone (Fig. IB-6). This could also explain the very high  $a^*$  values in G1100 and Gg1100.

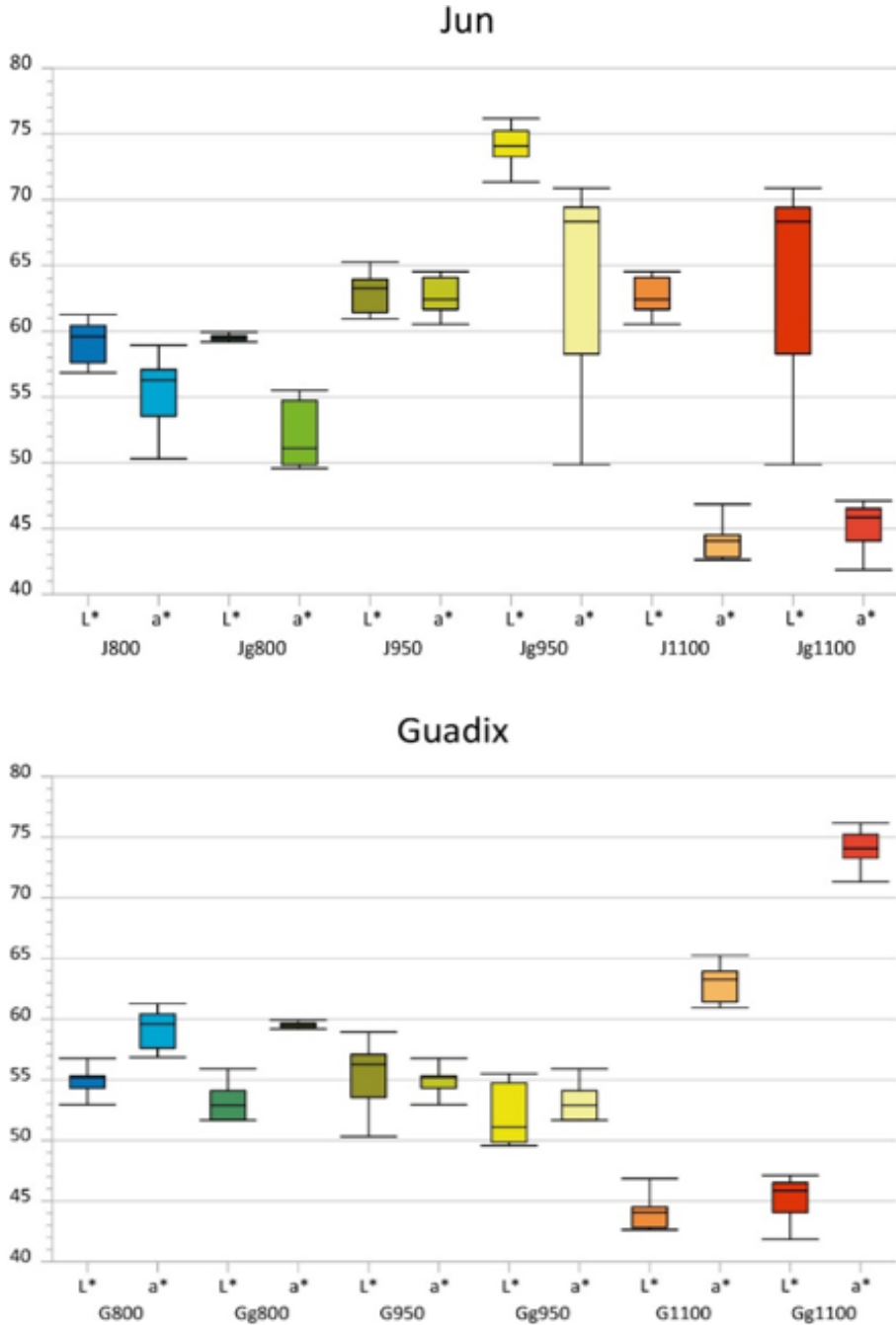


**Figure IB-6.** Volume chart showing the lightness (L\*) and a\* values for bricks made with or without glass and fired at 800, 950 and 1100 °C.

### 3.2.2.2. Radiography

The bricks with added household glass fired at higher temperatures have the highest densities. Figure IB-7 shows brick cubes with two types of images, grey scale (original) and green-red variation, the latter highlighting the denser areas of the samples. The contrast makes it easier to observe the density difference between the bricks. The highest density is reached at the edges and decreases as we move inwards towards the core, as firing takes effect from the outside-in.

Jun samples made with added glass and fired at 950 °C and 1100 °C (Jg950 and Jg1100) show similar contrast intensity, which suggests that they have similar densities. However, Guadix samples with glass fired at 1100 °C are quite similar to Jun samples with glass fired at 800 °C. In addition, there is hardly any difference between the samples from Guadix fired at 800 and 950 °C. Radiography images suggest that, as firing temperature increases, a more or less (depending on the composition of bricks) vitreous phase develops, which increases the compactness (Cultrone et al., 2004).

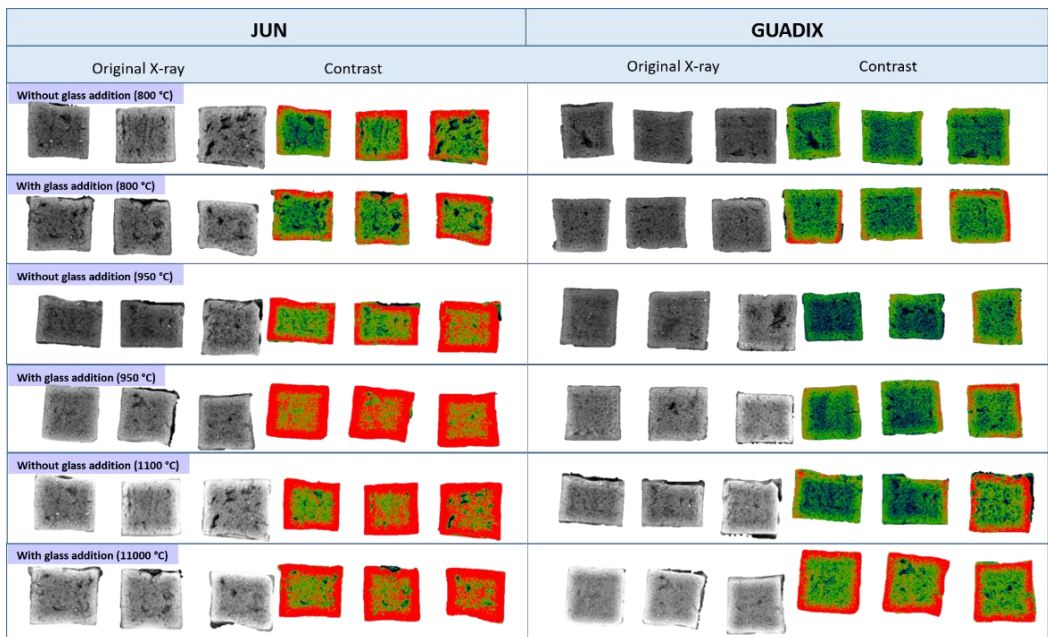


**Figure IB-7.** X-rays of the bricks made with clay from Jun and Guadix with or without added glass and fired at 800, 950 and 1100 °C.

### 3.2.3. Assessment of mechanical properties

#### 3.2.3.1. Leeb hardness (LH) test

The hardness test results coincide with those of radiography (Fig.IB-7). Figure IB-8 shows that the highest hardness values are observed on the surfaces and that they decrease towards the inside of the brick. This hardness is associated with higher density, i.e. the greater compactness of the bricks in these areas.

The bricks with added glass fired at 800 °C show similar hardness values (average values Jg800, 258 and Gg800, 267, respectively). This suggests that at 800 °C the glass is not yet acting as a flux agent and is not vitrifying the samples. Higher hardness values were obtained at 950 °C, especially in the bricks with added glass (average values of 304 in Jun and 272 in Guadix). The samples with the highest hardness values are those with added glass fired at 1100 °C (Jg1100 and Gg1100 with 449 and 393, respectively) (Fig.IB-8).

In the bricks made with clay from Guadix, the difference in hardness between the surface and the core increases by approximately 10% when household glass is added, regardless of the firing temperature. This is not so evident in the bricks from Jun for which a similar percentage difference between surface and core hardness to that of the Guadix bricks can only be observed at 1100 °C. This different behaviour of Jun bricks may be due to the fact that more energy is consumed during the formation of Ca-(Mg-) silicate phases (Cultrone et al., 2001).

#### 3.2.3.2. Ultrasonic pulse velocity (UPV)

Table IB-3 shows the UPV values measured in the bricks with or without added glass. The preferential orientation of the phyllosilicates and other planar grains during the preparation of the raw material was perpendicular to the pressure that was exerted on the clayey earth when it was placed in the moulds. The P waves move more slowly perpendicular to these grains.

The UPV of the brick samples with added glass ranges between 1368 (Gg800) and 4625 m/s (Jg1100) (Table IB-3). A tendency towards lower velocity values was observed in the samples with no added glass, and the lowest was measured in sample G800 (Table IB-3, 1260 m/s). For bricks to be considered durable, the UPV value should be at least 1000 m/s (Hei et al., 2003). This means that all the studied bricks studied here can be defined

as durable. UPV values increase not only with the addition of glass but also in line with increases in the firing temperature.

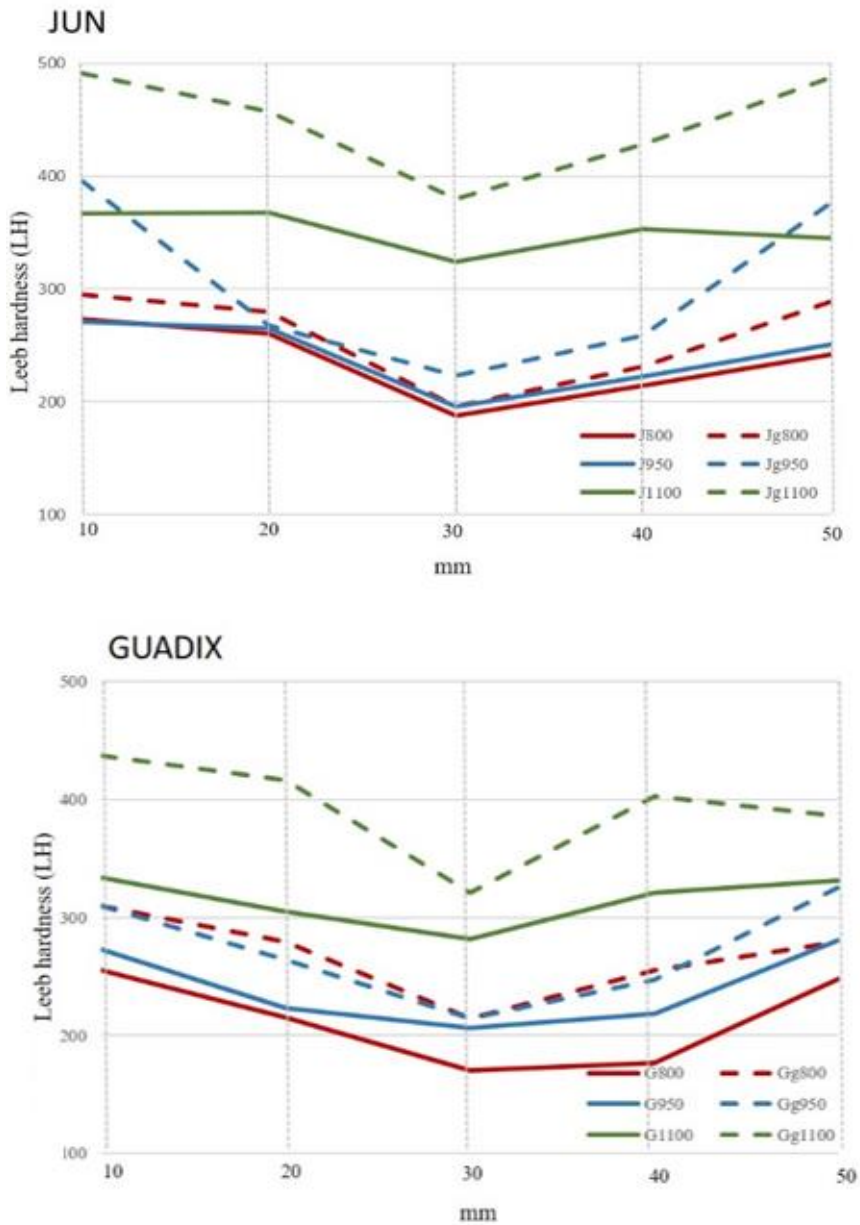


**Figure IB-8.** Hardness (in LH) of bricks made with raw materials from Jun and Guadix with or without added glass and fired at 800, 950 and 1100 °C.



### 3.2.3.3. Compressive strength (CS)

The bricks made with clay from Jun, with or without added glass, showed higher compressive strength than those from Guadix (Table IB-3). In mineralogical terms, Changizi and Haddad (2015) found that the compressive strength of bricks increases with the amount of quartz in the mix. However, if one looks at the mineralogy of the bricks from Jun and Guadix, the opposite applies: the bricks from Guadix are richer in quartz than those from Jun. In this case, the previous analyses show that the increase in compressive strength is related to the higher levels of vitrification produced by the addition of household glass (Crespo-López and Cultrone, 2022). In fact, the addition of glass always increases the strength of the bricks (Table IB-3). This increase is related to the textural and microstructural changes that take place in the bricks. As mentioned earlier, the glass acts as a flux agent bonding the particles together and reducing the porosity. The highest values were found for bricks fired at 1100 °C, due to their high level of vitrification. The sample with the highest compressive strength was Jg1100 (72.58 N/mm<sup>2</sup>).

Several authors have found that the compressive strength of bricks is more closely linked to the porosity and the degree of vitrification than to the mineralogy of the raw material (Dan et al., 1986; Elert et al., 2003; Cultrone et al., 2004; Changizi et al., 2015; Hei et al., 2023). Tite and Maniatis (1975) found that in bricks made with carbonate-rich clays, the structure formed at low temperatures (840-960 °C) remains almost unchanged until about 1080 °C. This is why the Jun samples (without added glass) fired at 800 and 950 °C show very similar CS values (Table IB-3 and Fig. IB-9). According to official specifications from the Spanish Ministry of Public Works (Pliego RL-88, 1988), all the samples, with the exception of G800, have enough compressive strength to be used for construction purposes.

In contrast to pore-forming additives, such as cigarette butts (Kadir and Mohajerani, 2015; Mohajerani et al., 2016) wood sawdust (Cultrone et al., 2020) or grape stalks (Coletti et al., 2023; Crespo-López et al., 2023c), or tea waste (Crespo-López et al., 2024), the addition of glass improves the mechanical properties of the bricks.

**Table IB-3.** Summary of average values ( $\bar{x}$ ) for LH, UPV (m/s) and CS (Rc, MPa) and standard deviation ( $\sigma$ ) values for handmade bricks made with raw materials from Jun and Guadix with or without added glass.

	LH		UPV (m/s)		CS (MPa)	
	$\bar{x}$	$\sigma$	$\bar{x}V$	$\sigma$	$\bar{x}$	$\sigma$
J800	235	34.52	2667	87.71	19.18	5.09
J950	241	31.47	2650	143.73	20.23	8.15
J1100	351	18.12	2952	67.13	26.56	3.28
Jg800	258	42.97	2922	105.71	31.39	4.11
Jg950	304	76.70	2905	169.38	26.84	12.98
Jg1100	449	46.02	4625	250.51	72.58	5.07
G800	213	39.17	1260	59.83	6.43	0.34
G950	240	34.27	1853	191.39	12.34	3.15
G1100	315	21.45	2726	149.36	29.05	9.2
Gg800	267	35.67	1368	51.99	8.88	2.54
Gg950	272	45.86	2018	126.38	17.35	1.02
Gg1100	393	44.15	3346	200.92	35.28	15.03

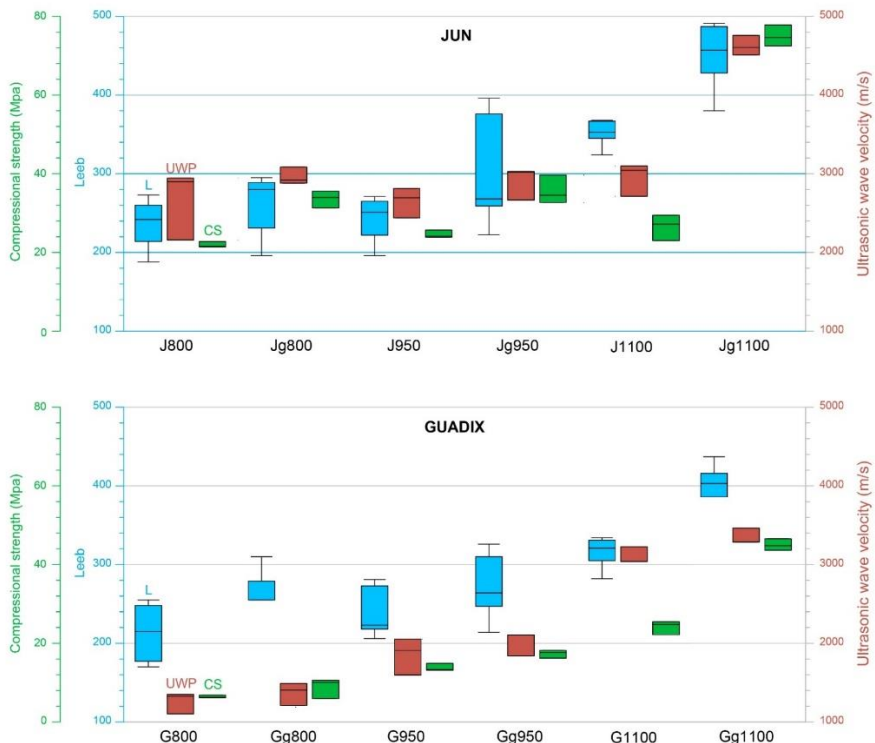


**Figure IB-9.** Volume chart showing the LH, UPV and CS values for bricks made with or without added glass and fired at 800, 950 and 1100 °C.

#### 4. Statistical analysis

The statistical analysis in this paper seeks to apply Tukey and Duncan's test ( $P < 5\%$ ) to predict homogeneous subsets for the lightness ( $L^*$ ) and chromatic values ( $a^*$ ) taking into account the three firing temperatures for the same data population. The two types of clay (Jun and Guadix) and the addition or not of household glass were not considered because there are only two variables per type and this method requires at least three.

Three subsets (a, b and c) for  $L^*$  and  $a^*$  and two subsets (a and b) for  $b^*$  were classified (Table IB-4). According to this method, there is a direct relationship between the lightness of the samples and the firing temperature, with higher temperature samples having higher lightness values. The average values for the bricks from Jun suggest that they follow this trend, while those from Guadix do not. This method also suggests that  $a^*$  values increase in line with firing temperature. This was true for the Guadix bricks but not for those from Jun. This suggests that this method was unsuitable in that the properties of the bricks could not be determined solely on the basis of the firing temperature. The different combinations of clay with or without added glass might change the appearance of the bricks, a crucial issue in the restoration of architectural heritage.

The relationships between the mechanical properties determined by NDT, namely superficial hardness (Leeb), UPV and compressive strength (Table IB-4), were also explored. The study of the anisotropy enabled the correlation of the ultrasonic velocities with the microstructure (especially the pores/voids) of the samples in order to better understand the technical quality of the bricks, which is associated with the concept of anisotropic resistance. Homogeneous subsets were obtained according to Tukey and Duncan for the UPV, Leeb and compressive strength values taking into account the three firing temperatures for the same data population. These subsets were analysed and the data obtained confirmed the results of the NDT. It should be noted that for the UPV and compressive strength values, the values are divided into 3 subsets with an upward trend in line with temperature, while the Leeb values are only divided into 2 subsets. This makes it more difficult to compare the Leeb results with the results of other tests on physical-mechanical properties, such as UPV and compressive strength. Even so, this predictive method could be very useful for determining the mechanical properties.

**Table IB-4.** Classification of subsets (a, b and c) for aesthetic (L\* a\* and b\*) and physical (UPV, LH and CS) properties according to the tests proposed by Tukey and by Duncan and the ANOVA method.

	<b>L*</b>	<b>a*</b>	<b>b*</b>	<b>UPV</b>	<b>LH</b>	<b>CS</b>
800 °C	53.75a	13.61a	18.98a	2054a	244a	17.58a
950 °C	56.63b	16.94b	26.53b	2356b	264a	20.85b
1100 °C	60.92c	19.02c	26.60b	3506c	377b	42.04c
<b>ANOVA P values</b>						
Raw material (RM)	0.000	0.000	0.000	0.000	0.036	0.000
Temperature (T)	0.000	0.000	0.000	0.000	0.000	0.000
Glass added (G)	0.023	0.000	0.000	0.000	0.000	0.000
RM x T	0.000	0.000	0.000	0.000	0.300	0.001
RM x G	0.000	0.000	0.000	0.000	0.770	0.000
G x T	0.019	0.000	0.000	0.000	0.153	0.000
RM x T x G	0.000	0.000	0.000	0.000	0.454	0.000

## 5. Conclusions

In this paper, NDT were used to characterize bricks that were handmade with raw materials from two different sources, Jun and Guadix (Granada, Spain), fired at three different temperatures (800, 950 and 1100 °C), with or without added glass. The following conclusions were reached:

- The use of non-destructive techniques (NDT) revealed that the addition of glass increased the vitrification of the bricks and augmented their compressive strength.
- The colour of the bricks was mainly dependent on the type of raw material used, while the addition of household glass enhanced the lightness in the bricks made with clay from Jun and the a\* parameter in the bricks made with clay from Guadix. Firing temperatures from 950 °C produced a significant aesthetic change in the bricks, which was especially visible in the samples with added glass, where glass bubbles can be seen "hatching" on the surface of the bricks.
- Radiography proved to be a very useful tool for observing the anisotropic distribution of density in the fired samples.

- In terms of mechanical properties, the bricks from Jun perform better than those from Guadix. However, the latter have better aesthetic properties, in the sense of more homogeneous colours, which can be a key factor when choosing a building material.
- The relationship between the aesthetic and the mechanical properties determined by NDT allows the results obtained from different analytical techniques to be compared, such as the relationship between density, as determined by x-rays, and surface hardness, as determined by Leeb. In this way, the density of the bricks can be compared with the hardness, both of which are greater on the surface and decrease towards the core, thus reducing the connectivity of the pores.
- According to the statistical predictions for the dependent variables of firing temperature using the tests proposed by Tukey and by Duncan, regardless of whether they are fired with or without glass, the bricks made with clay from Jun tend to have higher mean values for all the variables than the bricks made with clay from Guadix. ANOVA analysis reveals that the clay from Jun performs better than the clay from Guadix. However, the bricks from Jun fired at 1100 °C and with added glass show the highest colour variations, which could make them less suitable for the restoration of architectural heritage, in which colour is a crucial factor.

## CHAPTER II

*Carbon fibre from wind industry for making porous bricks*

Laura Crespo-López, Chiara Coletti, Salvador Morales-Ruano, Giuseppe Cultrone

Published in *Ceramics International*

Vol. 50, 9681-9696 (2024)

DOI: 10.1016/j.ceramint.2023.12.287

*Impact Factor: 5.2*

*Position 3/29 (Q1)*

*Category: Materials Science, Ceramics (JCR 2022)*





Ceramics International

Available online 26 December 2023

In Press, Corrected Proof [?](#) What's this? [↗](#)



# Use of recycled carbon fibre as an additive in the manufacture of porous bricks more durable against salt crystallization

[Laura Crespo-López](#)<sup>a</sup>  , [Chiara Coletti](#)<sup>b</sup>, [Salvador Morales-Ruano](#)<sup>a, c</sup>,  
[Giuseppe Cultrone](#)<sup>a</sup>

**Keywords:** bricks, carbon fibre, recycling, circular economy

## 1. Introduction

The circular economy is a sustainable economic model that aims to reduce resource consumption and waste generation by promoting the long-life usage, recycling and regeneration of materials (Stahel, 2016; Geisendorf and Pietrulla, 2018). By adopting circular practices, businesses and society can achieve long-term environmental and economic benefits, increasing resource efficiency and creating new employment opportunities in green industries (Webster, 2021; Corvellec and Stowell, 2022). Great efforts are currently being made to achieve sustainable development, inspired by the challenges outlined in the United Nations 2030 Agenda (Sustainable Development

Goals- SDG) (UN General Assembly, (<https://refworld.org>) in spite of these efforts, the Circularity Gap Report 2023 (<https://qwec.net>) reveals that the global economy is still only 7.2% circular. It is therefore necessary for each economic sector to assess how circularity can best be achieved. Within the construction sector, one option that is currently being explored is the use of alternative and/or local raw materials in the manufacture of building materials. To this end, Gencel et al. (2021a and b), Crespo-López and Cultrone (2022), Er et al. (2022), and Erdogmus et al. (2023) have recently studied the use of inorganic residues such as industrial slags, water treatment slag, household glass and metallurgical wastes as additives in brick production. These additives modify certain physical properties of the fired bricks (above all, porosity, mechanical strength and durability). The aim of this paper is to support the brick industry in its search for suitable alternative raw materials that can be used in the manufacture of bricks, so reducing the amount of clay required. In this case, the study focuses on the carbon fibre waste from decommissioned wind turbine blades. In line with the SDG challenges (in particular SDG 12, “Responsible Consumption and Production” which has the most targets specifically addressing waste management), there are two main objectives, namely to reduce the demand and therefore the extraction of natural resources and to reuse and recycle as raw materials the waste produced by other anthropogenic activities. Successful application of alternative raw materials of this kind would also have socioeconomic benefits in terms of cost savings.

Wind is a competitive, clean energy source and its industry is booming. If the wind targets set out in REPowerEU (2022) (<https://commission.europa.eu/>), the EU's energy security strategy, are successfully met, a massive 65 billion cubic meters of gas could be saved. Apart from reducing greenhouse gas emissions (GHG), this would also make Europe self-sufficient in terms of energy production and less reliant on imported fossil fuels. Wind is an increasingly stable form of power supply. New onshore wind farms now operate at capacity factors of 30-45%, and new offshore wind farms at 50% (Arshad and O`Kelly, 2019; Council, 2020). Wind power does not emit any CO<sub>2</sub>, SO<sub>x</sub>, NO<sub>x</sub>, or metal particles (Kalair et al., 2021). It emits ~95% less CO<sub>2</sub> than gas-based electricity production and ~98% less CO<sub>2</sub> than coal-based production (Higuchi et al., 2014) and consumes very little water. Wind meets 15% of electricity demand in the EU as a whole and much more in certain countries: Denmark 44%; Ireland 31%; Portugal 26%; Spain 24%, and Germany 23% (Ruska and Kiviluoma, 2011; González and Lacal-Arántegui, 2016; Bórawski et al., 2020). The International Energy Agency (IEA, <https://www.iea.org>) expects wind to be



the first source of power in Europe by 2027. The standard lifetime of a wind farm is around 20-25 years (Lecomte et al., 2017). When wind turbines reach the end of their life, project developers must take them down and restore the site to its pre-existing condition. According to WindEurope 2021 (<https://windeurope.org/>), the European Wind Energy Association (EWEA, 2013) (<https://www.ewea.org/>) and Recycling International (<https://recyclinginternational.com/>), around 14,000 blades may have to be dismantled across the continent in the next five years, which would create between 40,000 and 60,000 tonnes of waste.

Wind-turbine blades are typically composed of several materials, including glass fibre, carbon fibre, carbon/glass (hybrid) fibre, reinforced polymer composites and foam. The exact combination of materials used in wind turbine blades may vary depending on the manufacturer and the wind turbine model (Rani et al., 2021). Carbon fibre is the typical material used in the blades on the larger, higher-capacity turbines (Song et al., 2022). It is known for its high strength, stiffness and durability, making it an ideal material to support the load and stress experienced by blades during operation (Mishnaevsky et al., 2017). Another benefit is that it is lighter than other materials, so ensuring that the blades are lighter and more energy-efficient (Thomas and Ramachandra, 2018; Kalkanis et al., 2019). The use of carbon fibre also allows longer blades to be made, which increases the amount of energy that can be produced with each turn of the turbine (Hao et al., 2020). Although carbon fibre is expensive, its use as the raw material in wind turbine blades can lead to increased efficiency and durability of the turbines, so reducing long-term maintenance and operating costs (Albers et al., 2009). The wind industry has committed to recycling or recovering 100% of decommissioned wind turbines by 2025 and work is currently underway to boost recycling through different technologies, e.g. mechanical recycling, which involves shredding materials so that they can be reused for example as filler material in building materials or plastics; thermal recycling, which entails incinerating the blades to break down the composites, producing energy in the process; or chemical recycling, which uses solvents and thermal processes to separate the resins from the fibres so that both materials can be reused (Mishnaevsky et al., 2017; Sanjay et al., 2018; Rani et al., 2021). In this regard, the construction industry can play an important role in the recycling of these blades, by promoting the production of new materials. Yazdanbakhsh et al., 2018 investigated the addition of 5 to 10% volume of slender elements from wind turbine blades (known as “needles”) to a concrete mix. Results

revealed no negative effects on the steadiness or workability of the new concrete or on its tensile, compressive and flexural strength.

This paper aims to offer the wind industry a new perspective on blade waste recycling by using this residue as an additive in the production of bricks. It could also provide an opportunity for the brick industry to test the feasibility of using carbon fibres in the manufacture of what could potentially be high-performance materials. Carbon fibre is very light, so transport costs would be lower than with traditional bricks, and its use in the brick production process would provide direct benefits for the environment by reducing the depletion of clayey soils, which are non-renewable natural resources (Dabaieh, 2020; Dabaieh et al., 2020).

This paper breaks new ground in the brick industry sector, because although there have been studies that investigated the addition of carbon fibre to concrete for the construction of structural elements such as beams and columns (Babatunde, 2017; Vega and Torres, 2018; Krosomer et al., 2019), no specific research has been conducted on the reuse of carbon fibre from wind turbine blades in brick manufacture. With this in mind, the aim of this research is to produce a new type of brick which i) is environmentally friendly, ii) uses fewer raw materials, iii) contributes to the elimination of waste and iv) meets the relevant standards in terms of its physical-mechanical properties for use in the construction industry.

## **2. Materials and Method**

### **2.1. Geological context and supply of raw materials**

Bricks were made by mixing clayey materials from Viznar and Guadix (Granada, Spain). In geological terms, Viznar is part of the Granada basin, while Guadix belongs to the Guadix basin. Both basins are part of the central area of the Betic Cordillera. The clayey material from Guadix was deposited in the Middle-Late Pleistocene during the last stages of basin infilling, while the clay from Viznar was deposited during the late Turolian in a lacustrine environment with alluvial sediments (conglomerates and sands), deltaic sediments, small calcarenitic platforms and other minor materials from Sierra Nevada and Sierra Arana (García-Alix et al., 2008).

This work was carried out in partnership with the company Tesela, Materiales, Innovación y Patrimonio S.L. (Granada, Spain), who supplied carbon fibre powder (CF) from the

blades of decommissioned wind turbines from wind-farms in Spain, and with the brick manufacturer Cerámica Castillo Siles (Granada, Spain), who supplied the clayey materials.

## 2.2. Traditional brick production

In this study, the bricks were made using a mixture of clayey materials from Viznar and Guadix in proportions of 3/5 and 2/5 by weight, respectively. These proportions were chosen on the recommendation of the brick manufacturer who supplied the raw materials, because in his experience they produced the most workable mix and the best-quality end products. Figure II-S1 shows the different steps in the brickmaking process. Several kilograms of the two clayey materials from Viznar and Guadix were removed from piles of clay in the brick factory using a shovel. All coarse rock fragments and plant roots were discarded. Once in the laboratory, the clayey materials were sieved and fragments of over 1.5 mm in size were removed. The two types of clay were then mixed together in the proportions mentioned above. With a view to using as much residue as possible without affecting the workability of the clay mixture, and as there was no previous bibliography to follow, it was decided to use 5 and 10 wt.% of carbon fibre powder (CF). With higher amounts of carbon fibre, the clayey mass became less workable. The addition of carbon fibre means that less clay is required to produce the bricks (Table II-S1). The maximum amount of added CF was set at 10 wt.%, given that as CF is a very lightweight material in relation to its volume, the addition of over 10 wt.% CF could have prevented the residue from mixing properly with the clayey earth. The clay and CF mixtures were then mixed with water and moulded in moistened wooden moulds of 15 × 20 × 4 cm (Fig.II-S1 A and II-S1B). Table II-S1 shows the proportions of clayey material, carbon fibre powder (by weight percentage, wt.%) and water used in each mix design. A control group (CF0) of bricks with no added carbon fibre powder was also prepared.

Moulds were removed after one hour and the clayey pastes were cut into ~ 4 cm edge cubes using a stretched cotton thread and left to dry (Fig.II-S1C). Once the samples had dried, they were fired in a Herotec CR-35 electric oven at 800, 950 and 1100 °C (Fig.II-S1C). These three temperatures were selected on the following basis. The intermediate temperature (950 °C) was chosen because it is one of the most commonly used in the brick industry (the brick manufacturer who provided the raw materials fires his bricks at this temperature). The other two were chosen to enable the analysis of the mineralogical,

textural, physical and durability changes in the bricks with and without added CF over a range of 300 °C. Table II-S2 offers a summary of the samples analysed in this paper. The temperature inside the oven was initially kept constant for 1 hour at 100 °C to eliminate any residual moisture in the samples. Then, the temperature was increased at a rate of 2 °C/min (heating). Once the desired temperature had been reached, the oven was kept at a constant temperature for 3 hours (soaking). Finally, it was turned off and the samples were left to cool slowly (cooling). They were not removed from the oven until the next day. After removal from the oven, the bricks were immersed in water for about 1 hour to prevent possible “lime blowing” due to the presence of lime grains (Laird and Worcester, 1956).

### 2.3. Analytical techniques

#### *2.3.1. Chemistry, mineralogy and texture of the raw materials and fired bricks*

The granulometry of the raw material and of the CF was determined using a Galai CIS-1 laser gauge that uses laser diffraction to measure the range of the particles after 10 s sonication in water over a 0.02 - 1500 µm range. The thermal decomposition of the clayey material up to 950 °C was carried out using a METTLER-TOLEDO TGA/DSC1 thermogravimetric analyser coupled with differential scanning calorimetry (TG-DSC). About 20 mg of sample was deposited on an Al crucible and analysed in a flowing air atmosphere (50 ml/min) at a heating rate of 20 °C/min. The components of the carbon fibre in the IR spectrum were identified using a Fourier transform infrared spectroscopy with an attenuated total reflectance sample holder (ATR-FTIR), in a frequency range of 4000-400 cm<sup>-1</sup> and with a step size of 0.50 cm<sup>-1</sup>. X-ray fluorescence (XRF) was used to determine the major elements in the clayey material and in the CF with a PANalytical Zetium compact spectrometer with an Rh anode and a 4 kV X-ray generator. 5 g per sample were milled to powder in an agate mortar and then analysed. The Loss On Ignition (LOI) was determined by burning the samples at 1000 °C for one hour. The mineralogical composition of the raw material and the fired bricks was determined by powder X-ray diffraction (PXRD) using a PANalytical X'Pert PRO diffractometer. The working conditions were as follows: CuK $\alpha$  radiation, 45 kV voltage, 40 mA current, 3 to 70° 2 $\theta$  exploration range, 0.1 2 $\theta$  s<sup>-1</sup> goniometer speed. Mineral phase identification was first performed using the PANalytical X'pert Highscore Plus 3.0 software, matching the experimental diffraction peaks with those from the Joint Committee for Powder Diffraction

Standards (JCPDS) PDF-2 database. Quantitative estimations were also performed by adding 10 wt.% internal standard  $\alpha$ -Al<sub>2</sub>O<sub>3</sub> to the powder samples and detecting the peaks using open-source Profex-BGMN software, which has dedicated fitting functions (Tsipursky and Drits, 1984; Taut et al., 1998; Ufer et al., 2004; Dobelin and Kleeberg, 2015) for Rietveld refinements (Rietveld, 1969). The goodness-of-fit of the refinements (GoF) were between 1.68 and 1.87.

The petrographic features of the fired bricks were observed by means of polarized optical microscopy (POM). Observations under plane- and cross-polarized light were carried out on polished thin sections using a Carl Zeiss Jenapol-U microscope equipped with a Nikon D7000 digital camera. Detailed observations of the morphology of the carbon fibres and of the texture, pore morphology and degree of vitrification of the fired bricks were made using a high-resolution field emission scanning electron microscope (FESEM) Carl Zeiss SMT (AURIGA series) coupled with energy dispersive X-ray analysis (EDS). The carbon fibres and brick fragments were carbon-coated prior to their observation under FESEM.

### 2.3.2. *The pore system of the bricks*

The pore system of the fired bricks was investigated using hydric and porosimetric tests (Table II-S3). To this end, free (Ab, at atmospheric pressure (UNE-EN 13755, 2008) and forced (Af, under vacuum) water absorption and drying tests (Di, NORMAL 19/88, 1988) were carried out (according to the relevant standards, see Table II-S3). These tests enabled us to determine the degree of pore interconnectivity (Ax), the capillary rise (C) (UNE-EN 1926, 2007), the saturation coefficient (S) (RILEM, 1980), the apparent ( $\rho_a$ ) and real ( $\rho_r$ ) densities and the open porosity (Po) (Equations 1-9, Table II-S3) (UNE-EN 1936, 2007); ISRM, 1979). Hydric tests were performed under controlled thermo-hygrometric conditions (20 °C and 60% RH) using deionized water. Three samples per brick (~ 4 cm edge cube) group were analysed.

The pore system of the bricks within a range of 0.002 to 200  $\mu$ m was analysed by mercury intrusion porosimetry (MIP) using a Micromeritics Autopore V 9600 porosimeter with a mercury-brick contact angle of 130°. Open porosity ( $P_{oMIP}$ ) (Equations 6, Table II-S3) and specific surface area (SSA) were calculated.

### 2.3.3. *Durability of the bricks*

Fifteen salt crystallization cycles were performed to assess a theoretical degradation that could affect the lifetime of the bricks according to the UNE-EN 12370 (2020) standard. This test reproduces the decay that the bricks may undergo due to the dissolution and recrystallization of soluble salts within their porous systems. Three samples per brick type were used for this test.

#### 2.3.4. *Mechanical behaviour (Cs)*

In the analysis of compressive strength (Cs), three samples measuring 1.5 x 1.5 x 6 cm were tested for each brick type (Equation 10, Table II-S3) (UNE-EN 196-1, 2005)). The compressive strength of these samples was measured using a Controls Uniframe T1192 electromechanical universal tester, equipped with 100 kN and 25 kN load cells and a loading rate 0.6 of mm/min. This device was specially designed for measuring the compressive strength of small bricks.

#### 2.3.5. *The compactness of the bricks*

The ultrasound propagation velocity of compressional ( $V_p$ ) and shear ( $V_s$ ) waves was measured with a Panametrics HV Pulser/Receiver 5058PR coupled with a Tektronix TDS 3012B oscilloscope. It was measured in accordance with the ASTM D2845 (2000) (Equations 11, Table II-S3) standard for dry test samples using transducers of 1 MHz. These data were used to obtain information on the compactness of the bricks. A viscoelastic gel was applied to ensure good coupling between the transducers and the brick samples.  $V_p$  and  $V_s$  were measured in the three perpendicular directions on cubic samples. Once the ultrasound velocities had been determined, total anisotropy ( $\Delta M$ ), the Poisson coefficient ( $\nu$ ) and the Young (E), Shear (G) and Bulk (K) moduli were calculated (Equations 12-15, Table II-S3).

The Leeb Hardness (LH) tester PCE-2500N was used to measure the surface hardness of the bricks using a rebound hammer. Ten linear measurements were made from one edge of each brick to the opposite side passing through the centre. The harder the surface of the material, the higher the rebound velocity (Crespo-López et al., 2023a).

#### 2.3.6. *Colour*

Colour measurements were performed to quantify the lightness ( $L^*$ ) and chromatic coordinates ( $a^*$  and  $b^*$ ) of the fired bricks (UNE-EN 15886, 2011). A Konica Minolta CM-

700d spectrophotometer was used. Illuminant D65, 10° observer angle and 8 mm measurement area were used. Nine measurements per sample were performed. The total colour variation ( $\Delta E$ ) between the control bricks and those with added CF was calculated (Equation 16, Table II-S3).

### **3. Results and discussion**

#### **3.1. Grain size distribution, thermogravimetry and chemistry of the clayey material and CF**

The granulometric analysis shows that the clayey material has a unimodal particle size distribution with a maximum peak at 23.2  $\mu\text{m}$  (Fig.II-1A). As expected, the carbon fibre (CF) curve has a shorter size distribution compared to the clayey material. This curve is bimodal, although there is a dominant maximum peak at 14.1  $\mu\text{m}$  and a smaller one at 102.5  $\mu\text{m}$ .

Thermal analysis of the clayey material (Fig.II-1B) shows a weight loss of 5% at 86 °C due to the loss of hygroscopic water (Maritan et al., 2006). At 297 °C there is an inflection in the curve corresponding to the combustion of organic matter (Labus, 2017; Fernández et al., 2012).

At ~ 500°C, a gradual dehydroxylation of the phyllosilicates begins to occur, which continues up to 711 °C (Cultrone et al., 2001; Coquelle, 2014). Between 711 °C and 800 °C, the main weight loss of around 13% occurs. This is linked to the decomposition of carbonates and the release of CO<sub>2</sub> (Rodríguez-Navarro et al., 2009 and 2012; Coquelle, 2014). The clayey material starts losing weight again at ~ 840 °C, probably due to further dehydroxylation of the phyllosilicates (Cultrone et al., 2004; Hirono and Tanikawa, 2011; Heller-Kallai and Lapidés, 2015). Finally, an exothermic peak is observed at 925 °C due to the formation of new crystalline phases, which will later be identified using PXRD analysis.

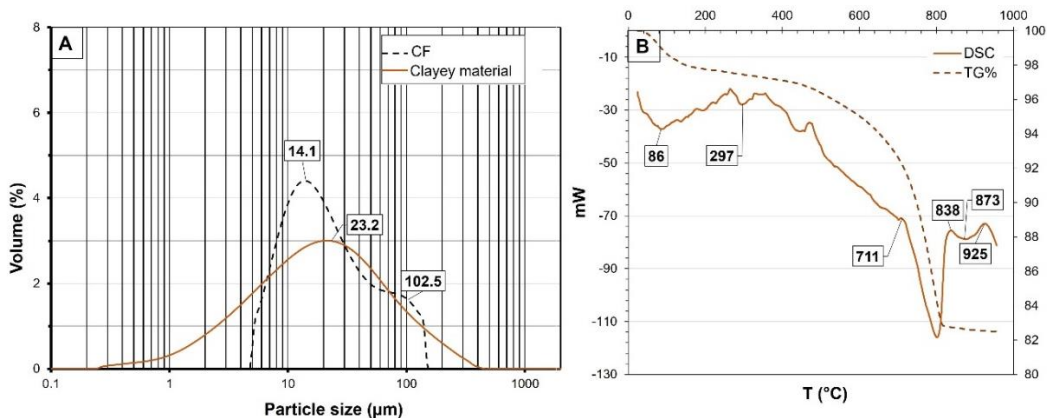


**Figure II-1.** Grain size distribution of the raw materials (clayey material and carbon fibre, CF) (A) and TG-DSC analysis of the clayey material (B). A) Particle size (in  $\mu\text{m}$ ) vs. volume (in %). B) Temperature (in  $^{\circ}\text{C}$ ) vs. weight loss (right ordinate, in %) and differential scanning calorimetry (left ordinate, in mW).

The IR spectrum obtained from the carbon fibre was compared with other spectra reported in the literature. Table II-1 shows a summary of the bands identified, their attribution and references. The IR spectrum revealed that at some earlier stage the carbon fibre had been carbonised at a temperature of approximately  $850^{\circ}\text{C}$  (Boccaro et al., 1997; Shin et al., 1997; Hanna et al., 2012), probably in order to make the blades stronger and more durable. Figure II-2 illustrates the infrared spectra of the carbon fibres, where the larger and thinner bands in the range  $1300\text{--}1800\text{ cm}^{-1}$  show a chaotic trend due to the presence of several compounds together with the carbon fibre. A peak at  $1730\text{ cm}^{-1}$  was evidence of the ester (arachidyl dodecanoate) functional group (Sellitti et al., 1990). Ketone and carboxylic acid  $\text{C}=\text{O}$  peaks were centred at  $1705\text{ cm}^{-1}$  (Starsinic et al., 1983). The peak of benzoic acid was present at a lower wavenumber,  $1640\text{ cm}^{-1}$ , probably because of the aromaticity of the compound (Nandiyanto et al., 2019). This peak is quite high due to the carbonisation detected in the sample. Peaks at  $2389$  and  $2667\text{ cm}^{-1}$  are related to C-H stretching of the monomer units (Barbosa et al., 2017).



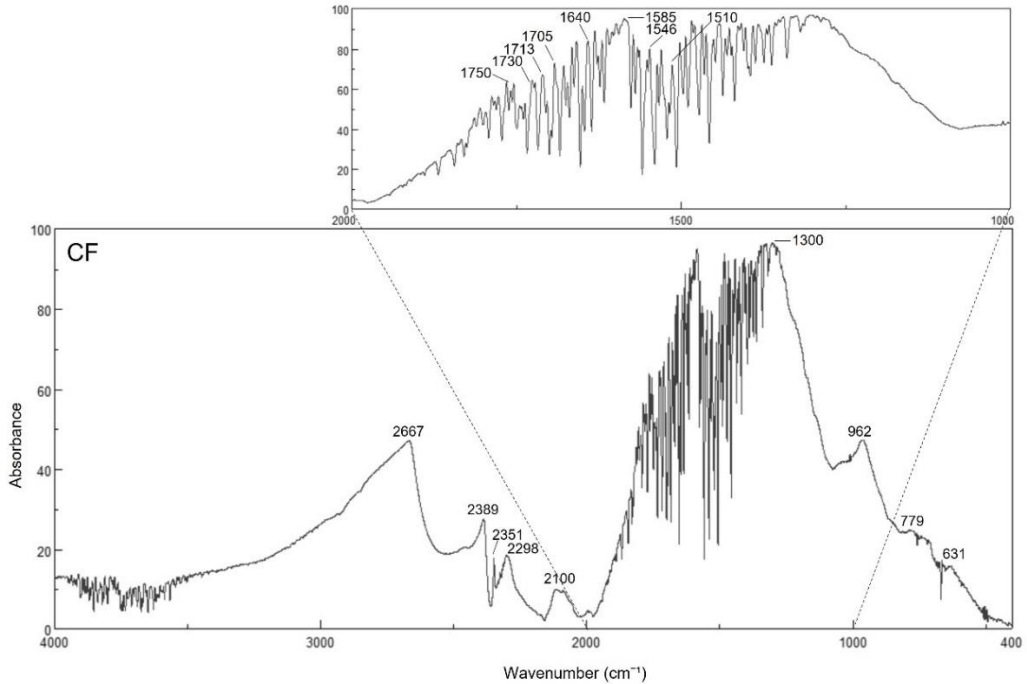


**Figure II-2.** Infrared spectrum of the carbon fibre used in this study. The range of the spectrum from 2000 to 1000  $\text{cm}^{-1}$  has been marked to highlight the presence of other components in the carbon fibre sample.

Other compounds detected in the CF sample were: free water ( $\text{H}_2\text{O}$ : 450–600  $\text{cm}^{-1}$ ; 1250–2000  $\text{cm}^{-1}$ ; 3500–4000  $\text{cm}^{-1}$ ) (Guan et al., 2011), carbon dioxide ( $\text{CO}_2$ : 3570–3750  $\text{cm}^{-1}$ ; 2298  $\text{cm}^{-1}$ ; 631–779  $\text{cm}^{-1}$ ), carbon monoxide ( $\text{CO}$ : 2000–2100  $\text{cm}^{-1}$ ) (Cusidó et al., 2003), carbonyl sulphide ( $\text{COS}$ : double peaks at 2100 and 2051  $\text{cm}^{-1}$ ), ammonia ( $\text{NH}_3$ : 965  $\text{cm}^{-1}$ ) (Süzer and Andrews, 1987) and sulphur dioxide ( $\text{SO}_2$ : 1300  $\text{cm}^{-1}$ ) (Guan et al., 2011). The degradation of thermoplastic products (mainly the peak of  $\epsilon$ -caprolactam (Poljansek and Krajnc, 2005) at 1713  $\text{cm}^{-1}$ ) and the release of phenol at 1510  $\text{cm}^{-1}$  (Cremades et al., 2018) were also observed. In relation to these compounds detected by FTIR, Cusidó et al. (2003) and Cremades et al. (2018) studied the hazardousness of the gases emitted during the firing of ceramics made with additives, recommending the use of technologies that minimize the emission of pollutants that are dangerous for human health. In this case, the addition of 5 to 10 wt.% carbon fibre would increase  $\text{CO}_2$  emissions during the firing process, as explained below.

**Table II-1.** FTIR bands identified for CF, their attribution and references.

Bands identified (cm <sup>-1</sup> )	Attribution	References
450–600	free water	Guan et al., 2011
965	ammonia	Süzer and Andrews, 1987
1250–2000	free water	Guan et al., 2011
1300	sulphur dioxide	Guan et al., 2011
1510	phenol	Cremades et al., 2018
1713	ε- caprolactam	Poljansek and Krajnc, 2005
1730	ester	Sellitti et al., 1990
1705	ketone and carboxylic acid	Starsinic et al., 1983
1640	benzoic acid	Nandiyanto et al., 2019
2000–2100	carbon monoxide	Cusidó et al., 2003
2100–2051	carbonyl sulphide	Süzer and Andrews, 1987
2298	carbon dioxide	Cusidó et al., 2003
2389–2667	monomer	Süzer and Andrews, 1987
3500–4000	free water	Guan et al., 2011
3570–3750	carbon dioxide	Cusidó et al., 2003

Table II-2 shows the chemistry of the clayey material and the carbon fibre (CF). The raw material is rich in SiO<sub>2</sub> and has a high Al<sub>2</sub>O<sub>3</sub> content. The presence of CaO (9.23%) and MgO (2.82%) is a sign of its carbonate content. The carbon fibre is composed almost exclusively of carbon, which is consumed during calcination of the sample, so explaining the very high loss on ignition (LOI) of over 99%. The calcination of carbon fibres results in the emission of CO<sub>2</sub> into the atmosphere, an issue that must be taken into account if this residue is to be used in the brick industry, as these factories are subject to carbon tax and CO<sub>2</sub> emission restrictions. Furthermore, the resin residues associated with the fibres will increase the total organic carbon in the flue gas (Cusidó et al., 2003). However, the use of carbon fibres as an additive in brick production is more environmentally friendly in terms of air pollution than other possible methods for dealing with decommissioned turbine blades such as incineration, pyrolysis, or chemical recycling. Cameán (2011) and

Rodríguez Vazquez (2014) have shown that if metals such as Fe, Ti and Al are present, even in small amounts, in the clayey material, they can promote the graphitization of carbon fibres during the firing process.

**Table II-2.** Chemical analysis of mayor oxides (in wt.%) in the raw material and CF.

	SiO <sub>2</sub>	Al <sub>2</sub> O <sub>3</sub>	Fe <sub>2</sub> O <sub>3</sub>	MnO	MgO	CaO	Na <sub>2</sub> O	K <sub>2</sub> O	TiO <sub>2</sub>	P <sub>2</sub> O <sub>5</sub>	LOI
Clayey material	48.78	15.97	5.69	0.07	2.80	9.43	1.27	2.70	0.83	0.16	12.40
CF	0.47	0.08	0.03	-	0.02	0.32	0.02	0.03	-	0.03	99.13

### 3.2. Mineralogy of the clayey material and fired bricks

Rietveld refinement of PXRD analysis reveals that the clay mixture is rich in quartz (41 wt.%) (Table II-2), which confirms the high SiO<sub>2</sub> content detected by XRF (see Table II-2). Other phases detected include carbonates (calcite and dolomite, 11 wt.%), K-feldspar (microcline 8 wt.%), hematite (5 wt.%) and phyllosilicates (smectite, illite, paragonite, kaolinite and chlorite, 21wt.%). The CaO and MgO content analysed by XRF (12%, Table II-2) is in accordance with the carbonate content determined by PXRD. Paragonite is a common phyllosilicate in the inner areas of the Betic Cordillera and is found in the raw material from Guadix (Cruz, 2008; Jiménez-Millán et al., 2022). For its part, the clay from Viznar is rich in carbonates from the different geological formations in the Granada Depression (Martin et al., 1984). The amorphous phase content in the clay mixture is 13 wt.%.

**Table II-3.** Mineralogical characterization by PXRD of the clayey material and the fired bricks with or without added CF. Data is provided in weight %. Abbreviations of minerals according to Warr (2020): Sme = smectite; Ill = illite; Pg = paragonite; Kln = kaolinite; Chl = chlorite; Mc = microcline; Qz = quartz; Cal = calcite; Dol = dolomite; Hem = hematite; Or = orthoclase; Sa = sanidine; Gh = gehlenite; An = anorthite; Mull = mullite; Wo = wollastonite; Di = diopside; Amph = amorphous phase.

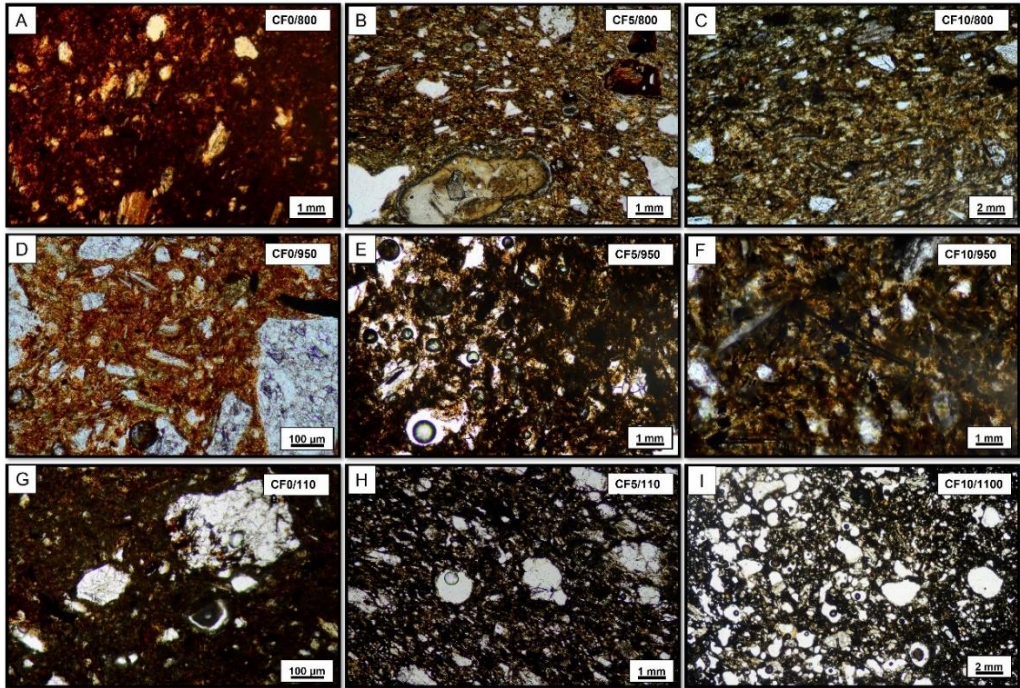
	Sme	Ill	Pg	Kln	Chl	Mc	Qz	Cal	Dol	Hem	Or	Sa	Gh	An	Mull	Wo	Di	Amph	ERROR
Clay mat.	3	12	2	2	1	8	41	6	5	5	-	-	-	-	-	-	-	13	±5
CF0/800	-	19	-	-	-	-	40	4	-	4	4	-	-	-	-	-	-	30	±2
CF5/800	-	18	-	-	-	-	39	4	-	2	2	-	-	-	-	-	-	35	±3
CF10/800	-	16	-	-	-	-	32	5	-	1	3	-	-	-	-	-	-	42	±4
CF0/950		16	-	-	-	-	31	-	-	5	-	1	7	12	-	-	-	30	±2
CF5/950	-	10	-	-	-	-	32	-	-	2	-	2	3	14	-	-	-	37	±2
CF10/950	-	14	-	-	-	-	20	-	-	1	-	1	7	11	-	-	-	47	±3
CF0/1100	-	-	-	-	-	-	26	-	-	5	-	2	4	19	3	2	9	33	±1
CF5/1100	-	-	-	-	-	-	23	-	-	1	-	2	2	22	3	2	10	41	±2
CF10/1100	-	-	-	-	-	-	24	-	-	0	-	3	2	22	4	3	12	48	±3

Table II-3 shows the changes in the mineralogy of the bricks after firing. These changes are more obvious at 1100 °C with the crystallization of high-temperature silicates, the increase in background noise due to the vitrification of the samples (Cultrone et al., 2004) and more extensive development of a graphite-type crystalline structure in the samples with added CF. The amorphous phase content (in wt.%) increases in line with the firing temperature and with the percentage of CF, reaching its highest value in the samples fired at 1100 °C and with 10wt.% CF. At the three firing temperatures studied (800, 950 and 1100 °C), quartz is the most abundant phase (ranging from 41 to 20 wt.%), while hematite and feldspars *s.l.* are detected in all the samples. At 800 °C, all the phyllosilicates have disappeared with the exception of a dehydroxylated illite. The fired bricks have a higher illite content than the raw unfired bricks. This seems to be due to an overestimation of this phase due to the decomposition of the other phyllosilicates and their absence in the phase count (they accounted for 8%, Table II-3). Illite can still be detected at 950 °C, although the reflection (001) at 10 Å is lower than that observed in the clay mixture, suggesting a lower concentration of this phase. Dehydroxylation can influence the properties of the surrounding material, such as the strength and porosity of the fired brick (Kingery et al., 1976). Calcite is detected in very small amounts at 800 °C (~ 4 wt.%) and disappears at higher temperatures, while dolomite has already disappeared at 800 °C (Table II-2). Microcline detected in the clayey material converted into its polymorphs, i.e. orthoclase at 800 °C and sanidine at 950 °C and 1100 °C (Goldsmith and Laves, 1954). The hematite concentration decreases with increasing firing temperature in the samples made with added CF, reaching values of <1 wt.% in CF10/1100 as compared to 5 wt.% in CF0/1100 (Table II-2). The decomposition of carbonates and their reactions with quartz and other silicates leads to the appearance of new Ca- (and Mg-) silicates such as gehlenite at 950 °C and wollastonite, anorthite and diopside at 1100°C. Another new phase, mullite, is identified at 1100 °C. The appearance of these phases is manifested in the exothermic peak observed in TG-DSC analysis at 925 °C (Fig.II-1B).

### 3.3. Texture and microtexture of the fired bricks

The observations under MOP of the bricks made with and without carbon fibre revealed the presence of fragments of mica-schists, gneiss and quartz grains with undulose extinction with a maximum length of about 1 mm. At 800 °C these fragments are homogeneously distributed in an orange matrix (Fig.II-3A) forming the temper of the

bricks. With the addition of carbon fibre, the matrix becomes browner in colour and disoriented carbon fibres are observed as part of the matrix (Figs.II-3B and C). These fibres probably encourage the development of a reducing environment in the oven and the formation of "black core". At 800 °C, other minerals can also be observed. The carbonate grains are partially decomposed and have lost their typical high interference colour (Fig.II-3B). Phyllosilicates appear unaltered and often have a preferential orientation due to the pressure exerted during kneading. Pores are mainly elongated and follow the same orientation as planar minerals. At 950 °C, the matrix is slightly darker (Fig.II-3D) due to the gradual vitrification and even more so in the samples with added CF (Fig.II-3E and F). The phyllosilicates become less birefringent, and carbonates are totally decomposed. In the bricks with carbon fibre (Figs.II-3E and F), it seems that the fibres start to form clumps and orient themselves slightly. Many of the fibres were severely affected, and some even disappeared, leaving imprints in their place. At 1100 °C, due to the high firing temperature, the pores become ellipsoidal-to-rounded and the matrix becomes dark (Fig.II-3G, H and I). This change is more noticeable in the samples made with CF. This is probably because of the combustion of fibres (remember the high LOI of CF weighed at 1000 °C in Table II-1), which brings more heat into the matrix. In these samples, the development of sandwiched structures, i.e. black cores, is more evident. The phyllosilicates have lost their birefringence and have a whitish interference colour. According to Pask and Tomsia (1991) and Rodríguez Navarro et al. (2003), the kaolinite and illite have probably been replaced by mullite, as also suggested by the PXRD results (Table II-3).



**Figure II-3.** Optical microscopy images of bricks with or without added carbon fibres fired at 800, 950 and 1100 °C, as observed in plane-polarized light. A) Orange matrix of sample FC0/800; B) and C) brown matrix of the samples fired at 800 °C with added CF (CF5/800 and CF10/800, respectively); D) phyllosilicate grains with a preferential orientation in the FC0/950 sample; E) and F) the matrix is slightly darker due to the gradual vitrification and the presence of imprints of CF; G) dark matrix in the CF0/1100 sample; H) and I) rounded pores in the samples fired at 1100 °C with added CF (CF5/1100 and CF10/1100).

Figure II-4 offers a schematic image of the distribution and orientation of the imprints of the carbon fibres and pores in the matrix of sample CF10/1100. Three concentric areas (A, B and C) can be distinguished. In the outer area of the sample (A zone), which has a more orangey colour, a small amount of randomly arranged imprints can be observed under the microscope, together with small, rounded pores. In the middle area (B zone), the imprints are shorter and thicker than those observed in the outer area and tend to orient themselves. In the core of the sample (C zone), the imprints remain thick but increase in length forming oriented aggregates in bundles. The additional heat provided by the combustion of the fibres is probably responsible for these textural changes. According to Cameán (2011), it is possible that carbon fibres are oriented by the pressure



applied during the preparation of handmade bricks prior to firing, an effect that becomes more intense as more carbon fibres are added.

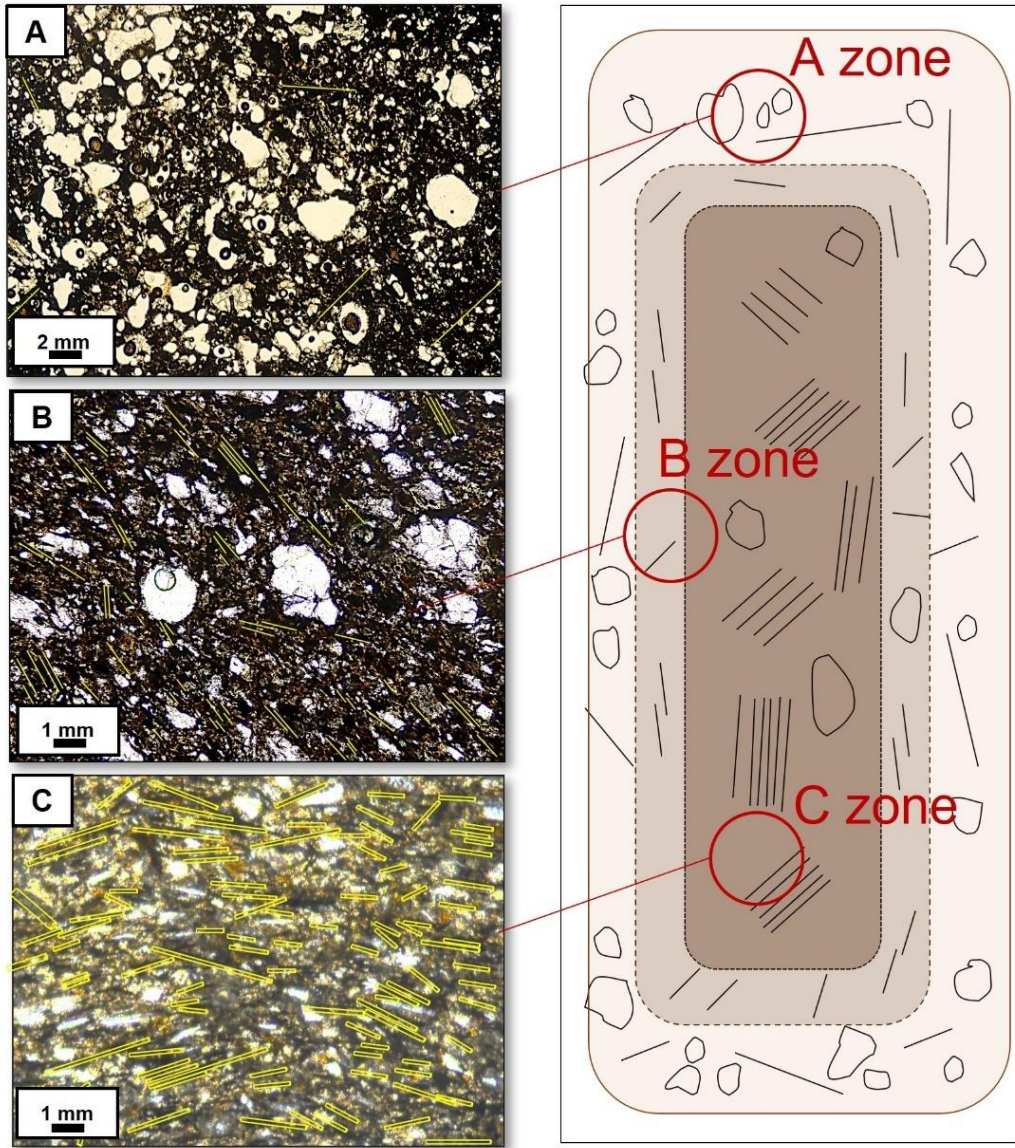


**Figure II-4.** Left – Optical microscopy images in plane-polarized light. The fibres and their imprints are highlighted in yellow. Right – schematic view of a thin section of the CF10/1100 brick. Moving inwards from the outside to the core of the brick, three quite distinct zones can be observed: Zone A, the outermost zone, corresponds to MOP image A, zone B to image B and zone C, the innermost area, to image C.



The FESEM observations were made on detached particles of carbon fibre before it was kneaded with the clayey material (Fig.II-5) and on fragments of the bricks made with 0 wt.% and 10 wt.% CF fired at 800 °C (Fig.II-6). The aim was to highlight the textural differences in the brick matrix caused by the addition of the highest amount of CF. Although this question was not analysed in our study, previous researchers argued that the microstructural changes resulting from the addition of CF could have improved the thermal properties of bricks, and in particular their thermal conductivity (Vilatela et al., 2015). Figure II-6 shows a general view of the carbon fibres used to make the bricks. As expected, this waste is not only composed of elongated fibres but also contains rough and irregular aggregates (Fig.II-5A-C). EDS analysis confirms the presence of C and O in the carbon fibres. These aggregates probably come from the reinforcing foam used in the construction of the blades (Sharma and Wetzel, 2010; Debnath et al., 2013; Linul and Marsavina, 2013). They are very sensitive to increases in temperature, forming pores in the fired bricks. The carbon fibres range in length from 5 to 90 µm and have a diameter of around 6-9 µm. The surface of the fibres appears striated (Fig.II-5D).

The addition of carbon fibres to the clayey mix results in a partial change in the texture of the fired bricks and the matrix becomes quite heterogeneous (Fig.II-6A, CF0/800 and Fig.II-6C, CF10/800). In both groups of bricks (CF0 and CF10), the phyllosilicate grains maintain their lamellar habit, although the lamellae tend to separate along their basal plane due to dehydroxylation (Fig.II-6B) (Cultrone and Carrillo Rosua, 2020). Carbonate grains are partially decomposed, confirming MOP observation and PXRD data. The carbon fibres in the fired bricks, when visible, show a change in their morphology compared to the unfired fibres (Fig.II-6D), as a result of firing. The striae observed on the unfired fibres (Fig.II-5D) have disappeared or thinned out. It is also possible to corroborate the changes in the size of the fibres noted during MOP observations. At 800 °C they have already started to thicken and shorten and by 1100 °C they are completely calcined. At 800 °C some fibres have disappeared due to combustion, leaving imprints in the matrix of the brick (Fig.II-6D), as already observed under POM. At the same time, greater porosity and irregular-shaped pores can be distinguished in the bricks made with CF. This may be linked to the burning of carbon fibres and reinforcing foam observed under FESEM (Fig.II-5B).

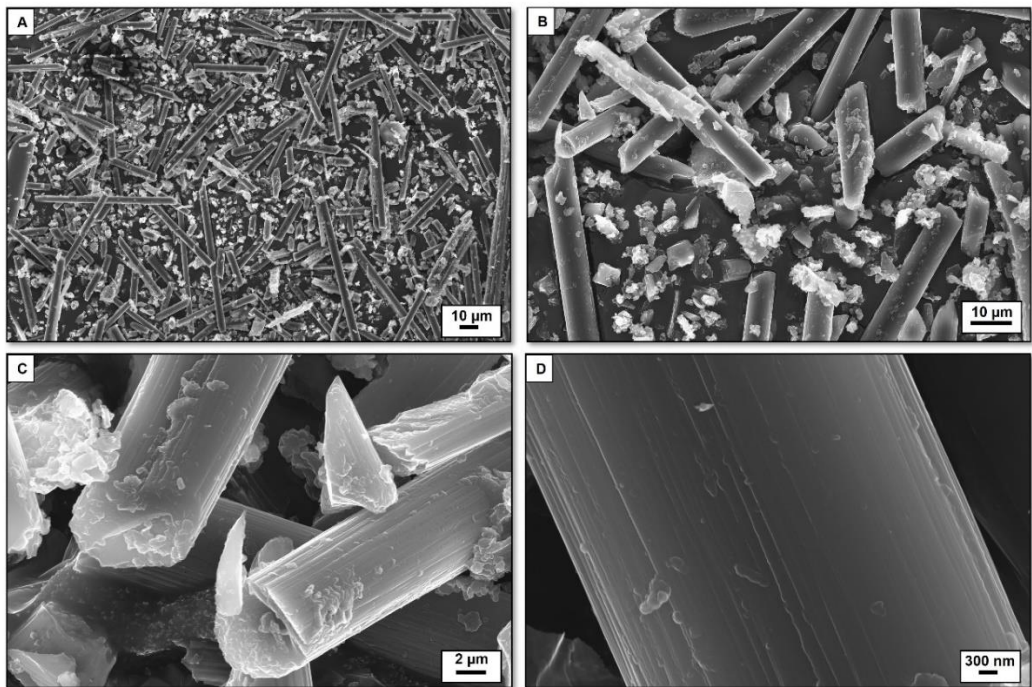


**Figure II-5.** FESEM secondary electron images of carbon fibres added to the clayey material to make the bricks. A) General view of carbon fibres and other particulate matter from wind turbines; B) unidentified aggregates with irregular morphology together with fibres; C) detailed image of the cylindrical morphology of the carbon fibres; D) detail of the surface morphology of a carbon fibre highlighting the presence of striae on the surface.

The orientation of the CF occurs because they are oxygen-rich organic compounds that develop a structure with aliphatic crosslinks that provide great rigidity to the carbonaceous structure. This structure is stable at 25 °C and 35% HR (Fig.II-7). When the temperature augments, the carbon fibre changes from a state of carbonisation (around 800 °C) to one of graphitization (over 900 °C) (Fig.II-7), in which there are far fewer crosslinks. This allows the fibres to reorganise themselves and acquire a graphitic structure as the temperature increases (Rodríguez Vázquez, 2014).

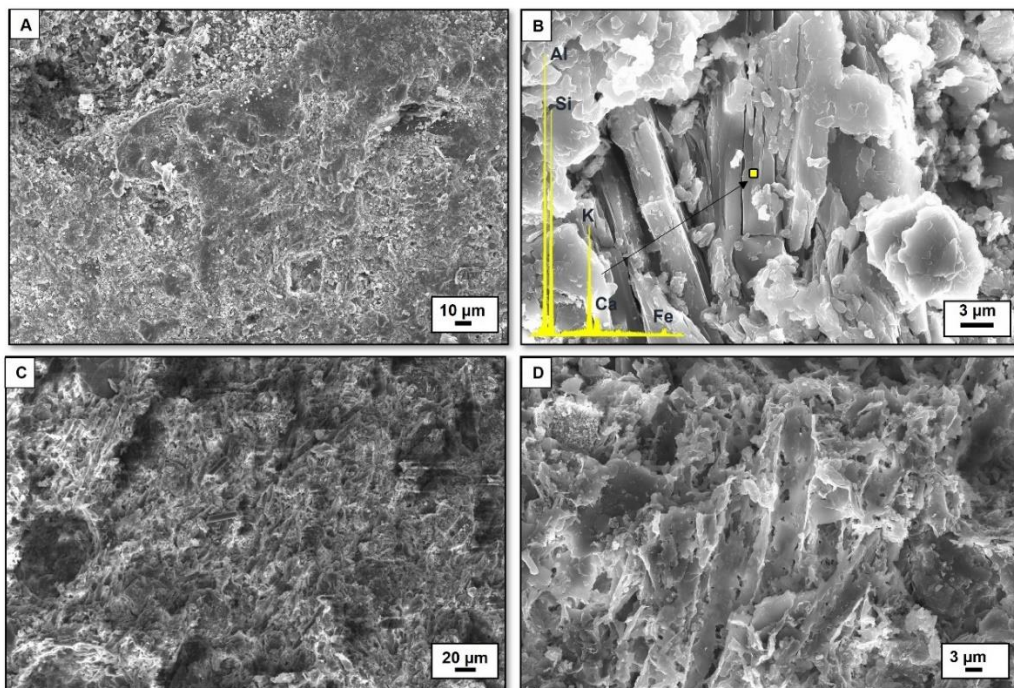


**Figure II-6.** FESEM secondary electron images. A) General view of the texture and porosity of the sample CF0/800; B) dehydroxylation of a phyllosilicate grain along (001) planes in CF0/800 (the EDS of the phyllosilicate can be seen in the inset); C) general view of the texture and porosity of the sample CF10/800; D) imprints left by carbon fibres in sample CF10/800.

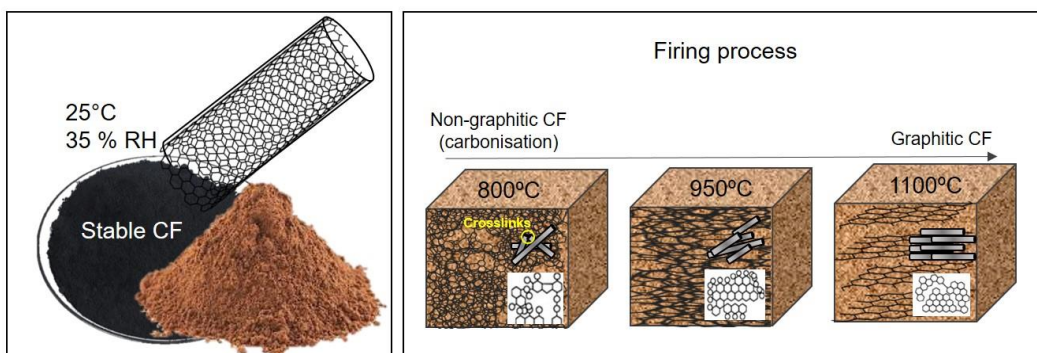


**Figure II-7.** Influence of temperature on the reorientation of carbon fibres.

Cameán (2011) and Rodríguez Vázquez (2014) demonstrated that temperatures close to 1800 °C are required for complete graphitisation of the CF, although this process can

be accelerated by the presence of resins and clays (as in this study), leading to further fibre orientation at 1100 °C as compared to 950 °C (Fig.II-7).

#### 3. 4. Hydric behaviour and pore system of fired bricks

The bricks fired at 800 and 950 °C show an increase in water absorption ( $A_b$  and  $A_f$ ) and open porosity ( $P_o$ ) values with the addition of carbon fibre, changes that can also be observed in line with increases in the firing temperature (Table II-4). CF0 samples showed lower values than CF5 and CF10 samples. This indicates that at low firing temperatures, the presence and amount of carbon fibre have a greater influence on the hydric behaviour of the fired pieces than the firing temperature does. The opposite trend can be observed at 1100 °C, where the addition of carbon fibre seems to hinder water absorption.

The addition of carbon fibre has a clear impact on the circulation of water in the pores and capillaries of the bricks. The bricks with no added CF achieve the best  $A_x$  values at all firing temperatures, although these values decline with the addition of CF and with increasing CF content (Table II-4).  $A_x$  also worsens with the increase in the firing temperature, reaching the worst values with FC10/1100. Bricks reach high saturation indices ( $S$ , Table II-4), except at 1100 °C when the extended vitrification of the ceramic mass makes them less absorbent (Cultrone et al., 2004). As for drying, bricks fired at 800 °C dry faster than those fired at 950 °C, and these in turn dry faster than those fired at 1100 °C ( $D_i$ , Table II-4). This is logical given that pore interconnection worsens as firing temperature increases and the water finds it more difficult to move around the pore network. As regards porosity, two trends can be recognised:  $P_o$  increases between 800 and 950 °C, but falls at 1100 °C (Table II-4). In all cases, the presence and percentage of CF lead to higher porosity because of the imprints left by CF in the matrix of the bricks. The different behaviour at the different firing temperatures can be explained by the change in size of the carbon fibres, a process that began at 800 °C, as seen in POM and FESEM observations. This could have encouraged the development of small fissures around the fibres. Although at 1100 °C the carbon fibres underwent the same change as at 950 °C, the vitrification of the matrix was so pronounced that it hampered the development of fissures.

Water absorption by capillarity tends to increase with the addition of CF and with the rise in the firing temperature (C, Table II-4). No clear trend can be observed with densities. Both,  $\rho_a$  and  $\rho_r$  are lower when CF is added, and their values fall further as higher amounts of CF are added. This is logical given the lower density of carbon fibres, as found in previous research ( $1.75 \text{ g cm}^{-3}$ ), compared to the silicate compounds present in the bricks.

The MIP analysis confirms the results obtained by HT (Table II-4) and shows how the addition of CF modifies the pore system of the bricks in terms of open porosity and pore size distribution. All bricks display a unimodal pore size distribution with a maximum peak at around  $0.1 \text{ }\mu\text{m}$  (Fig.II-8). The only exception is CF10/1100 which has a bimodal distribution, with a main peak between  $0.1$  and  $1 \text{ }\mu\text{m}$  and a second family of pores at around  $10 \text{ }\mu\text{m}$  (Fig.II-8).

When comparing the different types of bricks, the maximum peak always shifts towards the right of each diagram (i.e. towards larger pores), as the firing temperature increases. This causes a reduction in the specific surface area (SSA, Table II-4) because small pores fuse into new larger ones, above all, when CF is added, leaving empty spaces in the fired bricks.

**Table II-4.** Hydric parameters of bricks: Ab: free water absorption (%); Af: forced water absorption (%); Ax: degree of pore interconnection (%); S: saturation coefficient (%); Di: drying index; Po: open porosity (%); C: capillarity coefficient ( $\text{g}/\text{m}^2\text{s}^{0.5}$ );  $\rho_a$ : apparent density ( $\text{g cm}^{-3}$ );  $\rho_r$ : real density ( $\text{g cm}^{-3}$ ); MIP:  $\text{Po}_{\text{MIP}}$ : open porosity (%), determined by MIP); SSA: specific surface area ( $\text{m}^2 \text{g}^{-1}$ , determined by MIP). The standard deviation of each result is indicated in brackets.

	Hydric Test (HT)									MIP	
	Ab	Af	Ax	S	Di	Po	C	$\rho_a$	$\rho_r$	SSA	Po
CF0/800	18.30 (4.34)	18.96 (5.37)	0.21 (1.11)	91.73 (0.89)	0.92 (0.003)	38.46 (0.66)	2.09 (1.34)	1.84 (0.02)	2.93 (0.03)	9.65 (0.07)	37.23 (1.12)
CF5/800	26.63 (4.95)	26.79 (3.96)	1.46 (3.14)	93.30 (2.15)	0.90 (0.001)	39.31 (1.54)	2.47 (2.21)	1.71 (0.01)	2.88 (0.05)	2.46 (0.01)	38.47 (0.93)
CF10/800	32.45 (5.84)	32.74 (0.67)	19.55 (3.22)	92.21 (1.55)	0.89 (0.012)	40.14 (3.45)	2.84 (3.44)	1.64 (0.03)	2.61 (0.05)	2.57 (0.11)	41.11 (1.25)
CF0/950	21.46 (4.27)	21.97 (5.90)	3.87 (2.65)	91.08 (2.31)	0.89 (0.004)	41.89 (2.01)	2.05 (0.96)	1.73 (0.01)	2.74 (0.02)	8.37 (1.45)	43.89 (1.32)
CF5/950	29.87 (5.33)	30.09 (3.89)	15.79 (5.11)	91.74 (0.94)	0.90 (0.009)	44.96 (3.65)	2.38 (3.69)	1.56 (0.03)	2.48 (0.02)	2.21 (1.88)	45.11 (2.54)
CF10/950	36.22 (6.45)	36.69 (5.71)	27.27 (3.86)	92.64 (2.64)	0.90 (0.011)	46.82 (4.09)	2.64 (5.96)	1.48 (0.03)	2.22 (0.01)	1.64 (1.13)	46.38 (2.99)
CF0/1100	24.66 (3.17)	24.81 (0.56)	3.61 (3.14)	89.65 (0.99)	0.88 (0.007)	37.12 (1.34)	1.99 (3.74)	1.59 (0.02)	2.61 (0.03)	7.20 (2.74)	39.67 (0.89)
CF5/1100	15.48 (3.69)	15.86 (0.43)	30.59 (5.67)	82.03 (3.44)	0.88 (0.009)	39.94 (4.61)	1.69 (5.21)	1.42 (0.04)	2.54 (0.03)	1.38 (1.71)	40.97 (3.45)
CF10/1100	18.01 (3.70)	18.44 (2.52)	37.34 (5.31)	84.40 (2.89)	0.87 (0.009)	42.97 (6.33)	1.82 (6.12)	1.25 (0.04)	2.36 (0.02)	0.74 (0.09)	42.27 (4.65)

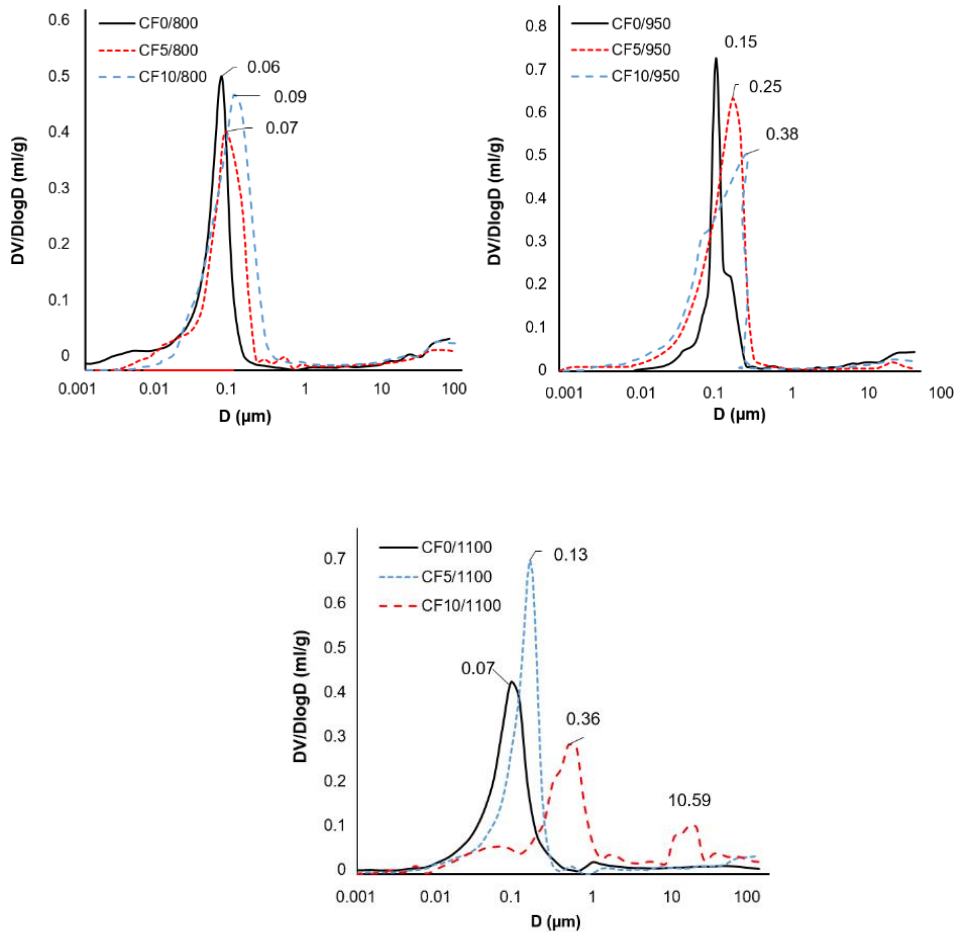


**Figure II-8.** MIP curves for bricks fired at 800, 950 and 1100 °C without additive (black continuous line) and with added CF (red and blue dashed lines, respectively). The pore diameter at the maximum peak in each porosimetric curve is indicated.

### 3.5. Salt crystallization test

The samples were also subjected to decay tests involving 15 salt crystallization cycles. The general trend observed in all the bricks was for an increase in weight at the beginning of the decay test, due to the presence of sodium sulphate in the pores and fissures, followed by a steep or more gradual decrease in the successive cycles. This trend was accentuated by the presence of carbon fibre. In the bricks made with added CF, after the initial crystallization of salts in the pore system (weight gain), the salts began to damage the brick, causing cracks to appear and fragments to break off (weight loss). However, at

the end of the test, the samples fired at 950 and 1100 °C with added CF had suffered the least loss of material. Because of their high vitrification, the bricks fired at 1100 °C, and especially those that contain CF, lost the least weight during this experiment and are therefore considered the most durable against salt attack.

### 3.6. Mechanical behaviour

The compressive strength of the bricks was tested according to the procedure described in Table II-S1 and the results of the tests are shown in Figure II-9. The addition of CF caused a progressive decline in compressive strength as compared to the control bricks, with a fall of about 25% in samples with 5 wt.% CF (CF5) and about 50% in those with 10 wt.% CF (CF10).

These results can be summarized in two main findings: i) the compressive strength of the bricks improves as the firing temperature increases; ii) the addition of carbon fibre to the clay mixture decreases the strength of the fired products. The latter is due at least in part to the increase in porosity (in CF5 and CF10) resulting from the combustion of the fibres, which causes pores to be formed (Table II-4). However, the decrease in strength is much higher than the increase in porosity. This suggests that other factors may have been involved in this loss of strength. These include, firstly, the manual processing of the samples which may have resulted in CF being unevenly distributed within the clay mass (as reflected in higher standard deviation values in CF5 and CF10, Fig.II-9) and secondly, the preferential orientation of the carbon fibres observed under the microscope (see Fig.II-4), especially at 950 and 1100 °C, which may have reduced the compressive strength of the bricks. This shows that the results for the mechanical and thermal properties of the bricks with added CF can vary depending on the direction of measurement (Pierson, 1993). If we look at the three groups of samples with 0, 5 and 10 wt.% of CF respectively, the mechanical strength improved as temperature increased (e.g. from 9.89 MPa to 11.07 MPa and to 12.22 MPa for samples CF10/800, CF10/950 and CF10/1100, respectively) (see Fig.II-9). Thus, the highest values were found in the bricks fired at 1100 °C, with the highest compressive strength (25.6 MPa) for sample CF0/1100. This direct relationship between the firing temperature and the mechanical properties of the samples is related to their different degree of vitrification, as suggested by PXRD analysis (Table II-3). These findings are consistent with earlier studies that show that compressive strength is more closely related with porosity and the degree of vitrification than with the mineralogy of the clay (Saravanapavan and Hench, 2003; Dondi



et al., 2009). Although the addition of CF impairs the mechanical behaviour of the bricks, the results demonstrate that all the samples, with the exception of CF10/800, have sufficient compressive strength to be used for construction purposes, according to official specifications from the Spanish Ministry of Public Works (Pliego RL-88, 1988).

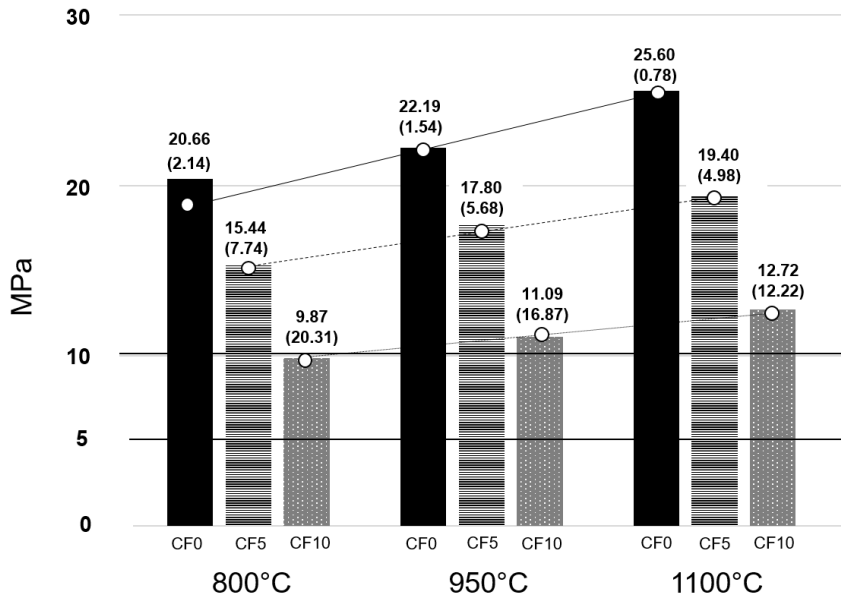


**Figure II-9.** Mechanical behaviour of the bricks fired at 800, 950 and 1100 °C made without additives (control group, CF0) and with added CF (CF5 and CF10). The standard deviation appears in brackets. The lines connecting the different brick types (CF0, CF5 and CF10) correspond to trend lines and the black lines at 10 and 5 MPa show minimum thresholds for solid and lightweight bricks respectively, according to the official specifications of the Spanish Ministry of Public Works (Pliego RL-88, 1988).

### 3.7. Non-destructive testing of fired bricks

Table II-5 shows the results of ultrasound measurements. The highest velocity values ( $V_p$  and  $V_s$ ) were measured in bricks fired at 1100 °C. The presence of CF reduces the ultrasound velocity at all three firing temperatures, especially at 950 °C and 1100 °C. These results are consistent with the lower density of the bricks fired at these two temperatures (see  $\rho_a$  and  $\rho_r$ , Table II-5). The anisotropy of the bricks increased in line with increased temperature and CF content. Poisson's ratio ( $\nu$ ) values were very similar in all the bricks, with a small rise in the samples with added CF fired at 950 and 1100 °C. The Young modulus ( $E$ , Table II-5) was higher in the control bricks (CF0) than in those

with added CF. The bricks with 5 and 10 wt.% CF obtained similar values at the same firing temperature. However, for all the samples, the Young modulus values increased in line with firing temperature, suggesting that firing temperature was a more important factor than the amount of CF. A similar pattern was observed in the shear (G) modulus values, although the bulk modulus (K) results showed no such correlation.

**Table II-5.** Average velocities (V) for the propagation of ultrasonic P and S pulses (m/s).  $\bar{x}$ : average values;  $\sigma$ : standard deviation;  $\Delta M$  total anisotropy (in %);  $\nu$ : Poisson's ratio; E: Young's modulus (GPa); G: shear modulus (GPa); K: bulk modulus (GPa).

	$V_P$ (m/s)		$V_S$ (m/s)		$\Delta M$	$\nu$	E	G	K
	$\bar{x}$	$\sigma$	$\bar{x}$	$\sigma$					
CF0/800	2434	2.29	1270	7.14	2.22	0.31	8.22	5.73	9.32
CF5/800	2418	51.47	1241	43.33	9.52	0.32	7.02	2.63	7.47
CF10/800	2308	278.12	1184	79.56	14.26	0.32	7.35	3.68	6.86
CF0/950	2576	3.77	1290	10.88	4.57	0.33	9.56	7.59	9.52
CF5/950	2000	76.70	1297	61.20	14.26	0.24	8.21	5.16	1.47
CF10/950	1937	212.02	1075	111.04	18.68	0.28	8.03	5.67	2.27
CF0/1100	2823	4.13	1426	12.65	7.20	0.33	10.78	6.33	7.57
CF5/1100	2693	84.27	1363	63.21	15.94	0.33	9.68	5.49	8.40
CF10/1100	2448	238.45	1871	126.34	20.46	0.20	9.99	5.61	1.90

The highest Leeb hardness values (LH) were observed in the bricks fired at the highest temperatures due to the high vitrification of the samples (Fig.II-10). This trend was maintained with the addition of CF. Some authors (Coletti et al., 2018; Crespo-López and Cultrone, 2022) have shown that the addition of inorganic waste improves the surface hardness of fired bricks, especially at high temperatures. Figure II-10 also shows that bricks fired at 800 and 950 °C reach similar values. This confirms that the extended vitrification of the bricks occurs more between 950 and 1100 °C than between 800 and 950 °C (Coletti et al., 2018). The bricks fired at 800 °C and with added carbon fibre obtained slightly higher hardness values than those made without additive, 2.3% higher with 5 wt.% carbon fibre and 5% with 10 wt.% CF. This suggests that at 800 °C the addition of carbon fibre improves the surface hardness of the bricks very slightly. The LH results for the samples fired at 950 °C show a similar trend to those for the samples fired at 800 °C. Sometimes the values are slightly lower, possibly due to the development of small fissures described above (see Section 3.4 on hydric behaviour).

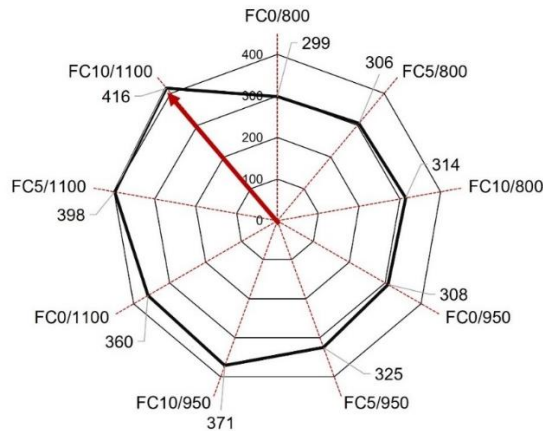


**Figure II-10.** Surface hardness of the bricks as determined by the Leeb Hardness Test (LH).

At 1100 °C the surface hardness of the bricks increases because of the extended vitrification as shown earlier by the POM and ultrasound techniques. The higher the carbon fibre content, the greater the increase in surface hardness. The highest hardness values were achieved by FC1100/10, with values that were 16% higher than FC0/1100 and 32.5% higher than FC10/800.

The fact that the surface hardness results show an opposite trend to that revealed by the compressive and ultrasonic strength tests could be due to the fact that the size and shape of both the pores and the fibres vary considerably within the brick. As we get nearer the core, the pores become larger and the fibres are shorter and thicker. This in turn confirms the heterogeneous matrix observed in the POM (Fig.II-3).

### 3.8. Colour

According to Kreimeyer (1987) and Karaman et al. (2006), the colour of fired clay products is primarily determined by the type and amount of iron oxide in the clay raw material, as well as the firing temperature and the atmosphere inside the oven. Brick colour can also be affected by CaO. The presence of CaO compounds (mainly calcite) can make the bricks appear yellower because the iron is "trapped" within the structure of Ca-rich silicate phases as gehlenite, developed by the reaction between carbonates and silicates (Maniatis et al., 1983), and cannot develop to hematite, so causing the bricks to lose their reddish hue. Regardless of the mineralogy of the clayey material, previous authors have also shown that the use of different additives can affect the colour of the bricks (Saenz et al., 2019; Crespo-López et al., 2023c).

The bricks fired at 800 and 950 °C with or without added carbon fibre had a reddish appearance (Fig.II-11). When the temperature reached 1100 °C, the difference in colour between the bricks made with and without added carbon fibre became more evident. In Figure II-10, the chromatic values ( $a^*$  and  $b^*$ ) are divided into three different areas according to the firing temperatures. It is interesting to note that the addition of carbon fibre causes a greater dispersion of the  $b^*$  parameter values. In fact, in the samples with no CF (FC0),  $b^*$  ranges between 20 and 25 approximately, while in those with added CF (samples CF5 and CF10) it ranges from 5 to 30. As regards the different firing temperatures, the samples fired at 800 °C had quite homogeneous values and were grouped within a limited area, while those at 950 °C and 1100 °C were more scattered. Bricks fired at 950 °C suffer a higher variation in the  $a^*$  value than in the  $b^*$  value but with no marked trend in relation to the CF content. Samples fired at 1100 °C generally show lower  $a^*$  and  $b^*$  values and there is a marked drop in the  $b^*$  value as the amount of carbon fibre augments. These bricks lose their reddish colour and turn yellow to dark-brown as the carbon fibre content increases. The lightness ( $L^*$ ) is not significantly affected by the firing temperature, although the lowest  $L^*$  values (47.28 and 42.50, respectively) were obtained by the bricks with 5 and 10 wt.% of carbon fibre fired at 1100 °C.

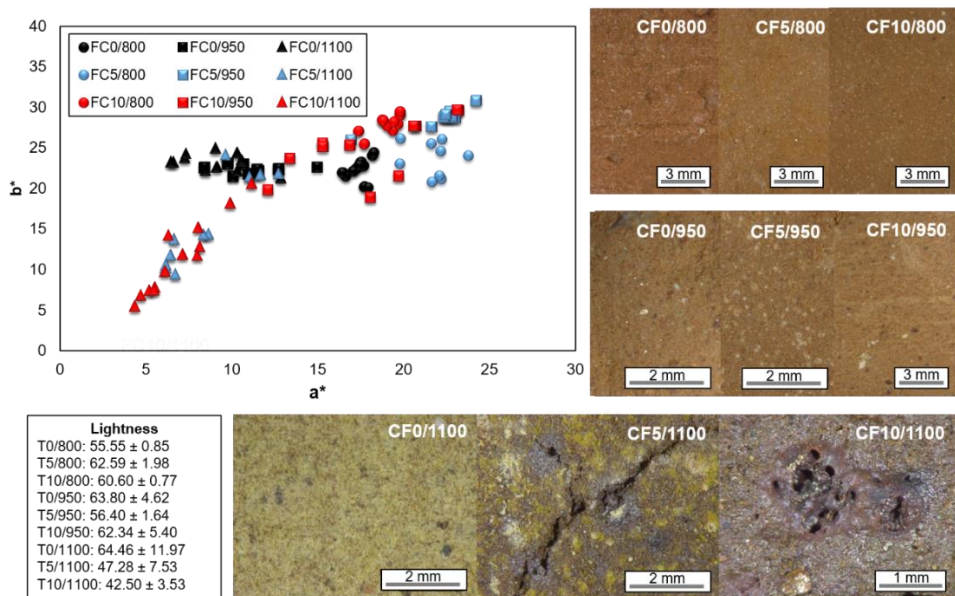


**Figure II-11.** Chromatic ( $a^*$  and  $b^*$ ) and lightness ( $L^*$ ) values for bricks with and without added CF. The visual appearance of the nine types of bricks is shown.

### 3.9. Socioeconomic importance of including clay and carbon fibre in the circular economy

Red clay is a natural material used to manufacture bricks. In a recent report by the United States Geological Survey (USGS) (<https://usgs.gov>), the recycling of clay was classified as "Insignificant" (U.S. Geological Survey, 2023). In those countries with an abundant supply of this material, its correct extraction and recycling can provide significant environmental and economic benefits and, in poorer countries especially, could be an important factor in their economic development.

According to the present study, the use of carbon fibres in brickmaking could result in a 23% reduction in red clay consumption (Table II-S1). The use of a mix composed of red clay and carbon fibre has various different benefits:

(1) Local sourcing: red clay is usually extracted from nearby quarries because it is widely available and because it is rarely viable in economic terms to source it from more distant sites, because of the high transport costs involved. Using materials in abundant supply in the immediate area not only reduces the environmental impact of transportation, but also contributes to the efficient use of regional resources.

(2) Saving natural resources: the use of 5 and 10 wt.% additive would result in respective savings of 994 and 1375 kt of clay per year in Spain (a reduction in clay consumption of up to 23%). In order to visualise what this might look like, if we assume a drilling depth of one metre, extracting 994 and 1375 kt/year would involve quarrying an area equivalent to 110 and 152 football fields with standard dimensions of 100 metres long and 50 metres wide. This simple visualisation highlights the potential benefits in terms of savings in natural resources and the safeguarding of the environment.

(3) Reducing damage to the landscape: reducing the demand for clay brings environmental benefits in the area around the quarry: the impact on the landscape, the topography, and the local flora and fauna is reduced, as is the amount of dust and noise. The reduction of quarrying activity also brings several economic savings by reducing spending on explosives, electricity, labour, and the transport of materials (on conveyor belts, trucks or other vehicles).

(4) Common efforts towards sustainability: the use of carbon fibre in the brick manufacturing process would contribute to the achievement of the Sustainable Development Goals of the United Nations (SDGs, <https://www.un.org/sustainabledevelopment/>), and in particular SDG 9 (Industry, innovation and infrastructure) and SDG 12 (Responsible consumption and production).

(5) Physical changes: one of the main aims of materials science is to optimise certain physical properties so as to enhance the performance of the materials. Among these, the thermal conductivity of materials is important to evaluate because of its impact on their energy efficiency. The thermal conductivity of any given material is directly related to the porosity inside it. The higher the porosity, the lower the thermal conductivity because the voids act as insulating barriers, preventing heat flow. Changes in the orientation of carbon fibres and the voids left behind by them after firing can change the heat transfer inside the bricks.

However, there are also a number of drawbacks to using carbon fibre as an additive in brick production:

(1) Gas emissions: when carbon fibre is incinerated or burnt, a number of gases can be released, including carbon dioxide (CO<sub>2</sub>) and total volatile organic compounds (TOC). CO<sub>2</sub> is a greenhouse gas that contributes to global warming. TOC can have adverse effects on air quality and human health, as some of these compounds can be precursors to harmful air pollutants. The presence of carbon fibre will increase CO<sub>2</sub> emissions into the atmosphere during firing. In addition to the negative impact on the environment, the CO<sub>2</sub> footprint of the finished products will be worse than that of bricks made without this residue.

(2) Quality of the final product: lower mechanical strength could make the bricks unsuitable for certain types of construction work. It is therefore essential to verify that these materials comply with the strength requirements established in current regulations.

(3) Economic impact and difficulties in production: although some financial savings can be made by replacing part of the clayey material by a waste product, the cost of

transporting the waste from the wind farms to the brick factories and the cost of grinding the residue to the size required for the brickmaking process must also be taken into account. The size of the carbon fibre particles is an important issue. The fibres used in this research were very small, which made shaping of the brick samples much easier. However, larger sizes could hinder the manufacturing process when it comes to moulding and cutting the unfired samples.

#### **4. Conclusions**

In this paper, the carbon fibre waste generated by decommissioned wind turbine blades was used as an alternative additional raw material in the production of durable bricks considered suitable for use in the construction industry and in Cultural and Architectural Heritage, so obtaining a series of important socioeconomic and environmental benefits. The most important results of this research are described below.

- It has been confirmed that carbon fibre from wind turbine blades also contains resin and thermoplastic compounds. During firing, the carbon fibre and these associated compounds are consumed, creating micropores in the bricks, so improving their thermal conductivity. On the downside, the main environmental problems arising from the manufacture of bricks with added carbon fibre are the gas emissions and unpleasant odors produced during firing. However, it is important to point out that the use of carbon fibre as an additive for brick production is less damaging, in terms of air pollution, than other "waste reduction" processes used in the wind power sector, such as incineration, pyrolysis or chemical recycling.
- The addition of carbon fibre to the clay mix partially modifies the mineralogical composition of the bricks. The concentration of hematite decreases in line with increasing firing temperature in the samples with added CF because they encourage the development of a reducing environment in the oven and the appearance of a black core.
- Texturally, the carbon fibres tend to orient themselves inside the brick. This may be influenced by the kneading and moulding of the raw bricks and by the firing temperature, as happens with the phyllosilicates.

- After firing, the carbon fibres start to degrade. As the temperature increases, they tend to disappear, leaving their imprints in the clay matrix. This increases the porosity, although the connectivity between the pores is worse in the bricks with added carbon fibre.
- Carbon fibre worsens the mechanical behaviour of the bricks. This is mainly due to their increased porosity, which was detected by analysing the porous system and the ultrasound propagation velocity. However, the samples made with CF were found to have higher surface hardness because most of the pores were in the inner part of the bricks. This could be due to the fact that the bricks were prepared by hand, which may have caused an uneven distribution of the CF particles within the clay matrix, which in turn may have affected the analysis.
- As regards the durability of the bricks, the salt crystallization test led initially to increases in weight, but with successive cycles, the bricks started to deteriorate, leading to weight loss. The presence of carbon fibre exacerbates this behaviour. However, the bricks fired at 950 and 1100 °C with added CF experienced the least material loss, making them highly resistant to salt attack and more durable.
- The colour changes resulting from CF addition did not affect the aesthetic properties of the bricks, which can make a valuable contribution as alternative building materials that are more sustainable than traditional ones.

When they reach the end of their useful life, a high percentage of turbine blades are not recycled, and have to be stored in warehouses. This could have a significant long-term impact on the environment. Within this context, the wind industry has committed to recycling or recovering 100% of decommissioned wind blades by 2025. In addition, wind turbines are becoming larger in order to be able to generate more power per turbine. This requires larger installations, with some prototypes reaching up to 280 metres in height. These huge turbines have 116-metre-long blades, which can produce up to 16 megawatts (MW), enough to power 20,000 homes over their 25-year lifespan. In recent decades, the capacity of wind power installations worldwide has grown steadily from 24 gigawatts (GW) in 2001 to 837 GW in 2022, with China, the United States of America, Germany, India and Spain accounting for 72% of global wind power installations. In terms



of the number of wind turbines, Spain has 21,574 wind turbines (Asociación Empresarial Eólica,), while the United States has 72,731.

The use of carbon fibre in the manufacture of bricks could therefore provide an excellent opportunity for both the reduction of clay consumption and the reuse of carbon fibre from wind turbine blades, so designing a circular economy process with two main benefits. Firstly, the use of raw materials (in this case clay) is minimized and secondly, the waste (carbon fibre) generated in a process, wind energy production, that is essential in the fight against climate change can be reused as an alternative building material. The results show that reusing carbon fibre waste from wind turbine blades in brick manufacture has great potential as part of a strategy for achieving the goals of the 2030 Agenda for Sustainable Development.

## Supplementary material



**Figure II-S1.** Brick making process. A) Raw materials are kneaded with water; B) the kneaded clayey mass is placed in the wooden mould; C) cut samples are left to dry in the laboratory; D) fired bricks: control group (bricks with no added carbon fibre) in the top row, bricks with 5 wt.% carbon fibre in the middle row, and bricks with 10 wt.% carbon fibre in the bottom row.

**Table II-S1.** Amount of clayey material, carbon fibre (CF) and water (in wt.%) used to produce the brick samples.

Clayey material	CF	Water
99.20	0	0.80
94.05	5	0.95
89.00	10	1

**Table II-S2.** Abbreviations used to identify the brick samples according to the firing temperatures and the amount of carbon fibre added (CF).

Firing temperature (°C)	CF (wt.%)		
	0	5	10
800	CF0/800	CF5/800	CF10/800
950	CF0/950	CF5/950	CF10/950
1100	CF0/1100	CF5/1100	CF10/1100

**Table II-S3.** Equations used to calculate the parameters from test data. Abbreviations:  $M_0$  = mass of dried sample;  $M_l$  = mass of sample saturated with water at atmospheric pressure;  $M_s$  = mass of sample saturated under vacuum;  $M_H$  = hydrostatic weight of sample saturated under vacuum;  $M_t$  = decreasing water weight content as a function of time;  $t_0$  and  $t_f$  = start and finish times of the drying test;  $t$  = time;  $h$  = height of water reached by capillary;  $F$  = is the breaking load (in N);  $A$  = cross-sectional area (in  $m^2$ );  $V_p$  = compressional pulse;  $V_s$  = shear pulse;  $V_{p1}$  = mean maximum velocity;  $V_{p2}$  = mean intermediate velocity;  $V_{p3}$  = mean minimum velocity in any of the three orthogonal directions;  $\Delta L$  = variation of the lightness parameter between control samples and those with carbon fibre;  $\Delta a^*$  and  $\Delta b^*$  = variation of the chromatic values ( $a^*$  and  $b^*$ ) between control samples and those with carbon fibre.

		Equation	Units	Norm/standards or reference
1	Free water absorption ( $A_f$ )	$A_f = \frac{M_l - M_0}{M_0} \cdot 100$	%	UNE-EN 13755 (2008)
2	Forced water absorption ( $A_f$ )	$A_f = \frac{M_s - M_0}{M_0} \cdot 100$	%	UNE-EN 1936 (2007)
3	Degree of pore interconnection ( $A_x$ )	$A_x = \frac{A_f - A_l}{A_f} \cdot 100$	%	ISRM (1979)
4	Drying Index (Di)	$Di = \frac{\int_{t_0}^{t_f} M_t dt}{M_f \times t_f}$	-	NORMAL 29/88
5	Saturation coefficient (S)	$S = \frac{M_s - M_0}{M_0 - M_H} \cdot 100$	%	RILEM (1980)
6	Open porosity ( $\rho_o$ , $\rho_oMIP$ )	$\rho_o = \frac{M_s - M_0}{M_s - M_H} \cdot 100$	%	UNE-EN 1936 (2007)
7	Apparent density ( $\rho_a$ , $\rho_aMIP$ )	$\rho_a = \frac{M_0}{M_s - M_H} \cdot 100$	$g\ cm^{-3}$	ISRM (1979)
8	Real density ( $\rho_r$ , $\rho_rMIP$ )	$\rho_r = \frac{M_0}{M_0 - M_H} \cdot 100$	$g\ cm^{-3}$	UNE-EN 1936 (2007)
9	Capillarity rise (C)	$C = \frac{h}{\sqrt{t}}$	$g/m^2s^{0.5}$	UNE-EN 1926 (2007)
10	Compressive strength ( $C_s$ )	$C_s = \frac{F}{A}$	MPa	UNE-EN 196-1 (2005)
11	Total anisotropy ( $\Delta M$ )	$\Delta M = (1 - \frac{2V_{p1}}{V_{p2} + V_{p3}}) \cdot 100$	%	ASTM D2845 (2000)
12	Poisson coefficient ( $\nu$ )	$\nu = \frac{(\frac{V_p}{V_s})^2 - 2}{2 [(\frac{V_p}{V_s})^2 - 1]}$	-	Cultrone and Sebastian, 2009 Coletti et al., 2016
13	Young modulus (E)	$E = 2\nu V_s^2 (1 + \nu)$	GPa	Cultrone and Sebastian, 2009 Coletti et al., 2016
14	Shear modulus (G)	$G = \frac{E}{2(1 - 2\nu)}$	GPa	Pande et al., 1989
15	Bulk modulus (K)	$K = \frac{E}{3(1 - 2\nu)}$	GPa	Cultrone and Sebastian, 2009
16	Colour variation ( $\Delta E$ )	$\Delta E = [(\Delta L^*)^2 + (\Delta a^*)^2 + (\Delta b^*)^2]^{1/2}$	-	UNE-EN 15886 (2011)

# CHAPTER III

***Waste pomace from wine industry as additive for making bricks***

Laura Crespo-López, Alberto Martínez-Ramirez, Eduardo Sebastián, Giuseppe Cultrone

Published in *Applied Clay Science*

Vol. 243, 107084 (2023)

DOI: 10.1016/j.clay.2023.107084

Impact Factor: 5.6

Position 2/29 (Q1, D1)

Category: Mineralogy (JCR 2022)





Applied Clay Science

Volume 243, October 2023, 107084






Review article

# Pomace from the wine industry as an additive in the production of traditional sustainable lightweight eco-bricks

[Laura Crespo-López](#)<sup>○</sup>  , [Alberto Martínez-Ramirez](#)<sup>b</sup>, [Eduardo Sebastián](#)<sup>○</sup>, [Giuseppe Cultrone](#)<sup>○</sup>

Show more 

 Add to Mendeley  Share  Cite

<https://doi.org/10.1016/j.clay.2023.107084>

[Get rights and content](#) 

**Keywords:** lightweight bricks; wine pomace; porosity; strength.

## 1. Introduction

Vine cultivation is one of the most common, most widespread crops in Mediterranean countries and in the world in general (Barbieri et al., 2013; Fontana et al., 2013). In 2021, over 74 million tonnes of fresh grapes were obtained from approximately 7.4 Mha of plantations worldwide, from which 262 million hL of wine were produced (data from the International Organisation of Vine and Wine, OIV, [www.oiv.int](http://www.oiv.int)). This vast scale of production clearly generates a huge volume of waste, known as pomace. The countries

with the highest worldwide production of wine pomace are Italy, France and Spain, with almost 1.4, 1.2 and 1 million tonnes respectively (OIV, [www.oiv.int](http://www.oiv.int)).

The chemical composition of wine pomace is affected by factors such as grape variety or climate (Bordiga et al., 2019; Taladrid et al., 2019a; Aresta et al., 2020; Kotsanopoulos et al., 2021). The presence of certain compounds, such as phenols (anthocyanins, flavan-3-ols, flavonols, hydroxybenzoic and hydroxycinnamic acids and stilbenes) (Lafka et al., 2007; Makris et al., 2007; Monad et al., 2010; Fogliano et al., 2011; Barcia et al., 2014) could make disposing of the wine pomace in landfills or its incineration a threat to the environment, as it could lower the pH of the soil leading to oxygen depletion. It could also increase resistance to biological degradation (Arvanitoyannis et al., 2006; Lafka et al., 2007; Fontana et al., 2013). According to Spanish Law 10/1998, these wastes must be treated before disposal to avoid environmental pollution. Wine companies that make unauthorised discharges of wastewater can be subject to heavy fines and waste disposal fees can be significant (González-Paramás et al., 2006; Devesa-Rey et al., 2011). This regulation could encourage wine industries to investigate new waste treatment technologies or new ways of using these residues profitably and sustainably. However, small wine producers often choose not to comply with this law and dispose of wine pomace and winery sludge in landfills.

Traditionally, pomace is used as a fertiliser, animal feed or for the production of distillates (Salinas et al., 2003; Paradelo et al., 2011; Meloni et al., 2015; Paradelo et al., 2013). Some researchers have also investigated its application as a biofuel, based on its high calorific value (Airado-Rodríguez et al., 2011; Ye et al., 2016; Maicas, 2020; Arya et al., 2022), and this seems to be the most promising sector for future research (Taladrid et al., 2019a and b; Perra et al., 2022).

Wine pomace is made up of grape skins, seeds and stems and wine lees (Bustamante et al., 2008). The proportions of each of the components of wine pomace vary, with some authors stating that seed content ranges between 38-52 wt.% and skin content between 5-10 wt.% (Nogales et al., 2005; Yu and Ahmedna, 2013; García-Lomillo and González-San José, 2017; Nardoia et al., 2017; Guardia et al., 2018). Sulphur dioxide is often added to the grape must during winemaking to inhibit wild yeasts and control microorganisms such as bacteria and moulds (Arvanitoyannis et al., 2006), which explains why it can also be found in wine waste products. As regards the possible use of wine pomace in the brick industry, certain types of residues (both organic and inorganic)

have been found to increase porosity in fired bricks, so reducing their thermal conductivity (Cultrone and Sebastián, 2009; La Rubia-García et al., 2012; Eliche-Quesada et al., 2017; Cultrone et al., 2020). When it comes to forming pores, organic wastes are generally cheaper than inorganic ones and also have the advantage of contributing to the heat required during the firing process (Bustamante et al., 2008; Guardia et al., 2018; Crespo-López et al., 2024). However, the amount of residue that can be added is limited by the fact that it can impair the mechanical properties of the bricks (Anjum et al., 2020). In addition, residues can have negative effects on the plasticity of the clayey material, causing an increase in the amount of water required during the moulding process (Demir, 2008). Another drawback of organic wastes is that CO<sub>2</sub> emission during firing is usually higher than when inorganic wastes are used.

At the same time, the widespread exploitation of clayey soils for brickmaking is leading to the depletion of these non-renewable natural resources (Demir, 2008). Clays are essential for making bricks in a process which briefly involves: the extraction of the raw materials, their crushing, sieving and, in some cases, mixing with other clays or additives, kneading with water and shaping the samples. After drying, the bricks are fired at temperatures that cause mineralogical and physical transformations. The composition of the raw material and the firing temperature are the two main factors that affect the final characteristics of the bricks (Cultrone, 2001). This paper aims to investigate the recycling of a winemaking by-product, pomace, by using it as an additive to make quality bricks for use in the construction industry, so reducing the amount of clay used and preventing its depletion. By using this waste material in the production of bricks, we could reduce the amount of wine pomace that is dumped in landfills and perhaps also make savings in production costs.

In this paper, we investigate the effects of the addition in different proportions (2.5, 5 and 10 wt.%) of wine pomace to a mix of two different clayey materials to produce lightweight bricks fired at three different temperatures (800, 950 and 1100 °C). The main objectives are to find out more about the properties of the wine pomace, to determine the optimum amount to use in the brick-making process, and to evaluate the quality and durability of the resulting bricks. The percentages of waste were chosen in view of the promising results obtained in previous research into wine pomace (La Rubia-García et al., 2012) and other organic wastes (Monteiro and Vieira, 2014). On this question, Coletti et al., 2023 recently observed that the addition of grape stalks increases the porosity and

thermal insulation properties of the bricks. However, high percentages of pomace seem inadvisable. In fact, Monteiro and Vieira (2014) and Muñoz et al. (2014) found that amounts of over 10 wt.% would produce excessively brittle bricks from a mechanical point of view.

## **2. Materials and Method**

### 2.1. Geological context of the clayey materials

The raw materials used to make the bricks come from Viznar and Guadix (Granada, Spain). The Viznar clay formation is part of the Granada basin, while the clay from Guadix belongs to the Guadix basin. Both basins are part of the central area of the Betic Cordillera.

The clay from Viznar was deposited during the late Turolian in a lacustrine environment, with alluvial sediments (conglomerates and sands), deltaic sediments, small calcarenitic platforms and other materials from the Sierra Nevada and Sierra Arana (García-Alix et al., 2008).

The clay from Guadix was deposited in the Middle-Late Pleistocene during the last stages of basin infilling (Braga et al., 2003; Pérez-Peña et al., 2009), mainly in small lagoons and marshes that appeared temporarily on the banks of braided rivers draining from the nearby Sierra Nevada (Vera and Rodríguez Fernández, 1988; Braga et al., 2003).

### 2.2. Traditional brick production

The bricks for this study were made by mixing the raw materials from Viznar and Guadix in proportions of 3/5 and 2/5 by weight, respectively, following the same proportions as those used by a brick manufacturer from Viznar (Granada, Spain), who provided the raw materials. The wine pomace was provided by a wine manufacturer from Valdepeñas (Ciudad Real, Spain). In order to remove all residual moisture, the pomace was dried at 60 °C in an electric oven for 8 h to avoid degradation of the polyphenols during the drying process. The clayey materials were sieved and fragments of over 1.5 mm in size were discarded, while the wine pomace was mechanically crushed to a particle size of up to 3 mm in size. The clayey material, wine pomace and water were mixed together to form a kneadable paste. Once enough plasticity had been achieved, the clayey paste was placed in moistened wooden moulds of 15 × 20 × 4 cm. After one hour, the moulds were removed and the clayey pastes were cut into ~ 4 cm edge cubes using a stretched cotton



thread and left to dry. When the bricks were dry, they were fired in a Herotec CR-35 electric oven at 800 °C, 950 °C and 1100 °C. Table III-1 summarizes the samples analysed in this paper. The samples were preheated for 1 hour at 100 °C so as to eliminate any residual moisture that might still be present inside them. Then, the temperature was increased at a rate of 2 °C/min. Once the maximum temperature was reached, it was maintained for the dwell time of 3 hours. Finally, the oven was turned off and the samples were left to cool slowly until the next day, so as to prevent fissures from developing due to the  $\beta$ -to- $\alpha$  quartz transition at 573 °C. After removal from the oven, the bricks were immersed in water for about 1 hour so as to prevent possible “lime blowing” due to the presence of lime grains (Laird and Worcester, 1956).

**Table III-1.** Reference and firing temperatures of brick samples made with (W samples) and without (Mi samples) added wine pomace.

Firing temperature (°C)	Control	Wine pomace (wt.%)		
		2.5	5	10
800	Mi800	W800/2.5	W800/5	W800/10
950	Mi950	W950/2.5	W950/5	W950/10
1100	Mi1100	W1100/2.5	W1100/5	W1100/10

### 2.3. Analytical techniques

#### *2.3.1. Chemical, mineralogical and textural study*

Elemental analysis of the wine pomace was conducted using a Thermo Scientific Elemental Analyser CHSN TM FlashSmart and its calorific value was determined using a calorimetric pump IKA Werke model C5003. The grain size of the raw material and the wine pomace were measured separately using a Galai CIS-1 laser gauge. X-ray fluorescence (XRF) was used to determine the major elements in the clayey material with a PANalytical Zetium compact spectrometer. 3 g of each sample was ground to powder prior to its analysis. The mineralogical composition of the raw sample and fired bricks was determined by powder X-ray diffraction (PXRD) using a PANalytical X'Pert PRO diffractometer. The samples were milled with an agate mortar to a particle size less than 53  $\mu\text{m}$  and then analysed. The working conditions were as follows: CuK $\alpha$  radiation, 45 kV voltage, 40 mA current, 3 to 70° 2 $\theta$  exploration range, 0.1 2 $\theta$  s<sup>-1</sup> goniometer speed. The mineral phases were identified using the PANalytical X'Pert Highscore Plus 3.0 software.

The thermal decomposition of the raw material up to 950 °C was determined using a METTLER-TOLEDO TGA/DSC1 thermogravimetric analyser coupled with differential scanning calorimetry. The sample was deposited on an Al crucible and analysed in a flowing air atmosphere (50 ml/min) at a heating rate of 20 °C/min up to 950 °C. The petrographic features (mineralogy and texture) of the fired samples were observed under plane- and cross-polarized light by means of polarized optical microscopy (POM) using a Carl Zeiss Jenapol-U microscope equipped with a Nikon D7000 digital camera. A high-resolution Carl Zeiss SMT (AURIGA series) field emission scanning electron microscope (FESEM) coupled with X-ray energy dispersive spectroscopy (EDS) was used to observe the texture and porosity of the samples in more detail.

### 2.3.2. *Pore system*

Hydric and porosimetric tests were carried out in order to analyse the pore system of the bricks and how it is altered by the addition of wine pomace. Free ( $A_b$ , at atmospheric pressure) and forced ( $A_f$ , under vacuum) water absorption, drying ( $D_i$ ) and capillarity tests ( $C$ ) were carried out according to UNE-EN 13755 (2008), NORMAL 29/88 (1988) and UNE-EN 1926 (2007) standards, respectively. These tests enabled us to determine the saturation coefficient ( $S$ ), the apparent ( $\rho_a$ ) and real ( $\rho_r$ ) densities, and the open porosity ( $P_o$ ). Hydric tests were performed under controlled thermo-hygrometric conditions (20 °C and 60% relative humidity) using deionized water. Three samples per brick group were analysed.

The pore system of the bricks within a range of 0.002 to 200  $\mu\text{m}$  was analysed by mercury intrusion porosimetry (MIP) using a Micromeritics Autopore IV 9500 porosimeter. Samples of about 1 g were dried in a ventilated oven for 48 h at 30 °C prior to analysis. Specific surface area (SSA), apparent and real densities ( $\rho_{a\text{MIP}}$  and  $\rho_{r\text{MIP}}$ ) and open porosity ( $P_{o\text{MIP}}$ ) were calculated.

### 2.3.3. *Physical-mechanical properties*

Ultrasound was used to determine the compactness of the bricks. Measurements were performed using a Control 58-E4800 ultrasonic pulse velocity tester with transducers of 54 kHz and a circular surface of 27 mm in diameter. A water-based eco-gel was used to enable homogeneous contact between the transducers and the brick. The measurements were carried out on three samples per brick type. P-wave propagation was measured in m/s according to the ASTM D2845 (2008) standard.

The compressive strength (CS) was measured using a Matest E181 hydraulic press with double frame 25 kN/300 kN, according to the UNE-EN1926 (2000) standard. CS was measured perpendicular to the compaction plane of the clayey mass and was calculated in MPa on three samples per brick type according to the following Eq. 1:

$$CS = \frac{F}{A} \quad (1)$$

Where F is the breaking load (in N) and A is the cross-sectional area (in m<sup>2</sup>).

#### 2.3.4. Colour

Colour measurements were carried out to quantify the lightness (L\*) and chromaticity (a\* and b\*) of the fired bricks. A Konica Minolta CM-700d spectrophotometer was used following the UNE-EN 15886 (2011) standard. Illuminant D65, 10° observer angle and 8 mm measurement area were used. Nine measurements per sample were performed. The total colour variation ( $\Delta E$ ) between bricks without additive and with added wine pomace was calculated as follows (Eq.2):

$$\Delta E = [(\Delta L^*)^2 + (\Delta a^*)^2 + (\Delta b^*)^2]^{(1/2)} \quad (2)$$

#### 2.3.5. Salt crystallization test

Fifteen salt crystallization cycles were performed to observe a theoretical degradation that could affect the lifetime of the bricks (made with and without wine pomace) according to the UNE-EN 12370 (2020). The salt crystallization test reproduces the deterioration that the bricks may undergo due to the dissolution and recrystallization of soluble salts within their porous systems.

### 3. Results and discussion

#### 3.1. Characterization of the raw material and the wine pomace

Table III-2 shows the elemental composition (in %) of the wine pomace used for the production of the bricks. It is clearly very high in C and it is interesting to note the absence of S, given that sulphur is widely used to prevent biological attacks on vines, as mentioned in the introduction section.

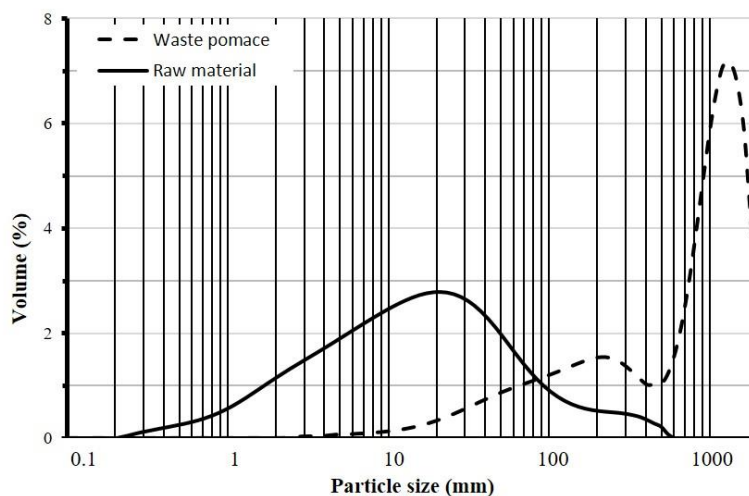
The calorific value of wine pomace is 19.2 kJ/g. Compared to the calorific value of other wastes such as avocado peel (14.7 kJ/g) or olive pits (18.4 kJ/g), which have also been

investigated for their possible use in the production of lightweight bricks (José et al., 2021; Limami et al., 2021; El Boukili et al., 2022), waste pomace could save a little more energy during brick firing due to its higher calorific value.

**Table III-2.** Elemental analysis (in %) of wine pomace.

N	C	H	S
2.39	50.77	6.11	0.00

The granulometric analysis shows that the raw material has unimodal particle size distribution while the wine pomace is bimodal (Fig.III-1). The raw material curve is quite symmetrical with a maximum at around 20  $\mu\text{m}$ . In contrast, the wine pomace curve has larger particle sizes with a main curve that peaks at 1345  $\mu\text{m}$  and a less intense second peak at 276  $\mu\text{m}$ .



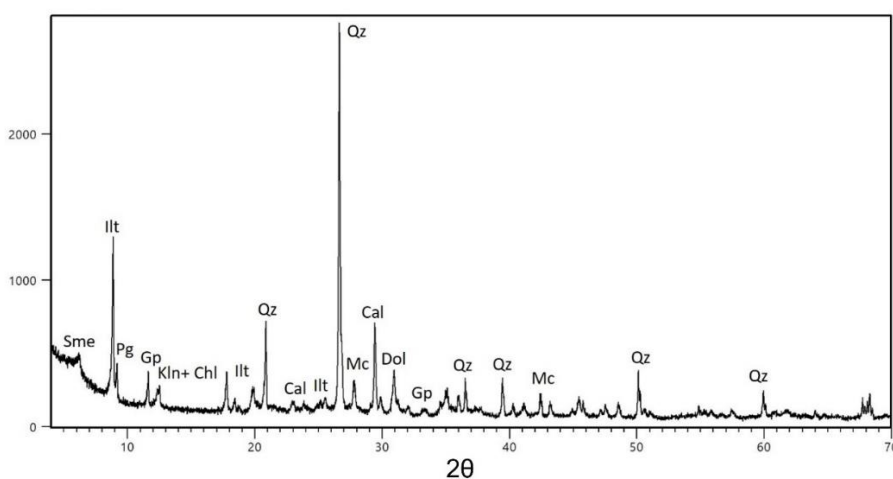
**Figure III-1.** Grain size distribution of the raw material and waste pomace.

Table III-3 shows the chemistry of the mixed clayey sample. It is rich in  $\text{SiO}_2$  and has high  $\text{Al}_2\text{O}_3$  and  $\text{Fe}_2\text{O}_3$  contents. The presence of  $\text{CaO}$  (9.23%) and  $\text{MgO}$  (2.82%) is a sign of its carbonate content and it can be classified as calcareous according to Tite (1975) and Maniatis and Tite (1981).

**Table III-3.** XRF results (in %) for the raw material used to manufacture the bricks.

$\text{SiO}_2$	$\text{Al}_2\text{O}_3$	$\text{Fe}_2\text{O}_3$	MnO	MgO	CaO	$\text{Na}_2\text{O}$	$\text{K}_2\text{O}$	$\text{TiO}_2$	$\text{P}_2\text{O}_5$	LOI
47.98	14.95	5.69	0.07	2.82	9.23	1.25	2.66	0.84	0.15	12.33

PXRD analysis reveals that the clay is rich in quartz (Fig.III-2), so confirming the high SiO<sub>2</sub> content detected by XRF. Various phyllosilicates were encountered including illite, paragonite, smectite, chlorite and kaolinite while the carbonates consist of calcite and dolomite. Gypsum and K-feldspar (microcline) were also detected. Paragonite is very common in the internal areas of the Betic Cordillera (Ramos et al., 1989; López and Cruz, 2016), an area from which part of the clay (Guadix) used to make the bricks was obtained. For its part, the clay from Viznar is made up above all of carbonates and gypsum, common features of the different geological formations that make up the Granada Depression (Ruiz-Bustos et al., 1992; Torres et al., 2020; Santamaría-López et al., 2022).



**Figure III-2.** X-ray diffraction pattern of the raw material. Legend according to Whitney and Evans (2010): Qz = quartz; Cal = calcite; Gp: Gypsum; Dol = dolomite; Illt = illite; Pg = paragonite; Kln= kaolinite; Chl = chlorite; Sme = smectite; Mc = microcline.

Thermal analysis (TG-DTA) of the clayey material (Fig.III-3) shows a weight loss of 5% at 98 °C due to the loss of hygroscopic water (Maritan et al., 2006; Nieto et al., 2008). At 289 °C there is an inflection in the curve corresponding to the combustion of organic matter (Geng and Sun, 2018; Touch et al., 2019; Achik et al., 2021). At around 500 °C, a gradual dehydroxylation of the phyllosilicates begins to occur which continues until just below 714 °C (Eberhart, 1963; Cultrone et al., 2001; Heller-Kallai and Lapides, 2015). Between this temperature and 800°C, the main weight loss of around 15% occurs, a value very similar to that detected by XRF (LOI, Table III-4) and linked to the decomposition of carbonates and the release of CO<sub>2</sub> (Rodríguez-Navarro et al., 2009 and 2012). The sample starts losing weight again at 841 °C, probably due to further

dehydroxylation of the phyllosilicates (Cultrone et al., 2004; Dubacq et al., 2010; Hirono and Tanikawa, 2011). Finally, an exothermic peak is observed at 920 °C due to the formation of new crystalline phases (Eliche-Quesada et al., 2012a and b; Taurino et al., 2019; Rodriguez-Navarro et al., 2003), which will be described later by PXRD.

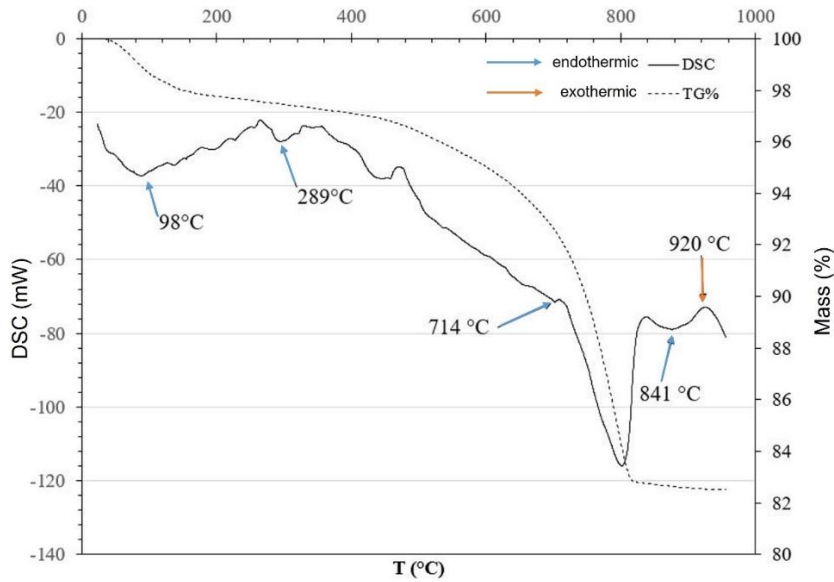


**Figure III-3.** TG-DSC analysis of the raw material. The abscissa represents the temperature (in °C) and the two ordinates represent the weight loss (right ordinate, in %) and the differential scanning calorimetry (left ordinate, in mW).

### 3.2. Chemistry, mineralogy and texture of fired bricks

#### 3.2.1. Weight difference and linear shrinkage

Fig.III-S1 shows the relationship between weight difference and linear shrinkage after firing. All samples show a shift downwards and to the right that is related to their composition.

Bricks without additives show a decrease in weight (from 4 to 6%) as the firing temperature increases. This trend is not observed in the bricks with added wine residues (Fig.III-S1). The bricks made with 2.5 wt.% pomace are clearly lighter (approximately 10.5% lighter at all three firing temperatures) than the Mi bricks. This trend continues as the amount of additive is increased. Those made with 5 wt.% wine pomace were up to 18% lighter than the control samples, while those made with 10 wt.% pomace were 22-

24% lighter. This weight reduction could represent an advantage for the construction industry in terms of cost savings, in that lighter bricks are cheaper to transport.

As regards linear shrinkage, all the bricks become shorter (Fig.III-S1). The control bricks show the least linear shrinkage and this is mainly due to the loss of the hygroscopic water still present in the samples and the dehydroxylation of phyllosilicates during firing (Ngon et al., 2012; Velasco et al., 2015; Saenz e al., 2019). This is why the bricks fired at 1100 °C (-1.80 mm) shrink more than those fired at 800 °C (-1.07 mm). The shrinkage of the bricks that contain wine pomace is directly related to the amount of waste added to the clay mixture. The more the additive, the greater the shrinkage, which reaches a maximum value of -4.6 mm in samples with 10 wt.% waste. These results are in line with those of other authors such as Demir (2008), Barbieri et al. (2013), and Eliche-Quesada et al. (2012a), who reported that linear shrinkage depends more on the amount of residue used in the mix than on the firing temperature (Wang et al., 2020). Our bricks all had shrinkage values of less than 8%, the maximum shrinkage value for producing good quality bricks, according to Laita et al. (2021).

### 3.2.2. Mineralogical composition of fired bricks

The evolution of the mineralogy of the bricks during the firing process determined by powder X-ray diffraction (PXRD) can be seen in Fig.III-4. No substantial differences can be observed in the bricks fired at 800 and 950 °C. However, at 1100 °C an increase in background noise is detected, probably due to the development of amorphous phase (i.e. vitrification of the samples) and the crystallization of high temperature phases, which increase in concentration in line with the increase in the amount of additive used. This indicates that the calorific value of the wine pomace plays a key role in the reaction between the mineral phases to promote further development of new silicates.

At the three firing temperatures studied (800, 950 and 1100 °C), quartz (as the main crystalline phase) and feldspars *s.l.* are present in all the samples regardless of the amount of wine pomace added. At 800 °C, all the phyllosilicates have disappeared with the exception of a dehydroxylated illite, which can still be detected at 950 °C. Calcite is detected in very small amounts at 800 °C, but not at the higher temperatures. According to Rodríguez-Navarro et al. (2009), calcite starts to decompose at 600 °C and disappears completely at 850 °C. As for K-feldspar, the microcline detected in the raw material

converts into orthoclase at 800 °C and sanidine at 950 °C and 1100 °C (Cultrone et al., 2001). Hematite, which was absent in the raw material, starts to appear in traces at 800 °C and increases in concentration as the firing temperature augments. It probably forms due to the decomposition of phyllosilicates, which favour Fe recrystallization (Cultrone and Sebastián, 2009). The decomposition of carbonates and their reactions with quartz and other silicates lead to the appearance of new Ca- (and Mg-) silicates such as gehlenite at 950 °C and wollastonite, anorthite and diopside at 1100 °C (Fig.III-4). The presence of gehlenite in the bricks fired at 950 °C could explain the appearance of the exothermic peak detected in the DSC curve at 920 °C (Fig.III-3). At 1100 °C, gehlenite content falls because it is involved in the formation of anorthite and wollastonite (Cultrone et al., 2001). Another new phase, mullite, is identified. This phase replaces illite, with which it shares certain specific crystallographic orientations (Rodríguez-Navarro et al., 2003).

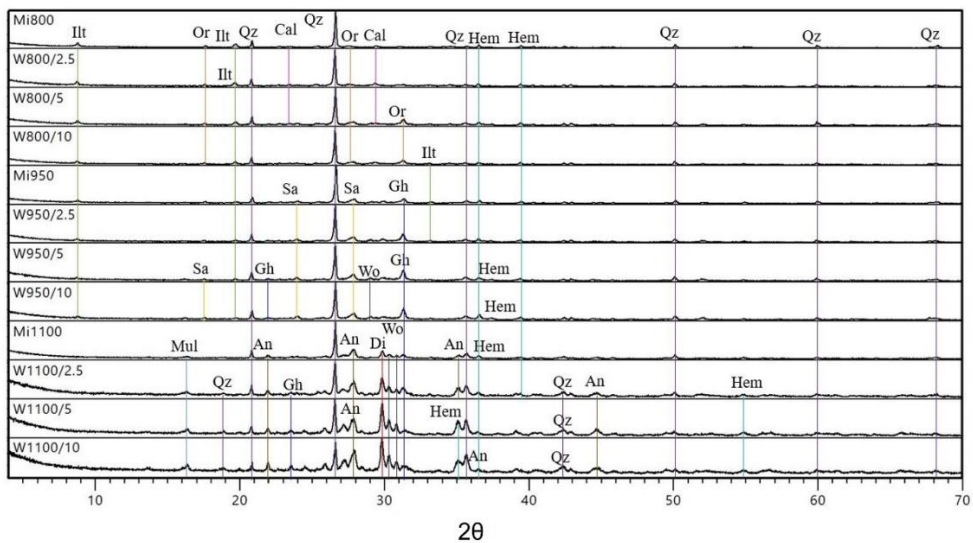


**Figure III-4.** PDRX patterns for control bricks (Mi) and bricks with added wine pomace (W) fired at 800, 950 and 1100 °C. Legend according to Whitney and Evans (2010): Qz = quartz; Cal = calcite; Ill = illite; Hem = hematite; Or = orthoclase; Sa = sanidine; An = anorthite; Gh = gehlenite; Di = diopside; Wo = wollastonite; Mul = mullite.

### 3.2.3. Structure of the fired bricks

Polarized optical microscope (POM) observation of the samples fired at 800 °C revealed the presence of fragments of metamorphic rocks (quartz grains with undulose extinction, mica-schists and gneiss, Fig.III-5A) of about 1 mm in length in an orange-to-brown matrix.



As expected, higher porosity can be observed when residues with irregularly-shaped pores are added and it increases in line with the amount of residue added to the clay (compare Figs.III-5A and B with Figs.III-5C to G). Phyllosilicates and elongated fragments often show a preferential orientation due to the pressure exerted on the raw material during the kneading process (Fig.III-5C). Phyllosilicates are composed of muscovite-type crystals and appear unaltered reaching second-order interference colour (Fig.III-5C and E). The carbonate grains are partially decomposed and have lost their typical high interference colour (Fig.III-5G). At 1100 °C, due to the high firing temperature, the pores become ellipsoidal-to-rounded in shape and the matrix becomes darker (Fig.III-5B, D, F and H). Muscovite-type crystals have lost their birefringence and have a whitish colour (Fig.III-5D, red arrows). According to Rodríguez Navarro et al. (2003) and the PXRD results (Fig.III-4), this phyllosilicate has probably been replaced by mullite.

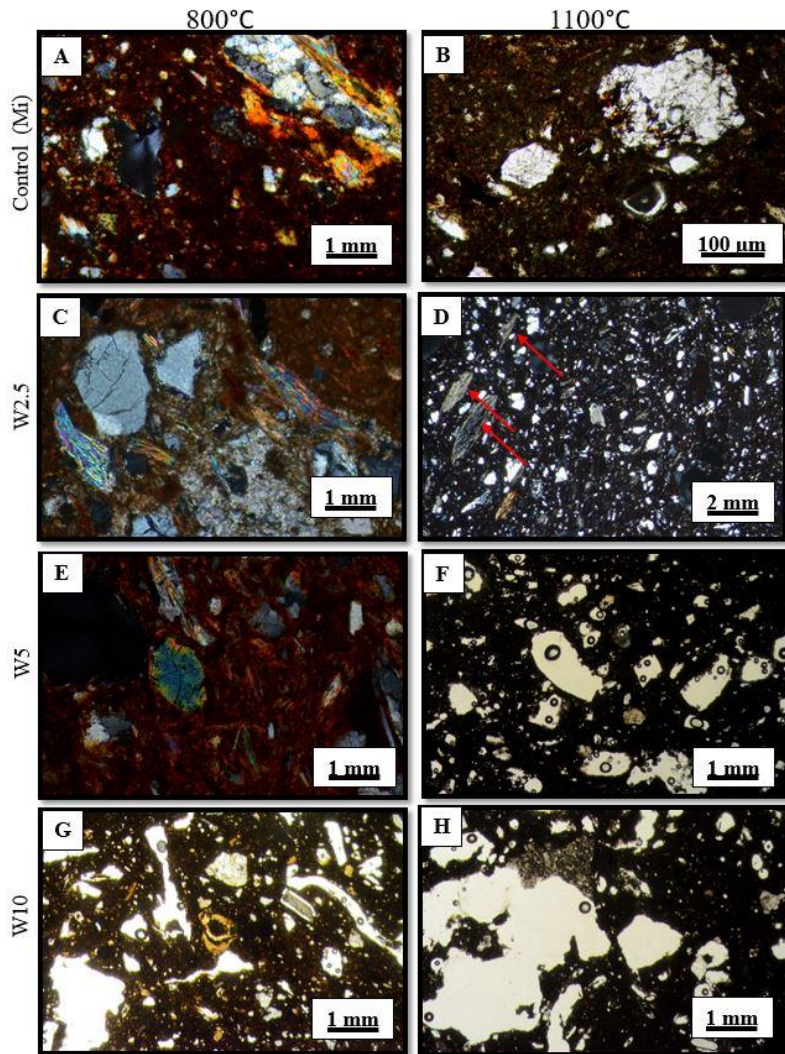
#### 3.2.4. *Microstructure of fired bricks*

FESEM observations were carried out on the bricks fired at 800 °C (Fig.III-6) and 1100 °C (Fig.III-7) with and without 5 wt.% wine pomace in order to highlight any textural differences between them.

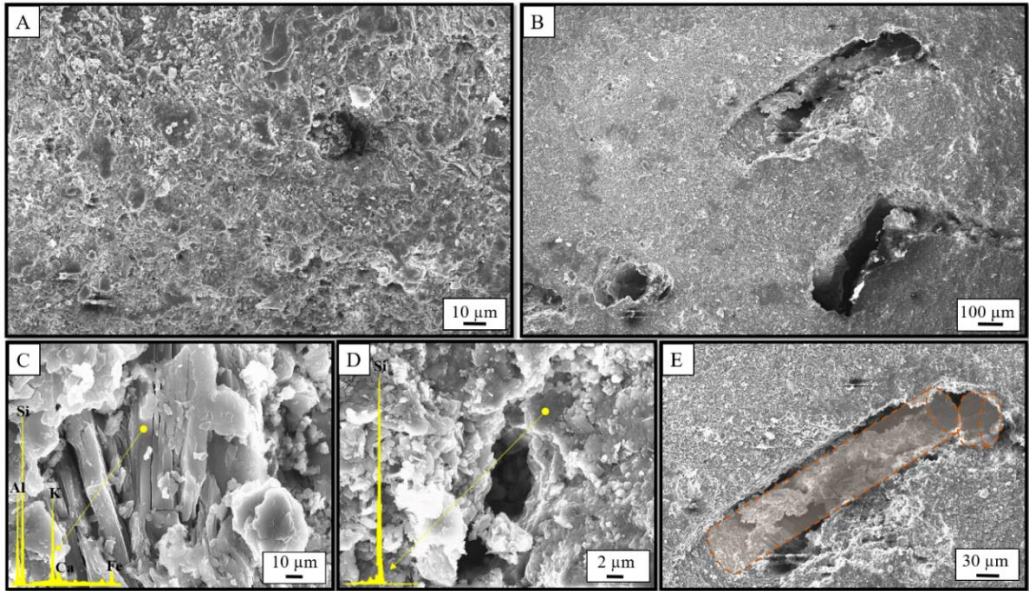
Fig.III-6A (Mi800) shows a dense structure with lower porosity than Fig.III-6B (W800/5) in which large pores with irregular shapes can be observed. These are due to the imprints left by the wine pomace particles (grape seeds, stems and skins) present in the clay mixture before firing. A detailed observation of the bricks made without (Fig.III-6C) and with 5 wt.% wine pomace (Fig.III-6D) shows that they are compositionally very similar, which corroborates the previous XRF and PXRD analyses. K-feldspar (Fig.III-6C) and quartz fragments (Fig.III-6D) have been detected by EDS analysis. Fig.III-6E is a zoomed version of Fig.III-6B, in which we have recreated the imprint left by an elongated, cylindrical stem after firing of the brick.

Fig.III-7A (Mi1100) shows an even more compact structure than in Fig.III-6A (Mi800) due to the vitrification process after firing the samples at 1100 °C, thus confirming the POM observations (see section 3.2.3.). Fig.III-7B (W1100/5) shows the same level of vitrification level as in Fig.III-7A (Mi1100), although the morphology of the surface is quite irregular due to the presence of larger pores as a result of the addition of the wine pomace. Detailed images of the bricks fired at 1100 °C (Figs.III-7C, D and E) highlight the presence of elongated and irregular-shaped pores, created by the vitrification of the

matrix. Pores tend to coalesce forming larger pores and remain larger in the bricks with added wine pomace (Fig.III-7D and 7E). The difference in the porosity of bricks made with and without wine pomace will be corroborated later by studying the pore system with hydric tests and MIP.



**Figure III-5.** Bricks with and without added wine pomace fired at 800 and 1100 °C. Abbreviation: PPL = plane-polarized light; PPX = cross-polarized light. A) Matrix of sample Mi800 (PPX); B) detailed image of extended vitrification in the matrix of Mi1100 (PPL); C) phyllosilicate grains with a preferential orientation (PPX); D) muscovite-type crystals with a whitish colour (red arrows, sample W1100/2.5, PPX); E) unaltered phyllosilicates in W800/2.5 sample (PPX); F) ellipsoidal-to-rounded pores and darker matrix in W1100/5 (PPL); G) decomposed carbonate grain in W10/800 sample (PPL); H) very large and rounded pores in W10/1100 sample (PPL).



**Figure III-6.** FESEM images of bricks fired at 800 °C without additives (A and C) and with wine pomace (B, D and E). EDS spectra of some of the mineral phases have been included.

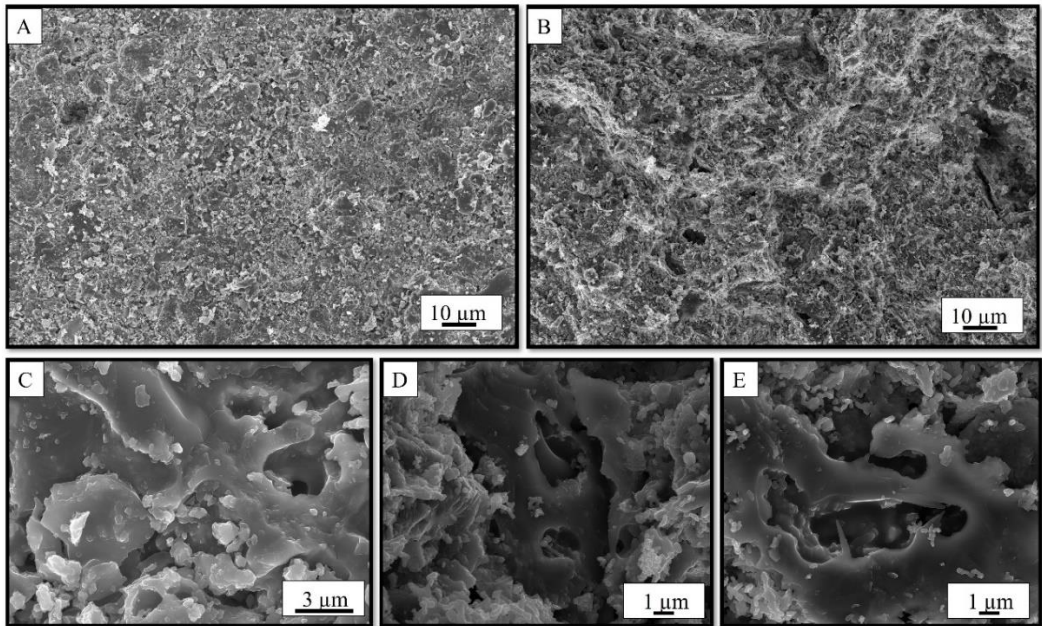


**Figure III-7.** FESEM images of bricks fired at 1100 °C made without (A and C) and with wine pomace (B, D and E).

### 3.2.5. Colour measurement of fired bricks

The colour of bricks is mainly dependent on the composition of the raw material, the firing temperature and time, and the oxidant-redox environment inside the oven (Weng et al., 2003; Bautista-Marín et al., 2021). The colour of bricks can also be modified by adding organic or inorganic compounds to the raw material (Rathossi and Pontikes, 2010; Ordieres and Cultrone, 2022). In this research, the fired bricks are generally yellowish-red in colour, but there are certain differences between those made without additive and those made with (Fig.III-S2). The addition of wine pomace increases the lightness ( $L^*$ ) and decreases the chromatic coordinates ( $a^*$  and  $b^*$ ) (Table III-4). The results show that the increased lightness in samples with wine pomace appears to be linked to the increase in firing temperature. Conversely, the decrease in the values of the chromatic coordinates, especially in those linked to the red colour ( $a^*$ ) could be related to changes in the size of the crystallized hematite particles, which give the bricks their reddish hue (Clifford, 1984; Crespo-López and Cultrone, 2022; Wang et al., 2022).

The differences in colour between the control samples and those made with wine pomace augment with the firing temperature, varying between 1.5 and 2.8 ( $\Delta E$ , Table III-4). According to Mokrzycki and Tatol (2011), this means that bricks with added pomace fired at 800 °C can only be distinguished from those without additive by an experienced observer, while those fired at 950 and 1100 °C can also be recognized by inexperienced observers. These results are particularly important in the construction sector, as colour is an essential feature of the first impression that the consumer gains of any brick and can strongly influence their choice.

**Table III-4.** Lightness ( $L^*$ ), chromatic coordinates ( $a^*$ ,  $b^*$ ) and colour change ( $\Delta E$ ) values in fired bricks.  $\sigma$  is the standard deviation of nine measurements per brick.

	$L^*$		$a^*$		$b^*$		$\Delta E$
	$\bar{x}$	$\sigma$	$\bar{x}$	$\sigma$	$\bar{x}$	$\sigma$	
Mi800	56.85	2.60	18.76	1.13	24.40	0.73	-
W800/2.5	60.68	1.41	16.17	0.85	23.60	1.07	1.48
W800/5	63.01	2.43	14.24	2.02	23.83	1.47	2.04
W800/10	63.51	2.11	9.64	2.29	18.76	1.63	2.69
Mi950	59.75	3.21	16.30	1.04	22.90	1.53	-
W950/2.5	60.28	2.19	13.51	1.18	20.15	1.64	1.68
W950/5	67.95	3.44	8.95	1.50	22.91	2.27	2.15
W950/10	63.22	2.15	6.55	1.38	18.71	2.11	2.79
Mi1100	67.30	4.69	7.66	1.70	23.12	0.86	-
W1100/2.5	76.13	3.00	4.11	0.90	23.45	1.76	1.74
W1100/5	76.10	3.01	4.08	0.46	22.22	1.11	2.55
W1100/10	72.74	4.41	3.56	0.59	23.39	1.67	2.75

### 3.3. Hydric tests

As expected, the porosity and water absorption of the bricks increase in line with the amount of residue added (Fig.III-8 and Table III-5). This indicates that the addition of pomace has a more substantial effect on the hydric behaviour of the bricks than the firing temperature. In particular, control bricks (Mi) absorb less water (Ab decreases from 27.3% at 800 °C to about 21% at 1100 °C, Table III-5) as the firing temperature increases. The same trend is observed when water absorption is forced under vacuum (Af, Table III-5). The open porosity values also fall (Po, Table III-5). This is due to a gradual vitrification of the matrix and, if we look at the curves for the Ab and Po values, it seems more pronounced from 950 to 1100 °C than from 800 to 950 °C. Other researchers found that in the raw materials that contain carbonates, the vitrification process does not occur at the same gradual rate throughout, but is slow at low firing temperatures (a stable structure is created) and then accelerates as high temperatures are reached (Cultrone et al., 2004; Tarvornpanich et al., 2008; Mokrzycki and Tatol, 2011; Gliozzo, 2020). However, this does not happen when wine pomace is added. In fact, these bricks are more porous and absorb more water as firing temperature increases (Table III-5). The large pores left by organic fibres in the wine pomace already observed under FESEM (Figs.III-6 and 7) clearly affect the hydric properties of the bricks, not only by increasing



their water absorption capacity, but also by improving water flow as the matrix sinters and vitrifies. The high calorific value of the residue used in this research may have favoured a partial fusion of the matrix around the fibres, so improving the connectivity between the capillaries. The observation that bricks made with and without additives have quite different hydric behaviour is confirmed by the drying index (Fig.III-8). While the control bricks tend to dry more slowly as firing temperature increases (Di augments, Table III-5), those made with wine pomace showed similar drying index values at all 3 firing temperatures, with a slight improvement at 950 °C (Table III-5). As for capillarity (C, Table III-5), the bricks tend to absorb water faster as the temperature increases and as the amount of wine pomace decreases. The control bricks have the highest C values. This is because the capillaries are larger in the bricks with added organic matter in which water rises more slowly (Dacuba et al., 2022; Micheal and Moussa, 2022). And the more organic matter added, the greater the proportion of larger capillaries in the bricks, and the slower the capillary rise. No clear trend is observed regarding the saturation coefficient (S, Table III-5). It is quite similar in brick samples and ranges from 75 to 93% ca. The increase in the amount of wine pomace always leads to the reduction of apparent density ( $\rho_a$ , Table III-5). Real density ( $\rho_r$ ) also appears to be affected at least in part by the addition of this organic matter. At 800 and 950 °C, real density fell as the % of additive increased. However, this tendency was not observed at 1100 °C.

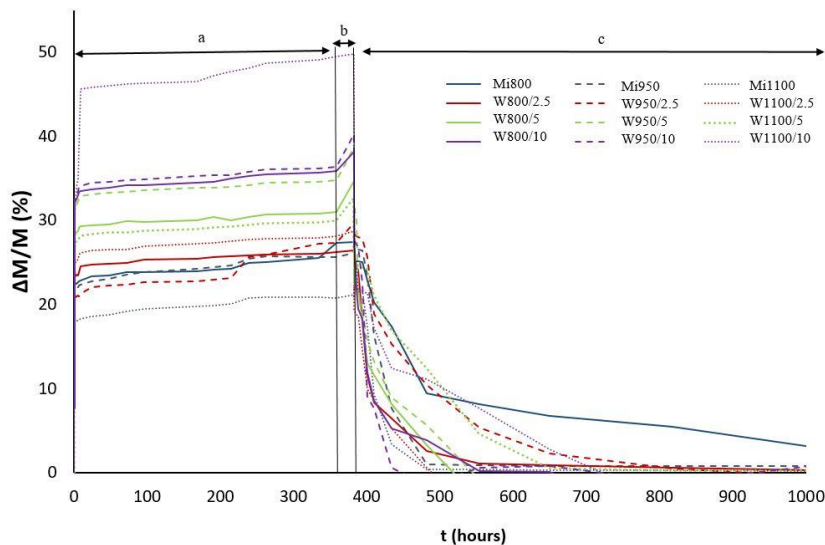


**Figure III-8.** Free (a) and forced water absorption (b) and drying curves (c) for bricks made without (Mi) and with wine pomace (W) fired at 800, 950 and 1100 °C.

**Table III-5.** Hydric parameters of bricks. Ab: free water absorption (%); Af: forced water absorption (%); S: saturation coefficient (%); Di: drying index; P<sub>o</sub>: open porosity (%); C: capillarity coefficient (g/m<sup>2</sup>s<sup>0.5</sup>); ρ<sub>a</sub>: apparent density (g cm<sup>-3</sup>); ρ<sub>r</sub>: real density (g cm<sup>-3</sup>). For sample acronyms, see Table III-1.

	Ab	Af	S	Di	P <sub>o</sub>	C	ρ <sub>a</sub>	ρ <sub>r</sub>
Mi800	27.31	27.43	85.39	1.08	38.66	3.21	1.84	2.93
W2.5/800	26.18	26.40	84.05	1.49	40.95	3.34	1.71	2.88
W5/800	31.01	34.72	85.11	1.74	43.12	3.59	1.64	2.61
W10/800	35.87	38.10	88.94	1.96	44.41	3.66	1.52	2.50
Mi950	25.65	26.13	88.33	1.16	37.65	2.15	1.27	1.98
W2.5/950	27.29	29.71	74.78	1.19	38.96	2.28	1.20	1.74
W5/950	34.79	38.63	86.17	1.46	44.85	2.46	1.09	1.60
W10/950	36.42	40.27	85.97	1.87	48.28	2.71	0.98	1.57
Mi1100	20.81	21.14	88.97	1.57	30.73	2.09	1.59	2.61
W2.5/1100	28.10	28.76	91.93	1.64	37.94	2.15	1.42	2.54
W5/1100	29.94	32.60	87.49	1.74	42.97	2.54	1.25	2.36
W10/1100	49.47	49.74	92.59	1.93	52.64	2.69	1.04	2.75

### 3.4. Mercury intrusion porosimetry (MIP)

The MIP analysis highlights the way the addition of wine pomace modifies the pore system of the bricks in terms of open porosity and pore size distribution. All bricks show unimodal pore size distribution at around 0.1 μm with the exception of W1100/10, where a second family of pores can be clearly observed in the 0.08-0.12 μm range (Fig.III-9). This second group was made up of the voids left by the organic particles after firing, as revealed in FESEM observations (Figs.III-6 and 7).

When comparing bricks fired at 800 and 1100 °C, the maximum peak always shifts towards larger pore sizes as the firing temperature increases. The porosity of the bricks increases with the percentage of wine pomace and also with the firing temperature (P<sub>oMIP</sub>, Table III-6), thus confirming the results of the hydric tests. This suggests that at 1100 °C, the small pores coalesce into new, larger ones, as the FESEM images showed (Figs.III-7C, D and E). In fact, the specific surface area decreases at 1100 °C, above all in bricks with added wine pomace, reaching 0.84 m<sup>2</sup>/g for the bricks with 5 and 10% (SSA, Table III-6). These data confirm what was previously suggested in the hydric tests, i.e. that the combustion of the fibres in the wine pomace improves the connectivity between the pores. The porosity and density values measured by MIP are in line with those calculated

in the hydric tests. Any differences between these two techniques are probably due to the use of two liquids with different intrusion pressures and different physical properties.

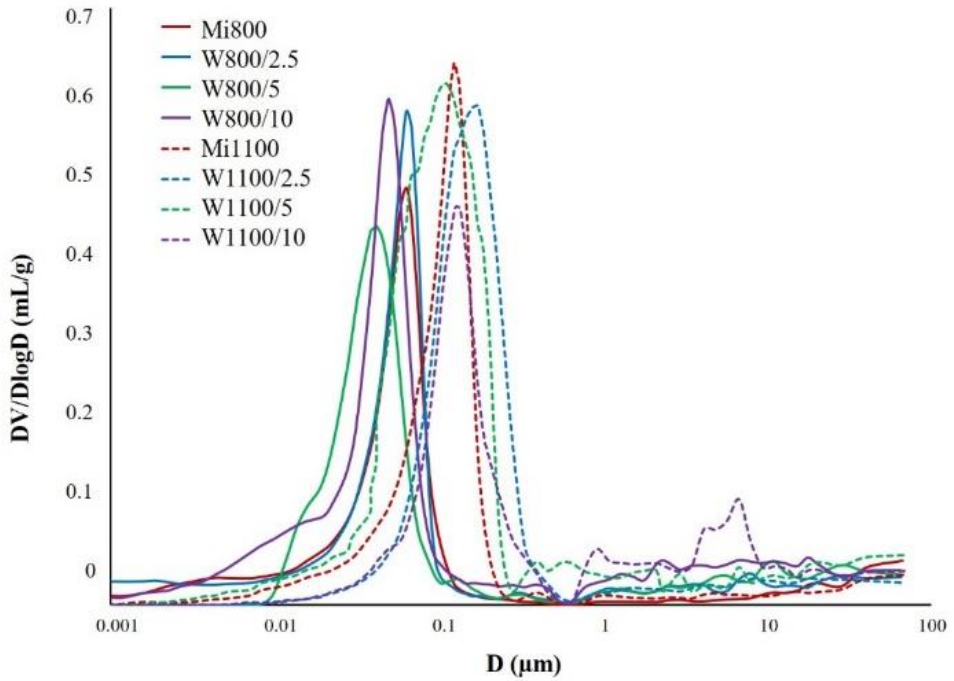


**Figure III-9.** MIP curves for bricks fired at 800, 950 and 1100 °C without additive (Mi, continuous line) and with added wine pomace (W, dashed line).

**Table III-6.** MIP parameters for bricks without additive (Mi) and with added wine pomace (W) fired at 800 and 1100 °C. SSA = specific surface area (m<sup>2</sup>/g);  $\rho_{aMIP}$  = apparent density (g·cm<sup>-3</sup>);  $\rho_{rMIP}$  = real density (g·cm<sup>-3</sup>);  $P_{OMIP}$  = open porosity (%).

	SSA	$\rho_{aMIP}$	$\rho_{rMIP}$	$P_{OMIP}$
Mi800	9.64	1.40	2.03	27.49
W800/2.5	1.21	1.11	2.11	36.60
W800/5	2.63	1.16	2.29	38.52
W800/10	2.11	1.34	1.98	41.43
Mi1100	7.21	1.45	2.55	36.65
W1100/2.5	1.04	1.36	2.40	39.67
W1100/5	0.84	1.22	2.36	46.53
W1100/10	0.84	1.14	1.93	51.61



### 3.5. Ultrasonic pulse velocity (UPV) and compressive strength (CS)

Table III-7 shows the average values for ultrasound velocities ( $\bar{x}V_p$ ) and compressive strength measured in bricks made with and without added wine pomace. It is commonly reported that UPV values in bricks increase in line with increasing firing temperature, so indicating a stronger structure due to vitrification and densification of the matrix (Cultrone et al., 2001; Anjum et al., 2020). If we analyse the bricks with wine pomace,  $V_p$  decreases in line with increases in the percentage of additive, a logical result given the increased porosity of these bricks (see hydric and MIP values in Tables III-5 and III-6). The lowest  $V_p$  value was for the samples containing 10 wt.% residue (Table III-7). Note how the standard deviation ( $\sigma$ , Table III-7) follows an opposite trend:  $\sigma$  increases in line with the amount of additive. This increase in  $\sigma$  is probably due to the fact that as the amount of wine pomace increases, mixing the pomace with the clayey material during the moulding process becomes more and more difficult. This leads to the appearance of more voids when the bricks are fired, which in turn cause greater standard deviation in the UPV values.

The bricks with the highest mechanical strength are the control bricks. This parameter increases in line with firing temperature reaching the highest value at 1100 °C (Mi1100 Table III-7). The wine pomace reduces the strength of the bricks due to their increased porosity, such that the higher the residue content, the lower the mechanical resistance. The lowest compressive strength value is obtained by W10/800 (2.1 MPa, Table III-7). According to the RL-88 (1988) standard, the minimum strength value recommended for bricks for use in building work in Spain is 10 MPa. The only bricks that meet this requirement are those fired at 1100 °C and those without additives fired at 950 °C. However, according to the same standard, bricks with a compressive strength of at least 5 MPa may be used as lightweight bricks in construction. In this case, only the bricks fired at 800 °C with 5 and 10 wt.% waste and those fired at 950 °C with 10 wt.% should be excluded. If we compare the mechanical strength values of these bricks with those obtained in other studies in which organic matter was added (Velasco et al., 2015; Taurino et al., 2019; Cultrone et al., 2020; Ordieres and Cultrone, 2022), our values are lower, especially at 800 and 950 °C. This means that lower concentrations of wine pomace or higher firing temperatures must be considered if we want to obtain mechanically stronger bricks.

**Table III-7.** Average UPV ( $\bar{x}V_p$ , in m/s) and compressive strength (CS, in MPa) values for handmade bricks made without (Mi) additive and with added wine pomace (W).  $\sigma$  is the standard deviation of  $\bar{x}V_p$  and CS values.

	$\bar{x}V_p$	$\sigma$	CS	$\sigma$
Mi800	2534	2.31	7.8	4.52
W800/2.5	2447	6.47	6.2	2.50
W800/5	2164	7.89	3.0	1.14
W800/10	861	10.55	2.1	1.64
Mi950	2576	3.74	10.1	7.92
W950/2.5	2400	7.85	6.9	2.22
W950/5	2371	7.94	5.5	9.45
W950/10	1147	12.33	3.5	7.10
Mi1100	2823	4.11	15.2	7.22
W1100/2.5	2676	5.23	12.3	9.41
W1100/5	2500	6.93	9.5	1.52
W1100/10	1053	13.08	6.7	2.43

#### 4. Salt crystallization test

During the salt crystallisation test, all the bricks show an increase in weight during the first five cycles, which is probably due to the deposition of sodium sulphate inside the pores (Fig.III-10). This initial increase in weight varies depending on the type of bricks tested, in that the bricks with the highest amount of added residue (W800/10, W950/10 and W1100/10) show the greatest weight increase. This confirms the results of the hydric tests (see section 3.3) where the bricks without additives gained the least weight.

A decrease in weight can be observed in the following two cycles. This decrease can be attributed to the loss of brick fragments because of the crystallization of salt crystals in confined spaces. As the test progresses, continuous fluctuations of the curves can be observed with increases and losses in weight respectively linked to the crystallization of the salt in new fissures generated by the crystallization pressure and to the consequent loss of new fragments (Fig.III-10). At the end of the test, the bricks with 10 wt.% wine pomace are those that suffer the highest weight variation and weight increase.

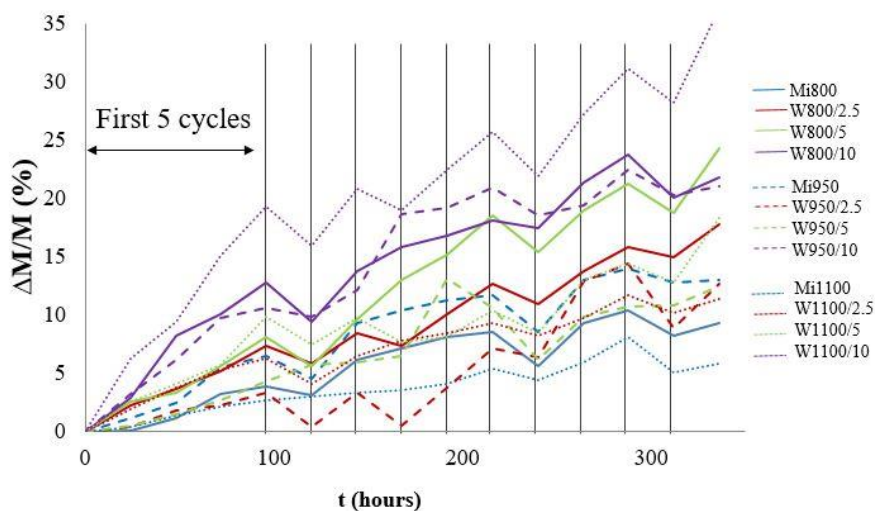


**Figure III-10.** Salt crystallization diagram for bricks made with and without wine pomace added and fired at 800, 950 and 1100 °C. Weight variation ( $\Delta M/M$ ) vs. time (in hours).

## 5. Conclusions

In this paper, we assessed the physical-mechanical behaviour of lightweight bricks made with a clayey material rich in quartz and phyllosilicates and a smaller amount of carbonates, which was mixed with wine pomace at three percentages (2.5, 5 or 10 wt.%). The samples were fired at 800, 950 and 1100 °C. The addition of the wine pomace did not affect the mineralogy of the brick samples. The wine pomace reduced the linear shrinkage of unfired samples and the samples were lighter after firing due to the consumption of this organic matter. The mineralogical changes that occur during firing were directly related to the composition of the raw material and were not affected by the addition of wine pomace.

In terms of texture, particles in the wine pomace were consumed during firing, which led to the appearance of voids. The bricks fired at 1100 °C are highly vitrified and have the highest compactness and lowest open porosity values. Conversely, the addition of wine pomace caused a fall in ultrasonic velocity. It also increased the water absorption capacity and open porosity of the bricks, while impairing their mechanical properties. The organic fibres in the wine pomace affected the hydric behaviour of the bricks, not only by increasing their water absorption capacity, but also by improving water flow within the

pore system. The addition of wine pomace influenced the lightness and the chromatism of the bricks, which ranged from reddish to yellowish depending on the amount of additive added and the firing temperature. It also reduced the mechanical strength of the bricks, especially at low firing temperatures. Suitable resistance values for use in construction work in Spain (10 MPa) are only reached at 1100 °C, when the samples are highly vitrified. However, the same standard allows bricks with a compressive strength of at least 5 MPa to be used as lightweight bricks in the construction industry. Most of the bricks studied here would meet this requirement. In terms of durability, the bricks made with the largest amount of additive suffer the highest variation in weight due to salt crystallization. This means that when used in a building they would be more vulnerable to damage from salt attack.

The advantage of reusing wine pomace in the brick industry is demonstrated by analysing the data on bricks produced and wine pomace generated in Spain. In 2019 (latest available data from the Geological and Mining Institute of Spain, IGME, <https://www.igme.es/>), 7.4 million tonnes of clay soils were extracted for the ceramic industry with an approximate value of 36.2 million euros. Of these clays, 4.3 million tonnes were destined for the manufacture of bricks, representing a value of 21 million euros. Regarding the amount of wine pomace generated per year (1 million tonnes, see Introduction section), the replacement of the clay material with up to 10% by weight of wine pomace would represent a maximum saving of 2 million euros and the use of 43% of this waste by the brick industry.

The wine pomace is at no cost, so the only expense is the transportation of the waste to the brick factories. The vineyard area in Spain is almost 1 million hectares ([www.oiv.int](http://www.oiv.int)), the largest in the world, which extends mainly in the flat and hilly areas of the Iberian Peninsula. These are the same areas where the brick factories are located, so the approximate average distance between the wine factories and the 130 brick factories registered in 2022 ([www.hspalyt.es](http://www.hspalyt.es)) is estimated at 100 km. Thus, the cost of the fuel used to transport the waste would be relatively low, certainly lower than the benefit produced by making bricks with wine pomace. Therefore, this common waste in some countries, especially those in the Mediterranean area, can be efficiently used in brick production by combining it with local natural resources.

The research carried out here has shed more light on the possible use of wine pomace in the production of lightweight bricks for use in the construction industry. This could lead

to environmental benefits by reducing the amount of clay required in brick production and by usefully disposing of the pomace, a waste product that might otherwise end up in landfills.

### Supplementary material

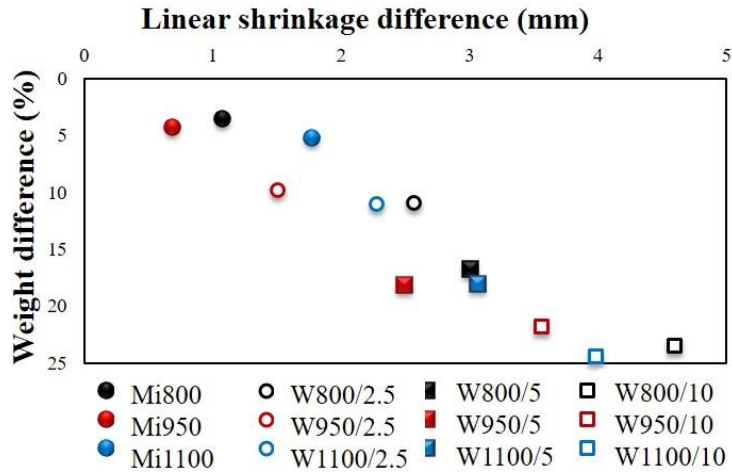


**Figure III-S1.** Relationship between weight difference (%) and linear shrinkage (mm) between unfired and fired bricks based on firing temperature (800, 950 and 1100 °C) and the amount of residue added (no residue, 2.5, 5 and 10 wt.%).

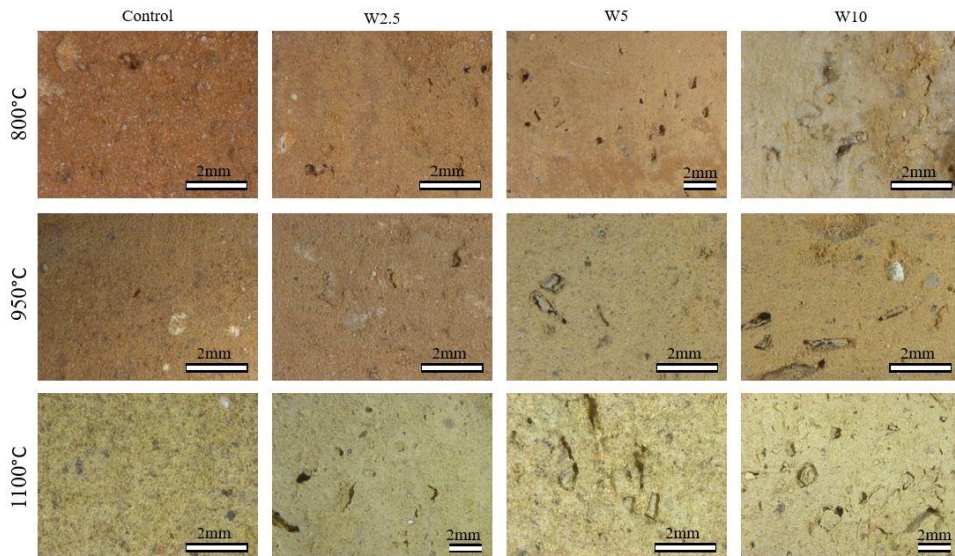


**Figure III-S2.** Macroscopic view of control bricks and bricks made with added wine pomace fired at 800, 950 and 1100 °C.

# CHAPTER IV

***Effect of tea waste as additive to solid bricks***

Laura Crespo-López, Chiara Coletti, Anna Arizzi, Giuseppe Cultrone

Published in *Sustainable Materials and Technologies*

DOI: 10.1016/j.susmat.2024.e00859

Impact Factor: 9.6

Position 18/119 (Q1)

Category: Energy & Fuels (JCR 2022)








Sustainable Materials and Technologies




Volume 39, April 2024, e00859



# Effects of using tea waste as an additive in the production of solid bricks in terms of their porosity, thermal conductivity, strength and durability

[Laura Crespo-López](#)<sup>a</sup>  , [Chiara Coletti](#)<sup>b</sup> , [Anna Arizzi](#)<sup>a</sup> ,  
[Giuseppe Cultrone](#)<sup>a</sup> 

[Show more](#) 

 Add to Mendeley  Share  Cite

<https://doi.org/10.1016/j.susmat.2024.e00859> 

[Get rights and content](#) 

**Keywords:** Bricks, Tea waste, recycling, thermal conductivity, innovation

## 1. Introduction

Tea is one of the oldest traditional beverages in the world and one of the most widely consumed non-alcoholic drinks after coffee, with consumption estimated at 85 litres per person per year. Tea is particularly important in Asia, Eastern Europe, and the UK (Wills, 2013). There are records of its consumption as early as 1500 BC in the Yunnan province of China (Zang et al., 2017), where it first appeared as a medicinal drink due to the antioxidant, diuretic and anti-inflammatory properties of *Camellia Sinesis* (Hamilton-Miller, 2001; Trouillas et al., 2003) the plant commonly known as tea. The particular variety of tea produced varied greatly depending on the harvesting process and the

treatment applied to it (Wang et al., 2000; Farag et al., 2023). However, it was not until the 16<sup>th</sup> century that its consumption became popular in the West, where it became the emblematic hot drink in the United Kingdom (Sumpio et al., 2006; Awasom and Tea, 2011). In the early 20<sup>th</sup> century, the sale of tea became even more popular worldwide due to the invention of the tea bag (Bajaj, 2016). In 2020, a total of just over seven million tonnes of tea were produced worldwide. Asia accounted for around 83% of this volume, growing and harvesting around 5.8 million tonnes (Debnath et al., 2023). The tea industry is on the rise, and is expected to grow by 4.22% per year between 2023 and 2025 (<https://statista.com>). In line with the increase in tea consumption, the amount of waste is growing rapidly, resulting in a substantial loss of biomass and increasing environmental stress. Tea residues, also known as tea waste or tea grounds, are known to be rich in certain organic compounds, in particular lignin and holocellulose (Guo et al., 2021; Tang et al., 2022). These compounds play a crucial role in the formation of porous structures in construction materials. During the tea-leaf manufacturing process, these components become interwoven within the plant's cell walls. Later, when the tea is brewed, they are released into the liquid phase, and after the tea is consumed, some remain behind in the residues (Feng et al., 2013). Hussain et al. (2018) and Li et al. (2022b) have postulated that tea residues could be used to produce biochar, which in turn could be used as a nitrogen-rich biomass precursor for preparing pollutant adsorbents. Research into the possible reuse of tea waste biomass in practical applications has so far centred on converting it into bioadsorbents (Zang et al., 2015), agricultural compost (De Corato, 2020; Orden et al., 2021) or animal feed (Ding et al., 2020; Li et al., 2022a) although more research is required in this field and other alternatives must be proposed.

For its part, clay is now considered an exhaustible resource, to such an extent that in some countries, such as Australia or China, its use in the manufacture of bricks has been restricted and the use of alternative waste or recycled materials is being actively promoted (Zhang; 2013; Zhang et al., 2018; Crespo-López et al., 2023a) . To this end, research has been conducted into the use of various organic additives in bricks (Ordieles and Cultrone, 2022; Coletti et al., 2023; Crespo-López et al., 2023b). Results have demonstrated their effectiveness as pore agents/developers, and the improvements they can bring in terms of insulation and the reduction of heat transmission (Coletti et al., 2023). The resulting bricks have also been shown to be well suited for use as lightweight building materials (Crespo-López et al., 2023b).



With this in mind, in this paper, we explore the possible use of tea residues (5 and 10 wt.%) as additives in the production of traditional handmade bricks. There are various reasons for research on this subject. Firstly, the use of additives reduces the depletion of natural supplies of clay, the main raw material used in brickmaking. Secondly, the reuse of the waste generated by tea-drinking in the brick manufacturing process can produce energy savings compared to conventional brickmaking. This is due to the biomass capacity of the additive, which produces additional heat during firing. Thirdly, the addition of tea waste enables the production of lightweight bricks with optimal thermal insulation properties that can help reduce domestic winter heating bills.

Although various research studies have already been conducted into the use of tea waste as an additive in brick manufacture, we believe that there are still many important gaps that our research seeks to fill. To this end we focus on various issues that we consider essential for appraising the technical quality of the bricks. These include: 1) measuring the colour of the fired bricks and assessing how the addition of tea waste influences the colour values. Colour is of great importance in the field of architectural heritage, in that it is one of the key factors in the choice of a replacement brick when restoring the front of a historic building; 2) the need to determine the compactness of bricks and relate it to their compressive strength. In this research, we combine the measurement of compressive strength with that of ultrasound velocity so as to provide a more complete picture of the performance of the bricks from a petrophysical point of view; 3) the study of the porous system and pore size distribution and how they are altered by the addition of the tea waste.

Previous research on this issue has thrown up interesting results albeit with certain important differences compared to our research, which we will now go on to explain. Hamilton and Hall (2013) considered that further studies were needed to understand the effect of added tea residue on the compressive strength and thermal conductivity of fired brick samples and on the development of macroscopic defects in the bricks. Saman (2017) used percentages from 2.5% to 10% by weight of tea waste to study the compressive strength, water absorption and thermal conductivity of bricks. His results showed that compressive strength and thermal conductivity decreased, while water absorption increased as the percentage of tea residue augmented. Ozturk et al. (2019) investigated extruded bricks made with added 10 wt.% tea waste and fired within a range of 950-1050 °C, whereas in our research, we prepared the samples using the traditional

manual kneading method. This produces important differences in the fired bricks. Compared to handmade bricks, extruded bricks show: 1) generally lower porosity and different pore size distribution; 2) more pronounced orientation of flattened minerals, pores and organic fibres (i.e., tea waste). It is also important to take into account the energy cost associated with the use of the hydraulic press to extrude the bricks. For their part, Anjum et al. (2021) also produced extruded bricks made with added tea waste fired at temperatures of 600 and 1000 °C. In our opinion, this temperature range does not enable us to fully identify the important mineralogical and textural changes that take place during the firing process in the matrix of the ceramic samples. Other studies mixed ground tea waste with inorganic additives (Sahu et al., 2020; Ibrahim et al., 2023). The particular approach adopted by these researchers made it impossible to assess the impact of the addition of tea waste on certain physical and mechanical properties of the bricks, one of the main objectives of our paper. For example, Sahu et al. (2020) used a single firing temperature (990 °C) and were therefore unable to analyse the effects of different firing temperatures on the texture of the fired samples. Similarly, the results obtained by Ibrahim et al. (2023) are difficult to compare with ours in that they did not use clay in the brickmaking process, instead mixing varying proportions of tea waste (from 0 to 12 wt.%) with zeolitic tuff (from 100 to 89 wt.%).

## **2. Materials and Method**

### ***2.1. Geological context and procurement of raw materials***

The clayey raw material (with a total mass of over 5 kg) was obtained from a site (lat. 40.311186, long.-1.13375) on the eastern edge of the Betic Cordillera, in the province of Teruel (Spain) (Fig.IV-S1), about 4.2 km from the centre of the city of Teruel. In geological terms, this region is located in the Aragonese Branch of the Betic System (Guimerá et al., 2004; De Vicente et al., 2009). The Teruel Basin is the largest Neogene extensional macrostructure within the central-eastern Iberian Chain (NE of Iberian Plate) (Ezquerro et al., 2020). The limonitic facies in which the raw material was obtained is made up of clays without exceptional structures, in which there are small sandy layers at the top and high carbonate concentration at the bottom with small subangular quartz grains, traces of K-feldspar, fragments of limestone rocks, fragments of quartzite, silex grains and iron oxides (Sinusia et al., 2004). The quarrying of rock for industrial use is an important sector in this area, involving above all Miocene (Neogene) clays for the brick and ceramic

industry (<https://igme.es>). Within a radius of 2 km around the city of Teruel, there are currently about fifteen quarries producing between 6,000 and 18,000 kT of clay per year (*Mining Overview*, Instituto Geológico y Minero de España, IGME 2018-2020, <https://igme.es>). As regards the tea residue, it came from the tea bags discarded by local households.

## 2.2. Production of traditional bricks using tea grounds as an additive

The residue from the tea bags (particles from leaves, flowers, small branches, etc.) was mixed and left to air dry for one month at a temperature of approximately 25 °C. The tea residue was not sieved before mixing with the clay to form a kneadable mixture (with 0, 5 or 10% by weight of added tea residue) that ensured homogeneity. Mixing the tea residue with the clay could provide energy savings compared to some of the previous research studies in which the tea residue was milled before mixing. Water was then added until a paste-like texture was achieved. The proportions of raw material, tea residue and water are shown in Fig.IV-1. The addition of residue meant that less water had to be added to the mixture. We observed that the additive gave the clay mixture a pleasant kneading texture, with a gel-like quality, possibly due to the organic nature of the tea. The clay paste was placed in a previously moistened wooden mould of 15 × 20 × 4 cm and pressed down. Once the mould was full, the surface was smoothed off with a ruler. After one hour, the moulds were removed and the clayey pastes were cut into ~ 4 cm edge cubes using a stretched cotton thread and left to dry at almost constant room temperature and humidity (20-23 °C, 40-50% RH) for one month.

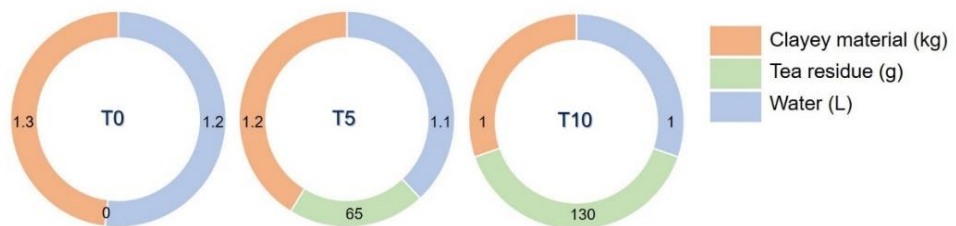


**Figure IV-1.** Amount of clay (kg) and water (L) used in relation to the amount of tea residue added (g).

Once the bricks were dry, they were fired in a Herotec CR-35 electric oven at 800 °C, 950 °C and 1100 °C. Table IV-1 sets out the acronyms given to the control samples made

with no added residue (T0) and to those with added 5 wt.% (T5) and 10 wt.% (T10) tea waste. The samples were preheated for 1 hour at 100°C so as to eliminate any residual moisture that might still be present inside them. The temperature was then increased at a rate of 2 °C/min. Once the maximum temperature was reached (800, 950 or 1100 °C), it was maintained for 3 hours.

Finally, the oven was turned off and the samples were left to cool slowly until the next day, so as to prevent the development of fissures due to the  $\beta$ -to- $\alpha$  quartz transition at 573 °C. After removal from the oven, the bricks were immersed in water for about 1 hour so as to prevent possible “lime blowing” due to the presence of lime grains (Cultrone et al., 2004).

**Table IV-1.** Acronyms assigned to the bricks according to the addition of 0, 5 or 10 wt.% of tea residue and the firing temperature (800, 950 or 1100 °C).

800°C	950°C	1100°C
T0/800	T0/950	T0/1100
T5/800	T5/950	T5/1100
T10/800	T10/950	T10/1100

### 2.3. Characterization and testing methods

#### *2.3.1. Chemical, mineralogical and textural study*

X-ray fluorescence (XRF) was used to determine the major elements in the raw material and the fired bricks with a PANalytical Zetium compact spectrometer. 3 g of each sample was ground to powder prior to its analysis. The mineralogical composition of the raw clay and the fired bricks was determined by powder X-ray diffraction (PXRD) using a PANalytical X'Pert PRO diffractometer. The working conditions were as follows: CuK $\alpha$  radiation ( $\lambda = 1.5405 \text{ \AA}$ ), 45 kV voltage, 40 mA current, 3 to 70° 2 $\theta$  exploration range, 0.1 2 $\theta \text{ s}^{-1}$  goniometer speed. A first qualitative mineral phase identification was performed using the PANalytical X'pert Highscore Plus 3.0 software matching the experimental diffraction peaks with those included in the Joint Committee for Powder Diffraction Standards (JCPDS) PDF-2 database. A quantitative phase analysis was carried out using open-source Profex-BGMN software with dedicated fitting functions (Dobelin and Kleeberg, 2015) and 10 wt.% internal standard  $\alpha$ -Al<sub>2</sub>O<sub>3</sub> was added to the powder samples

to comply with the Rietveld refinements (Kim et al., 2016; Zhou et al., 2018; Christidis et al., 2020).

The petrographic features (mineralogy, texture and development of vitrification in the matrix) of the samples fired at 800 and 1100 °C were observed by means of polarized optical microscopy (POM). Observations under plane- and cross-polarized light were carried out on polished thin sections using a Zeiss AXIO Scope.A1 microscope equipped with a Canon EOS 550D digital camera. In addition, detailed observations were made on the same thin sections of the samples fired at 800 and 1100 °C using a high-resolution field emission scanning electron microscope (HRSEM) TESCAN SOLARIS coupled with energy dispersive X-ray spectroscopy (EDS). The microscope operated at 5 and 10 kV with a working distance (WD) of 5 mm using a beam current of 300 pA and 1 nA.

### 2.3.2. Analysis of the pore system

A detailed study of the pore system of the bricks and how it is affected by firing temperature and the addition of tea waste was conducted using several physical tests. Hygroscopic water adsorption was measured according to the EN-ISO-12571 (2000) standard. Brick samples were oven-dried and then placed in an environmental chamber at a constant temperature of 23 °C and with relative humidity (RH) increasing according to the following sequence 30-50-70-75-80-85-90-95% and then decreasing through the same steps in reverse order. The mass of each sample was measured at each step after equilibration at constant RH.

Hydric tests were used to analyse the water flow through the pore network of the bricks. Free (Ab, at atmospheric pressure) and forced (Af, under vacuum) water absorption (UNE-EN 13755, 2008), drying (Di) (NORMAL 29/88, 1988) and capillarity tests (C) (UNE-EN 1926, 2007) were carried out. These tests enabled us to calculate the saturation coefficient (S), the apparent ( $\rho_a$ ) and real ( $\rho_r$ ) densities, and the open porosity ( $P_o$ ) (UNE-EN 1936, 2007). Hydric tests were performed under controlled thermo-hygrometric conditions (20 °C and 60% relative humidity) using deionized water.

The pore size distribution within a range of 0.002 to 200  $\mu\text{m}$  was analysed by mercury intrusion porosimetry (MIP) using a Micromeritics Autopore IV 9600 porosimeter. Samples of about 1 g were dried in a ventilated oven for 48 h at 30 °C prior to analysis. Apparent and real densities ( $\rho_{a\text{MIP}}$  and  $\rho_{r\text{MIP}}$ ,  $\text{g}/\text{cm}^3$ ), open porosity ( $P_{o\text{MIP}}$ , %) and specific surface area (SSA,  $\text{m}^2/\text{g}$ ) were calculated.

Finally, HRSEM images were analysed using digital image analysis (DIA) in order to estimate the percentage of pores of over 4  $\mu\text{m}$  in size in the bricks with and without tea waste fired at 800 and 1100  $^{\circ}\text{C}$ . For each sample a total of 250 images overlapped by 10% were acquired by the TESCAN SOLARIS using the same working conditions mentioned above and then automatically stitched together in order to cover as much of the thin section as possible, so increasing its representativeness (Coletti et al., 2016; Salvini et al., 2023). ImageJ software was used to calculate the pore ratio by segmenting and binarizing the BSE images and calculating the ratio of the pixels corresponding to pores to the total area of interest (Schneider et al., 2012). The resolution limit was 4  $\mu\text{m}$ , the size of one pixel.

#### 2.3.3. *Thermal conductivity*

A Thermal Conductivity Scanner (TCS) was used to assess the thermal behaviour of the bricks. This high precision noncontact method uses an optical scanning technology based on scanning a sample surface with a focused, mobile, continuously operated heat source in combination with infrared temperature sensors. The thermal conductivity range varied from 0.2 to 25 W/m·K, with an accuracy of 3%. The standards used for calibration were glass (Standard 1) and fused quartz (Standard 2), in line with the components of the bricks. The bricks were painted with acrylic black paint, with a stripe width of approximately 30 mm for each orthogonal side, so as to ensure proper infrared absorption to heat the sample. The thermal diffusivity ( $\alpha$ ,  $\text{mm}^2/\text{s}$ ) of the samples was determined indirectly on the basis of the apparent density values measured by MIP ( $\rho_{\text{aMIP}}$ ) and a mean heat capacity ( $C_p$ ) value of 800 kJ/g·K established in previous research (Bwayo and Obwoya, 2014; Kubiś et al., 2020).

#### 2.3.4. *Compactness and strength*

The ultrasound propagation velocity of compressional ( $V_p$ ) and shear ( $V_s$ ) waves was performed with a Panametrics HV Pulser/Receiver 5058PR coupled with an EPOCH650® Ultrasonic Flaw Detector (Olympus) performed with transducers of 1 MHz over a circular contact surface of 30 mm in diameter to determine the compactness of the bricks made with and without tea residue. A viscoelastic gel was used to ensure good coupling between transducers and brick samples.  $V_p$  and  $V_s$  were measured in the three perpendicular directions on three samples per brick type. Once the ultrasound velocities

had been determined, we then calculated the Poisson coefficient ( $\nu$ ) and the Young (E), Shear (G) and Bulk (K) moduli.

The compressive strength (Cs) was measured on three samples per brick type according to the requirements of the UNE-EN 196-1 (2005) standard. For this purpose, we used a Controls Uniframe T1192 electromechanical universal tester, equipped with 100 kN and 25 kN load cells. Samples with dimensions of 1.5 x 1.5 x 6 cm<sup>3</sup> were tested using a specifically designed device that is mounted on the press.

The PCE-2500N Leeb Hardness (LH) tester was used to determine whether the surface hardness of the bricks varied in line with the firing temperature or the amount of added residue. The rebound of the hammer was measured in ten different places along a line running from one edge of each brick to the opposite side, passing through the centre.

#### 2.3.5. Colour

The colour of the fired bricks was assessed using a Konica Minolta CM-700d spectrophotometer which quantified their lightness and chromaticity according to the UNE-EN 15886 (2011) standard. Illuminant D65, 10° observer and a measurement area of 8 mm were used. Nine measurements per sample were performed to determine their lightness ( $L^*$ ) and chromatic coordinates ( $a^*$  and  $b^*$ ). Once the  $L^*$ ,  $a^*$  and  $b^*$  values had been determined, we then calculated the total colour variation ( $\Delta E$ ) between bricks with and without tea residue as follows (Eq.1):

$$\Delta E = \sqrt{(L_1 - L_2)^2 + (a_1 - a_2)^2 + (b_1 - b_2)^2} \quad (1)$$

where  $L_1$ ,  $a_1$  and  $b_1$  are the lightness and chromaticity values for the control bricks made with no added residue and  $L_2$ ,  $a_2$  and  $b_2$  for those made with added tea waste.

#### 2.3.6. Durability

Fifteen salt crystallization cycles were performed according to the UNE-EN 12370 (2020) standard. The objective of this test is to reproduce a decay process that could affect the lifetime of the bricks due to the dissolution and recrystallization of soluble salts within their porous systems. Three samples (4 cm-edge cubes) per brick type were used for this test. To further determine the effect of the salts on the pore system of these samples,

ultrasound measurements were carried out before the decay test and after the 4<sup>th</sup>, 10<sup>th</sup> and 15<sup>th</sup> cycles.

### **3. Results and discussion**

#### 3.1. Changes in the weight of the bricks after firing

As expected, the difference in weight between unfired and fired bricks varies according to the amount of tea residue added and the firing temperature. i.e., the larger the amount of residue added and the higher the firing temperature, the greater the difference in weight between the fired and unfired bricks (Table IV-S1). The bricks made with added waste are lighter. The highest weight change was measured in T1100/10 for which a weight loss of about 30% was observed. This trend is in line with the findings of other authors, who reported a decrease in the weight of the samples made with added organic matter after firing (Martínez-García et al., 2012; Gliozzo, 2020; Crespo-López et al., 2023c).

#### 3.2. Chemical, mineralogical and textural study

##### 3.2.1. X-ray fluorescence (XRF)

Table IV-2 shows the chemistry of the raw material and the fired bricks. The main difference is that the fired bricks have lower Loss on Ignition (LOI) values. This is because the organic matter present in the raw material is consumed during firing, and the carbonates decompose, as manifested by the ~ 8% of CaO identified. The dehydroxylation of phyllosilicates will also have influenced the decrease in the LOI value. LOI increases in line with the amount of tea residue in the bricks ( $LOI_{T0} < LOI_{T5} < LOI_{T10}$ ). However, with firing temperature the opposite occurs. LOI falls as firing temperature increases. Chemically, the raw material and the bricks are rich in silica and alumina suggesting the presence of quartz and aluminium silicates. Based on its CaO content, the raw material can be classified as calcareous (Maniatis and Tite, 1981). Iron compounds are the fourth most abundant with values of between 3.8 and 4.1% and their presence enables the formation of iron oxides. Finally, K<sub>2</sub>O makes up around 2-2.5% and seems linked to the formation of feldspars and phyllosilicates, while the remaining elements account for less than 1%.



**Table IV-2.** XRF results (in %) for the raw material and for the fired bricks.

	SiO <sub>2</sub>	Al <sub>2</sub> O <sub>3</sub>	Fe <sub>2</sub> O <sub>3</sub>	MnO	MgO	CaO	Na <sub>2</sub> O	K <sub>2</sub> O	TiO <sub>2</sub>	P <sub>2</sub> O <sub>5</sub>	LOI	Total
Raw material	65.72	9.40	3.77	0.06	0.69	7.85	0.11	2.21	0.52	0.12	9.52	99.97
T0/800	73.18	9.28	3.8	0.05	0.66	6.98	0.11	2.19	0.54	0.12	3.07	99.98
T5/800	69.39	10.40	4.11	0.07	0.78	8.53	0.12	2.44	0.63	0.15	3.36	99.98
T10/800	68.43	10.13	3.95	0.07	0.78	8.75	0.12	2.46	0.60	0.17	4.53	99.99
T0/950	73.10	9.88	4.02	0.06	0.72	7.62	0.12	2.32	0.56	0.14	1.44	99.98
T5/950	71.84	10.07	4.08	0.07	0.77	7.98	0.13	2.43	0.56	0.16	1.90	99.99
T10/950	70.61	10.39	4.10	0.07	0.82	8.46	0.13	2.60	0.59	0.19	2.01	99.97
T0/1100	73.39	10.08	4.09	0.06	0.73	8.04	0.12	2.34	0.57	0.13	0.44	99.99
T5/1100	73.21	9.70	3.91	0.06	0.73	7.92	0.12	2.44	0.59	0.15	1.16	99.99
T10/1100	70.69	10.73	4.18	0.07	0.84	9.33	0.13	2.59	0.62	0.18	0.63	99.99

### 3.2.2. Powder X-ray diffraction (PXRD)

The Rietveld refinement of the PXRD analysis reveals that the raw material is mainly composed of quartz (64.78 wt.%). Calcite, phyllosilicates (illite and kaolinite), K-feldspar and hematite were also identified (Table IV-3). The clay has an amorphous phase content of 8.46 wt.%, which can be attributed to the presence of organic matter. Fig.IV-S2 shows the changes in the mineralogy of the bricks after firing, which are more evident at 1100 °C with the crystallization of high-temperature silicates and an increase in the background noise due to the vitrification of the samples (Cultrone et al., 2004; Crespo López and Cultrone, 2022). The amorphous phase content (in wt.%) increases in line with the firing temperature and with the percentage of tea residue added, reaching its highest value in the samples fired at 1100 °C and with 10 wt.% waste. It is possible that the tea residues generate additional heat, which results in a more pronounced vitrification of the matrix. If we look at the results in more detail, at the three firing temperatures investigated (800, 950 and 1100 °C), quartz is the most abundant phase although its concentration drops sharply when the firing temperature reaches 1100 °C and as the amount of residue increases, with values ranging from 45 to 27 wt.% (Table IV-3). The lower quartz values at 1100 °C suggest that at this temperature, some of the quartz has been consumed in mineralogical reactions to form new high-T silicate phases. At 800 °C, dehydroxylated illite-type phyllosilicates are still present (Fig.IV-S2), albeit in lower amounts compared to the raw material, while the kaolinite has decomposed (Table IV-3). Calcite is detected in smaller amounts compared to the raw material and disappears at higher temperatures (Fig.IV-S2 and Table IV-3). The microcline detected in the raw material is converted into more stable polymorphs, i.e. orthoclase at 800 °C and sanidine at 950 °C and 1100 °C (Brown and Parsons, 1989; Cultrone and Carrillo Rosua, 2020). Hematite is detected in

all the samples, irrespective of the amount of tea residue added. It has a higher concentration in the bricks fired at 800 °C than in the clay raw material due to the decomposition of the phyllosilicates, which favours the recrystallisation of Fe in the matrix. At higher temperatures, the hematite content falls to its lowest value of 0.78 wt.% in the T10/1100 sample (Table IV-3). This is because iron is trapped inside the structure of the new silicates, so hindering the formation of hematite (Cultrone et al., 2004; Nodari et al., 2007; Trincal et al., 2022; Daghmehchi et al., 2023). The decomposition of carbonates and their reactions with quartz and other silicates leads to the appearance of new Ca-silicates such as gehlenite at 950 °C and wollastonite and anorthite at 1100 °C.

**Table IV-3.** Mineralogical characterization by XRD of the clayey material and the fired bricks with or without tea residue. Data is provided in weight %. Abbreviations of minerals according to Warr (2020): Qz = quartz; Kln = kaolinite; Cal = calcite; Ill = illite; Hem = hematite; Mc = microcline; Or = orthoclase; Sa = sanidine; An = anorthite; Aug = augite; Gh = gehlenite; Wo = wollastonite; AM = amorphous phase.

	Qz	Kln	Cal	Ill	Hem	Mc	Or	Sa	An	Aug	Gh	AM	ERROR
Clayey material	64.78	4.30	6.65	11.81	2.08	1.90	0	0	0	0	0	8.46	±0.96
T0/800	44.04	0	6.91	9.88	4.80	5.66	0	0	0	0	0	28.61	±1.11
T5/800	35.48	0	5.25	13.71	5.82	0	3.01	0	0	0	0	36.72	±2.13
T10/800	33.76	0	5.04	10.67	6.01	0	1.88	0	0	0	0	42.67	±3.12
T0/950	45.13	0	0	0.20	4.52	0	0	1.78	5.12	0	7.14	31.54	±1.63
T5/950	43.15	0	0	2.00	4.93	0	0	2.36	5.77	0	6.04	36.17	±1.06
T10/950	36.34	0	0	0	3.44	0	0	3.64	6.06	0	7.23	44.41	±2.41
T0/1100	40.33	0	0	0	3.91	0	0	2.31	8.34	4.19	5.64	35.24	±1.99
T5/1100	34.24	0	0	0	1.40	0	0	2.74	9.65	5.40	4.22	42.65	±1.78
T10/1100	26.78	0	0	0	0.68	0	0	3.59	10.54	5.88	4.07	48.74	±3.82

### 3.2.3. Polarized optical microscope (POM)

Polarized optical microscopy (POM) observation of the T0/800 control bricks (samples with no added waste fired at 800 °C) revealed the presence of quartz grains with undulose extinction of over 1 mm in length in an orange-to-brown coloured matrix (Fig.IV-2A), which turns black in the bricks fired at 1100 °C (T0/1100) (Fig.IV-2D). Higher porosity was observed in the bricks with added tea residue (Fig.IV-2B, C, E and F), in which this organic matter disappears after combustion leaving imprints in the form of pores. The porosity increases in line with the percentage of residue (T5/800 and T10/800, Fig.IV-2B and C). The addition of tea residue also seems to affect the colour of the matrix, such that in the bricks made with 5 and 10 wt.% tea residue, the matrix is darker than in the control sample (T0/800). In addition to the quartz, calcite, phyllosilicates (muscovite-type)

and feldspar grains were also identified. Phyllosilicates and elongated fragments of other minerals often show a preferential orientation due to the pressure exerted on the raw material during the kneading process. Muscovite-type crystals appear unaltered reaching a second-order interference colour. The carbonate grains are partially decomposed and have lost their typical high birefringence colour. At 1100 °C, the bricks undergo major textural changes due to the high firing temperature (Fig.IV-2D, E and F), the pores become ellipsoidal-to-rounded in shape and the matrix becomes darker and loses its birefringence due to vitrification. Only quartz grains can be identified.

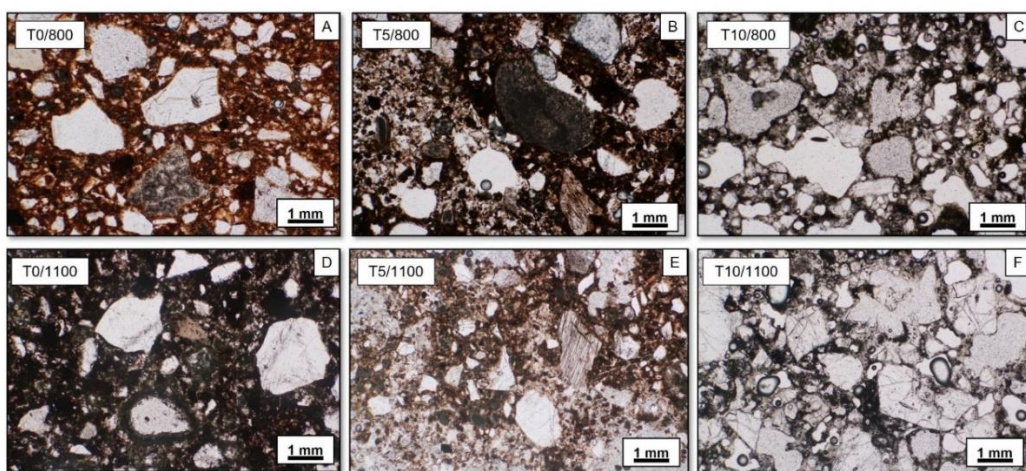


**Figure IV-2.** Bricks with and without added tea residue fired at 800 and 1100 °C. All photographs were taken with plane-polarized light (PPL).

#### 3.2.4. HRSEM

The textural features of the bricks vary considerably according to their firing temperature (800 and 1100 °C) and tea residue content (0, 5 or 10 wt.%). Both these factors alter the texture by improving the interconnection between mineral grains and increasing the porosity. These differences are reported in Figure IV-3 where SEM-BSE images show changes in the structures due to the firing process, such as the high sintering in sample T5/1100 due to the addition of tea residue. In samples fired at 800 °C, there are large gaps/pores between the grains. The pores are irregular in shape and clay minerals are still evident in the groundmass (Fig.IV-3A). Nuclei of new silicates phases are also present in the matrix of the bricks fired at 800 °C with 5 and 10 wt.% of tea waste (Fig.IV-3B and C). Even though they were not detected by PXRD due to their small quantities, their presence indicates a higher level of sintering as a result of the addition of tea

residue, as suggested by the increased amorphous phase revealed by the Rietveld refinements (see Table IV-3). Reaction rims, in particular on the edges of the quartz grains, are frequent (Fig.IV-3D). Fibrous phytoliths resulting from the addition of tea residues have been observed in bricks fired at 800 °C, where amorphous silica reacts with residual calcite grains (Cultrone et al., 2001), (Fig.IV-3E). This supports the mineralogical process in which new silicates are formed.

In the samples fired at 1100 °C, the illite has decomposed completely and melted in a highly sintered matrix, which displays the growth of new silicates and the development of larger, rounded pores (Fig.IV3G and H). Reaction rims on the edges of the quartz grains are also frequent at this temperature (Fig.IV-3J). Framboidal hematite, with microcrystallites of between 0.5 µm and 5 µm in diameter, was found in some bricks (Fig.IV-3K and L). The framboidal texture suggests that they were pyrite crystals, which probably formed due to the presence of organic matter (Love, 1957; Berner, 1969; Sawlowicz, 1993) and the establishment of an anoxic environment that enhanced the activity of sulphate-reducing bacteria (Germinario et al., 2019; Cultrone et al., 2020). During the firing of the bricks, the sulphur content of the framboids fell due to the decomposition of these sulphides at 588 °C and, in an oxidising atmosphere, were transformed into Fe<sub>2</sub>O<sub>3</sub> (Brownell and Brownell, 1976).

The chemical composition maps (area and linear) in Figure IVA-4 reveal the growth of new Ca-silicate phases (mainly wollastonite and maybe gehlenite) close to quartz and calcite grains.

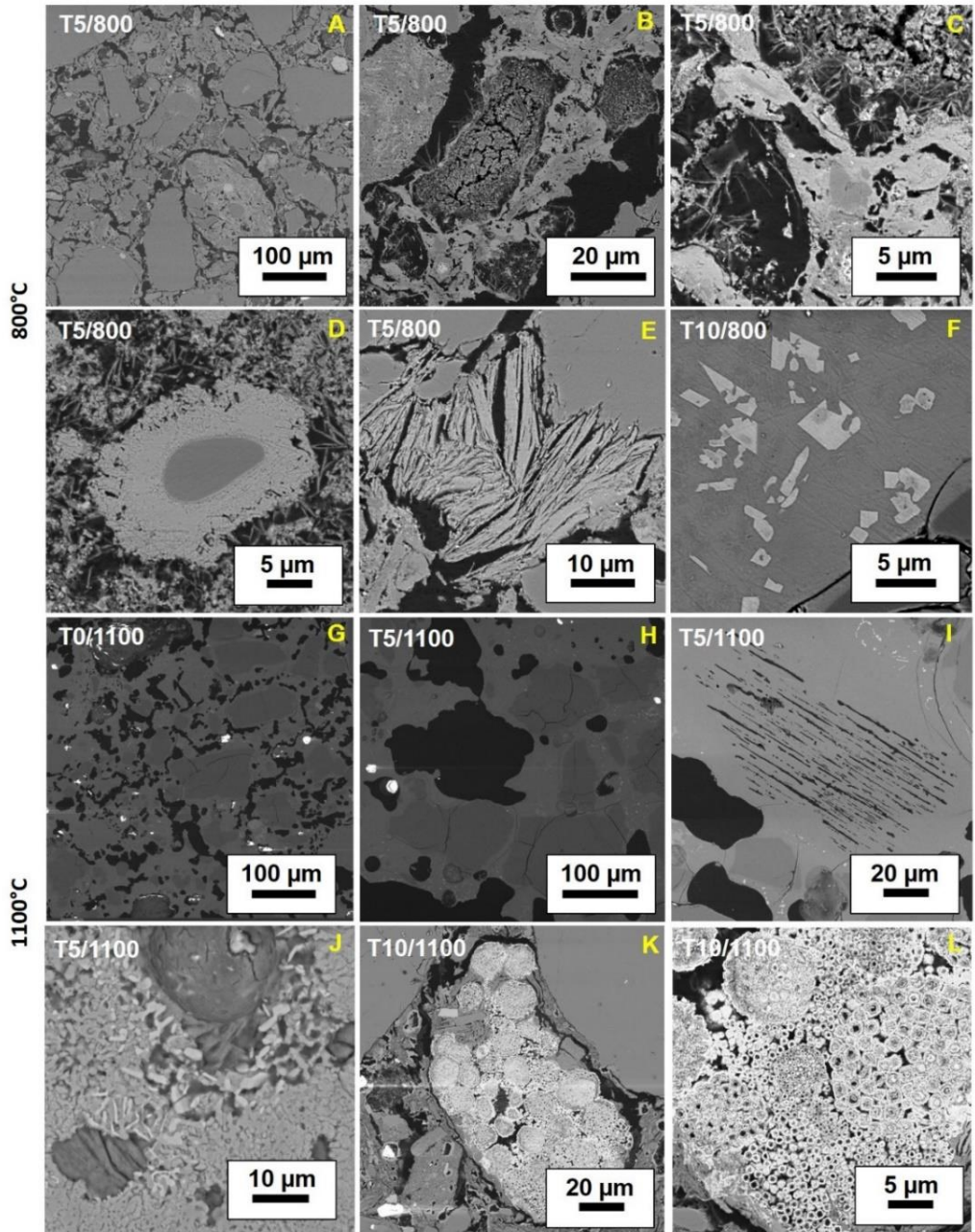


**Figure IV-3.** High resolution SEM-BSE images of bricks made with and without added tea residue fired at 800 and 1100 °C.



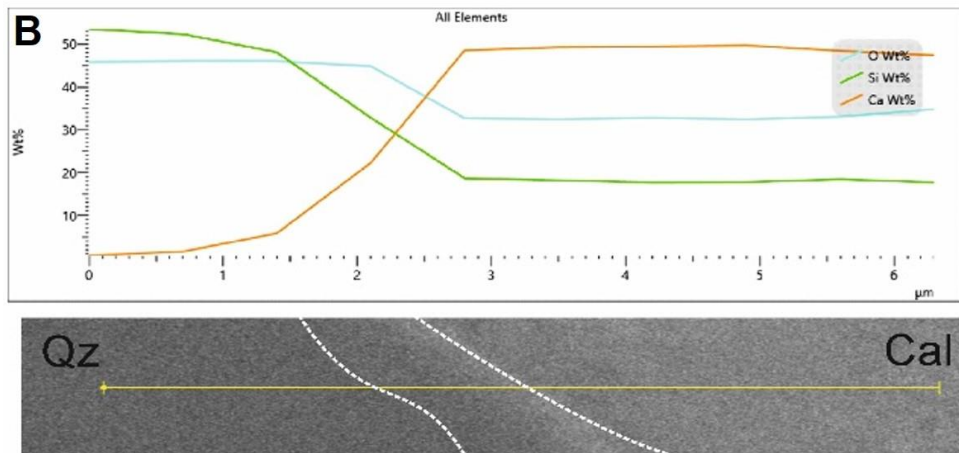
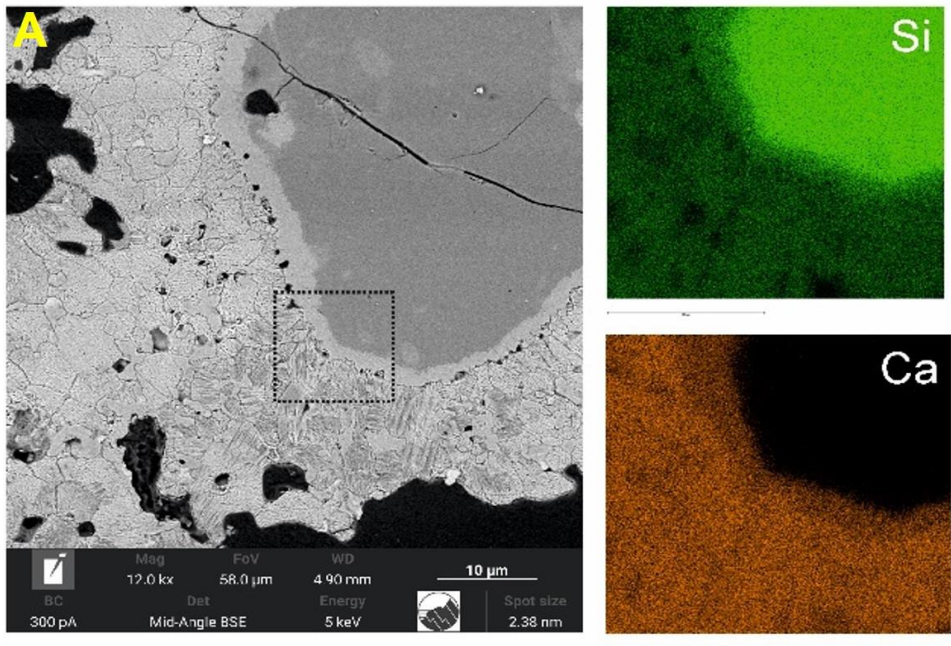


**Figure IV-4.** A) SEM-EDS elemental maps and B) a linear chemical analysis along a reaction rim between quartz and calcite grains.

### 3.3. Pore system

As regards the interaction of the bricks with water vapour and their behaviour with respect to RH variations, Figure IV-5 shows that the bricks fired at 800 °C adsorb more vapour than those fired at higher temperatures. As for the tea residue, the samples with higher amounts of additive are those in which mass increases most, because they have more empty spaces and are able to absorb more water vapour. The samples fired at 800 °C experienced the greatest increase in mass of around 3-3.5%, values that were reached at 90-95% RH. The mass of these samples increased progressively, as RH increased from 30 to 90-95% and then went down again as RH went back to 30%, still retaining some moisture at the end of the test. In the samples fired at 1100 °C, the mass only increased during the first cycle (from 0 to 30% RH) and thereafter remained almost stable (Fig.IV-5).

As regards the hydric tests on the bricks, the porosity and water absorption of the bricks increase in line with increasing amounts of tea residue (Fig.IV-5 and Table IV-4). This indicates that the hydric behaviour of the bricks is more affected by the addition of tea residue than by the firing temperature. At 800 °C,  $A_b$  increases from 12.9% (T0) to 22.4% (T10) (Table IV-4). The same trend is observed with forced water absorption ( $A_f$ , Table IV-4). The interconnection between the pores improves (i.e.,  $A_x$  values decrease) and open porosity augments ( $P_o$ , Table IV-4) as the amount of tea residue increases, so making the bricks more absorbent ( $S$ , Table IV-4).  $A_x$  and  $P_o$  values are more or less the same for each group of bricks (T0, T5 and T10) at the three firing temperatures. As for capillarity ( $C$ , Table IV-4), the bricks tend to absorb water more slowly as the amount of tea residue increases. The control bricks have the highest  $C$  values. This is because the capillaries are larger in the bricks with added organic matter, so hampering capillary rise (Dacuba et al., 2022; Crespo-López et al., 2023c). The increase in the amount of tea residue always leads to a decrease in apparent density ( $\rho_a$ , Table IVA-4). There is less variation in real density ( $\rho_r$ ), which is mainly influenced by the mineralogy of the bricks.

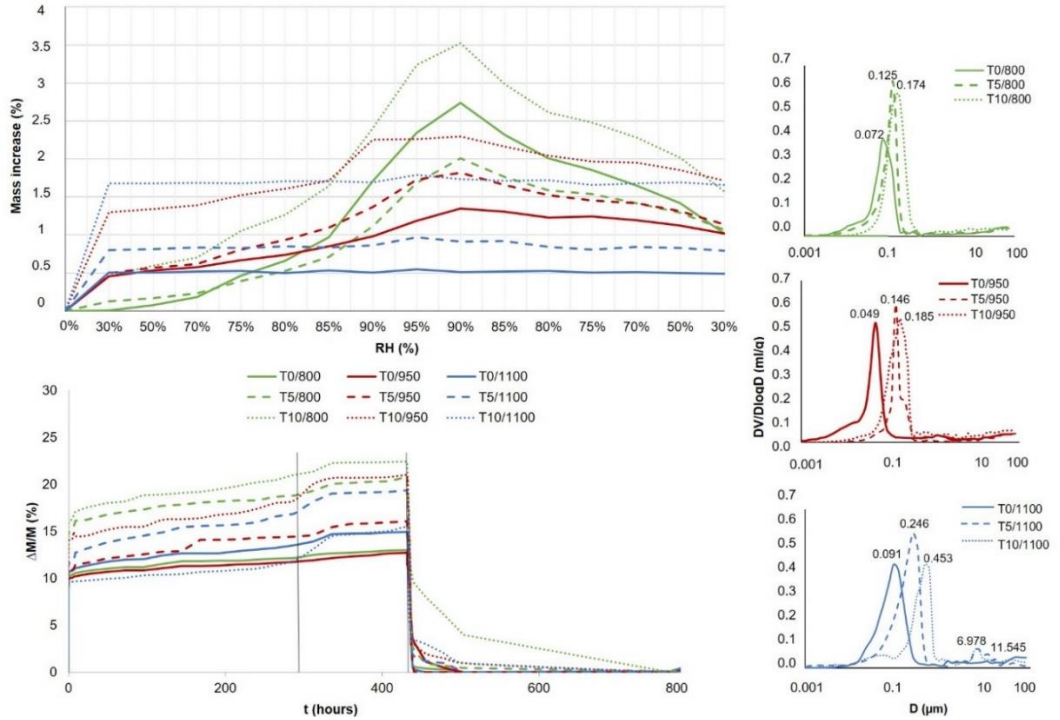


**Figure IV-5.** Interaction of the bricks with water vapour and their behaviour in relation to RH variations (mass increase versus relative humidity both in %), hydric behaviour of the bricks (weight variation in % versus time in hours) and MIP curves (frequency in % versus pore diameter in  $\mu m$ ) for bricks fired at 800, 950 and 1100 °C with no additive (continuous line) and with added tea residue (dashed lines)



**Table IV-4.** Hydric, MIP and DIA parameters for bricks with and without tea residue. Ab: free water absorption (%); Af: forced water absorption (%); Ax: degree of pore interconnection (%); S: saturation coefficient (%); Di: drying index. P<sub>o</sub>: open porosity by hydric test (%); C: capillarity coefficient (g/m<sup>2</sup>s<sup>0.5</sup>); ρ<sub>a</sub>: apparent density (g cm<sup>-3</sup>); ρ<sub>r</sub>: real density (g cm<sup>-3</sup>). P<sub>oMIP</sub> = open porosity by MIP (%); ρ<sub>aMIP</sub> = apparent density (g cm<sup>-3</sup>); ρ<sub>rMIP</sub> = real density (g cm<sup>-3</sup>); SSA = specific surface area (m<sup>2</sup>/g); P<sub>oDIA</sub> = open porosity by DIA (%); MinFeret = the largest MinFeret diameter measured by DIA.

	Hydric behaviour									MIP				DIA	
	Ab	Af	Ax	S	Di	Po	C	ρ <sub>a</sub>	ρ <sub>r</sub>	P <sub>oMIP</sub>	ρ <sub>aMIP</sub>	ρ <sub>rMIP</sub>	SSA	P <sub>oDIA</sub>	MinFeret
T0/800	12.94	13.01	11.46	85.12	1.30	40.56	3.80	1.92	3.06	36.47	1.54	2.42	10.06	11.18	1386
T5/800	20.34	20.76	8.90	91.88	2.07	44.91	3.59	1.65	2.88	39.67	1.44	2.39	3.72	19.96	1382
T10/800	22.37	22.42	6.28	93.74	2.24	48.67	3.11	1.55	2.53	46.53	1.36	2.55	2.09	32.89	3529
T0/950	12.68	12.73	11.25	86.46	1.27	42.34	3.56	1.69	2.19	41.43	1.96	1.98	9.72	-	-
T5/950	15.94	16.05	7.75	93.46	1.60	45.70	2.91	1.09	1.94	44.44	1.66	1.99	2.8	-	-
T10/950	20.78	21.02	5.30	94.65	2.10	49.03	2.14	0.92	1.48	51.61	1.14	1.35	1.49	-	-
T0/1100	14.87	14.87	12.95	82.07	1.49	42.81	3.82	1.53	2.40	41.97	1.63	2.81	8.44	14.56	1141
T5/1100	19.20	19.38	6.11	93.34	1.93	44.46	2.46	1.21	2.16	47.12	1.45	2.74	1.43	34.24	3513
T10/1100	15.05	15.46	5.08	95.97	1.54	49.22	1.98	0.98	2.64	54.11	1.51	3.09	1.22	38.92	13153

MIP analysis revealed that the addition of tea residue alters the pore size distribution in the bricks. All the bricks show a unimodal pore size distribution with a maximum peak at around 0.1  $\mu\text{m}$  in bricks fired at 800 °C and 950 °C and 0.2  $\mu\text{m}$  in those fired at 1100 °C. The addition of residue causes the main peak to shift to the right of the diagrams, i.e. towards higher pore sizes. This is most evident at 1100 °C where the peaks for T5/1100 and T10/1100 are at 0.25 and 0.45  $\mu\text{m}$ , respectively. At 1100 °C, a second family of pores can be clearly distinguished at around 10  $\mu\text{m}$  (Fig.IV-5). The open porosity is influenced by the addition of residue, so confirming the results of the hydric tests ( $P_{\text{oMIP}}$ , Table IV-4).

Digital image analysis (DIA) was performed on the two sets of samples fired at 800 °C (T0/800, T5/800, T10/800) and 1100 °C (T0/1100, T5/1100, T10/1100) (Table IV-4). This highlighted the increase in both porosity and pore size in line with the increase in firing temperature and in the percentage of tea residue added, so confirming the qualitative observations reported in sections 3.2.3 and 3.2.4. The abundance of pores of over 4  $\mu\text{m}$  explains the differences observed in the weight of the bricks after firing (Table IV-S1). The pores were also affected by the addition of tea waste, as is clear in the samples fired at 800 °C where porosity increased in line with the tea percentages, from 11.18% (T0/800) to 19.96% and 32.89% (T5/800 and T10/800, respectively). A large difference was noted in the bricks fired at 1100 °C. The high firing temperature increased the porosity (Crespo-López et al., 2023a; Coletti et al., 2018), as confirmed by the T0/1100 sample, which had 20% more pores than the T0/800 sample. At 1100 °C, the addition of tea waste caused a significant increase in porosity from 14.56% to 34.24% and 38.92% for T5/1100 and T10/1100, respectively. The combined effects of firing temperature and tea waste addition are also detectable in pore size analysis. Table IV-5 sets out the maximum and minimum diameter found in each section in terms of caliper diameter (MinFeret) (Coletti et al., 2016; Salvini et al., 2023), which increases in line with increasing firing temperature and tea waste percentage. While the samples T0/800, T5/800, and T0/1100 display the largest minFeret of about 1100-1300  $\mu\text{m}$  and the samples T10/800 and T5/1100 show a minFeret of around 3500  $\mu\text{m}$ , the sample fired at 1100 °C made with 10% of tea residue (T10/1100) has pores with a minFeret of just over 13000  $\mu\text{m}$  (i.e., more than 1 cm).

### 3.4. Thermal conductivity

The results of the thermal conductivity measurements are shown in Table IV-5. Values measured on the three orthogonal directions revealed that the thermal behaviour of the bricks is anisotropic. This is due to the brickmaking process applied here, which was based on the traditional method of pressing and moulding by hand (a = perpendicular to the pressure exerted, b and c = parallel to the pressure exerted). The highest values were found normal to the side of brick ( $\lambda(c)$ ), while  $\lambda(a)$  and  $\lambda(b)$  showed similar thermal conductivity values, which were about 10% lower than for ( $\lambda(c)$ ). The mean thermal conductivity ( $\lambda_{\text{mean}}$ ) ranges from 0.34 to 0.91 (W/(m·K)), in accordance with the findings of previous research (Ten et al., 2010; Sutcu, 2015; Kubiś et al., 2020; Coletti et al., 2023). Values decrease in line with the increase in temperature from 800°C to 1100°C and with the increase in tea residue content (0, 5 or 10 wt.%), suggesting a direct relationship between  $\lambda$  and porosity (Ten et al., 2010; Allegretta et al., 2017). When thermal conductivity is plotted against porosity (Fig.IV-S3), an  $R^2 > 0.8$  is found. The best correlation was obtained by the hydric test analysis of open porosity ( $P_o$ , Table IV-4) ( $R^2 = 0.9552$ ), in which a medium-sized pore range was observed, as compared to the smaller sizes measured by MIP ( $R^2 = 0.8061$ ) and the larger ones recorded by DIA ( $R^2 = 0.8864$ ) (Fig.IV-S3).

The estimated heat diffusivity  $\alpha$  also decreases with an increase in firing temperature and in tea waste content.  $\alpha$  varied from  $2.01 \cdot 10^{-7}$  mm/s and  $2.87 \cdot 10^{-7}$  mm/s for samples with 10 wt.% of tea residues to  $3.71 \cdot 10^{-7}$  mm/s to  $4.89 \cdot 10^{-7}$  mm/s for samples with no added tea residue. Those with 5 wt.% of added residue obtained intermediate values for all three firing temperatures (Table IV-5). These results indicate that the addition of tea residue strongly decreases both thermal conductivity and heat diffusion capacity, suggesting that bricks made with this additive would have good thermal insulation properties.

**Table IV-5.** Thermal behaviour:  $\lambda(a)$ ,  $\lambda(b)$  and  $\lambda(c)$  = thermal conductivity measured normal to the sides a (perpendicular to the pressure exerted), b and c (parallel to the pressure exerted) of the sample (W/(m·K));  $\lambda_{\text{mean}}$  = mean thermal conductivity (W/(m·K)) calculated on the three sides  $\lambda(a)$ ,  $\lambda(b)$  and  $\lambda(c)$ ;  $\alpha$  = thermal diffusivity calculated by  $\lambda_{\text{mean}}$  (mm/s).

	$\lambda(a)$	$\lambda(b)$	$\lambda(c)$	$\lambda_{\text{mean}}$	$\alpha$
T0/800	0.83	0.89	1.01	0.91	$3.71 \cdot 10^{-7}$
T5/800	0.64	0.68	0.75	0.69	$3.01 \cdot 10^{-7}$
T10/800	0.45	0.47	0.48	0.47	$2.32 \cdot 10^{-7}$
T0/950	0.76	0.82	0.99	0.85	$4.89 \cdot 10^{-7}$
T5/950	0.53	0.60	0.72	0.61	$3.97 \cdot 10^{-7}$
T10/950	0.32	0.33	0.37	0.34	$2.87 \cdot 10^{-7}$
T0/1100	0.75	0.83	0.84	0.81	$4.20 \cdot 10^{-7}$
T5/1100	0.56	0.63	0.68	0.62	$3.62 \cdot 10^{-7}$
T10/1100	0.35	0.43	0.49	0.42	$2.01 \cdot 10^{-7}$

### 3.5. Compactness and strength

The control bricks (T0) show higher compressive strength than those with added tea residue (T5 and T10), which is logical considering the large number of new pores formed in the T5 and T10 bricks after the combustion of the organic matter during firing (see Po, Table IV-4). The sample with the highest compressive strength was T0/1100 (29.3 MPa, Fig.IVA-6). If we look at the three groups of samples with 0, 5 and 10 wt.% of tea residue, the bricks fired at 1100 °C always had the highest compressive strength values (Fig.IV-6), due to their higher level of vitrification, as was demonstrated by PXRD analysis and microscope observations. These results are in line with those of previous research studies in which it was found that compressive strength is more closely related with porosity and the degree of vitrification of bricks than with the mineralogy of the raw material (Saravanapavan and Hench, 2003; Cultrone et al., 2004; Dondi et al., 2009; Crespo-López et al., 2023c). In a similar trend to compressive strength, the highest surface hardness values were observed in the bricks with no tea residue fired at 950 and 1100 °C (385.7 and 446.8, respectively) (Fig.IV-S4). In all the bricks, the higher the amount of tea residue added, the lower the surface hardness. The lowest hardness values were obtained in the bricks fired at 800 °C and with 10 wt.% tea residue. These were 34% lower than those made without the additive and fired at the same temperature. However, according to official specifications from the Spanish Ministry of Public Works (Pliego RL-88, 1988), the minimum compressive strength value for bricks to be used in

the construction industry is 10 MPa. All the samples obtained compressive strength values above this threshold, so making them suitable for use as building materials.

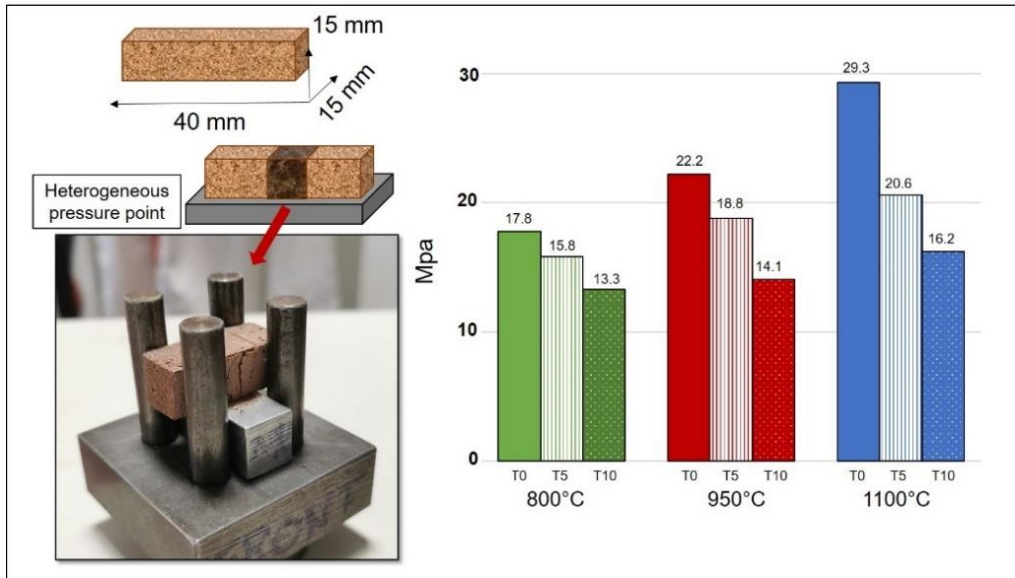


**Figure IV-6.** Mechanical behaviour for bricks fired at 800, 950 and 1100 °C made without additives (control group, T0) and with added tea residue (T5 and T10).

Table IV-6 shows the average values for ultrasound velocities ( $V_p$  and  $V_s$ ) measured in bricks made with and without tea residue. The highest  $V_p$  and  $V_s$  values were measured in bricks fired at 1100 °C. The increase in velocity is not gradual from 800 to 1100 °C, in that  $V_p$  and  $V_s$  are similar at 800 and 950 °C. In some cases (when residue is added) they are lower at 950 °C and experience a significant rise at 1100 °C. The higher velocity is a sign of greater compactness (Crespo-López et al., 2023a). This indicates that vitrification occurs more between 950 and 1100 °C than between 800 and 950 °C. The formation of new pores due to use of added tea waste results in a decrease in  $V_p$  and  $V_s$ .

The lowest ultrasound value was for the samples fired at 950 °C with 10 wt.% residue (Table IV-6). In this case, it is possible that the combustion of organic matter together with the total decomposition of the calcite grains and the higher phyllosilicate dehydroxylation at 950 °C reduced the compactness of the bricks compared to those fired at 800 °C.

The Poisson's ratio ( $\nu$ ) values are very similar for all the samples regardless of the firing temperature or the addition or not of tea residue. The mean values of around 0.30 indicate a value similar to that of shale, a sedimentary rock with a mineralogy comparable to that

of bricks (Molina et al., 2017). This value decreases slightly for bricks with added tea residue (about 0.27, Table IV-6), a value closer to silty materials, loose sands or soft clays (Kumar Thota et al., 2021). The Young (E), shear (G) and bulk (K) moduli (Table IV-6) decrease in line with the increases in the amount of tea residue.

**Table IV-6.** Average velocities for the propagation of ultrasonic  $V_P$  and  $V_S$  (in m/s).  $\nu$ : Poisson's ratio; E: Young's modulus (in GPa); G: shear modulus (in GPa); K: bulk modulus (in GPa).

	Mean $V_P$ (m/s)	Mean $V_S$ (m/s)	$\nu$	E ( $\times 10^3$ )	G ( $\times 10^3$ )	K ( $\times 10^3$ )
T0/800	2357	1212	0.31	7.39	2.82	0.93
T5/800	2125	1011	0.28	4.34	1.69	0.64
T10/800	1861	939	0.27	2.55	1.00	0.39
T0/950	2443	1238	0.31	6.79	2.59	0.86
T5/950	2101	995	0.30	2.81	1.07	0.37
T10/950	1581	753	0.28	1.34	0.52	0.19
T0/1100	2526	1292	0.32	6.74	2.55	0.81
T5/1100	2346	1088	0.27	3.64	1.43	0.56
T10/1100	2221	1156	0.26	3.30	1.30	0.53

### 3.6. Colour

The colour of bricks is the result of a combination of factors such as the temperature, the type of raw material used (in particular the presence and concentration of Fe oxide, which gives the bricks their reddish colour (Perez-Monserrat et al., 2022b and 2024) and the addition of residue. These factors determine the final shade and hue of the samples. During firing, our brick samples underwent certain changes in colour.

The bricks fired at 800 °C are red and have some of the highest  $a^*$  and  $b^*$  values (Fig.IV-S5). Higher firing temperatures tend to result in darker shades. The chromatic values and the lightness ( $L^*$ ) tend to decrease in bricks without residues. It is interesting to note that  $L^*$  is higher for bricks without residues, e.g. at T0/800,  $L^*=54.25$ , going down to 43.47 at T10/800.

At 1100 °C, bricks without additive (T0) reach mean values of 11.75 ( $a^*$ ) and 19.24 ( $b^*$ ). The addition of 10% wt. of tea residue results in bricks with a lighter colour (Table IV-S2). The general trend in lightness ( $L^*$ ) is related to the amount of tea residue added, and is

higher in the residue-free bricks fired at 800 and 950 °C (T0/800: 54.25 and T0/950: 56.24) than in the T10/800 samples (43.47). The samples fired at 800 and 950 °C have a rough appearance, with numerous pores (Fig.IV-S5) and an orangey shade of red. As the firing temperature increases to 1100 °C, the difference in colour between the bricks produced with and without the addition of tea residue becomes more pronounced. By contrast, the lightness values are more similar.

### 3.7. Durability

During the salt crystallisation test, all the samples gain weight. This is because of the deposition of sodium sulphate inside the pores and fissures of the bricks (Fig.IV-7A). At the beginning of this ageing test, the weight increase varies from one type of brick to another, with the greatest increases being observed in those with 10 wt.% tea residue (T10/800, T10/950 and T10/1100). This confirms the results of the hydric tests in which the bricks without residue gained the least weight. This is because less saline solution can enter the pore system and damage the bricks. As the ageing test progresses, small fluctuations of the curves can be observed with increases and losses in weight which are linked respectively to the crystallization of the salt in new fissures and the consequent loss of fragments due to crystallization pressure. Using ultrasound, we were able to monitor the behaviour of the bricks during the salt crystallization decay test (Fig.IV-7B). Again, the P waves move faster in the bricks without additives and slower in those with 10 wt.% residue. Over the course of the test, all the samples showed an increase in the average wave velocity, which was especially evident after the 4<sup>th</sup> cycle, because of the crystallization of salts in the pores of the bricks.

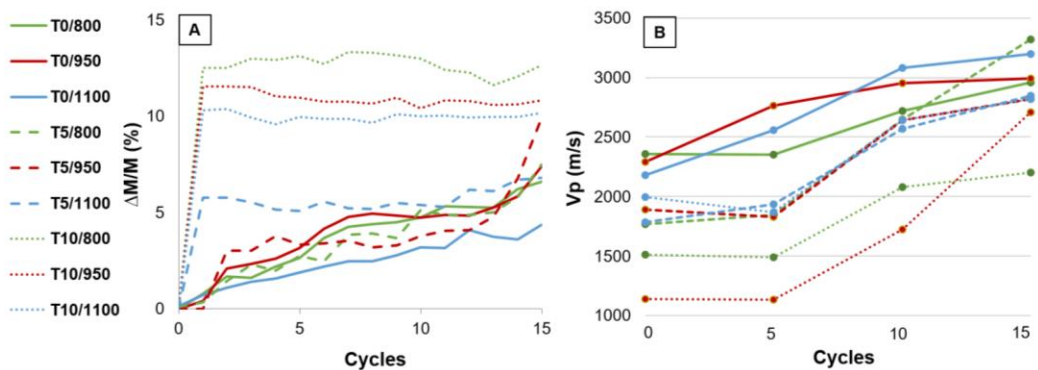


**Figure IV-7.** A) Weight variation in the bricks made without additives (T0) and with added tea residue (T5 and T10) over 15 salt crystallization test cycles. Each curve represents the mean of three measurements. B)  $V_p$

velocities during the salt crystallization test for bricks fired at 800, 950 and 1100 °C without additives and with added tea residue.

#### **4. Conclusions**

In this paper, chemical, mineralogical and physical techniques were applied to assess the behaviour of solid bricks that were handmade with a clayey raw material from Teruel (Spain) to which 0, 5 or 10 wt.% of tea waste was added. The samples were fired at temperatures of 800, 950 and 1100 °C. The following conclusions were reached:

- Tea residue did not affect the mineralogy of the bricks. The mineralogical changes that occurred during firing were dependent on the raw material and the firing temperature, with higher temperatures leading to increased amounts of amorphous phase due to the vitrification of the brick matrix.
- The tea waste had a more significant effect on the hydric behaviour of the bricks than the firing temperature, increasing porosity and water vapour absorption in proportion to the amount of added residue. This is because the residue is consumed during firing, creating more empty spaces.
- Mercury intrusion porosimetry and digital image analysis highlighted that pore sizes and porosity increased in line with increases in the amount of added waste and in firing temperature.
- The addition of tea waste reduced thermal conductivity and heat diffusion in the bricks, making them suitable for thermal insulation.
- The bricks made without added waste were mechanically stronger than those made with the additive, but both comply with the specifications required by the construction industry.
- The addition of tea waste created new pores, so reducing ultrasound velocities. This indicates a reduction in the compactness of the bricks. The higher the amount of added residue, the lower the velocity.
- The addition of tea waste gave the bricks a more greyish colour, decreasing the lightness and the chromaticity parameters.



- In terms of durability, the bricks made with the highest amount of tea waste (10 wt.%) undergo the greatest variation in weight due to salt crystallization regardless of the firing temperature. The bricks with no added waste or with 5 wt.% showed similar decay behaviour. Therefore, the addition of this percentage of waste does not reduce the durability of the bricks when exposed to salt crystallization.

**Supplementary material**

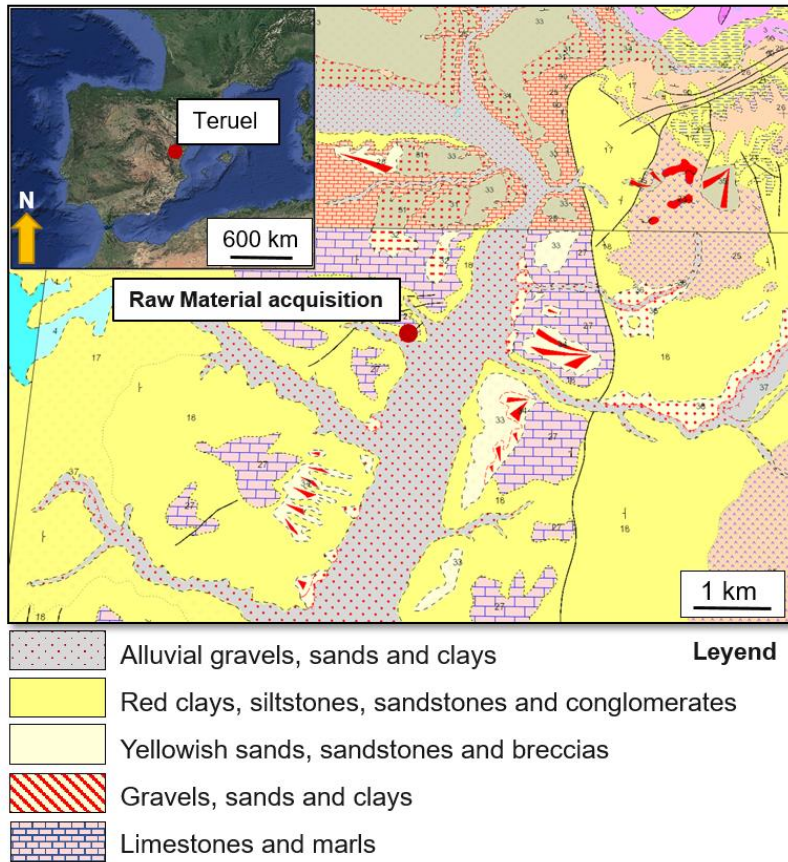


**Figure IV-S1.** Geological mapping of the Teruel area from where the raw material was obtained (red point). Map obtained and modified from IGME (<https://igme.es>).

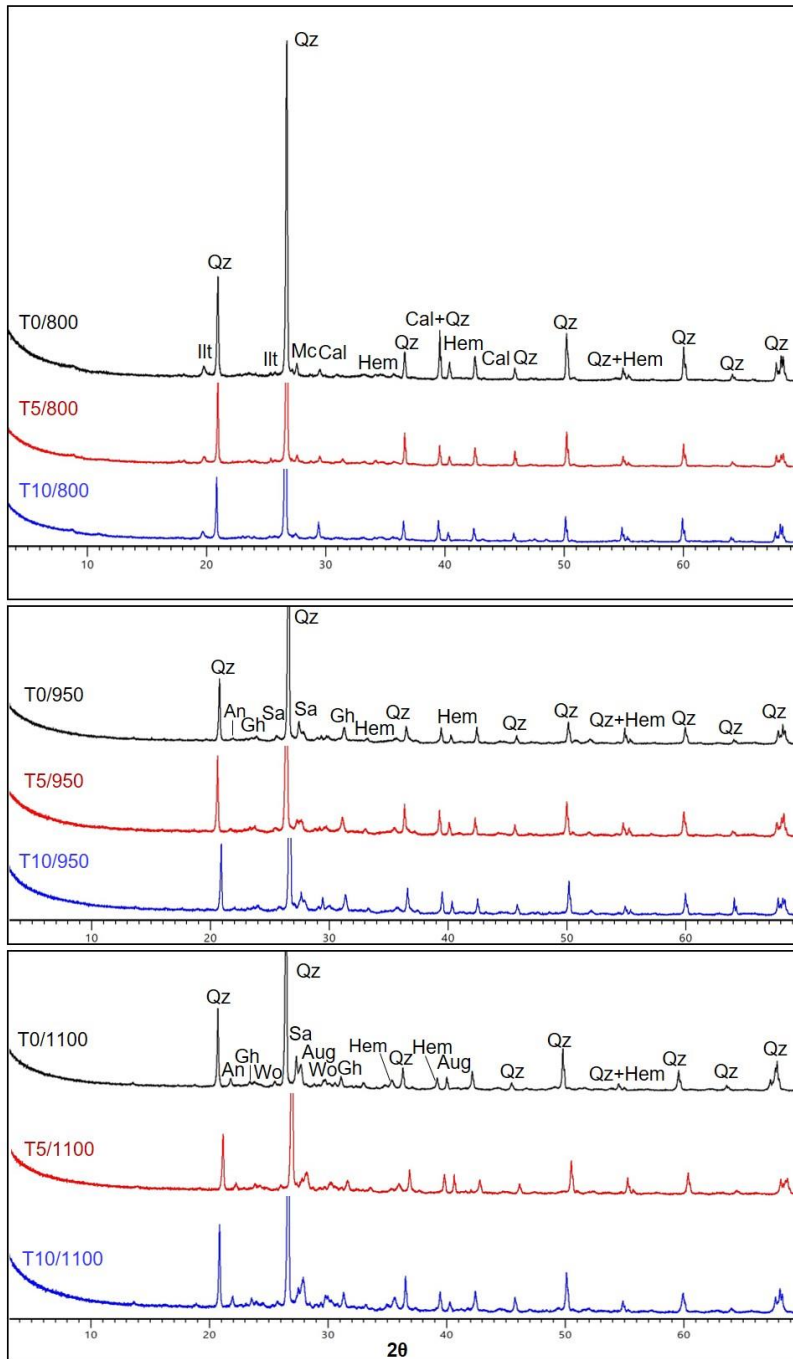


**Figure IV-S2.** Mineralogy of the bricks with and without tea residue added and fired at different temperatures. Legend (mineral acronyms according to Warr (2020): Qz = quartz; Cal = calcite; Ilit = illite; Hem = hematite; Mc = microcline; Or = orthoclase; Sa = sanidine; An = anorthite; Aug = augite; Gh = gehlenite; Wo = wollastonite.

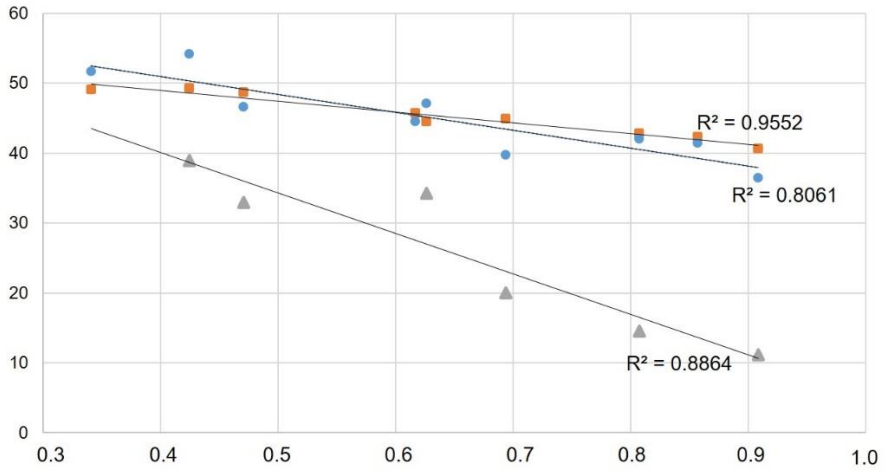


**Figure IV-S3:** Correlation between thermal conductivity and porosity measured by hydric test (orange spot,  $R^2 = 0.9552$ ), MIP (blue circles,  $R^2 = 0.8061$ ) and DIA (grey triangles,  $R^2 = 0.8864$ ).

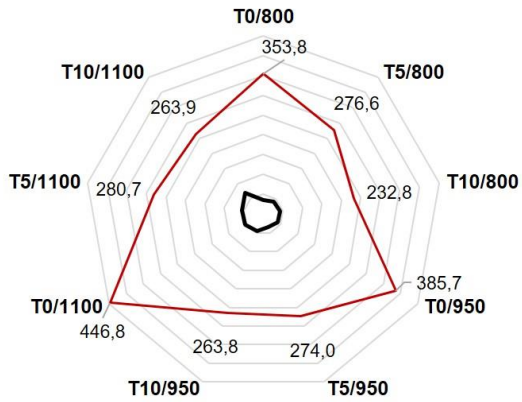


**Figure IV-S4.** Surface hardness as determined from the Leeb Hardness Test (LH) on the bricks studied.

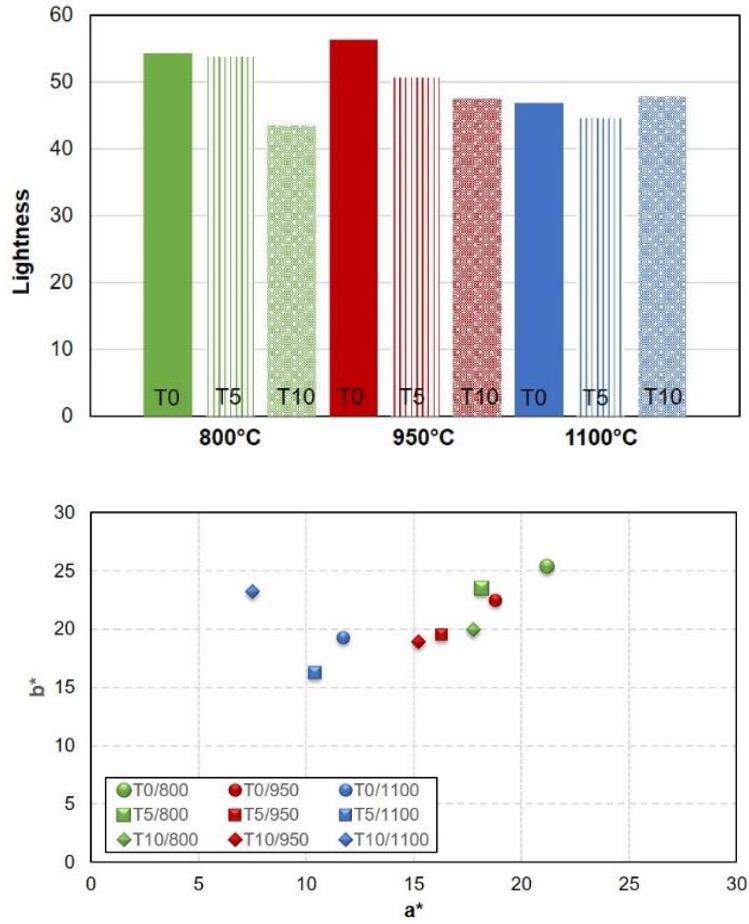


**Figure IV-S5.** Lightness (up) and chromaticity (down) of fired bricks with and without tea residue added.

**Table IV-S1.** Weight difference average and standard deviation of fired bricks with and without tea residues added

		Pre-fired	Post-fired	Weight difference (%)
Control bricks	T0/800	106.64 (11.01)	97.30 (11.23)	-9.34
	T0/950	113.50 (8.58)	100.83 (9.26)	-10.62
	T0/1100	107.94 (5.59)	87.12 (7.22)	-19.44
Bricks + Tea residue	T5/950	107.69 (11.38)	99.73 (12.12)	-7.41
	T5/800	97.18 (8.38)	86.15 (7.11)	-11.34
	T5/1100	105.37 (9.01)	84.12 (7.92)	-20.01
	T10/800	94.62 (13.99)	80.20 (11.35)	-15.79
	T10/950	95.05 (12.04)	67.60 (9.46)	-28.42
	T10/1100	102.45 (3.71)	71.12 (2.65)	-30.39

**Table IV-S2.** Colour difference ( $\Delta E$ ) due to the addition of tea residue to the brick samples as compared to those made without additive.

	$\Delta E$		
	T0	T5	T10
800°C	-	3.59	5.52
950°C	-	3.78	6.27
1100°C	-	3.97	7.85

## 6. CONCLUSIONS

In this research, bricks were made using two different production methods (manual and extrusion) and various different clayey materials (Guadix, Jun, a specific mixture of Guadix and Viznar, and Teruel) to which various different inorganic and organic residues were added in different proportions. The properties of the fired bricks were then compared with those of the control samples made solely with clay. All the samples, regardless of their production method, were fired in the same electric oven and oxidizing atmosphere at 800, 950 and 1100°C.

The following **inorganic wastes** were selected: household glass and carbon fibre from wind turbine blades.

The addition of 20% by weight of ground household glass powder was shown to improve the strength of solid bricks made from two different clayey materials, one rich in carbonates (Jun) and the other rich in quartz and other silicates (Guadix), and using two production processes (by hand or by extrusion). The difference in the mineralogy of the raw materials led to differences in the mineralogy of the bricks after firing, i.e. the development of new Ca-(Mg-) silicate phases such as gehlenite, diopside, wollastonite and anorthite when the raw material from Jun was used, while mullite appeared in the bricks made from clay from Guadix. The increase in firing temperature also led to an increase in the amount of amorphous phase due to the vitrification of the bricks, which in turn modified the porous system. Bricks made with household glass and fired at high temperature absorbed less water and dried faster than the bricks without additive. Extruded bricks were also less porous than handmade bricks due to the different manufacturing process. However, the porosity of both handmade and extruded bricks decreased as the firing temperature increased. In terms of strength, the bricks with added glass were found to be more resistant to the compressive strength test than those made solely with clay. This was more evident in the Jun bricks and was confirmed by ultrasound testing. This non-destructive technique (NDT) showed that the compactness of the bricks increased in line with both the firing temperature and the amount of glass added. Another NDT technique, radiography, proved to be a valuable tool to identify the anisotropic density distribution in the bricks, which was higher on the surface of the samples and decreased towards the core. This suggests greater vitrification and consequently greater hardness on the surface of the samples.

The colour of any brick depends on the composition of the raw materials and the mineralogical and textural changes that occur during firing. The bricks from Jun varied from orange to yellow, while those from Guadix tended towards dark red. The addition of

household glass enhanced the lightness of the Jun bricks and the  $a^*$  parameter in the Guadix bricks. Firing temperatures of 950°C caused significant aesthetic changes, especially evident in the samples with added glass, where glass bubbles were seen "hatching" on the surface of the bricks.

The correlation between the aesthetic and mechanical properties assessed by NDT (such as the relationship between density and surface hardness (determined by Leeb microhardness) enabled us to compare the results obtained with the different analytical techniques.

The Jun bricks performed better in the accelerated ageing tests. This was attributed to several factors such as the fact that the carbonates present in the Jun clay melt at low firing temperatures.

According to the statistical predictions for the firing temperature variable, using the tests proposed by Tukey and Duncan and the ANOVA analysis, the Jun clay bricks tended to have better mean values for all the parameters than the Guadix clay bricks, regardless of whether they were fired with or without glass. However, the bricks from Jun fired at 1100°C and with added glass showed the greatest variations in colour, which could make them less suitable for architectural heritage restoration, where colour is a crucial factor.

In our research into the possible use of carbon fibre from wind turbine blades as an additive in brickmaking, it was observed that the carbon fibre residues also contain resin and thermoplastic compounds. During firing, the carbon fibre is consumed together with these additional compounds. This creates micropores in the bricks, which improve their thermal conductivity. The main inconveniences of using this additive in brick manufacture were the gas emissions and unpleasant odours produced during firing. Despite this, it is important to note that the use of carbon fibre as an additive in brick production is less harmful in terms of air pollution than other "waste reduction" processes used in the wind energy sector, such as incineration, pyrolysis or chemical recycling.

The addition of carbon fibre to the clay mixture partially modified the mineralogical composition of the bricks. The concentration of hematite decreased with increases in the firing temperature, because the fibres promote the development of a reducing environment in the oven and the appearance of a black core in the bricks. Texturally, the carbon fibres tended to orient themselves within the brick, possibly influenced by the kneading and moulding processes and by the firing temperature, as happens with phyllosilicates. During firing, the carbon fibres began to degrade. As the temperature



increased, they started to disappear, leaving traces in the clay matrix in the form of increased porosity, although the connectivity between the pores was worse in bricks with added carbon fibre. The addition of carbon fibre impaired the mechanical behaviour of the bricks, mainly due to their higher porosity, as detected by mercury intrusion porosimetry and ultrasound.

As for the durability of the bricks, the salt crystallization test led initially to weight gains, but with successive cycles, the bricks began to deteriorate. The presence of carbon fibre intensified this behaviour. However, the bricks fired at 950 and 1100°C with added carbon fibre experienced the least material loss, making them highly resistant to salt attack. The colour changes resulting from the addition of carbon fibre did not affect the aesthetic properties of the bricks, which means they could be used as a sustainable alternative to traditional building materials.

The **organic wastes** selected for this research were: wine pomace and tea residue.

In our research into wine pomace, this waste product was mixed in three different percentages (2.5, 5 or 10% by weight) with a combination of the raw materials from Guadix and Viznar to make lightweight bricks, whose physical and mechanical behaviour were then evaluated. The wine pomace reduced the linear shrinkage of the unfired samples and the resulting bricks were lighter after firing due to the combustion of this organic matter. The mineralogical changes that occurred during firing were directly related to the composition of the clay raw material and were unaffected by the addition of wine pomace.

In terms of texture, the particles of the wine pomace were consumed during firing, leading to the formation of new voids. The bricks fired at 1100°C were highly vitrified and had the highest values of compactness and the lowest values of open porosity. By contrast, the addition of wine pomace caused a decrease in the ultrasonic velocity. It also increased the water absorption capacity and open porosity of the bricks, which in turn affected their mechanical properties, especially at low firing temperatures. In terms of compressive strength values, the only bricks that met the specifications for use in construction work in Spain (10 MPa) were those fired at 1100 °C, when the samples were highly vitrified. However, the regulations state that bricks with a compressive strength of at least 5 MPa may be used as lightweight bricks in the construction industry. Most of the bricks studied here fulfilled this requirement.

The addition of wine pomace changed the chroma of the bricks, which varied from reddish to yellowish depending on the amount of additive added and the firing temperature.

In terms of durability, the bricks with the highest amount of residue suffered the greatest variation in weight due to salt crystallization. This means that, when used in construction, they would be more vulnerable to damage from salt attack.

As regards the addition of 5 and 10% by weight of tea residue, chemical, mineralogical and physical techniques were applied to assess how it affected the behaviour of bricks that were handmade with clay from Teruel. As happened with wine pomace, the addition of tea residues did not affect the mineralogy of the bricks. The mineralogical changes depended on the composition of the clay material and the firing temperature, with higher temperatures leading to more amorphous phase due to vitrification of the brick matrix. The addition of tea residues had a more significant effect on the hydric behaviour of the bricks than firing temperature did. Porosity and water vapour absorption increased in proportion with the amount of residue added. This is because the residues were consumed during firing, so creating voids and reducing the ultrasonic velocities and compactness of the bricks.

Porosity and pore sizes increased in line with the amount of residue added and the firing temperature, according to mercury intrusion porosimetry and digital image analysis.

The addition of tea residues reduced the thermal conductivity and the diffusion of heat in the bricks, making them suitable for thermal insulation. However, the bricks made without tea residues were mechanically stronger than those made with them, although both met the specifications required by the construction industry.

The addition of tea residues gave the bricks a darker colour, decreasing the brightness and chromatic parameters.

In terms of durability, the bricks made with the highest amount of tea residues (10% by weight) experienced the greatest variation in weight due to salt crystallization, regardless of the firing temperature. The bricks with 5% added residue showed similar decay behaviour to those made solely with clay. Therefore, the addition of this percentage of residue did not reduce the durability of the bricks when exposed to salt crystallization.

In conclusion, the use of inorganic residues, household glass or carbon fibre, as additives in brickmaking influences various properties of the fired bricks. There is a slight increase in new silicate phases when glass is added. However, the main mineralogical changes

are due to the composition of the raw material and the firing temperature. The mechanical strength of the bricks is improved by the addition of household glass, while carbon fibre increases porosity with negative consequences for mechanical strength. In terms of durability, the bricks with glass are more resistant to salt attack, due to their highly vitrified matrix enhanced by glass particles. Despite these differences, both additives could improve specific physical properties of the bricks and contribute to more sustainable construction.

Although the use of organic wastes such as wine pomace and tea residues as additives in brick manufacture does not alter the mineralogy of the bricks, it does affect their hydric and thermal behaviour, as they act as pore-forming agents. Both wine pomace and tea residues reduce the linear shrinkage of the unfired bricks and increase their porosity and water absorption capacity. They are also likely to decrease the thermal conductivity of the bricks, so making them suitable for thermal insulation. The bricks made with tea residue are mechanically stronger than those made with wine pomace and both residues influence the chromatism of the samples. In terms of durability, both types of brick are vulnerable to the salt crystallization test, suffering significant changes in weight due to the crystallization of salts within the pores. The bricks with added wine pomace suffered more severe damage.

# CONCLUSIONES

Se fabricaron ladrillos con dos métodos de producción (manual y extrusión) y diferentes materiales arcillosos (Guadix, Jun, una mezcla específica de Guadix y Viznar, y Teruel) a los que se añadieron residuos inorgánicos y orgánicos, y se compararon sus propiedades con las de las muestras fabricadas sin residuos. Todas las muestras, independientemente de su método de producción, se cocieron en el mismo horno eléctrico y atmósfera oxidante a 800, 950 y 1100 °C.

Se seleccionaron los siguientes residuos inorgánicos: vidrio doméstico y fibra de carbono procedente de las palas de los aerogeneradores.

Se demostró que la adición de un 20% en peso de polvo de vidrio doméstico molido mejoraba la resistencia de los ladrillos macizos fabricados a partir de dos materiales arcillosos diferentes, uno rico en carbonatos (Jun) y otro rico en cuarzo y otros silicatos (Guadix), y procedentes de dos procesos de producción (a mano y por extrusión). La diferencia en la mineralogía de las materias primas dio lugar a diferencias en la mineralogía de los ladrillos tras la cocción, es decir, el desarrollo de nuevas fases de silicato de Ca-(Mg-) como gehlenita, diópsido, wollastonita y anortita cuando se utilizó la materia prima procedente de Jun, mientras que la mullita apareció con la de Guadix. El aumento de la temperatura de cocción también provocó un aumento de la cantidad de fase amorfa debido a la vitrificación de los ladrillos, lo que a su vez modificó el sistema poroso. Los ladrillos fabricados con vidrio doméstico y cocidos a alta temperatura absorbían menos agua y se secaban más rápidamente que los ladrillos sin aditivo. Los ladrillos extruidos también eran menos porosos que los hechos a mano debido al diferente proceso de fabricación. Sin embargo, la porosidad tanto de los ladrillos hechos a mano como de los extruidos disminuía a medida que aumentaba la temperatura de cocción. En cuanto a la resistencia, los ladrillos con vidrio añadido resultaron ser más resistentes a la prueba de resistencia a la compresión que los fabricados sólo con arcilla. Esto fue más evidente en los ladrillos fabricados con la materia prima de Jun y se confirmó mediante el uso de ultrasonidos. Esta técnica no destructiva (END) demostró que la compacidad de los ladrillos aumentaba con la temperatura de cocción y con la adición de vidrio. Otra técnica END, la radiografía, demostró ser una herramienta valiosa para identificar la distribución anisotrópica de la densidad en los ladrillos, que era mayor en la superficie de las muestras y disminuía hacia el núcleo. Esto sugiere una mayor

vitrificación y, en consecuencia, una mayor dureza en la superficie de las muestras en comparación con el interior.

El color de los ladrillos refleja la composición de las dos materias primas y los cambios mineralógicos y texturales que se producen durante la cocción. Los ladrillos de Jun variaban del naranja al amarillo, mientras que los de Guadix tendían al rojo oscuro. La adición de vidrio doméstico aumentó la ligereza en los ladrillos de Jun y el parámetro  $a^*$  en los de Guadix. Las temperaturas de cocción de 950 °C provocaron cambios estéticos significativos, especialmente evidentes en las muestras con vidrio añadido, donde se observaron burbujas de vidrio "eclosionando" en la superficie de los ladrillos.

La correlación entre las propiedades estéticas y mecánicas evaluadas por END permitió comparar los resultados obtenidos por diferentes técnicas analíticas, como la relación entre la densidad y la dureza superficial (determinada por microdureza Leeb).

El mejor comportamiento de los ladrillos Jun en los ensayos de envejecimiento acelerado se atribuyó a varios factores, como la fusión a bajas temperaturas de cocción de los carbonatos presentes en esta materia prima.

De acuerdo con las predicciones estadísticas para las variables en función de la temperatura de cocción, utilizando las pruebas propuestas por Tukey y Duncan y el análisis ANOVA, los ladrillos de arcilla de Jun tendieron a presentar valores medios más óptimos que los ladrillos de arcilla de Guadix, independientemente de que fueran cocidos con o sin vidrio. Sin embargo, los ladrillos de Jun cocidos a 1100 °C y con vidrio añadido presentaron las mayores variaciones de color, lo que podría hacerlos menos adecuados para la restauración del patrimonio arquitectónico, donde el color es un factor crucial.

El mejor comportamiento de los ladrillos Jun en las pruebas de envejecimiento acelerado se atribuyó a varios factores, como la fusión a bajas temperaturas de cocción de los carbonatos presentes en esta materia prima.

En cuanto a la fibra de carbono de las palas de los aerogeneradores utilizada como residuo en la fabricación de ladrillos, se observó que también contiene resina y compuestos termoplásticos. Durante la cocción, la fibra de carbono y estos compuestos se consumen, creando microporos en los ladrillos, que mejoran su conductividad térmica. Los principales inconvenientes derivados de la fabricación de estos ladrillos eran las emisiones de gases y los olores desagradables producidos durante la cocción. A pesar de ello, es importante señalar que el uso de fibra de carbono como aditivo para la producción de ladrillos es menos perjudicial en términos de contaminación atmosférica

que otros procesos de "reducción de residuos" utilizados en el sector de la energía eólica, como la incineración, la pirólisis o el reciclado químico.

La adición de fibra de carbono a la mezcla de arcilla modificó parcialmente la composición mineralógica de los ladrillos. La concentración de hematites disminuyó al aumentar la temperatura de cocción en las muestras con estas fibras, ya que favorecen el desarrollo de un ambiente reductor en el horno y la aparición de un núcleo negro en los ladrillos. Texturalmente, las fibras de carbono tendieron a orientarse dentro del ladrillo, posiblemente influenciadas por los procesos de amasado y moldeado y por la temperatura de cocción, como es el caso de los filosilicatos. Tras la cocción, las fibras de carbono empezaron a degradarse. Al aumentar la temperatura, empezaron a desaparecer, dejando sus huellas en la matriz de arcilla. Esto aumentó la porosidad, aunque la conectividad entre los poros fue peor en los ladrillos con fibra de carbono añadida. La fibra de carbono empeoró el comportamiento mecánico de los ladrillos, principalmente debido a su mayor porosidad, detectada por porosimetría de intrusión de mercurio y ultrasonidos.

En cuanto a la durabilidad de los ladrillos, el ensayo de cristalización de sales produjo inicialmente aumentos de peso, pero con los ciclos sucesivos, los ladrillos empezaron a deteriorarse. La presencia de fibra de carbono intensificó este comportamiento. Sin embargo, los ladrillos cocidos a 950 y 1100 °C con fibra de carbono añadida experimentaron la menor pérdida de material, lo que los hizo muy resistentes al ataque de la sal. Los cambios de color resultantes de la adición de fibra de carbono no afectaron a las propiedades estéticas de los ladrillos, que pueden ser materiales de construcción alternativos y más sostenibles que los tradicionales.

Los residuos orgánicos seleccionados para esta investigación fueron: orujo de vino y residuo de té.

Se evaluó el comportamiento físico y mecánico de ladrillos ligeros fabricados a partir de una mezcla de las materias primas procedentes de Guadix y Viznar y mezcladas con orujo de vino en tres porcentajes (2,5, 5 ó 10% en peso). El orujo de vino redujo la contracción lineal de las muestras sin cocer y los ladrillos resultantes fueron más ligeros después de la cocción debido a la combustión de esta materia orgánica. Los cambios mineralógicos que se produjeron durante la cocción estaban directamente relacionados con la composición de la materia prima y no se vieron afectados por la adición de orujo de vino.

En cuanto a la textura, las partículas del orujo de vino se consumieron durante la cocción, dando lugar a la formación de nuevos huecos. Los ladrillos cocidos a 1100 °C estaban muy vitrificados y presentaban los valores más altos de compacidad y los más bajos de porosidad abierta. Por el contrario, la adición de orujo de vino provocó una disminución de la velocidad ultrasónica. También aumentó la capacidad de absorción de agua y la porosidad abierta de los ladrillos, al tiempo que afectó a sus propiedades mecánicas, especialmente a bajas temperaturas de cocción. Valores de resistencia adecuados para su uso en la construcción en España (10 MPa) sólo se alcanzaron a 1100 °C, cuando las muestras estaban muy vitrificadas. Sin embargo, la normativa permite utilizar ladrillos con una resistencia a la compresión de al menos 5 MPa como ladrillos ligeros en la industria de la construcción. La mayoría de los ladrillos estudiados aquí cumplían este requisito.

La adición de orujo de vino modificó el croma de los ladrillos, que varió de rojizo a amarillento en función de la cantidad de aditivo añadido y de la temperatura de cocción.

En cuanto a la durabilidad, los ladrillos fabricados con la mayor cantidad de residuo sufrieron la mayor variación de peso debido a la cristalización de las sales. Esto significa que, al utilizarse en la construcción, serían más vulnerables a los daños causados por el ataque de la sal.

Con respecto a la adición de 5 y 10% en peso de residuo de té, se aplicaron técnicas químicas, mineralógicas y físicas para evaluar su comportamiento en ladrillos macizos hechos a mano con un material arcilloso de Teruel. Se comprobó que, al igual que en el caso de la adición de orujo de vino, los residuos de té no afectaron a la mineralogía de los ladrillos. Los cambios mineralógicos dependían de la composición del material arcilloso y de la temperatura de cocción, con temperaturas más altas que conducían a una fase más amorfa debido a la vitrificación de la matriz del ladrillo. Los residuos de té tuvieron un efecto más significativo en el comportamiento hídrico de los ladrillos que la temperatura de cocción, aumentando la porosidad y la absorción de vapor de agua en proporción a la cantidad de residuos añadidos. Esto se debe a que los residuos se consumieron durante la cocción, creando más huecos y reduciendo las velocidades ultrasónicas y la compacidad de los ladrillos.

La porosidad y el tamaño de los poros aumentaron con la cantidad de residuos añadidos y la temperatura de cocción alcanzada, según la porosimetría de intrusión de mercurio y el análisis digital de imágenes.

La adición de residuos de té redujo la conductividad térmica y la difusión del calor en los ladrillos, haciéndolos adecuados para el aislamiento térmico. Sin embargo, los ladrillos fabricados sin residuos añadidos eran mecánicamente más resistentes que los fabricados con residuos de té, pero ambos cumplían las especificaciones exigidas por la industria de la construcción.

La adición de residuos de té dio a los ladrillos un color más oscuro, disminuyendo el brillo y los parámetros cromáticos.

En términos de durabilidad, los ladrillos fabricados con la mayor cantidad de residuos de té (10% en peso) experimentaron la mayor variación de peso debido a la cristalización de sales, independientemente de la temperatura de cocción. Los ladrillos sin residuos añadidos o con un 5% mostraron un comportamiento similar de deterioro. Por lo tanto, la adición de este porcentaje de residuo no redujo la durabilidad de los ladrillos cuando se expusieron a la cristalización de la sal.

En conclusión, la adición de residuos inorgánicos, vidrio doméstico o fibra de carbono, como aditivos influye en diversas propiedades de los ladrillos macizos. Hay un ligero aumento de nuevas fases de silicato cuando se añade vidrio. Sin embargo, los principales cambios mineralógicos están condicionados por la composición de la materia prima y la temperatura de cocción. La resistencia mecánica mejora con la adición de vidrio doméstico, mientras que la fibra de carbono afecta negativamente a la porosidad y a la resistencia mecánica. En cuanto a la durabilidad, los ladrillos con vidrio muestran una mayor resistencia al ataque de la sal, debido a su elevada vitrificación de la matriz potenciada por las partículas de vidrio. A pesar de estas diferencias, ambos aditivos tienen potencial para mejorar las propiedades físicas específicas de los ladrillos y contribuir a una construcción más sostenible. El efecto de la adición de residuos orgánicos como el orujo de vino y los residuos de té en la fabricación de ladrillos macizos no altera la mineralogía de los ladrillos, pero afecta a su comportamiento hídrico y térmico, ya que actúan como agentes formadores de poros. Tanto el orujo de vino como los residuos de té reducen la contracción lineal de los ladrillos sin cocer y aumentan su porosidad y capacidad de absorción de agua. Además, es probable que disminuyan la conductividad térmica, haciendo que los ladrillos sean adecuados para el aislamiento térmico. Los ladrillos con residuos de té son mecánicamente más resistentes que los fabricados con orujo de vino y ambos residuos influyen en el cromatismo de las muestras. En cuanto a la durabilidad, ambos tipos de ladrillos son vulnerables a la prueba de cristalización de sales, sufriendo importantes variaciones de peso debido a la



cristalización de sales en el interior de los poros. Se observó que los daños eran mayores en los ladrillos con adición de orujo de vino.

# FUTURE RESEARCH

The results of the research carried out in this PhD Thesis have revealed various other important issues that need to be addressed. Further research is required to identify more efficient, more sustainable methods for the production of bricks with waste product additives, reducing the energy required for their manufacture, the amount of water with which the clay is mixed and the emission of polluting particles into the atmosphere. Firstly, therefore, the aim is to explore the potential of other wastes, assessing their impact on the mineralogical, physical, mechanical and durability properties of the bricks and on the environment in general. A second promising line of research would be to explore new ways of processing and treating the waste before using it in brick manufacture. This could include pre-treatment techniques to improve the compatibility of the waste with the clay matrix, as well as more efficient recycling methods to reduce the demand for clay raw materials in brick production.

Research in this field can also contribute to the establishment of specific standards and regulations for the manufacture and use of waste bricks, in order to guarantee the quality and performance of these bricks in construction applications and the safety of the buildings in which they are used. Long-term tests must be carried out to evaluate the durability, stability and resistance of waste-based bricks in real conditions of use and exposure to environmental factors such as humidity, temperature changes and chemical agents. At the same time, research must be conducted into the development of new technologies and advanced manufacturing processes for the production of these bricks, such as 3D printing or the application of nano-engineering techniques to improve their properties. On this particular question, experiments have already been conducted with some success in other research centres.

Another area of interest would be to evaluate the socioeconomic impacts of the manufacture and use of waste-based bricks, including aspects such as local job creation, the development of sustainable supply chains and access to affordable housing. It would also be interesting to investigate market acceptance and consumer attitudes towards bricks made from waste products, identifying possible barriers and opportunities for their large-scale adoption by the construction industry.

# FUTURAS INVESTIGACIONES

Como resultado de los estudios realizados en esta Tesis Doctoral, aún quedan cuestiones por abordar. La necesidad de investigar métodos más eficientes y sostenibles para la producción de ladrillos a partir de residuos, reduciendo la energía necesaria para su fabricación, la cantidad de agua para su mezcla y la emisión de partículas contaminantes a la atmósfera, requiere una mayor atención. Por ello, por un lado, se pretende explorar el potencial de otros residuos, determinando su impacto en las propiedades mineralógicas, físicas, mecánicas, de durabilidad y medioambientales. Por otro lado, una línea de investigación prometedora sería explorar nuevas formas de procesar y tratar los residuos antes de incorporarlos a la fabricación de ladrillos. Esto podría incluir técnicas de pretratamiento para mejorar la compatibilidad de los residuos con la matriz de arcilla, así como métodos de reciclado más eficaces para reducir la necesidad de materias primas arcillosas en la producción de ladrillos.

Paralelamente, contribuir al establecimiento de normas y reglamentos específicos para la fabricación y uso de ladrillos de desecho, con el fin de garantizar la seguridad de las construcciones en las que se utilizan estos materiales, la calidad y el rendimiento en las aplicaciones constructivas; y realizar ensayos a largo plazo para evaluar la durabilidad, estabilidad y resistencia de los ladrillos de desecho en condiciones reales de uso y exposición a factores ambientales como la humedad, los cambios de temperatura y los agentes químicos. A su vez, investigar en el desarrollo de nuevas tecnologías y procesos de fabricación avanzados para la producción de ladrillos de desecho, como la impresión 3D o la aplicación de técnicas de nanoingeniería para mejorar sus propiedades, que ya se están experimentando con cierto éxito en otros centros de investigación.

Otra área de interés se centra en evaluar estudios sobre las repercusiones socioeconómicas relacionadas con la fabricación y el uso de ladrillos de desecho, incluidos aspectos como la creación de empleo local, el desarrollo de cadenas de suministro sostenibles y el acceso a viviendas asequibles. Investigar la aceptación del mercado y las actitudes de los consumidores hacia los ladrillos fabricados a partir de residuos, identificando las barreras y oportunidades para su adopción a gran escala en la industria de la construcción.

## 7. REFERENCES

- Aboudi Mana, S. C., Hanafiah, M. M. and Chowdhury, A. J. K. (2017). Environmental characteristics of clay and clay-based minerals. *Geology, ecology, and landscapes*, 1(3), 155-161. <https://doi.org/10.1080/24749508.2017.1361128>
- Achik, M., Benmoussa, H., Oulmekki, A., Ijjaali, M., El Moudden, N., Touache A. and Kizinievic, O. (2021). Evaluation of technological properties of fired clay bricks containing pyrrhotite ash. *Construction and Building Materials.*, 269, 121312. <https://doi.org/10.1016/j.conbuildmat.2020.121312>
- Adamo, N. and Al-Ansari, N. (2020). The Sumerians and the Akkadians: the forerunners of the first civilization (2900-2003BC). *Journal of Earth Sciences and Geotechnical Engineering*, 10(3), 17-39.
- Adeloye, E. K. (2017). Development of Brick Making Machine (Doctoral dissertation, Obafemi Awolowo University, Nigeria), 124 pp.
- Airado-Rodríguez, D., Durán-Merás, I., Galeano-Díaz, T. and Wold, J. P. (2011). Front-face fluorescence spectroscopy: A new tool for control in the wine industry. *Journal of Food Composition and Analysis*, 24(2), 257-264. <https://doi.org/10.1016/j.jfca.2010.10.005>
- Alami, A. H. (2013). Mechanical and thermal properties of solid waste-based clay composites utilized as insulating materials. *International Journal of Thermal & Environmental Engineering*, 6(2), 89-94. <https://doi.org/10.5383/ijtee.06.02.007>
- Albers, H., Greiner, S., Seifert, H. and Kühne, U. (2009). Recycling of wind turbine rotor blades. Fact or fiction?; Recycling von Rotorblättern aus Windenergieanlagen. Fakt oder Fiktion?. DEWI-Magazin. Germany: N. p., 2009. Web.
- Al-Fakih, A., Mohammed, B. S., Liew, M. S. and Nikbakht, E. (2019). Incorporation of waste materials in the manufacture of masonry bricks: An update review. *Journal Building Engineering*, 21, 37-54. <https://doi.org/10.1016/j.jobbe.2018.09.023>
- Alia, J. M., Edwards, H. G. M., Garcia-Navarro, F. J., Parras-Armenteros, J. and Sanchez-Jimenez, C. J. (1999). Application of FT-Raman spectroscopy to quality control in brick clays firing process. *Talanta*, 50 (2), 291-298. [https://doi.org/10.1016/S0039-9140\(99\)00031-4](https://doi.org/10.1016/S0039-9140(99)00031-4)
- Allegretta, I., Eramo, G., Pinto, D. and Hein, A. (2017). The effect of mineralogy, microstructure and firing temperature on the effective thermal conductivity of traditional hot processing ceramics. *Applied Clay Science*, 135, 260-270. <https://doi.org/10.1016/j.clay.2016.10.001>
- Allwright, R. K. (1997). Special interest: Art Deco. Its history and influence on architecture. (Doctoral dissertation, California State University, United States), 345 pp.

- Almssad, A., Almusaed, A. and Homod, R. Z. (2022). Masonry in the context of sustainable buildings: A review of the brick role in architecture. *Sustainability*, 14(22), 14734. <https://doi.org/10.3390/su142214734>
- Almusaed, A., and Almssad, A. (2023). Introductory Chapter: Bricks between the Historical Usage and Sustainable Building Concept. *Masonry for Sustainable Construction*. IntechOpen, 122 pp. <https://doi.org/10.5772/intechopen.109287>,
- Alonso-Zarza, A.M. and Calvo, J. P. (2000). Palustrine sedimentation in an episodically subsiding basin: the Miocene of the northern Teruel Graben (Spain). *Palaeogeography Palaeoclimatology Palaeoecology*, 160, 1-21. [https://doi.org/10.1016/S0031-0182\(00\)00041-9](https://doi.org/10.1016/S0031-0182(00)00041-9)
- Altoaguirre, Y., Schulz, M., Gibert, L. and Bruch, A. A. (2021). Mapping Early Pleistocene environments and the availability of plant food as a potential driver of early Homo presence in the Guadix-Baza Basin (Spain). *Journal of Human Evolution*, 155, 102986. <https://doi.org/10.1016/j.jhevol.2021.102986>
- Amritphale, S. S., Chandra, N. and Kumar, R. (1992). Sintering behaviour of pyrophyllite mineral: effect of some alkali and alkaline-earth metal carbonates. *Journal of Materials Sciences*, 27(17), 4797-4804. <https://doi.org/10.1007/BF01166022>
- Anadón, P. and Moissenet, E. (1996). Neogene basins in the Eastern Iberian Range. In: Friend, P.F., Dabrio, C.F., (Eds.), *Tertiary Basins of Spain. The Stratigraphic Record of Crustal Kinematics*. World and Regional Geology Series 6. Cambridge University Press, Cambridge, p. 68–76.
- Anderson, C. (2013). *Renaissance architecture*. Oxford University Press, 272 pp.
- Anjum, F., Naz, M. Y., Ghaffar, A., Shukrullah, S., Abd El-Salam, N. M. and Ibrahim, K. A. (2020). Study of thermal and mechanical traits of organic waste incorporated fired clay porous material. *Physica B: Physics and Condensed Matter*, 599, 412479. <https://doi.org/10.1016/j.physb.2020.412479>
- Antico, F. C., Wiener, M. J., Araya-Letelier, G. and Retamal, R. G. (2017). Eco-bricks: a sustainable substitute for construction materials. *Revista de la Construcción. Journal of Construction*, 16(3), 518-526. <https://doi.org/10.7764/RDLC.16.3.518>
- Aresta, A., Cotugno, P., De Vietro, N., Massari, F. and Zambonin, C. (2020). Determination of polyphenols and vitamins in wine-making by-products by supercritical fluid extraction (SFE). *Analytical Letters*, 53(16), 2585-2595. <https://doi.org/10.1080/00032719.2020.1749846>
- Arshad, M. and O'Kelly, B. (2019). Global status of wind power generation: theory, practice, and challenges. *International Journal of Green Energy*, 16(14), 1073-1090. <https://doi.org/10.1080/15435075.2019.1597369>
- Artioli, G., Secco, M. and Addis, A. (2019). The Vitruvian legacy: Mortars and binders before and after the Roman world. *EMU Notes in Mineralogy*, Vol. 20, Chapter 4, 151–202 <https://doi.org/10.1180/EMU-notes.20>

- Arvanitoyannis, I. S., Ladas, D. and Mavromatis, A. (2006). Potential uses and applications of treated wine waste: a review. *International Journal of Food Science*, 41(5), 475-487. <https://doi.org/10.1111/j.1365-2621.2005.01111.x>
- Arya, A. S., Boen, T. and Ishiyama, Y. (2014). Guidelines for earthquake resistant non-engineered construction. UNESCO.
- ASTM D2845 (2000). Standard test method for laboratory determination of pulse velocities and ultrasonic elastic constants of rock. J. ASTM Int., West Conshohocken, PA, USA.
- ASTM D5313 (2004). Standard Test Method for Evaluation of Durability of Rock for Erosion Control Under Wetting and Drying Conditions. J. ASTM Int, West Conshohocken, PA, USA.
- Awason, I. (2011). Tea. *Journal of Agricultural and Food Information*. 12(1) 2011, 12-22. <https://doi.org/10.1080/10496505.2011.540552>

## B

- Babatunde, S. A. (2017). Review of strengthening techniques for masonry using fiber reinforced polymers. *Composition. Structure*, 161, 246-255. <https://doi.org/10.1016/j.compstruct.2016.10.132>
- Bajaj, S. (2016). Tea bags filter paper-A miniature textile creation. *Contemporary Social Sciences*, 25, 131-138.
- Balan, E., Aufort, J., Saldi, G. D., Brouder, C. and Lazzeri, M. (2019). Line-broadening and anharmonic effects in the attenuated total reflectance infrared spectra of calcite, *European Journal of Mineral.*, 31, 73-81. <https://doi.org/10.1127/ejm/2018/0030-2802>
- Barbieri, L., Andreola, F., Lancellotti, I., Taurino, R. (2013). Management of agricultural biomass wastes: Preliminary study on characterization and valorisation in clay matrix bricks. *Journal of Waste Management*, 33(11), 2307-2315. <https://doi.org/10.1016/j.wasman.2013.03.014>
- Barbosa, A. P. C., Fulco, A. P. P., Guerra, E. S., Arakaki, F. K., Tosatto, M., Costa, M. C. B. and Melo, J. (2017). Accelerated aging effects on carbon fiber/epoxy composites. *Composites. B: Engineering*, 110, 298-306. <https://doi.org/10.1016/j.compositesb.2016.11.004>
- Barcia, M. T., Pertuzatti, P. B., Gómez-Alonso, S., Godoy, H. T. and Hermosín-Gutiérrez, I. (2014). Phenolic composition of grape and winemaking by-products of Brazilian

- hybrid cultivars BRS Violeta and BRS Lorena. *Food Chemistry*, 159, 95-105. <https://doi.org/10.1016/j.foodchem.2014.02.163>
- Barde, R. V., Nemade, K. R. and Waghuley, S. A. (2015). AC conductivity and dielectric relaxation in  $V_2O_5$ - $P_2O_5$ - $B_2O_3$  glasses. *Journal of Asian Ceramic Society*, 3(1), 116-122. <https://doi.org/10.1016/j.jascer.2014.11.006>
- Barlow, S. G. and Manning, D. A. C. (1999). Influence of time and temperature on reactions and transformations of muscovite mica. *Transactions and journal of the British Ceramic Society*, 98(3), 122-126. <https://doi.org/10.1179/096797899680327>
- Barnhisel, R. I. and Rich, C. I. (1967). Clay mineral formation in different rock types of a weathering boulder conglomerate. *Soil Science Society of America Journal*, 31(5), 627-631. <https://doi.org/10.2136/sssaj1967.03615995003100050007x>
- Basumatary, V., Saikia, R., Narzari, R., Bordoloi, N., Gogoi, L., Sut, D. and Kataki, R. (2018). Tea factory waste as a feedstock for thermo-chemical conversion to biofuel and biomaterial. *Materials Today: Proceedings*, 5(11), 23413-23422. <https://doi.org/10.1016/j.matpr.2018.11.081>
- Bautista-Marín, J. D., Esguerra-Arce, A. and Esguerra-Arce, J. (2021). Use of an industrial solid waste as a pigment in clay bricks and its effects on the mechanical properties. *Construction and Building Materials*, 306, 124848. <https://doi.org/10.1016/j.conbuildmat.2021.124848>
- Benavente, D., Brimblecombe, P., and Grossi, C. M. (2015). Thermodynamic calculations for the salt crystallisation damage in porous built heritage using PHREEQC. *Environmental Earth Sciences*, 74, 2297-2313. <https://doi.org/10.1007/s12665-015-4221-1>
- Benavente, D., del Cura, M. G., García-Guinea, J., Sánchez-Moral, S., and Ordóñez, S. (2004). Role of pore structure in salt crystallization in unsaturated porous stone. *Journal of crystal growth*, 260(3-4), 532-544. <https://doi.org/10.1016/j.jcrysgro.2003.09.004>
- Berge, B. (2007). *Ecology of building materials*. Routledge. Taylor and Francis, 448 pp. <https://doi.org/10.4324/9780080949741>
- Bertman, S. (2005). *Handbook to life in ancient Mesopotamia*. Oxford University Press, USA.
- Betzler, C., Braga, J. C., Martín, J. M., Sánchez-Almazo, I. M. and Lindhorst, S. (2006). Closure of a seaway: Stratigraphic record and facies (Guadix basin, southern Spain). *International Journal of Earth Sciences*, 95, 903-910. <https://doi.org/10.1007/s00531-006-0073-y>
- Blight, G. E. (1997). Origin and formation of residual soils. *Mechanics of Residual Soil*, 1, 15.



- Boccarda, A. C., Fournier, D., Kumar, A. and Pandey, G. C. (1997). Nondestructive evaluation of carbon fiber by mirage-FTIR spectroscopy. *Journal of Applied Polymer Science*, 63(13), 1785-1791. [https://doi.org/10.1002/\(SICI\)1097-4628](https://doi.org/10.1002/(SICI)1097-4628)
- Bórawski, P., Bedycka-Bórawska, A., Jankowski, K. J., Dubis, B. and Dunn, J. W. (2020). Development of wind energy market in the European Union. *Renewable Energy*, 161, 691-700. <https://doi.org/10.1016/j.renene.2020.07.081>
- Bolden, J., Abu-Lebdeh, T. and Fini, E. (2013). Utilization of recycled and waste materials in various construction applications. *American Journal of Environment Science*, 9 (1), 14-24. <https://doi.org/10.3844/ajessp.2013.14.24>
- Bordiga, M., Travaglia, F. and Locatelli, M. (2019). Valorisation of grape pomace: an approach that is increasingly reaching its maturity—a review. *International Journal of Food Sciences*, 54(4), 933-942. <https://doi.org/10.1111/ijfs.14118>
- Braga, J. C., Jiménez, A. P., Martín, J. M. and Rivas, P. (1996). Middle Miocene, coral-oyster reefs (Murchas, Granada, Southern Spain). In: Franseen, E., Esteban, M., Ward, B., Rouchy, J.M., (Eds), *Models for Carbonate Stratigraphy from Miocene Reef Complexes of the Mediterranean Regions*. SEPM, Concepts in Sedimentology and Paleontology Series 5, Tulsa, Oklahoma, p. 131.139. <https://doi.org/10.2110/csp.96.01.0131>
- Braga, J. C. and Martín, J. M. (1988). Neogene coralline-algal growth-forms and their palaeoenvironments in the Almanzora River valley (Almería, SE Spain). *Palaeogeography Palaeoclimatology Palaeoecology*, 67, 285-303. [https://doi.org/10.1016/0031-0182\(88\)90157-5](https://doi.org/10.1016/0031-0182(88)90157-5)
- Braga, J. C., Martín, J. M. and Alcalá, B. (1990). Coral reefs in coarse-terrigenous sedimentary environments (Upper Tortonian, Granada Basin, Southern Spain). *Sedimentary Geology*, 66, 135-150. [https://doi.org/10.1016/0037-0738\(90\)90011-H](https://doi.org/10.1016/0037-0738(90)90011-H)
- Braga, J. C., Martín, J. M. and Quesada, C. (2003). Patterns and average rates of late Neogene–Recent uplift of the Betic Cordillera, SE Spain. *Geomorphology*, 50(1-3), 3-26. [https://doi.org/10.1016/S0169-555X\(02\)00205-2](https://doi.org/10.1016/S0169-555X(02)00205-2)
- Brindley, G. W. and Nakahira, M. (1959). The kaolinite-mullite reaction series: I, a survey of outstanding problems. *Journal of American Ceramics Society*, 42(7), 311-314. <https://doi.org/10.1111/j.1151-2916.1959.tb14314.x>
- Brøndsted, P., Lilholt, H., and Lystrup, A. (2005). Composite materials for wind power turbine blades. *The Annual Review of Materials Research*, 35, 505-538. <https://doi.org/10.1146/annurev.matsci.35.100303.110641>
- Brown, W. L. (1989). Parsons, I. Alkali feldspars: ordering rates, phase transformations and behaviour diagrams for igneous rocks. *Mineralogical Magazine*, 53(369), 25-42. <https://doi.org/10.1180/minmag.1989.053.369.03>
- Brownell, W. E. and Brownell, W. E. (1976). History and Classification. *Structural Clay Products*, 1-23. [https://doi.org/10.1007/978-3-7091-8449-3\\_1](https://doi.org/10.1007/978-3-7091-8449-3_1)

- Bugini, R., and Folli, L. (2021). Masonries and stone materials of Romanesque architecture (Northern Italy). *International Journal of Masonry Research and Innovation*, 6(1), 45-59. <https://doi.org/10.1504/IJMRI.2021.112068>
- Bühler, D. (2020). Models in civil engineering from ancient times to the Industrial Revolution. *Physical Models: Their historical and current use in civil and building engineering design*, 3-30 pp.
- Bustamante, M. A., Moral, R., Paredes, C., Pérez-Espinosa, A., Moreno-Caselles, J. and Pérez-Murcia, M. D. (2008). Agrochemical characterisation of the solid by-products and residues from the winery and distillery industry. *Journal of Waste Management*, 28(2), 372-380. <https://doi.org/10.1016/j.wasman.2007.01.013>
- Bwayo, E. and Obwoya, S. K. (2014). Coefficient of Thermal Diffusivity of Insulation Brick Developed from Sawdust and Clays. *Journal of Ceramics*. 14, 6 pp. <http://dx.doi.org/10.1155/2014/861726>



- Calatan, G., Hegyi, A., Dico, C., and Mircea, C. (2016). Determining the optimum addition of vegetable materials in adobe bricks. *Procedia technology*, 22, 259-265. <https://doi.org/10.1016/j.protcy.2016.01.077>
- Calatan, G., Hegyi, A., Dico, C. and Mircea, C. (2017). Experimental research on the recyclability of the clay material used in the fabrication of adobe bricks type masonry units. *Procedia Engineering*, 181, 363-369. <https://doi.org/10.1016/j.proeng.2017.02.402>
- Calvache, M. L., and Viseras, C. (1997). Long-term control mechanisms of stream piracy processes in Southeast Spain. *Earth Surface Processes and Landforms: The Journal of the British Geomorphological Group*, 22(2), 93-105. [https://doi.org/10.1002/\(SICI\)1096-9837\(199702\)22:2<93::AID-ESP673>3.0.CO;2-W](https://doi.org/10.1002/(SICI)1096-9837(199702)22:2<93::AID-ESP673>3.0.CO;2-W)
- Cameán, I (2011). Preparación de materiales gráficos: aplicación como ánodos en baterías de ión-litio (Doctoral dissertation, Universidad de Oviedo, Spain). 268 pp.
- Capel, J., Huertas, F. and Linares, J. (1985). High temperature reactions and use of Bronze Age pottery from La Mancha, central Spain. *Mineralogica et Petrographica Acta*, 29, 563-575.
- Capote R., Muñoz J.A., Simón J.L., Liesa C.L. and Arlegui L.E. (2002). Alpine tectonics I: the Alpine system north of the Betic Cordillera. In: Gibbons, W., Moreno, T. (Eds.), *The Geology of Spain*, The Geological Society, London, p. 367-400. <https://doi.org/10.1144/GOSPP.15>

- Caro, D., Lodato, C., Damgaard, A., Cristóbal, J., Foster, G., Flachenecker, F. and Tonini, D. (2024). Environmental and socio-economic effects of construction and demolition waste recycling in the European Union. *Science of the Total Environment*, 908, 168295. <https://doi.org/10.1016/j.scitotenv.2023.168295>
- Chakraborty, A. K. (2014). Phase transformation of kaolinite clay (p. 342). New Delhi: Springer India. <https://doi.org/10.1007/978-81-322-1154-9>
- Changizi, F. and Haddad, A. (2015). Strength properties of soft clay treated with mixture of nano-SiO<sub>2</sub> and recycled polyester fiber. *Journal of Rock Mechanics and Geotechnical Engineering*, 7(4), 367-378. <https://doi.org/10.1016/j.jrmge.2015.03.013>
- Chen, J., Wang, J. and Ni, A. (2019). Recycling and reuse of composite materials for wind turbine blades: An overview. *Journal of Reinforced Plastics and Composites*, 38(12), 567-577. <https://doi.org/10.1177/0731684419833470>
- Chidiac, S. E. and Federico, L. M. (2007). Effects of waste glass additions on the properties and durability of fired clay brick. *Canadian Journal of Civil Engineering*, 34(11), 1458-1466. <https://doi.org/10.1139/L07-120>
- Chindaprasirt, P., Srisuwan, A., Saengthong, C., Lawanwadeekul, S. and Phonphuak, N. (2021). Synergistic effect of fly ash and glass cullet additive on properties of fire clay bricks. *Journal of Building Engineering*, 44, 102942. <https://doi.org/10.1016/j.jobbe.2021.102942>
- Choudhary, H. K., Anupama, A. V., Kumar, R., Panzi, M. E., Matteppanavar, S., Sherikar, B. N. and Sahoo, B. (2015). Observation of phase transformations in cement during hydration. *Construction and Building Materials*, 101, 122-129. <https://doi.org/10.1016/j.conbuildmat.2015.10.027>
- Christidis, G., Paipoutlidi, K., Marantos, I. and Perdikatsis, V (2020). Determination of amorphous matter in industrial minerals with X-ray diffraction using Rietveld refinement. *Bulletin of the Geological Society of Greece*, 56(1), 1-16. <https://doi.org/10.12681/bgsg.20940>
- Clark, P. (2009). *European cities and towns: 400-2000*. Oxford University Press, USA, 432 pp. [https://doi.org/10.1111/j.1468-0289.2009.00511\\_22.x](https://doi.org/10.1111/j.1468-0289.2009.00511_22.x)
- Clifford, J. F. (1984). High temperature reactions and colour development in brick clays. (Doctoral dissertation, University of Surrey, United Kingdom Spain). 436 pp.
- Coletti, C., Bragié, E., Dalconi, M.C., Mazzoli, C., Hein, A. and Maritan, L. (2023). A new brick-type using grape stalks waste from wine production as pore-agent. *Open Ceramics*, 14, 100365. <https://doi.org/10.1016/j.oceram.2023.100365>
- Coletti, C., Cultrone, G., Maritan, L. and Mazzoli, C. (2016). Combined multi-analytical approach for study of pore system in bricks: How much porosity is there?, *Materials Characterization*, Volume 121, 82-92, <https://doi.org/10.1016/j.matchar.2016.09.024>.

- Coletti, C., Maritan, L., Cultrone, G., Dalconi, M. C., Hein, A., Molina, E. and Mazzoli, C. (2018). Recycling trachyte waste from the quarry to the brick industry: Effects on physical and mechanical properties, and durability of new bricks. *Construction and Building Materials*, 166, 792-807. <https://doi.org/10.1016/j.conbuildmat.2018.01.158>
- Coquelle, M. (2014). Flame retardancy of polyamide 6 fibers: the use of sulfamate salts. Doctoral dissertation, Lille, France. 129 pp.
- Corbí, H., Lancis, C., García-García, F., Pina, J. A., Soria, J. M., Tent-Manclús, J. E. and Viseras, C. (2012). Updating the marine biostratigraphy of the Granada Basin (central Betic Cordillera). Insight for the Late Miocene palaeogeographic evolution of the Atlantic–Mediterranean seaway. *Geobios*, 45, 249-263. <https://doi.org/10.1016/j.geobios.2011.10.006>
- Corvellec, H. and Stowell, A. F. and Johansson, N. (2022). Critiques of the circular economy. *J. Ind. Ecol.*, 26(2), 421-432. <https://doi.org/10.1111/jiec.13187>
- Council, G. W. E. (2020). Global offshore wind report 2020. GWEC: Brussels, Belgium, 19, 10-12.
- Crawford, V. E. (1972). Excavations in the Swamps of Sumer. *Expedition Magazine*, 14(2), 12-20.
- Crawford, H. E. (2004). *Sumer and the Sumerians*. Cambridge University Press
- Cremades, L. V., Soriano, C. and Cusidó, J. A. (2018). Tackling environmental issues in industrial ceramic sintering of sewage sludge: odors and gas emissions. *Environment, Development and Sustainability*, 20, 1651-1663. <https://doi.org/10.1007/s10668-017-9958-0>
- Crespo-López, L., Benavente, D., Morales-Ruano, S., Vázquez-Vílchez, M., and Cultrone, G. (2023a). Non-destructive techniques (NDT) and statistical analysis for the characterization of bricks made with added glass. *Construction and Building Materials*, 408, 133583. <https://doi.org/10.1016/j.conbuildmat.2023.133583>
- Crespo-López, L., Coletti, C., Arizzi, A., and Cultrone, G. (2024). Effects of using tea waste as an additive in the production of solid bricks in terms of their porosity, thermal conductivity, strength and durability. *Sustainable Materials and Technologies*, 39, e00859. <https://doi.org/10.1016/j.susmat.2024.e00859>
- Crespo-López, L., Coletti, C., Morales-Ruano, S. and Cultrone, G. (2023b). Use of recycled carbon fibre as an additive in the manufacture of porous bricks more durable against salt crystallization. *Ceramics International*, <https://doi.org/10.1016/j.ceramint.2023.12.287>
- Crespo-López, L. and Cultrone, G. (2022). Improvement in the petrophysical properties of solid bricks by adding household glass waste. *Journal of Building Engineering*, 59, 105039. <https://doi.org/10.1016/j.job.2022.105039>

- Crespo-López, L., Martínez-Ramírez, A., Sebastián, E. and Cultrone, G., (2023c). Pomace from the wine industry as an additive in the production of traditional sustainable lightweight eco-bricks. *Applied Clay Science* 243, 107084. <https://doi.org/10.1016/j.clay.2023.107084>
- Critelli, S., Martín-Martín, M., Capobianco, W. and Perri, F. (2021). Sedimentary history and palaeogeography of the Cenozoic clastic wedges of the Malaguide Complex, Internal Betic Cordillera, southern Spain. *Marine and Petroleum Geology*, 124, 104775. <https://doi.org/10.1016/j.marpetgeo.2020.104775>
- Cruz, M. D. R. (2008). Na-bearing white micas from Triassic rocks of the transition between the Malaguide and Alpujarride complexes (Betic Cordillera, Spain). *Clays and Clay Minerals*, 56(3), 344-358. <https://doi.org/10.1346/CCMN.2008.0560305>
- Cultrone, G. (2001). Estudio mineralógico-petrográfico y físico-mecánico de ladrillos macizos para su aplicación en intervenciones del patrimonio histórico (Doctoral dissertation, Universidad de Granada, Spain) 292 pp.
- Cultrone, G. (2022). The use of Mount Etna volcanic ash in the production of bricks with good physical-mechanical performance: Converting a problematic waste product into a resource for the construction industry. *Ceramics International*, 48(4), 5724-5736. <https://doi.org/10.1016/j.ceramint.2021.11.119>
- Cultrone, G., Aurrekoetxea, I., Casado, C. and Arizzi, A. (2020). Sawdust recycling in the production of lightweight bricks: How the amount of additive and the firing temperature influence the physical properties of the bricks. *Construction and Building Materials*, 235, 117436. <https://doi.org/10.1016/j.conbuildmat.2019.117436>.
- Cultrone, G. and Carrillo Rosua, F. J. C. (2020). Growth of metastable phases during brick firing: Mineralogical and microtextural changes induced by the composition of the raw material and the presence of additives. *Applied Clay Science*, 185, 105419. <https://doi.org/10.1016/j.clay.2019.105419>.
- Cultrone, G., De La Torre, M. J., Sebastián, E., Cazalla, O. (2003). Evaluation of bricks durability using destructive and non destructive methods (DT and NDT). *Materiales de Construcción*, 53(269), 41-60. <https://doi.org/10.3989/mc.2003.v53.i269.267>.
- Cultrone, G., Rodríguez-Navarro, C., Sebastián, E., Cazalla, O. and De La Torre, M. J. (2001). Carbonate and silicate phase reactions during ceramic firing. *European Journal of Mineralogy*, 13(3), 621-634. <https://doi.org/10.1127/0935-1221/2001/0013-0621>
- Cultrone, G., and Sebastián, E. (2009). Fly ash addition in clayey materials to improve the quality of solid bricks. *Construction and Building Materials*, 23(2), 1178-1184. <https://doi.org/10.1016/j.conbuildmat.2008.07.001>

- Cultrone, G., Sebastian, E. and De la Torre, M. J. (2005). Mineralogical and physical behaviour of solid bricks with additives. *Construction and Building Materials*, 19(1), 39-48. <https://doi.org/10.1016/j.conbuildmat.2004.04.035>
- Cultrone, G., Sebastián, E., Elert, K., De la Torre, M. J., Cazalla, O. and Rodríguez–Navarro, C. (2004). Influence of mineralogy and firing temperature on the porosity of bricks. *Journal of the European Ceramic Society*, 24(3), 547-564. [https://doi.org/10.1016/S0955-2219\(03\)00249-8](https://doi.org/10.1016/S0955-2219(03)00249-8).
- Cusidó, J. A., Cremades, L. V. and González, M. (2003). Gaseous emissions from ceramics manufactured with urban sewage sludge during firing processes. *Waste management* 23(3), 273-280. [https://doi.org/10.1016/S0956-053X\(02\)00060-0](https://doi.org/10.1016/S0956-053X(02)00060-0)

## D

- Dabaieh, M., Heinonen, J., El-Mahdy D. and Hassan, D. M. (2020). A comparative study of life cycle carbon emissions and embodied energy between sun-dried bricks and fired clay bricks. *Journal of Cleaner Production*, 275, 122998. <https://doi.org/10.1016/j.jclepro.2020.122998>
- Dachowski, R. and Kostrzewa, P. (2016). The use of waste materials in the construction industry. *Procedia Engineering*, 161, 754-758. <https://doi.org/10.1016/j.proeng.2016.08.764>.
- Dacuba, J., Cifrián, E., Romero, M., Llano, T. and Andrés, A. (2022). Influence of Unburned Carbon on Environmental-Technical Behaviour of Coal Fly Ash Fired Clay Bricks. *Applied Sciences*, 12(8), 3765. <https://doi.org/10.3390/app12083765>
- Daghmehchi, M., Coletti, C., Moon, D. H., Jelodar, M. E. E., Omrani, H., Reka, A. A., Emami, M. (2023). Mineralogical and microstructural characterization of ceramics from the fifth and fourth millennium BC in the central plateau of Iran. *Open Ceramics*, 15, 100427. <https://doi.org/10.1016/j.oceram.2023.100427>
- Dale, G., Dotro, G., Srivastava, P., Austin, D., Hutchinson, S., Head, P. and Schönborn, A. (2021). Education in ecological engineering-a need whose time has come. *Circular Economy and Sustainability*, 1(1), 333-373. <https://doi.org/10.1007/s43615-021-00067-4>
- Dalin, C. (1984). The Great Wall of China. *Borders and Border Politics in a Globalizing World*, 11-20.
- Dan, T. K. and Raman, S. (1986). Physico-chemical analysis of a raw brick clays of Bhopal. *Indian Ceramics*.
- D'Angelo, G.; Fumo, M.; Merino, M. R.; Capasso, I.; Campanile, A.; Iucolano, F.; Caputo, D. and Liguori, B. (2021). Crushed Bricks: Demolition Waste as a Sustainable

- Raw Material for Geopolymers. Sustainability, 13, 7572. <https://doi.org/10.3390/su13147572>
- Darezereshki, E. (2010). Synthesis of maghemite ( $\gamma$ -Fe<sub>2</sub>O<sub>3</sub>) nanoparticles by wet chemical method at room temperature. Materials Letters, 64(13), 1471-1472. <https://doi.org/10.1016/j.matlet.2010.03.064>
- Davidovits, J. (2008). They built the Pyramids. Geopolymer Institute. 288pp.
- Debnath, B., Duarah and P., Purkait, M. K. (2023). Microwave-assisted quick synthesis of microcrystalline cellulose from black tea waste (*Camellia sinensis*) and characterization. International Journal of Biological Macromolecules, 244, 125354. <https://doi.org/10.1016/j.ijbiomac.2023.125354>
- Debnath, B., Haldar, D., and Purkait, M. K. (2021). Potential and sustainable utilization of tea waste: A review on present status and future trends. Journal of Environmental Chemical Engineering, 9(5), 106179. <https://doi.org/10.1016/j.jece.2021.106179>
- Debnath, K., Singh, I., Dvivedi, A. and Kumar, P. (2013). Natural fibre-reinforced polymer composites for wind turbine blades: Challenges and opportunities. Recent advances in composite materials for wind turbine blades, 237 pp.
- De Bonis, A., Cultrone, G., Grifa, C., Langella, A., Leone, A. P., Mercurio, M., Morra, V. (2017). Different shades of red: The complexity of mineralogical and physico-chemical factors influencing the colour of ceramics. Ceramics International, 43(11), 8065-8074. <https://doi.org/10.1016/j.ceramint.2017.03.127>.
- De Corato, U. (2020). Agricultural waste recycling in horticultural intensive farming systems by on-farm composting and compost-based tea application improves soil quality and plant health: A review under the perspective of a circular economy. Science of the Total Environment, 738, 139840. <https://doi.org/10.1016/j.scitotenv.2020.139840>
- Demir, I. (2008). Effect of organic residues addition on the technological properties of clay bricks. Journal of Waste Management, 28(3), 622-627. <https://doi.org/10.1016/j.wasman.2007.03.019>
- Devesa-Rey, R., Vecino, X., Varela-Alende, J. L., Barral, M. T., Cruz, J. M. and Moldes, A. B. (2011). Valorization of winery waste vs. the costs of not recycling. Journal of Waste Management 31(11), 2327-2335. <https://doi.org/10.1016/j.wasman.2011.06.001>
- De Vicente, G., Vegas, R., Muñoz-Martín, A., Van Wees, J. D., Casas-Sáinz, A., Sopeña, A., Fernández-Lozano, J. (2009). Oblique strain partitioning and transpression on an inverted rift: The Castilian Branch of the Iberian Chain. Tectonophysics, 470(3-4), 224-242. <https://doi.org/10.1016/j.tecto.2008.11.003>

- Di Cosmo, N. (1993). The origins of the Great Wall. American University, 129 pp.
- Ding, X., Li, H., Wen, Z., Hou, Y., Wang, G., Fan, J. and Qian, L. (2020). Effects of fermented tea residue on fattening performance, meat quality, digestive performance, serum antioxidant capacity, and intestinal morphology in fatteners. *Animals*, 10(2) 185. <https://doi.org/10.3390/ani10020185>
- Djangang, C. N., Kamseu, E., Elimbi, A., Lecomte, G. L. and Blanchart, P. (2014). Net-shape clay ceramics with glass waste additive. *International Journal of Materials Science and Applications*, 5(8), 592- 602. <https://doi.org/10.4236/msa.2014.58061>.
- Dobelin, N. and Kleeberg, R. (2015). Profex: a graphical user interface for the Rietveld refinement program BGMN, *Journal of Applied Crystallography* 48, 1573 –1580. <https://doi.org/10.1107/S1600576715014685>
- Dondi, M., Guarini, G., Raimondo, M. and Zanelli, C. (2009). Recycling PC and TV waste glass in clay bricks and roof tiles. *Journal of Waste Management*, 29(6), 1945-1951. <https://doi.org/10.1016/j.wasman.2008.12.003>.
- Drew, L. J., Langer, W. H., and Sachs, J. S. (2002). Environmentalism and natural aggregate mining. *Natural Resources Research*, 11, 19-28. <https://doi.org/10.1023/A:1014283519471>
- Drysdale, R. G., Hamid, A. A. and Baker, L. R. (1994). *Masonry structures: behavior and design*. The Masonry Society, Boulder, Colorado, USA. 888 pp.
- Dubacq, B., Vidal, O. and De Andrade, V. (2010). Dehydration of dioctahedral aluminous phyllosilicates: thermodynamic modelling and implications for thermobarometric estimates. *Contributions to Mineralogy and Petrology*, 159(2), 159-174. <https://doi.org/10.1007/s00410-009-0421-6>
- Durand-Delga, M. and Foucault A. (1967). La Dorsale Bétique, nouvel élément paléogéographique et structural des Cordillères Bétiques au bord Sud de la Sierra Arana (Province de Grenade, Espagne). *Bulletin de la Société Géologique de France*, 7, 723-728. <https://doi.org/10.2113/gssgfbull.S7-IX.5.723>

E

- Eberhart, J. P. (1963). Etude des transformations du mica muscovite par chauffage entre 700 et 1200 C. *Bulletin de Minéralogie*, 86(3), 213-251. <https://doi.org/10.3406/bulmi.1963.5644>



- Edike, U. E., Ameh, O. J., and Dada, M. O. (2020). Production and optimization of eco-bricks. *Journal of Cleaner Production*, 266, 121640. <https://doi.org/10.1016/j.jclepro.2020.121640>
- Egeler, C.G. and Simon, O.J. (1969). Orogenic evolution of the Betic Zone (Betic Cordilleras, Spain), with emphasis on the nappe structures. *Geologie en Mijnbouw*, 48, 296-305.
- El-Badry, A. (2019). Deterioration mechanisms affecting the bricks used in the building of the water wells at karnak temples, luxor, egypt. *Egyptian Journal of Archaeological and Restoration Studies*, 9(1), 13-25. <https://doi.org/10.21608/EJARS.2019.38426>
- El Boukili, G., Ouakarrouch, M., Lechheb, M., Kifani-Sahban, F. and Khaldoune, A. (2022). Recycling of olive pomace bottom ash (by-product of the clay brick industry) for manufacturing sustainable fired clay bricks. *Silicon*, 14(9), 4849-4863. <https://doi.org/10.1007/s12633-021-01279-x>
- Elert, K., Cultrone, G., Navarro, C. R. and Pardo, E. S. (2003). Durability of bricks used in the conservation of historic buildings—influence of composition and microstructure. *Journal of Cultural Heritage*, 4(2), 91-99. [https://doi.org/10.1016/S1296-2074\(03\)00020-7](https://doi.org/10.1016/S1296-2074(03)00020-7).
- Eliche-Quesada, D., Corpas-Iglesias, F. A., Pérez-Villarejo, L. and Iglesias-Godino, F. J. (2012a). Recycling of sawdust, spent earth from oil filtration, compost and marble residues for brick manufacturing. *Construction and Building Materials*, 34, 275-284. <https://doi.org/10.1016/j.conbuildmat.2012.02.079>
- Eliche-Quesada, D., Felipe-Sesé, M. A., López-Pérez, J. A., Infantes-Molina, A. (2017). Characterization and evaluation of rice husk ash and wood ash in sustainable clay matrix bricks. *Ceramics International*, 43(1), 463-475. <https://doi.org/10.1016/j.ceramint.2016.09.181>.
- Eliche-Quesada, D., Martínez-García, C., Martínez-Cartas, M. L., Cotes-Palomino, M. T., Pérez-Villarejo, L., Cruz-Pérez, N. and Corpas-Iglesias, F. A. (2011). The use of different forms of waste in the manufacture of ceramic bricks. *Applied Clay Science*, 52(3), 270-276. <https://doi.org/10.1016/j.clay.2011.03.003>
- Eliche-Quesada, D., Martínez-Martínez, S., Pérez-Villarejo, L., Iglesias-Godino, F. J., Martínez-García, C. and Corpas-Iglesias, F. A. (2012b). Valorization of biodiesel production residues in making porous clay brick. *Fuel Processing Technology*, 103, 166-173. <https://doi.org/10.1016/j.fuproc.2011.11.013>
- Elimbi, A., Tchakoute and H. K., Njopwouo, D. (2011). Effects of calcination temperature of kaolinite clays on the properties of geopolymer cements. *Construction and Building Materials*, 25(6), 2805-2812. <https://doi.org/10.1016/j.conbuildmat.2010.12.055>

- Er, Y., Sutcu, M., Gencel, O., Totic, E., Erdogmus, E., Cay, V. V. and Kazmi, S. M. S. (2022). Recycling of metallurgical wastes in ceramics: A sustainable approach. *Construction and Building Materials*, 349, 128713. <https://doi.org/10.1016/j.conbuildmat.2022.128713>
- Eramo, G. (2020). Ceramic technology: how to recognize clay processing. *Archaeological and Anthropological Sciences*, 12(8), 164. [doi.org/10.1007/s12520-020-01132-z](https://doi.org/10.1007/s12520-020-01132-z)
- Erdogmus, E., Sutcu, M., Gencel, O., Kazmi, S. M. S., Munir, M. J., Velasco, P. M. and Ozbakkaloglu, T. (2023). Enhancing thermal efficiency and durability of sintered clay bricks through incorporation of polymeric waste materials. *Journal of Cleaner Production*, 420, 138456. <https://doi.org/10.1016/j.jclepro.2023.138456>
- Ezquerro, L. (2017). El sector norte de la cuenca neógena de Teruel: tectónica, clima y sedimentación. (Doctoral dissertation, University of Zaragoza, Spain) 456 pp.
- Ezquerro, L., Simón, J. L., Luzón, A. and Liesa, C. L. (2020). Segmentation and increasing activity in the Neogene-Quaternary Teruel Basin rift (Spain) revealed by morphotectonic approach. *Journal of Structural Geology*, 135, 104043. <https://doi.org/10.1016/j.jsg.2020.104043>

## F

- Farag, M. A., Elmetwally, F., Elghanam, R., Kamal, N., Hellal, K., Hamezah, H. S. and Mediani, A. (2023) Metabolomics in tea products; a compile of applications for enhancing agricultural traits and quality control analysis of *Camellia sinensis*. *Food Chemistry*, 404, 134628. <https://doi.org/10.1016/j.foodchem.2022.134628>
- Feng, Y., Jiang, J., Zhu, L., Yue, L., Zhang, J. and Han, S. (2013) Effects of tea saponin on glucan conversion and bonding behaviour of cellulolytic enzymes during enzymatic hydrolysis of corncob residue with high lignin content. *Biotechnol. Biofuels*, 6(1) 1-8. <https://doi.org/10.1186/1754-6834-6-161>
- Fernandes, F. M., Lourenço, P. B., and Castro, F. (2010). Ancient clay bricks: manufacture and properties. In *Materials, technologies and practice in historic heritage structures*. Dordrecht: Springer Netherlands (29-48 pp.). [https://doi.org/10.1007/978-90-481-2684-2\\_3](https://doi.org/10.1007/978-90-481-2684-2_3)
- Fernández, J., Bluck, B.J. and Viseras, C. (1993). The effects of fluctuating base level on the structure of alluvial fan and associated fan delta deposits: an example from the Tertiary of the Betic Cordillera, Spain. *Sedimentology*, 40, 879-893. <https://doi.org/10.1111/j.1365-3091.1993.tb01367.x>

Fernández, J. M., Peltre, C., Craine, J. M. and Plante, A. F. (2012). Improved characterization of soil organic matter by thermal analysis using CO<sub>2</sub>/H<sub>2</sub>O evolved gas analysis. *Environmental Science & Technology*, 46(16), 8921-8927. <https://doi.org/10.1021/es301375d>

Fernández, J. and Soria, J.M., (1986-1987). Evolución sedimentaria en el borde norte de la Depresión de Granada a partir del Turolense terminal. *Acta Geológica Hispánica*, 21-22, 73-81.

Fernie, E. (2006). Romanesque architecture. *A Companion to Medieval Art: Romanesque and Gothic in Northern Europe*, 295-313 pp. <https://doi.org/10.1002/9780470996997>

Figaredo, A. T., and Dhanya, M. (2018). Development of Sustainable Brick Materials Incorporating Agro-Wastes: An Overview. *Development*, 5(11).

Fogliano, V., Corollaro, M. L., Vitaglione, P., Napolitano, A., Ferracane, R., Travaglia, F. and Gibson, G. (2011). In vitro bioaccessibility and gut biotransformation of polyphenols present in the water-insoluble cocoa fraction. *Molecular Nutrition and Food Research*, 55(S1), S44-S55. <https://doi.org/10.1002/mnfr.201000360>

Fontana, A. R., Antonioli, A. and Bottini, R. (2013). Grape pomace as a sustainable source of bioactive compounds: extraction, characterization, and biotechnological applications of phenolics. *Journal of Agricultural and Food Chemistry*, 61(38), 8987-9003. <https://doi.org/10.1021/jf402586f>

## G

Gallipoli, D., Bruno, A. W., Perlot, C., and Mendes, J. (2017). A geotechnical perspective of raw earth building. *Acta Geotechnica*, 12, 463-478. <https://doi.org/10.1007/s11440-016-0521-1>

Galindo-Zaldívar, J., Gil, A.J., Borque, M.J., González-Lodeiro, F., Jabaloy, A., Marín-Lechado, C., Ruano, P., Sanz de Galdeano, C. (2003). Active faulting in the internal zones of the central Betic Cordilleras (SE, Spain). *Journal of Geodynamics*, 36, 239-250. [https://doi.org/10.1016/S0264-3707\(03\)00049-8](https://doi.org/10.1016/S0264-3707(03)00049-8)

Galindo-Zaldívar, J., Braga, J.C., Marín-Lechado, C., Ercilla, G., Martín, J.M., Pedrera, A., Casas, D., Aguirre, J., Ruiz-Constán, Á., Estrada, F., Puga-Bernabéu, Á., Sanz de Galdeano, C., Juan, C., García-Alix, A., Tomás Vázquez, J., Alonso, B. (2019). *The Geology of Iberia: A Geodynamic Approach*, Regional Geology Reviews, vol. 4, Springer, 61-93 pp. [https://doi.org/10.1007/978-3-030-11190-8\\_3](https://doi.org/10.1007/978-3-030-11190-8_3)

- Galvao, A. C. P., Farias, A. C. M. and Mendes, J. U. L. (2015). Characterization of waste of soda-lime glass generated from lapping process to reuse as filler in composite materials as thermal insulation. *Ceramica*, 61(359), 367–373. <https://doi.org/10.1590/0366-69132015613591987>
- García-Aguilar, J. M. and Martín, J. M. (2000). Late Neogene to recent continental history and evolution of the Guadix-Baza Basin (SE Spain). *Revista de la Sociedad Geológica de España*, 13, 65-77.
- García-Alix, A., Minwer-Barakat, R., Martín, J. M., Martín-Suárez, E. and Freudenthal, M. (2008). Biostratigraphy and sedimentary evolution of late Miocene and Pliocene continental deposits of the Granada Basin (southern Spain). *Lethaia*, 41, 431-446. <https://doi.org/10.1111/j.1502-3931.2008.00097.x>.
- García-Hernández, M., López-Garrido, A. C., Rivas, P., Sanz de Galdeano, C. and Vera, J. A. (1980). Mesozoic palaeogeographic evolution of the External Zones of the Betic Cordillera. *Geologie en Mijnbouw*, 59, 155-168.
- García-Lomillo, J., González-San José, M. L. (2017). Applications of wine pomace in the food industry: Approaches and functions. *Comprehensive Reviews in Food Science and Food Safety*, 16(1), 3-22. <https://doi.org/10.1111/1541-4337.12238>
- García-Veigas, J., Rosell, L., Cendón, D. I., Gibert, L., Martín, J. M., Torres Ruiz, J. and Ortí, F. (2015). Large celestine orebodies formed by early-diagenetic replacement of gypsified stromatolites (upper Miocene, Monteivive-Escúzar deposits, Granada basin, Spain). *Ore Geology Reviews*, 64, 187-199. <https://doi.org/10.1016/j.oregeorev.2014.07.009>
- Garric, J. P. (2017). The French Beaux-Arts. *Companion to the History of Architecture*, 1-15.
- Geisendorf, S. and Pietrulla, F. (2018). The circular economy and circular economic concepts a literature analysis and redefinition. *Thunderbird International Business Review*, 60(5), 771-782. <https://doi.org/10.1002/tie.21924>
- Geng, J. and Sun, Q. (2018). Effects of high temperature treatment on physical-thermal properties of clay. *Thermochemica Acta*, 666, 148-155. <https://doi.org/10.1016/j.tca.2018.06.018>
- Gencel, O., Kazmi, S. M. S., Munir, M. J., Sutcu, M., Erdogmus, E. and Yaras, A. (2021a). Feasibility of using clay-free bricks manufactured from water treatment sludge, glass, and marble wastes: An exploratory study. *Construction and Building Materials*, 298, 123843. <https://doi.org/10.1016/j.conbuildmat.2021.123843>
- Gencel, O., Munir, M. J., Kazmi, S. M. S., Sutcu, M., Erdogmus, E., Velasco, P. M., Quesada, D. E. Recycling industrial slags in production of fired clay bricks for sustainable manufacturing. *Ceramics International*, 47(21) (2021b), 30425-30438. <https://doi.org/10.1016/j.ceramint.2021.07.222>

- Germinario, C., Cultrone, G., Cavassa, L., De Bonis, A., Izzo, F., Langella, A. and Grifa, C. (2019). Local production and imitations of Late Roman pottery from a well in the Roman necropolis of Cuma in Naples, Italy. *Geoarchaeology*, 34(1), 62-79. <https://doi.org/10.1002/gea.21703>
- Gliozzo, E. (2020). Ceramic technology. How to reconstruct the firing process. *Archaeological and Anthropological Sciences*, 12(11), 1-35. <https://doi.org/10.1007/s12520-020-01133-y>
- Goldsmith, J. R. and Laves, F. (1954). The microcline-sanidine stability relations. *Geochimica et Cosmochimica Acta*, 5(1), 1-19. [https://doi.org/10.1016/0016-7037\(54\)90058-7](https://doi.org/10.1016/0016-7037(54)90058-7)
- Gomes, E. and Hossain, I. (2003). Transition from traditional brick manufacturing to more sustainable practices. *Energy for Sustainable Development*, 7(2), 66-76. [https://doi.org/10.1016/S0973-0826\(08\)60356-7](https://doi.org/10.1016/S0973-0826(08)60356-7)
- Gómez-Pugnaire, M. T., Braga, J. C., Martín, J. M., Sassi, F. P. and Del Moro, A. (2000). The age of the Nevado-Filábride cover (Betic Cordilleras, S Spain): regional implications. *Schweizerische Mineralogische und Petrographische*, 80, 45-52.
- Gomez-Heras, M., Benavente, D., Pla, C., Martinez-Martinez, J., Fort, R. and Brotons, V. (2020). Ultrasonic pulse velocity as a way of improving uniaxial compressive strength estimations from Leeb hardness measurements. *Construction and Building Materials*, 261, 119996. <https://doi.org/10.1016/j.conbuildmat.2020.119996>
- González, J. S. and Lacal-Aránegui, R. (2016). A review of regulatory framework for wind energy in European Union countries: Current state and expected developments. *Renewable and Sustainable Energy Reviews*, 56, 588-602. <https://doi.org/10.1016/j.rser.2015.11.091>
- González, A., Pardo, G., Villena, J. and Pérez, A. (1984). Estratigrafía y Sedimentología del Terciario de la Cubeta de Alloza (Prov. De Teruel). *Boletín Geológico y Minero*, 95, 404-428.
- González-Paramás, A. M., da Silva, F. L., Martín-López, P., Macz-Pop, G., González-Manzano, S., Alcalde-Eon, C. and Santos-Buelga, C. (2006). Flavanol-anthocyanin condensed pigments in plant extracts. *Food Chemistry*, 94(3), 428-436. <https://doi.org/10.1016/j.foodchem.2004.11.037>
- Granados, A., Oms, O., Anadón, P., Ibanez-Insa, J., Kaakinen, A. and Jiménez-Arenas, J. M. (2021). Geochemical and sedimentary constraints on the formation of the Venta Micena Early Pleistocene site (Guadix-Baza basin, Spain). *Scientific Reports*, 11(1), 1-13. <https://doi.org/10.1038/s41598-021-01711-7>
- Grilli, E., Vigliotti, R. C., Rossetti, L., Scognamiglio, M., Fiumano, V., Fiorentino, A. and Ganga, A. (2021). Restoration of quarry areas in Mediterranean regions through a low-cost soil rebuilding technique for profitable

- pedotechnosystems development. *Soil and Tillage Research*, 209, 104936. <https://doi.org/10.1016/j.still.2021.104936>
- Grossi, C. M., Brimblecombe, P., Esbert, R. M. and Alonso, F. J. (2007). Colour changes in architectural limestones from pollution and cleaning. *Color Research & Application*, 32: 320-331. <https://doi.org/10.1002/col.20322>.
- Grosso, M., Motta, A., and Rigamonti, L. (2010). Efficiency of energy recovery from waste incineration, in the light of the new Waste Framework Directive. *Waste Management*, 30(7), 1238-1243. <https://doi.org/10.1016/j.wasman.2010.02.036>
- Guan, L., Xu, H. and Huang, D. (2011). The investigation on states of water in different hydrophilic polymers by DSC and FTIR. *Journal of Polymer Research*, 18, 681-689. <https://doi.org/10.1007/s10965-010-9464-7>
- Guardia, L., Suárez, L., Querejeta, N., Pevida, C. and Centeno, T. A. (2018). Winery wastes as precursors of sustainable porous carbons for environmental applications. *Journal of Cleaner Production*, 193, 614-624. <https://doi.org/10.1016/j.jclepro.2018.05.085>
- Guimera, J. (2018). Structure of an intraplate fold-and-thrust belt: The Iberian Chain. A synthesis. *Geologica Acta*, 16, 427-438. <https://doi.org/10.1344/GeologicaActa2018.16.4.6>
- Guimera, J., Mas, R. and Alonso, A. (2004). Intraplate deformation in the NW Iberian Chain: Mesozoic extension and Tertiary contractional inversion. *Journal of the Geological Society*, 161(2), 291-303. <https://doi.org/10.1144/0016-764903-055>
- Gulghane, A. A. and Khandve, P. V. (2015). Management for construction materials and control of construction waste in construction industry: a review. *International Journal of Engineering*, 5(4), 59-64.
- Guo, S., Awasthi, M. K., Wang, Y. and Xu, P. (2021) Current understanding in conversion and application of tea waste biomass: A review. *Bioresource Technology*, 338, 125530. <https://doi.org/10.1016/j.biortech.2021.125530>
- Guo, F., Wu, F., Mu, Y., Hu, Y., Zhao, X., Meng, W. and Lin, Y. (2016). Characterization of organic matter of plants from lakes by thermal analysis in a N<sub>2</sub> atmosphere. *Scientific Reports*, 6(1), 1-7. <https://doi.org/10.1038/srep22877>.
- Gutiérrez, F., Gutiérrez, M., Gracia, F.J., McCalpin, J.P., Lucha, P., Guerrero, J. (2008). Plio- Quaternary extensional seismotectonics and drainage network development in the central sector of the Iberian Range (NE Spain). *Geomorphology*, 102, 21-42. <https://doi.org/10.1016/j.geomorph.2007.07.020>

Guyader, J. and Denis, A. (1986). Propagation des ondes dans les roches anisotropes sous contrainte évaluation de la qualité des schistes ardoisiers. Bulletin of the International Association of Engineering Geology-Bulletin de l'Association Internationale de Géologie de l'Ingénieur, 33(1), 49-55. <https://doi.org/10.1007/BF02594705>

## H

Hafez, R. D. A., Tayeh, B. A., and Abd-Al Ftah, R. O. (2022). Development and evaluation of green fired clay bricks using industrial and agricultural wastes. Case Studies in Construction Materials, 17, e01391. <https://doi.org/10.1016/j.cscm.2022.e01391>

Hamilton, A., Hall, C. (2013). The mechanics of moisture-expansion cracking in fired-clay ceramics. Journal of Physics D: Applied Physics, 46(9), 092003. <https://doi.org/10.1088/0022-3727/46/9/092003>

Hamilton-Miller, J. M. T. (2001). Anti-cariogenic properties of tea (*Camellia sinensis*). Journal of Medical Microbiology, 50(4), 299-302. <https://doi.org/10.1099/0022-1317-50-4-299>

Hanna, S. B., Yehia, A. A., Ismail, M. N. and Khalaf, A. I. (2012). Preparation and characterization of carbon fibers from polyacrylonitrile precursors. Journal of Applied Polymer Science, 123(4), 2074-2083. <https://doi.org/10.1002/app.34704>

Hao, S., Kuah, A. T., Rudd, C. D., Wong, K. H., Lai, N. Y. G., Mao, J. and Liu, X. (2020). A circular economy approach to green energy: Wind turbine, waste, and material recovery. Science of The Total Environment, 702, 135054. <https://doi.org/10.1016/j.scitotenv.2019.135054>

Hasan, M., Siddika, A., Akanda, M., Ali, P. and Islam, M. (2021). Effects of waste glass addition on the physical and mechanical properties of brick. Innovative Infrastructure Solutions, 6(1), 1-13. <https://doi.org/10.1007/s41062-020-00401-z>

Hayman, B., Wedel-Heinen, J., and Brøndsted, P. (2008). Materials challenges in present and future wind energy. Materials Research Society Bulletin, 33(4), 343-353.

Heathcote, K. A. (1995). Durability of earthwall buildings. Construction and Building Materials, 9(3), 185-189. [https://doi.org/10.1016/0950-0618\(95\)00035-E](https://doi.org/10.1016/0950-0618(95)00035-E)

Hei, F., Liu, Q., Zhao, G., Ou, J., Xu, F. (2023). Preparation and Characteristics of the Fired Bricks Produced from Polyaluminum Chloride Slag and Glass Powder. Applied Sciences, 13(3). <https://doi.org/10.3390/app13031989>

- Heller-Kallai, L. and Lapidés, I. (2015). Dehydroxylation of muscovite: study of quenched samples. *Physics and Chemistry of Minerals*, 42(10), 835-845. <https://doi.org/10.1007/s00269-015-0767-4>
- Hellwege, K. H., Lesch, W., Plihal, M. and Schaack, G. (1970). Zwei-phononen-absorptionsspektren und dispersion der schwingungszweige in kristallen der kalkspatstruktur. *Zeitschrift für Physik A Hadrons and nuclei*, 232(1), 61-86. <https://doi.org/10.1007/BF01394946>
- Heywood, S. (1985). Stone Building in Romanesque East Anglia. *Archaeology*, 28, 23-25.
- Higgott, A. (2018). Key modern architects: 50 short histories of modern architecture. Bloomsbury Publishing. 312 pp.
- Higuchi, T., Morioka, M., Yoshioka, I. and Yokozeki, K. (2014). Development of a new ecological concrete with CO<sub>2</sub> emissions below zero. *Construction and Building Materials*, 67, 338-343. <https://doi.org/10.1016/j.conbuildmat.2014.01.029>
- Hirono, T. and Tanikawa, W. (2011). Implications of the thermal properties and kinetic parameters of dehydroxylation of mica minerals for fault weakening, frictional heating, and earthquake energetics. *Earth and Planetary Science Letters*, 307(1-2), 161-172. <https://doi.org/10.1016/j.epsl.2011.04.042>
- Hnainen, K. H. (2020). The appearance of bricks in ancient mesopotamia. *Athens Journal of History*, 6(1), 73-96. <https://doi.org/10.30958/ajhis.6-1-4>
- Huarachi, D. A. R., Gonçalves, G., de Francisco, A. C., Canteri, M. H. G. and Piekarski, C. M. (2020). Life cycle assessment of traditional and alternative bricks: A review. *Environmental Impact Assessment Review*, 80, 106335. <https://doi.org/10.1016/j.eiar.2019.106335>
- Hughes, R. E., and Bargh, B. L. (1982). The weathering of brick: Causes, assessment and measurement (83, 272). Reston, VA, USA: US Geological Survey.
- Hussain, F., Hussain, I., Khan, A. H. A., Muhammad, Y. S., Iqbal, M., Soja, G. and Yousaf, S. (2018). Combined application of biochar, compost, and bacterial consortia with Italian ryegrass enhanced phytoremediation of petroleum hydrocarbon contaminated soil. *Environmental and Experimental Botany*, 153, 80-88. <https://doi.org/10.1016/j.envexpbot.2018.05.012>
- Husung, R. D. and Doremus, R. H. (1990). The infrared transmission spectra of four silicate glasses before and after exposure to water. *Journal of Materials Research*, 5(10), 2209-2217. <https://doi.org/10.1557/JMR.1990.2209>



## I

- Ibrahim, J. E. F., Tihtih, M., Şahin, E. İ., Basyooni, M. A. and Kocserha, I. (2023). Sustainable Zeolitic Tuff Incorporating Tea Waste Fired Ceramic Bricks: Development and Investigation. *Case Studies in Construction Materials*, e02238. <https://doi.org/10.1016/j.cscm.2023.e02238>
- ISO, EN 12571 (2000). Hygrothermal performance of building materials and products- Determination of hygroscopic sorption properties. Belgium: CEN. 1997.
- ISRM (1979). Suggested methods for determining water content, porosity, density and related properties, and swelling. *International Journal of Rock Mechanics & Mining Science*, 16 (2) 141-156.

## J

- Jensen, J. P., and Skelton, K. (2018). Wind turbine blade recycling: Experiences, challenges and possibilities in a circular economy. *Renewable and Sustainable Energy Reviews*, 97, 165-176. <https://doi.org/10.1016/j.rser.2018.08.041>
- Jiménez-Millán, J., Abad, I., García-Tortosa, F. J. and Jiménez-Espinosa, R. (2022). Structural Diagenesis in Clay Smearing Bands Developed on Plio-Pleistocene Sediments Affected by the Baza Fault (S Spain). *Minerals*, 12(10), 1255. <https://doi.org/10.3390/min12101255>
- Joglekar, S. N., Kharkar, R. A., Mandavgane, S. A., and Kulkarni, B. D. (2018). Sustainability assessment of brick work for low-cost housing: A comparison between waste based bricks and burnt clay bricks. *Sustainable Cities and Society*, 37, 396-406. <https://doi.org/10.1016/j.scs.2017.11.025>
- Jollands, M. C., Blanchard, M. and Balan, E. (2020). Structure and theoretical infrared spectra of OH defects in quartz, *European Journal of Mineralogy*, 32, 311-323. <https://doi.org/10.5194/ejm-32-311-2020>
- José, A., Bueno, J. S. and Castro, E. (2021). Recycling of residues from the olive cultivation and olive oil production process for manufacturing of ceramic materials. A comprehensive review. *Journal of Cleaner Production*, 296, 126436. <https://doi.org/10.1016/j.jclepro.2021.126436>
- Joustra, J., Flipsen, B., and Balkenende, R. (2021). Structural reuse of high end composite products: A design case study on wind turbine blades. *Resources, Conservation and Recycling*, 167, 105393. <https://doi.org/10.1016/j.resconrec.2020.105393>

- Kadir, A. A. and Mohajerani, A. (2015). Effect of heating rate on gas emissions and properties of fired clay bricks and fired clay bricks incorporated with cigarette butts. *Applied Clay Science*, 104, 269-276  
<https://doi.org/10.1016/j.clay.2014.12.005>
- Kalair, A. R., Seyedmahmoudian, M., Stojcevski, A., Abas, N. and Khan, N. (2021). Waste to energy conversion for a sustainable future. *Heliyon*, 7(10).  
<https://doi.org/10.1016/j.heliyon.2021.e08155>
- Kalkanis, K., Psomopoulos, C. S., Kaminaris, S., Ioannidis, G. and Pachos, P. (2019). Wind turbine blade composite materials-End of life treatment methods. *Energy Procedia*, 157, 1136-1143. <https://doi.org/10.1016/j.egypro.2018.11.281>
- Karaman, S., Gunal, H. and Ersahin, S. (2006). Assesment of clay bricks compressive strength using quantitative values of colour components. *Construction and Building Materials*, 20(5), 348-354.  
<https://doi.org/10.1016/j.conbuildmat.2004.11.003>
- Karavida, S. and Nömmik, R. (2015). Waste management of end-of-service wind turbines. (Thesis dissertation, Aalborg University, Denmark). 69 pp.
- Karslioğlu, A., Balaban, E. and Onur, M. İ. (2021). Insulation properties of bricks with waste rubber and plastic: A Review. *Journal of Natural Products*, 1, 20-27.  
<https://doi.org/10.36937/janset2021.001.004>
- Kazmi, S. M., Abbas, S., Nehdi, M. L., Saleem, M. A. and Munir, M. J. (2017). Feasibility of using waste glass sludge in production of ecofriendly clay bricks. *Journal of Materials in Civil Engineering*, 29(8), 04017056.  
[https://doi.org/10.1061/\(ASCE\)MT.1943-5533.0001928](https://doi.org/10.1061/(ASCE)MT.1943-5533.0001928).
- Khan, M., and Ali, M. (2020). Optimization of concrete stiffeners for confined brick masonry structures. *Journal of Building Engineering*, 32, 101689.  
<https://doi.org/10.1016/j.jobe.2020.101689>
- Kim, J., Heo, E., Kim, S. J. and Kim, J. Y. (2016). Investigation of the mineral components of porcelain raw material and their phase evolution during a firing process by using a Rietveld quantitative analysis. *Journal of the Korean Physical Society*, 68, 126-130. <https://doi.org/10.3938/jkps.68.126>
- Kingery, W. D., Bowen, H. K. and Uhlmann, D. R. (1976). *Introduction to ceramics* (Vol. 17). John Wiley & Sons. 1056 pp.
- Kotsanopoulos, K. V., Ray, R. C. and Behera, S. S. (2021). Biovalorisation of Winery Wastes. In *Winemaking* (pp. 635-653). CRC Press.

- Kramer, S. N. (2010). *The Sumerians: Their history, culture, and character*. University of Chicago Press. 372 pp.
- Kreimeyer, R. (1987). Some notes on the firing colour of clay bricks. *Applied Clay Science*, 2(2), 175-183. [https://doi.org/10.1016/0169-1317\(87\)90007-X](https://doi.org/10.1016/0169-1317(87)90007-X)
- Kroger, S. A. (2005). *Architecture Built to Last: The Timelessness of Brick* (Doctoral dissertation, University of Cincinnati).
- Kromoser, B., Preinstorfer, P. and Kollegger, J. (2019). Building lightweight structures with carbon-fiber-reinforced polymer-reinforced ultra-high-performance concrete: Research approach, construction materials, and conceptual design of three building components. *Structural Concrete*, 20(2), 730-744. <https://doi.org/10.1002/suco.201700225>
- Kubiś M., Pietrak K., Cieslikiewicz Ł., Furmański P., Wasik M., Seredyński M., Wiśniewski T.S. and Łapka P. (2020). On the anisotropy of thermal conductivity in ceramic bricks. *Journal of Building Engineering* 31, 101418, <https://doi.org/10.1016/j.jobe.2020.101418>.
- Kumar Thota, S., Duc Cao, T. and Vahedifard, F (2021). Poisson's ratio characteristic curve of unsaturated soils. *Journal of Geotechnical and Geoenvironmental Engineering*, 147(1), 04020149. [https://doi.org/10.1061/\(ASCE\)GT.1943-5606.0002424](https://doi.org/10.1061/(ASCE)GT.1943-5606.0002424)

## L

- Labus, M. (2017). Thermal methods implementation in analysis of fine-grained rocks containing organic matter. *Journal of Thermal Analysis and Calorimetry*, 129(2), 965-973. <https://doi.org/10.1007/s10973-017-6259-7>
- Lafka, T. I., Sinanoglou, V. and Lazos, E. S. (2007). On the extraction and antioxidant activity of phenolic compounds from winery wastes. *Food chemistry*, 104(3), 1206-1214. <https://doi.org/10.1016/j.foodchem.2007.01.068>
- Laird, R. T. and Worcester, M. (1956). The inhibiting of lime blowing. *Transactions and journal of the British Ceramic Society*, 55, 545-563.
- Laita, E., Bauluz, B., Mayayo, M. J. and Yuste, A. (2021). Mineral and textural transformations in mixtures of Al-rich and Al-K-rich clays with firing: Refractory potential of the fired products. *Ceramics International*, 47(10), 14527-14539. <https://doi.org/10.1016/j.ceramint.2021.02.032>
- Lancaster, L. (2007). The brick relieving arch and urban redevelopment in ancient Rome. *Lexicon Topographicum Urbis Romae*, 4, 133-44.

- La Rubia-García, M. D., Yebra-Rodríguez, Á., Eliche-Quesada, D., Corpas-Iglesias, F. A. and López-Galindo, A. (2012). Assessment of olive mill solid residue (pomace) as an additive in lightweight brick production. *Construction and Building Materials*, 36, 495-500. <https://doi.org/10.1016/j.conbuildmat.2012.06.009>
- Lavat, A. E., Grasselli, M. C. and Tasca, J. E. (2007). Phase changes of ceramic whiteware slip-casting bodies studied by XRD and FTIR. *Ceramics International*, 33(6), 1111-1117. <https://doi.org/10.1016/j.ceramint.2006.03.016>
- Lecomte, T., Ferrería de la Fuente, J. F., Neuwahl, F., Canova, M.A. Pinasseau, I. J., Brinkmann, T., Roudier, S., Delgado Sancho, L. (2017). Control Reference Document on Best Available Techniques for Large Combustion Plants. Best Available Techniques (BAT). Reference Document for Large Combustion Plants; EUR 2883. <https://doi.org/10.2760/949>
- Leshina, V.A. and Pivnev, A.L. (2002). Ceramic Wall Materials Using Glass Waste. *Glass and Ceramics* 59, 356–358. <https://doi.org/10.1023/A:1022090814669>.
- Li, L., Sun, X., Luo, J., Chen, T., Xi, Q., Zhang, Y. and Sun, J. (2022a). Effects of herbal tea residue on growth performance, meat quality, muscle metabolome, and rumen microbiota characteristics in finishing steers. *Frontiers in Microbiology*, 12, 821293. <https://doi.org/10.3389/fmicb.2021.821293>
- Li, M., Wang, Y., Shen, Z., Chi, M., Lv, C., Li, C. and Zhao, X. (2022b). Investigation on the evolution of hydrothermal biochar. *Chemosphere*, 307, 135774. <https://doi.org/10.1016/j.chemosphere.2022.135774>
- Liesa, C. L., Soria, A. R., Casas, A., Aurell, M., Meléndez, N., Bádenas, B., Fregenal-Martínez, M., Navarrete, R., Peropadre, C. and Rodríguez-López, J. P. (2019). The South Iberian, Central-Iberian and Maestrazgo basins. In: Quesada, C., Oliveira, J.T. (Eds.), *The Geology of Iberia: A Geodynamic Approach*, vol. 3, Springer, Cham. Nature Switzerland
- Limami, H., Manssouri, I., Cherkaoui, K. and Khaldoun, A. (2021). Physicochemical, mechanical and thermal performance of lightweight bricks with recycled date pits waste additives. *Journal of Building Engineering*, 34, 101867. <https://doi.org/10.1016/j.jobbe.2020.101867>
- Lin, K. L., Huang, L. S., Shie, J. L., Cheng, C. J., Lee, C. H. and Chang, T. C. (2013). Elucidating the effects of solar panel waste glass substitution on the physical and mechanical characteristics of clay bricks. *Environmental Technology*, 34(1), 15-24. <https://doi.org/10.1080/09593330.2012.679693>.
- Linul, E. and Marsavina, L. (2013). Mechanical characterization of rigid pur foams used for wind turbine blades construction. *Recent Advances in Composite Materials for Wind Turbines Blades; WAP-AMSA*. 24 pp.
- Liu, H., Wei, Y., Li, P., Zhang, Y. and Sun, Y. (2007). Catalytic synthesis of nanosized hematite particles in solution. *Materials Chemistry and Physics*, 102(1), 1-6. <https://doi.org/10.1016/j.matchemphys.2006.10.001>

- López, Á. S. and Cruz, M. D. R. (2016). Las micas blancas del manto del Veleta (cordillera Bética, España). *Geotemas* (Madrid), (16), 419-422.
- López Gómez, M. and Cultrone, G. (2023). The Use of Expanded Polystyrene and Olive Stones in the Manufacture of Lightweight Bricks: Evaluation of Their Properties and Durability. *Materials*, 16(4), 1330. <https://doi.org/10.3390/ma16041330>
- Loryuenyong, V., Panyachai, T., Kaewsimork, K. and Siritai, C. (2009). Effects of recycled glass substitution on the physical and mechanical properties of clay bricks. *Journal of Waste Management*, 29(10), 2717-2721. <https://doi.org/10.1016/j.wasman.2009.05.015>.
- Love, L. G. (1957). Micro-organisms and the presence of syngenetic pyrite. *The Quarterly Journal of the Geological Society of London*, 113(1-4), 1957, 429-440. <https://doi.org/10.1144/GSL.JGS.1957.113.01-04.18>
- Lozano-Miralles, J. A., Hermoso-Orzáez, M. J., Martínez-García, C., and Rojas-Sola, J. I. (2018). Comparative study on the environmental impact of traditional clay bricks mixed with organic waste using life cycle analysis. *Sustainability*, 10(8), 2917. <https://doi.org/10.3390/su10082917>
- Lubelli, B., Cnudde, V., Diaz-Goncalves, T., Franzoni, E., van Hees, R. P., Ioannou, I. and Viles, H. (2018). Towards a more effective and reliable salt crystallization test for porous building materials: state of the art. *Materials and Structures*, 51, 1-21. <https://doi.org/10.1617/s11527-018-1180-5>

## M

- Maaze, M. R., and Shrivastava, S. (2023). Selection of eco-friendly alternative brick for sustainable development. A study on Technical, Economic, Environmental and Social feasibility. *Construction and Building Materials*, 408, 133808. <https://doi.org/10.1016/j.conbuildmat.2023.133808>
- MacDonald, S. A., Schardt, C. R., Masiello, D. J. and Simmons, J. H. (2000). Dispersion analysis of FTIR reflection measurements in silicate glasses. *Journal of Non-Crystalline Solids*, 275(1-2), 72-82 [https://doi.org/10.1016/S0022-3093\(00\)00121-6](https://doi.org/10.1016/S0022-3093(00)00121-6)
- Macfarlane, A., and Macfarlane, I. (2009). *The empire of tea*. Abrams. 308 pp.
- Maicas, S. (2020). The role of yeasts in fermentation processes. *Microorganisms*, 8(8), 1142. <https://doi.org/10.3390/microorganisms8081142>
- Majewski, P., Florin, N., Jit, J. and Stewart, R. A. (2022). End-of-life policy considerations for wind turbine blades. *Renewable and Sustainable Energy Reviews*, 164, 112538. <https://doi.org/10.1016/j.rser.2022.112538>

- Makris, D. P., Boskou, G. and Andrikopoulos, N. K. (2007). Polyphenolic content and in vitro antioxidant characteristics of wine industry and other agri-food solid waste extracts. *Journal of Food Composition and Analysis*, 20(2), 125-132. <https://doi.org/10.1016/j.jfca.2006.04.010>
- Małek, M., Grzelak, K., Łasica, W., Jackowski, M., Kluczyński, J., Szachogluchowicz, I., Torzewski and Łuszczek, J. (2022). Cement-glass composite bricks (CGCB) with interior 3D printed PET-G scaffolding. *Journal of Building Engineering*, 52, 104429. <https://doi.org/10.1016/j.jobbe.2022.104429>.
- Mandal, A. K., and Sen, R. (2017). An overview on microwave processing of material: a special emphasis on glass melting. *Materials and Manufacturing Processes*, 32(1), 1-20. <https://doi.org/10.1080/10426914.2016.1151046>
- Maniatis, Y., Simopoulos, A., Kostikas, A. and Perdikatsis, V. (1983). Effect of reducing atmosphere on minerals and iron oxides developed in fired clays: the role of Ca. *Journal of the American Ceramic Society*, 66(11), 773-781. <https://doi.org/10.1111/j.1151-2916.1983.tb10561.x>.
- Maniatis, Y. and Tite, M. S. (1981). Technological examination of Neolithic-Bronze Age pottery from central and southeast Europe and from the Near East. *Journal of Archaeological Science*, 8(1), 59-76. [https://doi.org/10.1016/0305-4403\(81\)90012-1](https://doi.org/10.1016/0305-4403(81)90012-1).
- Manohar, S., Santhanam, M., and Chockalingam, N. (2019). Performance and microstructure of bricks with protective coatings subjected to salt weathering. *Construction and Building Materials*, 226, 94-105. <https://doi.org/10.1016/j.conbuildmat.2019.07.180>
- Mao, L., Wu, Y., Zhang, W. and Huang, Q. (2019). The reuse of waste glass for enhancement of heavy metals immobilization during the introduction of galvanized sludge in brick manufacturing. *Journal of Environmental Management*, 231, 780-787. <https://doi.org/10.1016/j.jenvman.2018.10.120>
- Mao, L., Zhou, H., Peng, M., Hu, L. and Zhang, W. (2020). Effects of waste glass particle size on improving the property and environmental safety of fired brick containing electroplating sludge. *Construction and Building Materials*, 257, 119583. <https://doi.org/10.1016/j.conbuildmat.2020.119583>
- Maritan, L., Nodari, L., Mazzoli, C., Milano, A. and Russo, U. (2006). Influence of firing conditions on ceramic products: experimental study on clay rich in organic matter. *Applied Clay Science*, 31(1-2), 1-15. <https://doi.org/10.1016/j.clay.2005.08.007>
- Martin, J. M., Ortega-Huertas M. and Torres-Ruiz, J. (1984). Genesis and evolution of strontium deposits of the Granada Basin (southeastern Spain): evidence of diagenetic replacement of a stromatolite belt. *Sedimentary Geology*, 39(3-4), 281-298. [https://doi.org/10.1016/0037-0738\(84\)90055-1](https://doi.org/10.1016/0037-0738(84)90055-1)

- Martín-Algarra, A. Mazzoli, S. Perrone, V. and Rodríguez-Cañero, R. (2009). Variscan tectonics in the Malaguide Complex (Betic Cordillera, southern Spain): stratigraphic and structural constraints from the Ardales area (Province of Malaga). Part II: structure. *Journal of Geology*, 117, 263-284. <https://doi.org/10.1086/597364>
- Martín-Suárez, E., Freudenthal, M. and Agusti, J. (1993). Micromammals from the Middle Miocene of the Granada Basin (Spain). *Geobios*, 26, 377-387. [https://doi.org/10.1016/S0016-6995\(93\)80028-P](https://doi.org/10.1016/S0016-6995(93)80028-P)
- Martínez-Martínez, J., Benavente, D. and Del Cura, M. G. (2007). Petrographic quantification of brecciated rocks by image analysis. Application to the interpretation of elastic wave velocities. *Engineering Geology*, 90(1-2), 41-54. <https://doi.org/10.1016/j.enggeo.2006.12.002>
- Martínez, J. M., Benavente, D. and del Cura, M. G. (2011). Spatial attenuation: the most sensitive ultrasonic parameter for detecting petrographic features and decay processes in carbonatic rocks. *Engineering Geology*, 119, 84-95. <https://doi.org/10.1016/j.enggeo.2011.02.002>
- Martínez-García, C., Eliche-Quesada, D., Pérez-Villarejo, L., Iglesias-Godino, F. J., Corpas-Iglesias, F. A. (2012). Sludge valorization from wastewater treatment plant to its application on the ceramic industry. *Journal of Environmental Management*, 95, S343-S348. <https://doi.org/10.1016/j.jenvman.2011.06.016>
- Martinez-Marquez, D., Florin, N., Hall, W., Majewski, P., Wang, H. and Stewart, R. A. (2022). State-of-the-art review of product stewardship strategies for large composite wind turbine blades. *Resources, Conservation & Recycling Advances*, 15, 200109. <https://doi.org/10.1016/j.rcradv.2022.200109>
- Massoud, M. (2007). Analysis study of the Bricks Religious Architecture and archaeological evidence and the role religious of Bricks" Nile-Mud" in Ancient Egypt. *Magazine General Union of Arab Archaeologists*, (8).
- Mattsson, C., André, A., Juntikka, M., Tränkle, T. and Sott, R. (2020). Chemical recycling of End-of-Life wind turbine blades by solvolysis/HTL. In *IOP conference series: materials science and engineering*. 942, (1), 012013. IOP Publishing.
- Mazzanti, C. (2016). A multidisciplinary study on the exposed brick walls of the baroque architecture of Penne in Italy. In *Further Studies in the History of Construction: the Proceedings of the Third Annual Conference of the Construction History Society: The Proceedings of the Third Annual Conference of the Construction History Society* (241 pp.).
- McClendon, C. B. (2005). *The origins of medieval architecture: building in Europe, AD 600-900*. University of Yale Press. 208 pp.

- McHenry, P. G. (1989). *Adobe and rammed earth buildings: design and construction*. University of Arizona Press. 235pp.
- Meloni, B., Farinella, D. and Cois, E. (2015). Food and territory: local strategies of the Sardinian family farms in the dairy and wine sectors. In XXVIh Congress of the European Society for Rural Sociology, Places of Possibility (pp. 45-46).
- Mendes, B. C., Pedroti, L. G., Fontes, M. P., Ribeiro, J. C. L., Vieira, C. M., Pacheco, A. A., and de Azevedo, A. R. (2019). Technical and environmental assessment of the incorporation of iron ore tailings in construction clay bricks. *Construction and Building Materials*, 227, 116669. <https://doi.org/10.1016/j.conbuildmat.2019.08.050>
- Meseguer, S., Jordan, M. M. and Sanfeliu, T. (2009). Use of mine spoils from Teruel coal mining district (NE, Spain). *Environmental Geology*, 56, 845-853. <https://doi.org/10.1007/s00254-007-1185-9>
- Mesquita E., Antunes P., Coelho F. and Andre P. (2016). Global overview on advances in structural health monitoring platforms. *Journal of Civil Structural Health Monitoring*, 6(3):461–475. <https://doi.org/10.1007/s13349-016-0184-5>
- Mesquita E., Martini R., Alves A., Antunes P. and Varum H. (2018). Non-destructive characterization of ancient clay brick walls by indirect ultrasonic measurements. *Journal of Building Engineering*, 19:172–180. <https://doi.org/10.1016/j.jobe.2018.05.011>
- Micheal, A. and Moussa, R. R. (2022). Evaluating the Effect of Adding Sugarcane Bagasse to the Fire Clay Brick's Properties. *Civil Engineering and Architecture-HPUB*, 10(1), 71-78. <https://doi.org/10.13189/cea.2022.100106>
- Minke, G. (2006). *Building with earth: design and technology of a sustainable architecture*. Birkhäuser. 208 pp.
- Minwer-Barakat, R., García-Alix, A., Martín-Suárez, E., Freudenthal, M. (2012). The late Miocene continentalization of the Guadix Basin (southern Spain) reconsidered: A comment on Hüsing et al. (2010). *Geobios*, 45, 611-615. <https://doi.org/10.1016/j.geobios.2012.05.001>
- Miranda LF., Rio J., Miranda Guedes J. and Costa A. (2012). Sonic impact method—a new technique for characterization of stone masonry walls. *Construction and Building Materials*, 36:27–35. <https://doi.org/10.1016/j.conbuildmat.2012.04.018>
- Mishnaevsky Jr, L., Branner, K., Petersen, H. N., Beauson, J., McGugan, M., and Sørensen, B. F. (2017). Materials for wind turbine blades: An overview. *Materials*, 10(11), 1285. <https://doi.org/10.3390/ma10111285>
- Mogetta, M. (2021). *The origins of concrete construction in roman architecture: technology and society in Republican Italy*. Cambridge University Press. 350 pp.



- Mohajerani, A., Kadir, A. A. and Larobina, L. (2016). A practical proposal for solving the world's cigarette butt problem: Recycling in fired clay bricks. *Journal of Waste Management*, 52, 228-244 <https://doi.org/10.1016/j.wasman.2016.03.012>
- Mohsen, K. S., and Hameed, A. T. (2021). The Supreme temples (Ziggurats) in the Kashi era in Babylonia and their impact on archaeological tourism Ziggurat of Aqarquf- an example. *Review of International Geographical Education Online*, 11(7). <https://doi.org/10.48047/rigeo.11.07.112>
- Moissenet, E. (1983). Aspectos de la neotectónica en la Fosa de Teruel. In: Comba, J.A., (Ed.), *Geología de España, Libro Jubilar J.M. Ríos, IGME, Madrid, vol. II*, p. 427-446.
- Mokrzycki, W. S. and Tatol, M. (2011). Colour difference  $\Delta E$ -A survey. *Mach. Graph. Vis*, 20(4), 383-411.
- Molina, O., Vilarrasa, V. and Zeidouni, M. (2017). Geologic carbon storage for shale gas recovery. *Energy Procedia*, 114, 5748-5760. <https://doi.org/10.1016/j.egypro.2017.03.1713>
- Momčilović-Petronijević, A., Topličić-Ćurčić, G., and Ćurčić, A. (2018). Architecture and ceramic materials, development through time: adobe and brick. *Facta Universitatis-series: Architecture and Civil Engineering*, 16(3), 387-400. <https://doi.org/10.2298/FUACE180521016M>
- Monrad, J. K., Howard, L. R., King, J. W., Srinivas, K. and Mauromoustakos, A. (2010). Subcritical solvent extraction of anthocyanins from dried red grape pomace. *Journal of Agricultural and Food Chemistry*, 58(5), 2862-2866. <https://doi.org/10.1021/jf904087n>
- Montana, G. (2017). Ceramic raw materials. *The Oxford handbook of archaeological ceramic analysis*, 87-100.
- Monteiro, S. N. and Vieira, C. M. F. (2014). On the production of fired clay bricks from waste materials: A critical update. *Construction and Building Materials*, 68, 599-610. <https://doi.org/10.1016/j.conbuildmat.2014.07.006>.
- Moore, D. M. and Reynolds Jr, R. C. (1989). *X-ray Diffraction and the Identification and Analysis of Clay Minerals*. Oxford University Press. 396 pp.
- Morales, J., Vidal, F., de Miguel, D., Aguacil, G., Posadas, A. M., Ibáñez, J. M., Guzmán, A. and Guirao, J.M., (1990). Basement structure of the Granada Basin, Betic Cordilleras, southern Spain. *Tectonophysics*, 177, 337-348. [https://doi.org/10.1016/0040-1951\(90\)90394-N](https://doi.org/10.1016/0040-1951(90)90394-N)
- Moudry, R. (Ed.). (2005). *The American Skyscraper: Cultural Histories*. Cambridge University Press. 298 pp.

- Mould, O. (2017). Brutalism redux: Relational monumentality and the urban politics of brutalist architecture. *Antipode*, 49(3), 701-720. <https://doi.org/10.1111/anti.12306>
- Mukherjee, S. (2013). Environmental Degradations during Clay Mining and Beneficiation. *The Science of Clays*. 264-279 pp. Springer, Dordrecht. [https://doi.org/10.1007/978-94-007-6683-9\\_18](https://doi.org/10.1007/978-94-007-6683-9_18)
- Mukherjee, D. P. and Das, S. K. (2013). Effects of nano silica on synthesis and properties of glass ceramics in  $\text{SiO}_2\text{-Al}_2\text{O}_3\text{-CaO-CaF}_2$  glass system: A comparison. *Journal of Non-Crystalline Solids*, 368, 98-104. <https://doi.org/10.1016/j.jnoncrysol.2013.03.012>
- Mukhopadhyay, T. K., Ghatak, S. and Maiti, H. S. (2010). Pyrophyllite as raw material for ceramic applications in the perspective of its pyro-chemical properties. *Ceramics International*, 36(3), 909-916. <https://doi.org/10.1016/j.ceramint.2009.10.026>
- Muñoz, P., Morales, M. P., Mendivil, M. A., Juárez, M. C. and Muñoz, L. (2014). Using of waste pomace from winery industry to improve thermal insulation of fired clay bricks. Eco-friendly way of building construction. *Construction and Building Materials*, 71, 181-187. <https://doi.org/10.1016/j.conbuildmat.2014.08.027>

## N

- Nandiyanto, A. B. D., Oktiani, R. and Ragadhita, R. (2019). How to read and interpret FTIR spectroscopy of organic material. *Indonesian Journal of Science and Technology*, 4(1), 97-118. <https://doi.org/10.17509/ijost.v4i1.15806>
- Nardoia, M., Ruiz-Capillas, C., Herrero, A. M., Pintado, T., Jiménez Colmenero, F., Chamorro, S. and Brenes, A. (2017). Effect of added grape seed and skin on chicken thigh patties during chilled storage. *International Journal of Food and Nutritional Science*. 4,1 (67-73 pp.). <https://doi.org/10.15436/2377-0619.17.1497>
- Nascimento, E. S. S., de Souza, P. C., de Oliveira, H. A., Júnior, C. M. M., de Oliveira Almeida, V. G., and de Melo, F. M. C. (2021). Soil-cement brick with granite cutting residue reuse. *Journal of Cleaner Production*, 321, 129002. <https://doi.org/10.1016/j.jclepro.2021.129002>
- Nesbitt, A. (1863). VI.—On the Brick Architecture of the North of Germany. *Archaeologia*, 39(1), 93-111. <https://doi.org/10.1017/S0261340900004252>
- Nesbitt, H. W., Bancroft, G. M. and Henderson, G. S. (2018). Temperature dependence of Raman shifts and line widths for  $Q^0$  and  $Q^2$  crystals of silicates, phosphates, and sulphates. *American Mineralogist*, 103, 966-976. <https://doi.org/10.2138/am-2018-6314>

- Ngon, G. N., Fouateu, R. Y., Nana, G. L., Bitom, D. L., Bilong, P. and Lecomte, G. (2012). Study of physical and mechanical applications on ceramics of the lateritic and alluvial clayey mixtures of the Yaoundé region (Cameroon). *Construction and Building Materials*, 31, 294-299. <https://doi.org/10.1016/j.conbuildmat.2011.12.108>
- Nieto, F., Abad, I. and Azañón, J. M. (2008). Smectite quantification in sediments and soils by thermogravimetric analyses. *Applied Clay Science*, 38(3-4), 288-296. <https://doi.org/10.1016/j.clay.2007.04.001>
- Nigam, M., Rajoriya, S., Singh, S. R. and Kumar, P. (2019). Adsorption of Cr (VI) ion from tannery wastewater on tea waste: kinetics, equilibrium and thermodynamics studies. *Journal of Environmental Chemical Engineering*, 7(3), 103188. <https://doi.org/10.1016/j.jece.2019.103188>
- Nodari, L., Marcuz, E., Maritan, L., Mazzoli, C. and Russo, U. (2007). Hematite nucleation and growth in the firing of carbonate-rich clay for pottery production. *Journal of the American Ceramic Society*, 27(16), 4665-4673. <https://doi.org/10.1016/j.jeurceramsoc.2007.03.031>
- Nogales, R., Cifuentes, C. and Benitez, E. (2005). Vermicomposting of winery wastes: a laboratory study. *Journal of Environmental Science and Health, Part B*, 40(4), 659-673. <https://doi.org/10.1081/PFC-200061595>
- NORMAL 29/88, 1988. Misura dell'indice di asciugamento (drying index). CNR-ICR, Roma, Italia.



- Oppenheim, A. L. (2013). *Ancient Mesopotamia: portrait of a dead civilization* (444 pp.). University of Chicago Press.
- Orden, L., Ferreiro, N., Satti, P., Navas-Gracia, L. M., Chico-Santamarta, L. and Rodríguez, R. A. (2021). Effects of onion residue, bovine manure compost and compost tea on soils and on the agroecological production of onions. *Agriculture*, 11(10), 962 pp. <https://doi.org/10.3390/agriculture11100962>
- Ordieres, R. and Cultrone, G. (2022). Technical quality of solid bricks made using clayey earth with added coffee grounds and fly ash. *Construction and Building Materials*, 341, 127757. <https://doi.org/10.1016/j.conbuildmat.2022.127757>
- Ortí, F., Rosell, L. and Anadón, P. (2003). Deep to shallow lacustrine evaporites in the Libros Gypsum (southern Teruel Basin, Miocene, NE Spain): an occurrence of pelletal gypsum rhythmites. *Sedimentology*, 50, 361-386. <https://doi.org/10.1046/j.1365-3091.2003.00558.x>
- Ozturk, S., Sutcu, M., Erdogmus, E. and Gencel, O. Influence of tea waste concentration in the physical, mechanical and thermal properties of brick clay

mixtures. *Construction and Building Materials*, 217, 2019, 592-599.  
<https://doi.org/10.1016/j.conbuildmat.2019.05.114>

## P

- Palaniyappan, S., Annamalai, V. E., Ashwinkumaran, S., Thenmuhil, D. and Veeman, D. (2022). Utilization of abrasive industry waste as a substitute material for the production of fireclay brick. *Journal of Building Engineering*, 45, 103606. <https://doi.org/10.1016/j.jobe.2021.103606>.
- Panda, R. N., Hsieh, M. F., Chung, R. J. and Chin, T. S. (2003). FTIR, XRD, SEM and solid state NMR investigations of carbonate-containing hydroxyapatite nanoparticles synthesized by hydroxide-gel technique. *Journal of Physics and Chemistry of Solids*, 64(2), 193-199. [https://doi.org/10.1016/S0022-3697\(02\)00257-3](https://doi.org/10.1016/S0022-3697(02)00257-3)
- Pande, G. N., Liang, J. X., and Middleton, J. (1989). Equivalent elastic moduli for brick masonry. *Computers and Geotechnics*, 8(3), 243-265. [https://doi.org/10.1016/0266-352X\(89\)90045-1](https://doi.org/10.1016/0266-352X(89)90045-1)
- Paradelo, R., Moldes, A. B. and Barral, M. T. (2011). Carbon and nitrogen mineralization in a vineyard soil amended with grape marc vermicompost. *Waste Management and Research*, 29(11), 1177-1184. <https://doi.org/10.1016/j.jenvman.2012.12.001>
- Paradelo, R., Moldes, A. B. and Barral, M. T. (2013). Evolution of organic matter during the mesophilic composting of lignocellulosic winery wastes. *Journal of Environmental Management*, 116, 18-26. <https://doi.org/10.1016/j.jenvman.2012.12.001>
- Parisi, F., Asprone, D., Fenu, L. and Prota, A. (2015). Experimental characterization of Italian composite adobe bricks reinforced with straw fibers. *Composite Structures*, 122, 300-307. <https://doi.org/10.1016/j.compstruct.2014.11.060>
- Parras, J., Sánchez-Jimeñez, C., Rodas, M. and Luque, F. J., (1996). Ceramic applications of Middle Ordovician shales from central Spain. *Applied Clay Science*, 11(1), 25-41. [https://doi.org/10.1016/0169-1317\(96\)00003-8](https://doi.org/10.1016/0169-1317(96)00003-8).
- Pask, J. A. and Tomsia, A. P. (1991). Formation of mullite from sol-gel mixtures and kaolinite. *Journal of the American Ceramic Society*, 74(10), 2367-2373. <https://doi.org/10.1111/j.1151-2916.1991.tb06770.x>
- Pendón, J.G. (1978). *Sedimentación turbidítica en las unidades del Campo de Gibraltar*. Thesis Dissertation, Universidad de Granada, Spain. 260 pp.
- Pérez-Monserrat, E. M., Causarano, M. A., Maritan, L., Chavarria, A., Brogiolo, G. P., and Cultrone, G. (2022a). Roman brick production technologies in Padua (Northern Italy) along the Late Antiquity and Medieval Times: Durable bricks on

- high humid environs. *Journal of Cultural Heritage*, 54, 12-20. <https://doi.org/10.1016/j.culher.2022.01.007>
- Pérez-Monserrat, E. M., Crespo-López, L., Cultrone, G., Mozzi, P., and Maritan, L. (2024). Clayey materials for traditional bricks production in North-Eastern Italy through a combined compositional study: From firing dynamics to provenance. *Journal of Archaeological Science: Reports*, 54, 104400. <https://doi.org/10.1016/j.jasrep.2024.104400>
- Pérez-Monserrat, E. M., Maritan, L., and Cultrone, G. (2022b). Firing and post-firing dynamics of Mg- and Ca-rich bricks used in the built heritage of the city of Padua (northeastern Italy). *European Journal of Mineralogy*, 34(3), 301-319. <https://doi.org/10.5194/ejm-34-301-2022>
- Pérez-Peña, J. V., Azañón, J. M., Azor, A., Tuccimei, P., Della Seta, M. and Soligo, M. (2009). Quaternary landscape evolution and erosion rates for an intramontane Neogene basin (Guadix–Baza basin, SE Spain). *Geomorphology*, 106(3-4), 206-218. <https://doi.org/10.1016/j.geomorph.2008.10.018>
- Phonphuak, N., Kanyakam, S. and Chindapasirt, P. (2016). Utilization of waste glass to enhance physical–mechanical properties of fired clay brick. *Journal of Cleaner Production*, 112, 3057-3062. <https://doi.org/10.1016/j.jclepro.2015.10.084>.
- Perra, M., Bacchetta, G., Muntoni, A., De Gioannis, G., Castangia, I., Rajha, H. N. and Manconi, M. (2022). An outlook on modern and sustainable approaches to the management of grape pomace by integrating green processes, biotechnologies and advanced biomedical approaches. *Journal of Functional Foods*, 98, 105276. <https://doi.org/10.1016/j.jff.2022.105276>
- Pierson, H. O. (1993). Graphite structure and properties. *Handbook of carbon, graphite, diamonds and fullerenes*, 43-69.
- Pla-Pueyo, S. (2009). Contexto estratigráfico y sedimentario de los yacimientos de grandes mamíferos del sector central de la cuenca de Guadix (Cordillera Bética). Thesis Dissertation, Universidad de Granada, Spain, 271 pp.
- Platt, J., Behr, W., Johanesen, K. and Williams, J. (2013). The Betic-Rif Arc and Its Orogenic Hinterland: *Annual Review of Earth and Planetary Sciences*, 41, 313-357. <https://doi.org/10.1146/annurev-earth-050212-123951>
- Pliego RL-88 (1988). Pliego General de Condiciones para la Recepción de Ladrillos Cerámicos en las Obras de Construcción, Ministerio de Obras Públicas, Transportes y Medio Ambiente, Spain.
- Poljansek, I. and Krajnc, M. (2005). Characterization of phenol-formaldehyde prepolymer resins by in line FT-IR spectroscopy. *Acta Chimica Slovenica*, 52(3), 238.
- Pollock, S. (1999). *Ancient mesopotamia* (Vol. 1) Cambridge University Press. 272 pp.
- Post, J. L. and Borer, L. (2002). Physical properties of selected illites, beidellites and mixed-layer illite–beidellites from southwestern Idaho, and their infrared spectra.

Applied Clay Science, 22(3), 77-91. [https://doi.org/10.1016/S0169-1317\(02\)00129-1](https://doi.org/10.1016/S0169-1317(02)00129-1)

Prasad, M. S., Reid, K. J., and Murray, H. H. (1991). Kaolin: processing, properties and applications. *Applied clay science*, 6(2), 87-119. [https://doi.org/10.1016/0169-1317\(91\)90001-P](https://doi.org/10.1016/0169-1317(91)90001-P)

Preethi, S., Prasannadevi, R., Preethi, K., Prasad, S. R., Banuchander, T. R. (2019). Reuse of plastic bottles in construction of buildings. *Ratio*, 1(10).

Priyadarshini, M., Giri, J. P., and Patnaik, M. (2021). Variability in the Compressive Strength of Non-Conventional Bricks Containing Agro and Industrial Waste. *Case Studies in Construction Materials*, e00506. <https://doi.org/10.1016/j.cscm.2021.e00506>

Puga-Bernabéu, Á., Martín, J. M. and Braga, J. C. (2008). Sedimentary processes in a submarine canyon excavated into a temperate-carbonate ramp (Granada basin, S. Spain). *Sedimentology*, 55, 1449-1466. <https://doi.org/10.1111/j.1365-3091.2008.00952.x>

Puga-Bernabéu, Á., Martín, J. M., Braga, J. C. and Sánchez-Almazo, I. M. (2010). Downslope-migrating sandwaves and platform-margin clinoforms in a current dominated distally steepened temperate-carbonate ramp (Guadix Basin, Southern Spain). *Sedimentology*, 57, 293-311. <https://doi.org/10.1111/j.1365-3091.2009.01079.x>

## R

Radovic, L. R. (2001). Carbons and graphites, reactivity of. *Encyclopedia of materials: science and technology*, 975-984. <https://doi.org/10.1016/B0-08-043152-6/00182-0>

Ramos, J. M., Hidalgo, M. Á., Gallego, M. R. and Muñoz, F. O. (1989). Estudio cristalográfico de micas de Sierra Nevada. Cordillera Bética. *Boletín de la Sociedad Española de Mineralogía*, 12, 101-111.

Ramos L.F., Marques L., Lourenço P.B., De Roeck G., Campos-Costa A. and Roque J. (2010). Monitoring historical masonry structures with operational modal analysis: two case studies. *Mechanical Systems and Signal Processing*, 24(5):1291–1305. <https://doi.org/10.1016/j.ymssp.2010.01.011>

Rani, M., Choudhary, P., Krishnan, V. and Zafar, S. (2021). A review on recycling and reuse methods for carbon fiber/glass fiber composites waste from wind turbine blades. *Composites Part B: Engineering*, 215, 108768. <https://doi.org/10.1016/j.compositesb.2021.108768>

- Rathossi, C. and Pontikes, Y. (2010). Effect of firing temperature and atmosphere on ceramics made of NW Peloponnese clay sediments. Part I: Reaction paths, crystalline phases, microstructure and colour. *Journal of the European Ceramic Society*, 30(9), 1841-1851. <https://doi.org/10.1016/j.jeurceramsoc.2010.02.002>.
- Reddy, B. V., and Jagadish, K. S. (2003). Embodied energy of common and alternative building materials and technologies. *Energy and buildings*, 35(2), 129-137. [https://doi.org/10.1016/S0378-7788\(01\)00141-4](https://doi.org/10.1016/S0378-7788(01)00141-4)
- Richardson, S. (2015). Building Larsa: Labor-Value, Scale and Scope-of-Economy in Ancient Mesopotamia. *Labor in the Ancient World*, 5, 237-328.
- Rietveld, H.M. (1969). A profile refinement method for nuclear and magnetic structures, *Journal of Applied Crystallography*, 2, 65–71. <https://doi.org/10.1107/S0021889869006558>
- Righi, D., and Meunier, A. (1995). Origin of clays by rock weathering and soil formation. *Origin and mineralogy of clays: clays and the environment*. Berlin, Heidelberg: Springer Berlin Heidelberg. 43-161 pp.
- RILEM (1980). Recommended tests to measure the deterioration of stone and to assess the effectiveness of treatment methods. *Commission 25-PEM: Protection et Erosion des Monuments, Mater. Struct.*, 13(75), 175-253.
- RILEM (1998a). MS-A.1 Determination of the resistance of wallstones against sulphates and chlorides." *Materials and Structures*, 31 (1): 2–19.
- RILEM (1998b). Recommendation MS-A2: Unidirectional salt crystallization test for masonry units. *Materials and Structures* 31 (1): 10–11.
- Rivas, P., Braga, J.C. and Sánchez-Almazo, I.M. (1999). Arrecifes del Tortonense inferior en la cuenca de Granada (Cordillera Bética, España). *Trabajos Geológicos, Universidad de Oviedo*, 21, 309-320.
- RL-88, (1988). Pliego general de condiciones para la recepción de los ladrillos cerámicos en las obras de construcción. *Boletín Oficial del Estado (BOE)*.
- Rodríguez-Fernández, J. (1982). El Mioceno del sector central de las Cordilleras Béticas. Thesis Dissertation, Universidad de Granada, Spain, 224 p.
- Rodríguez-Fernández, J. and Sanz de Galdeano, C. (2006). Late orogenic intramontane basin development: the Granada basin, Betics (southern Spain). *Basin Research*, 18, 85-102. <https://doi.org/10.1111/j.1365-2117.2006.00284.x>
- Rodriguez-Navarro, C., Doehne, E. and Sebastian, E. (2000). How does sodium sulfate crystallize? Implications for the decay and testing of building materials. *Cement and Concrete Research*, 30(10), 1527-1534. [https://doi.org/10.1016/S0008-8846\(00\)00381-1](https://doi.org/10.1016/S0008-8846(00)00381-1)

- Rodriguez-Navarro, C., Cultrone, G., Sanchez-Navas, A. and Sebastian, E. (2003). TEM study of mullite growth after muscovite breakdown. *American Mineralogist*, 88(5-6), 713-724. <https://doi.org/10.2138/am-2003-5-601>.
- Rodriguez-Navarro, C., Ruiz-Agudo, E., Luque, A., Rodriguez-Navarro, A. B. and Ortega-Huertas, M. (2009). Thermal decomposition of calcite: Mechanisms of formation and textural evolution of CaO nanocrystals. *American Mineralogist*, 94(4), 578-593. <https://doi.org/10.2138/am.2009.3021>.
- Rodríguez Navarro, C; Kudlacz, K. and Ruiz Agudo, E. (2012). The mechanism of thermal decomposition of dolomite: new insights from 2D-XRD and TEM analyses. *American Mineralogist*, 97(1), 38-51. <https://doi.org/10.2138/am.2011.3813>.
- Rodríguez Vázquez, E. (2014). Espumas de carbono con propiedades avanzadas derivadas de carbones bituminosos. Thesis Dissertation, Universidad de Oviedo, Spain. 253 pp.
- Rosa M., Lorenzoni F., Deiana R., Taffarel S. and Modena C. (2019). Non-destructive investigations for structural qualification of the Sarno Baths, Pompeii. 280-287. *Journal of Cultural Heritage*, <https://doi.org/10.1016/j.culher.2019.04.015>
- Rosembaum, G., Lister, S.G. and Duboz, C. (2002). Relative motions of Africa, Iberia and Europe during Alpine orogeny. *Tectonophysics* 359, 117-129. [https://doi.org/10.1016/S0040-1951\(02\)00442-0](https://doi.org/10.1016/S0040-1951(02)00442-0)
- Ruiz-Bustos, A., Martín Martín, M. and Martín Algarra, A. (1992). Nuevos datos sobre el neógeno continental en el sector noreste de la cuenta de Granada, Cordillera Bética. *Geogaceta* (12), 52-56.
- Rush, S. J. N. (2022). The first Romanesque architecture of Conflent, Pyrénées-Orientales, France. Tradition, system and style. Thesis dissertation, University of London, United Kingdom. 328 pp.
- Ruska, M. and Kiviluoma, J. (2011). Renewable electricity in Europe. Current state, drivers, and scenarios for 2020. Technical Report. 72 pp.

S

- Saenz, N., Sebastián, E. and Cultrone, G. (2019). Analysis of tempered bricks: from raw material and additives to fired bricks for use in construction and heritage conservation. *European Journal of Mineralogy*, 31(2), 301-312. <https://doi.org/10.1127/ejm/2019/0031-2832>.
- Sahu, V., Attri, R., Gupta, P. and Yadav, R. (2020). Development of eco friendly brick using water treatment plant sludge and processed tea waste. *Journal of Engineering, Design and Technology*, 18(3), 727-738. <https://doi.org/10.1108/JEDT-06-2019-0168>



- Saidur, R., Rahim, N. A., Islam, M. R. and Solangi, K. H. (2011). Environmental impact of wind energy. *Renewable and sustainable energy reviews*, 15(5), 2423-2430. <https://doi.org/10.1016/j.rser.2011.02.024>
- Salinas, M. R., Garijo, J., Pardo, F., Zalacain, A. and Alonso, G. L. (2003). Color, polyphenol, and aroma compounds in rosé wines after prefermentative maceration and enzymatic treatments. *American Journal of Enology and Viticulture*, 54(3), 195-202. <https://doi.org/10.5344/ajev.2003.54.3.195>
- Salvini, S., Coletti, C., Maritan, L., Massironi, M., Balsamo, M. and Mazzoli, C. (2023). Exploring the Pore System of Carbonate Rocks through a Multi- Analytical Approach. *Environmental Earth Sciences*. <https://doi.org/10.21203/rs.3.rs-3289391/v1>
- Saman, N. S. (2017). Assessing low thermal conductivity of bricks which contain rice husk, corn cob and waste tea as an additive material (Doctoral Dissertation, Universiti Tun Hussein Onn Malaysia). 32 pp.
- Sánchez-Jiménez, N., Gismera, M. J., Sevilla, M. T., Cuevas, J., Rodríguez-Rastrero, M., and Procopio, J. R. (2012). Clayey materials as geologic barrier in urban landfills: Comprehensive study of the interaction of selected quarry materials with heavy metals. *Applied Clay Science*, 56, 23-29. <https://doi.org/10.1016/j.clay.2011.11.016>
- Sanchez-Navas, A. (1999). Sequential kinetics of a muscovite-out reaction: A natural example. *American Mineralogist*, 84(9), 1270-1286. <https://doi.org/10.2138/am-1999-0905>.
- Sanjay, M. R., Madhu, P., Jawaid, M., Sentharamaikannan, P., Senthil, S. and Pradeep, S. (2018). Characterization and properties of natural fiber polymer composites: A comprehensive review. *Journal of Cleaner Production*, 172, 566-581. <https://doi.org/10.1016/j.jclepro.2017.10.101>
- Santamaría-López, Á., González-Castillo, L., Galindo-Zaldívar, J. and Sanz de Galdeano, C. (2022). Geological Setting of Sierra Nevada in the Landscape of the Sierra Nevada (pp. 71-81). Springer, Cham. [https://doi.org/10.1007/978-3-030-94219-9\\_5](https://doi.org/10.1007/978-3-030-94219-9_5)
- Santhosh, K. G., Subhani, S. M. and Bahurudeen, A. (2022). Sustainable reuse of palm oil fuel ash in concrete, alkali-activated binders, soil stabilisation, bricks and adsorbent: A waste to wealth approach. *Industrial Crops and Products*, 183, 114954. <https://doi.org/10.1016/j.indcrop.2022.114954>
- Sanz de Galdeano, C., 2008. The Cádiz-Alicante fault: an important discontinuity in the Betic Cordillera. *Revista de la Sociedad Geológica de España*, 21, 49-58. <http://hdl.handle.net/10261/29430>
- Sanz de Galdeano, C. and Vera, J.A. (1992). Stratigraphic record and paleogeographical context of Neogene basins in the Betic Cordillera, Spain. *Basin Research*, 4, 21-36. <https://doi.org/10.1111/j.1365-2117.1992.tb00040.x>

- Sanz de Galdeano, C. and López-Garrido, A.C. (2003). Revisión de las unidades alpujarrides de las sierras de Tejada, Aljara y Guájares (sector central de la Zona Interna Bética, provincias de Granada y Málaga). *Revista de la Sociedad Geológica de España*, 16, 135-149. <http://hdl.handle.net/10261/29373>
- Sanz de Galdeano, C., García-Tortosa, F.J., Alfaro, P., Azañón, J.M., Galindo-Zaldívar, J., López-Casado, C., López-Garrido, A.C., Rodríguez-Fernández, J. and Ruano, P. (2012). Main active faults in the Granada and Guadix-Baza Basins (Betic Cordillera). *Journal of Iberian Geology*, 38, 209-223. <http://hdl.handle.net/10045/35319>
- Saravanapavan, P. and Hench, L. L. (2003). Mesoporous calcium silicate glasses. I. *Synthesis Journal of Non-Crystalline Solids*, 318(1-2), 1-13. [https://doi.org/10.1016/S0022-3093\(02\)01864-1](https://doi.org/10.1016/S0022-3093(02)01864-1).
- Sawlowicz, Z. (1993). Pyrite framboids and their development: a new conceptual mechanism. *Geologische Rundschau*, 82, 148-156. <https://doi.org/10.1007/BF00563277>
- Schneider, C. A., Rasband, W. S. and Eliceiri, K. W. (2012). NIH Image to ImageJ: 25 years of image analysis. *Nature methods*, 9(7), 671-675. <https://doi.org/10.1038/nmeth.2089>
- Sellitti, C., Koenig, J. L. and Ishida, H. (1990). Surface characterization of graphitized carbon fibers by attenuated total reflection Fourier transform infrared spectroscopy. *Carbon*, 28(1), 221-228. [https://doi.org/10.1016/0008-6223\(90\)90116-G](https://doi.org/10.1016/0008-6223(90)90116-G)
- Shannon, H. A. (1934). Bricks-A trade index, 1785-1849. *Economica*, 1(3), 300-318. <https://doi.org/10.2307/2548806>
- Shakir, A. A., and Mohammed, A. A. (2013). Manufacturing of Bricks in the Past, in the Present and in the Future: A state of the Art Review. *International Journal of Advances in Applied Sciences*, 2(3), 145-156.
- Sharma, S. and Wetzal, K. K. (2010). Process development issues of glass-carbon hybrid-reinforced polymer composite wind turbine blades. *Journal of Composite Materials*, 44(4), 437-456. <https://doi.org/10.1177/0021998309347569>
- Shimanouchi, T. (1973). Tables of molecular vibrational frequencies. US Government Printing Office. 176 pp.
- Shin, S., Jang, J., Yoon, S. H. and Mochida, I. (1997). A study on the effect of heat treatment on functional groups of pitch based activated carbon fiber using FTIR. *Carbon*, 35(12), 1739-1743. [https://doi.org/10.1016/S0008-6223\(97\)00132-2](https://doi.org/10.1016/S0008-6223(97)00132-2)
- Silva, V. J. D., Taveira, S. K., Silva, K. R., Neves, G. A., Lira, H. L., and Santana, L. N. (2021). Refractory ceramics of clay and alumina waste. *Materials Research*, 24, e20200485. <https://doi.org/10.1590/1980-5373-MR-2020-0485>

- Silveira, D., Varum, H. and Costa, A. (2013). Influence of the testing procedures in the mechanical characterization of adobe bricks. *Construction and Building Materials*, 40, 719-728. <https://doi.org/10.1016/j.conbuildmat.2012.11.058>
- Silveira, D., Varum, H., Costa, A., Martins, T., Pereira, H., and Almeida, J. (2012). Mechanical properties of adobe bricks in ancient constructions. *Construction and Building Materials*, 28(1), 36-44. <https://doi.org/10.1016/j.conbuildmat.2011.08.046>
- Simão, F. V., Chambart, H., Vandemeulebroeke, L., Nielsen, P., Adrianto, L. R., Pfister, S., and Cappuyens, V. (2022). Mine waste as a sustainable resource for facing bricks. *Journal of Cleaner Production*, 368, 133118. <https://doi.org/10.1016/j.jclepro.2022.133118>
- Simón, J.L., Arlegui, L.E., Lafunete, P., Liesa, C.L. (2012). Active extensional faults in the central-eastern Iberian Chain, Spain. *Journal of Iberian Geology*, 38, 127-144. [https://doi.org/10.5209/rev\\_JIGE.2012.v38.n1.39209](https://doi.org/10.5209/rev_JIGE.2012.v38.n1.39209)
- Sinusía, C., Pueyo, E. L., Azanza, B. and Pocoví, A. (2004). Datación magnetoestratigráfica del yacimiento paleontológico de la Puebla de Valverde (Teruel). *Geo-Temas*, 6(4), 339-342.
- Smith, T. R. (1896). *Architecture, Gothic and Renaissance*. S. Low, Marston.
- Sohling, U., Ruf, F., Schurz, K., Emmerich, K., Steudel, A., Schuhmann, R. and Scheper, T. (2009). Natural mixture of silica and smectite as a new clayey material for industrial applications. *Clay Minerals*, 44(4), 525-537. <https://doi.org/10.1180/claymin2009.044.4.525>
- Song, D., Li, Z., Wang, L., Jin, F., Huang, C., Xia, E., R. M. Rizk-Allah., J. Yang, M. Su and Joo, Y. H. (2022). Energy capture efficiency enhancement of wind turbines via stochastic model predictive yaw control based on intelligent scenarios generation. *Applied Energy*, 312, 118773. <https://doi.org/10.1016/j.apenergy.2022.118773>
- Soni, A., Das, P. K., Hashmi, A. W., Yusuf, M., Kamyab, H. and Chelliapan, S. (2022). Challenges and opportunities of utilizing municipal solid waste as alternative building materials for sustainable development goals: A review. *Sustainable Chemistry and Pharmacy*, 27, 100706. <https://doi.org/10.1016/j.scp.2022.100706>
- Soria, J.M., Fernández, J., García, F. and Viseras, C. (2003). Correlative lowstand deltaic and shelf systems in the Guadix Basin (Late Miocene, Betic Cordillera, Spain): the stratigraphic record of forced and normal regressions. *Journal of Sedimentary Research*, 73, 912-925. <https://doi.org/10.1306/031103730912>
- Spencer, A. J. (2023). *Brick architecture in ancient Egypt* (Vol. 16). Oxbow Books. 192 pp.
- Stahel, W. R. (2016). The circular economy. *Nature*, 531(7595), 435-438. <https://doi.org/10.1038/531435a>

- Starsinic, M., Taylor, R. L., Walker Jr, P. L. and Painter, P. C. (1983). FTIR studies of Saran chars. *Carbon*, 21(1), 69-74. [https://doi.org/10.1016/0008-6223\(83\)90158-6](https://doi.org/10.1016/0008-6223(83)90158-6)
- Stoianovich, T. (1971). Material Foundations of Preindustrial Civilization in the Balkans. *Journal of Social History*, 4(3), 205-262.
- Stromberg, S.G. and Bluck, B., (1998). Turbidite facies, fluid-escape structures and mechanisms of emplacement of the Oligo-Miocene Aljibe Flysch, Gibraltar Arc, Betics, southern Spain. *Sedimentary Geology*, 115, 267-288. [https://doi.org/10.1016/S0037-0738\(97\)00096-1](https://doi.org/10.1016/S0037-0738(97)00096-1)
- Stuart, B. H. (2004). *Infrared spectroscopy: fundamentals and applications*. John Wiley and Sons. 224 pp.
- Sudharsan, N. and Sivalingam, K. (2019). Potential utilization of waste material for sustainable development in construction industry. *International Journal of Recent Technology and Engineering*, 8(3), 3435-3438. <https://doi.org/10.35940/ijrte.C5062.098319>.
- Suctu M. (2015). Influence of expanded vermiculite on physical properties and thermal conductivity of clay bricks, *Ceramics International*, 41, 2819–2827. <https://doi.org/10.1016/j.ceramint.2014.10.102>
- Sumpio, B. E., Cordova, A. C., Berke-Schlessel, D. W., Qin, F. and Chen, Q. H. (2006). Green tea, the “Asian paradox,” and cardiovascular disease. *Journal of the American College of Surgeons*, 202(5) 813-825. <https://doi.org/10.1016/j.jamcollsurg.2006.01.018>
- Süzer, S. and Andrews, L. (1987). FTIR spectra of ammonia clusters in noble gas matrices. *The Journal of Chemical Physics*, 87(9), 5131-5140. <https://doi.org/10.1063/1.453681>

T

- Taladrid, D., Laguna, L., Bartolomé, B. and Moreno-Arribas, M. V. (2019a). Aplicaciones y nuevos usos de subproductos de la vinificación. *Interempresas: Canales Sectoriales*. <https://doi.org/10.1007/s00217-020-03581-1>
- Taladrid, D., Lorente, L., Bartolomé, B., Moreno-Arribas, M. V. and Laguna, L. (2019b). An integrative salivary approach regarding palate cleansers in wine tasting. *Journal of Texture Studies*, 50(1), 75-82. <https://doi.org/10.1111/jtxs.12361>
- Tang, N., Tan, X., Cai, Y., He, M. Y., Xiang, Z. Y., Ye, H. and Ma, J. L. (2022) Characterizations and application potentials of the hemicelluloses in waste oil-tea camellia fruit shells from Southern China. *Industrial Crops and Products*, 178, 114551. <https://doi.org/10.1016/j.indcrop.2022.114551>

- Tarvornpanich, T., Souza, G. P. and Lee, W. E. (2008). Microstructural Evolution in Clay-Based Ceramics I: Single Components and Binary Mixtures of Clay, Flux, and Quartz Filler. *Journal of the American Ceramic Society*, 91(7), 2264-2271. <https://doi.org/10.1111/j.1551-2916.2008.02393.x>
- Taurino, R., Ferretti, D., Cattani, L., Bozzoli, F. and Bondioli, F. (2019). Lightweight clay bricks manufactured by using locally available wine industry waste. *Journal of Building Engineering*, 26, 100892. <https://doi.org/10.1016/j.job.2019.100892>
- Taut, T., Kleeberg R. and Bergmann J. (1998). The new seifert rietveld program BGMN and its application to quantitative phase analysis, *Materials Structure* 5 (1) 55–64.
- Tay, J. H. (1987). Bricks manufactured from sludge. *Journal of Environmental Engineering*, 113(2), 278-284.
- Ten, J. G., Orts, M. J., Saburit, A. and Silva, G. (2010). Thermal conductivity of traditional ceramics. Part I: Influence of bulk density and firing temperature. *Ceramics International*, 36(6), 1951-1959. <https://doi.org/10.1016/j.ceramint.2010.05.012>
- Teschemacher, T., Wilson, P., Wüchner, R. and Bletzinger, K. U. (2022). Macroscopic characterization of modern masonry. *Engineering Structures*, 268, 114630 <https://doi.org/10.1016/j.engstruct.2022.114630>
- Thomas, L. and Ramachandra, M. (2018). Advanced materials for wind turbine blade-A Review. *Materials Today: Proceedings*, 5(1), 2635-2640. <https://doi.org/10.1016/j.matpr.2018.01.043>
- Thorat, P. K., Papal, M., Kacha, V., Sarnobat, T. and Gaikwad, S. (2015). Hollow concrete blocks-A new trend. *International Journal of Engineering & Research*, 5(5), 9-26.
- Tiffo, E., Elimbi, A., Manga, J. D. and Tchamba, A. B. (2015). Red ceramics produced from mixtures of kaolinite clay and waste glass. *Brazilian Journal of Science*, 2(1), 1-13. <https://doi.org/10.1186/s40552-015-0009-9>.
- Tite, M. S. (1975). Scanning electron microscopy of fired calcareous clays. *Transactions and journal of the British Ceramic Society*, 74, 19-22.
- Tite, M. S. and Maniatis, Y., (1975). Scanning Electron Microscope of Fired Calcareous Clays. *Transactions and journal of the British Ceramic Society*, No. 74, 19-22.
- Torres, T., Ortiz, J. E., Soler, V., Delgado, A., Araujo, R., Valle, M. and Vega-Panizo, R. (2020). An analogue of dominance of tectonic over climatic forcing in intermontane coal-bearing basins: Padul (SE Spain). *International Journal of Coal Geology*, 227, 103530. <https://doi.org/10.1016/j.coal.2020.103530>
- Touch, N., Nakamura, T. and Hibino, T. (2019). Changes in the State of Organic Matter Present in Sediment by Different Methods of Electrokinetic Treatment. *IJERD*, 10(1), 47-52. [https://doi.org/10.32115/ijerd.10.1\\_47](https://doi.org/10.32115/ijerd.10.1_47)

- Trevelyan, F. C. and Haslam, R. A. (2001). Musculoskeletal disorders in a handmade brick manufacturing plant. *International Journal of Industrial Ergonomics*, 27(1), 43-55. [https://doi.org/10.1016/S0169-8141\(00\)00036-6](https://doi.org/10.1016/S0169-8141(00)00036-6).
- Trincal, V., Benavent, V., Lahalle, H., Balsamo, B., Samson, G., Patapy, C. and Cyr, M. (2022). Effect of drying temperature on the properties of alkali-activated binders- recommendations for sample preconditioning. *Cement and Concrete Research*, 151, 106617. <https://doi.org/10.1016/j.cemconres.2021.106617>
- Trotti, F., Mozzo, P., Temporin, A., Lanciai, M., Predicatori, F., Righetti, F. and Tacconi, A. (1996). CR-39 track detectors applied to measurements of <sup>210</sup>Po embedded in household glass. *Environment International*, 22, 863-869. [https://doi.org/10.1016/S0160-4120\(96\)00194-8](https://doi.org/10.1016/S0160-4120(96)00194-8).
- Trouillas, P., Calliste, C. A., Allais, D. P., Simon, A., Marfak, A., Delage, C. and Duroux, J. L. (2003) Antioxidant, anti-inflammatory and antiproliferative properties of sixteen water plant extracts used in the Limousin countryside as herbal teas. *Food Chemistry*, 80(3), 399-407 [https://doi.org/10.1016/S0308-8146\(02\)00282-0](https://doi.org/10.1016/S0308-8146(02)00282-0)
- Tsipursky, S.I. and Drits V.A. (1984). The distribution of octahedral cations in the 2:1 layers of dioctahedral smectites studied by oblique-texture electron diffraction. *Clay Minerals*. 19177–193. <https://doi.org/10.1180/claymin.1984.019.2.05>
- Tyrrell, M. E. and Goode, A. H. (1972). Waste glass as a flux for brick clays (Vol. 7701). US Department of Interior, Bureau of Mines. 9 pp.
- Tyrrell, M. E., Feld, I. L. and Barclay, J. A. (1972). Fabrication and cost evaluation of experimental building brick from waste glass (Vol. 7605). US Department of Interior, Bureau of Mines. 33pp.

## U

- Ufer, K., Roth, G., Kleeberg, R., Stanjek, H., Dohrmann, R. and Bergmann J. (2004). Description of X-ray powder pattern of turbostratically disordered layer structures with a Rietveld compatible approach, *Zeitschrift für Kristallographie* 219, 519–527. <https://doi.org/10.1524/zkri.219.9.519.44039>
- Ugidos, J. M., Armenteros, I., Barba, P., Valladares, M. I., and Colmenero, J. R. (1997). Geochemistry and petrology of recycled orogen-derived sediments: a case study from Upper Precambrian siliciclastic rocks of the Central Iberian Zone, Iberian Massif, Spain. *Precambrian Research*, 84(3-4), 163-180. [https://doi.org/10.1016/S0301-9268\(97\)00023-5](https://doi.org/10.1016/S0301-9268(97)00023-5)
- UNE-EN 12370 (2020). Métodos de ensayo para piedra natural. Determinación de la resistencia a la cristalización de sales. AENOR, Madrid.

- UNE-EN 12371 (2011). Métodos de ensayo para piedra natural. Determinación de la resistencia a la heladicidad. AENOR, Madrid.
- UNE-EN 13755 (2008). Métodos de ensayo para piedra natural. Determinación de la absorción de agua a presión atmosférica. AENOR, Madrid.
- UNE-EN 1925 (1999). Métodos de ensayo para piedra natural. Determinación de la resistencia a la compresión uniaxial. AENOR, Madrid.
- UNE-EN 1926 (2007). Métodos de ensayo para piedra natural. Determinación del coeficiente de absorción de agua por capilaridad. AENOR, Madrid.
- UNE-EN 14147 (2004). Métodos de ensayo para la piedra natural. Determinación de la resistencia al envejecimiento por niebla salina. AENOR, Madrid.
- UNE-EN 1936 (2007). Métodos de ensayo para piedra natural. Determinación de la densidad real y aparente y de la porosidad abierta y total. AENOR, Madrid.
- UNE-EN 196-1 (2005). Métodos de ensayo de cementos. Parte 1: Determinación de resistencias mecánicas. AENOR, Madrid.
- UNE-EN 15886 (2011). Métodos de ensayo. Medición del color de superficies. AENOR, Madrid.



- Vega, C. and Torres, N. (2018). External strengthening of unreinforced masonry walls with polymers reinforced with carbon fiber. *Ingeniería e Investigación*, 38(3), 15-23. <https://doi.org/10.15446/ing.investig.v38n3.73151>
- Velasco, P. M., Ortiz, M. P. M., Giró, M. A. M., Melia, D. M. and Rehbein, J. H. (2015). Development of sustainable fired clay bricks by adding kindling from vine shoot: Study of thermal and mechanical properties. *Applied Clay Science*, 107, 156-164. <https://doi.org/10.1016/j.clay.2015.01.017>
- Velde, B. (1966). Upper stability of muscovite. *American Mineralogist*, 51(5-6), 924-929.
- Vera, J. A. and Rodríguez Fernández, J. (1988). Una modificación al modelo genético para la Formación Molicias (Tortoniense superior, Depresión de Guadix, S de España). *Geogaceta*, 5, 26-29.
- Vera, J.A. (Ed.) (2004). *Geología de España*. Sociedad Geológica de España-Instituto Geológico y Minero de España, Madrid, 890 p.
- Vichaphund, S., Kitiwan, M., Atong, D. and Thavorniti, P. (2011). Microwave synthesis of wollastonite powder from eggshells. *Journal of the European Ceramic Society*, 31(14), 2435-2440. <https://doi.org/10.1016/j.jeurceramsoc.2011.02.026>.

- Vieira, C. M. F., Sánchez, R. and Monteiro, S. N. (2008). Characteristics of clays and properties of building ceramics in the state of Rio de Janeiro, Brazil. *Construction and Building Materials*, 22(5), 781-787. <https://doi.org/10.1016/j.conbuildmat.2007.01.006>.
- Vilatela, J. J., Rabanal, M. E., Cervantes-Sodi, F., García-Ruiz, M., Jiménez-Rodríguez, J. A., Reiband, G. and Terrones, M. (2015). A spray pyrolysis method to grow carbon nanotubes on carbon fibres, steel and ceramic bricks. *Journal of Nanoscience and Nanotechnology*, 15(4), 2858-2864. <https://doi.org/10.1166/jnn.2015.9601>
- Viseras, C. (1991). *Estratigrafía y sedimentología del relleno aluvial de la Cuenca de Guadix (Cordilleras Béticas)*. Doctoral Dissertation, Universidad de Granada, Spain. 327 pp.
- Viseras, C. and Fernández, J. (1995). The role of erosion and deposition in the construction of alluvial fan sequences in the Guadix Formation (SE Spain). *Geologie en Mijnbouw*, 74, 21-33.
- Vu, D. H., Wang, K. S., Chen, J. H., Nam, B. X. and Bac, B. H. (2012). Glass–ceramic from mixtures of bottom ash and fly ash. *Journal of Waste Management*, 32(12), 2306-2314. <https://doi.org/10.1016/j.wasman.2012.05.040>.

W

- Walker Jr, P. L., Taylor, R. L. and Ranish, J. M. An update on the carbon-oxygen reaction. *Carbon*, 29(3) (1991), 411-421. [https://doi.org/10.1016/0008-6223\(91\)90210-A](https://doi.org/10.1016/0008-6223(91)90210-A)
- Wang, S., Gainey, L., Wang, X., Mackinnon, I. D. and Xi, Y. (2022). Influence of palygorskite on in-situ thermal behaviours of clay mixtures and properties of fired bricks. *Applied Clay Science*, 216, 106384. <https://doi.org/10.1016/j.clay.2021.106384>
- Wang, H., Provan, G. J. and Helliwell, K. (2000). Tea flavonoids: their functions, utilisation and analysis. *Trends in Food Science & Technology*, 11(4-5), 152-160. [https://doi.org/10.1016/S0924-2244\(00\)00061-3](https://doi.org/10.1016/S0924-2244(00)00061-3)
- Wang, H., Sun, Y., Chu, J., Wang, X. and Zhang, M. (2020). Crystalline structure variation within phlogopite, muscovite and talc under 0–1000 kGy  $\gamma$  ray irradiation: A clear dependence on intrinsic characteristic. *Applied Clay Science*, 187, 105475. <https://doi.org/10.1016/j.clay.2020.105475>
- Wang, H., Zhang, Q., Yang, H. and Sun, H. (2008). Synthesis and microwave dielectric properties of CaSiO<sub>3</sub> nanopowder by the sol–gel process. *Ceramics International*, 34(6), 1405-1408. <https://doi.org/10.1016/j.ceramint.2007.05.001>.



- Warr, L. N. (2020). Recommended abbreviations for the names of clay minerals and associated phases. *Clay Minerals*, 55(3), 261-264. <https://doi.org/10.1180/clm.2020.30>
- Waters, L. M., Bernazzani, P., and Jao, M. (2016). Optimal Proportioning, Tempering, and Testing of Adobe Brick, Compressed Stabilized Earthen Block, and Rammed Earth for Low-Cost, Sustainable Construction: A Literature Review. *Bulletin of the American Physical Society*, 61.
- Webster, K. (2021). A circular economy is about the economy. *Circular Economy and Sustainable Strategies*, 1(1), 115-126. <https://doi.org/10.1007/s43615-021-00034-z>
- Weng, C. H., Lin, D. F. and Chiang, P. C. (2003). Utilization of sludge as brick materials. *Advances in Environmental Research*, 7(3), 679-685. [https://doi.org/10.1016/S1093-0191\(02\)00037-0](https://doi.org/10.1016/S1093-0191(02)00037-0)
- Whitehouse, D. (2012). *Glass: a short history*. Smithsonian Inst Press.
- Whitney, D. L. and Evans, B. W. (2010). Abbreviations for names of rock-forming minerals. *American Mineralogist*, 95, 185–187. <https://doi.org/10.2138/am.2010.3371>.
- Wilkinson, R. G. (1988). The English industrial revolution. *The ends of the Earth: Perspectives on modern environmental history*, 80. 325 pp.
- Wills, J. E. (2013). European consumption and Asian production in the seventeenth and eighteenth centuries. In *Consumption and the World of Goods*. Routledge. 133-147 pp.
- Willhauk, E. and Harikantha, R. (2005). *Glass ceramics for household appliances. Low thermal expansion glass-ceramics*, 2nd edn. Springer Verlag, Heidelberg, 51-58.
- Wilson, A. (2006). The economic impact of technological advances in the Roman construction industry. *Innovazione tecnica e progresso economico nel mondo romano*, 225-236.
- Woodforde, J. (1976). *Bricks: to build a house*. Routledge. 208 pp.



- Yang, C., Cui, C., Qin, J. and Cui, X. (2014). Characteristics of the fired bricks with low-silicon iron tailings. *Construction and Building materials*, 70, 36-42. <https://doi.org/10.1016/j.conbuildmat.2014.07.075>
- Yazdanbakhsh, A., Bank, L. C., Rieder, K. A., Tian, Y. and Chen, C. (2018). Concrete with discrete slender elements from mechanically recycled wind turbine blades.

- Resources, Conservation and Recycling, 128, 11-21.  
<https://doi.org/10.1016/j.resconrec.2017.08.005>
- Ye, Z., Harrison, R., Cheng, V. J. and Bekhit, A. E. A. (2016). Wine making by-products. Valorization of Wine Making By-Products; CRC Press: Boca Raton, FL, USA, 73-116. <https://doi.org/10.3389/fimmu.2017.01418>
- Youssef, N., Lafhaj, Z., and Chapiseau, C. (2020). Economic analysis of geopolymers brick manufacturing: A french case study. Sustainability, 12(18), 7403. <https://doi.org/10.3390/su12187403>
- Yu, J., Ahmedna, M. (2013). Functional components of grape pomace: their composition, biological properties and potential applications. Int. J. Food Sci. Technol., 48(2), 221-237. <https://doi.org/10.1111/j.1365-2621.2012.03197.x>

## Z

- Zellmer, L. A. and White, W. B. (1984). Characterization of hydrated surface layers on nuclear waste glasses by infrared reflectance spectroscopy. MRS Online Proceedings Library (OPL), 44. <https://doi.org/10.1557/PROC-44-73>
- Zhang, L. (2013). Production of bricks from waste materials—A review. Construction and Building Materials, 47, 643-655. <https://doi.org/10.1016/j.conbuildmat.2013.05.043>
- Zhang, Y., Li, X. and Li, Y. (2015). Influence of solution chemistry on heavy metals removal by bioadsorbent tea waste modified by poly (vinyl alcohol). Desalination and Water Treatment, 53(8), 2134-2143. <https://doi.org/10.1080/19443994.2013.861775>
- Zhang, J., Ma, G., Chen, L., Liu, T., Liu, X. and Lu, C. (2017). Profiling elements in Puerh tea from Yunnan province, China. Food Additives & Contaminants: Part B, 10(3), 155-164. <https://doi.org/10.1080/19393210.2017.1278726>
- Zhang, Z., Wong, Y. C., Sofi, M. and Mendis, P. (2022). Incorporation of Glass and Plastic Waste into Alkali-Activated Mill Residue Bricks. Sustainability, 14(24), 16533. <https://doi.org/10.3390/su142416533>
- Zhou, X., Liu, D., Bu, H., Deng, L., Liu, H., Yuan, P. and Song, H. (2018). XRD-based quantitative analysis of clay minerals using reference intensity ratios, mineral intensity factors, Rietveld, and full pattern summation methods: A critical review. Solid Earth Sciences, 3(1), 16-29. <https://doi.org/10.1016/j.sesci.2017.12.002>

## **Web pages:**

Asociación Empresarial Eólica. Number of wind turbines installed in Spain from 2011 to 2021. [www.statista.com/statistics/1230487/wind-turbines-installed-in-spain/](http://www.statista.com/statistics/1230487/wind-turbines-installed-in-spain/) (accessed July, 2023).

European Wind Energy Association: [ewea.org/](http://ewea.org/) (accessed September, 2023).

Global Wind Report 2022: [gwec.net/wp-content/uploads/2022/03/GWEC-GLOBAL-WIND-REPORT-2022.pdf](http://gwec.net/wp-content/uploads/2022/03/GWEC-GLOBAL-WIND-REPORT-2022.pdf) (accessed July, 2023).

La corriente: [lacorriente.com](http://lacorriente.com) (accessed January, 2024).

National Geographic: [nationalgeographic.com](http://nationalgeographic.com) (accessed January, 2024).

Panorama Minero 2018-2020 (Instituto Geológico y Minero de España): [igme.es/PanoramaMinero/actual/ARCILLA%202019.pdf](http://igme.es/PanoramaMinero/actual/ARCILLA%202019.pdf) (accessed July, 2023).

Recycling International: [recyclinginternational.com/](http://recyclinginternational.com/) (accessed September, 2023).

Reddit: [reddit.com](http://reddit.com) (accessed January, 2024).

REPowerEU: [commission.europa.eu/](http://commission.europa.eu/) (accessed July, 2023).

Research Gate: [researchgate.net/](http://researchgate.net/) (accessed January, 2024).

Roman Stamped Bricks: Linge, H.: [worldhistory.org/image/5559/roman-stamped-bricks/](http://worldhistory.org/image/5559/roman-stamped-bricks/) (accessed January, 2024).

The International Energy Agency (2020): [iea.org/reports/world-energy-outlook-2020](http://iea.org/reports/world-energy-outlook-2020) (accessed July, 2023).

UN General Assembly. Transforming our world: the 2030. Agenda for Sustainable Development: [refworld.org/docid/57b6e3e44.html](http://refworld.org/docid/57b6e3e44.html) (accessed July, 2023).

U.S. Geological Survey. Mineral commodity summaries 2023: U.S. Geological Survey (2023), 210 p., <https://doi.org/10.3133/mcs2023> (accessed July, 2023).

U.S. Geological Survey, American Clean Power Association, and Lawrence Berkeley National Laboratory data release, <https://doi.org/10.5066/F7TX3DN0>. Viewer: <https://eerscmap.usgs.gov/uswtodb/viewer/#3/37.25/-96.25> (accessed July, 2023).

Visit Lübeck: [visit-luebeck.com](http://visit-luebeck.com) (accessed January, 2024).

Visual Capitalist (2022). [visualcapitalist.com/visualizing-the-worlds-biggest-wind-turbines/](http://visualcapitalist.com/visualizing-the-worlds-biggest-wind-turbines/) (accessed July, 2023).

WindEurope 2021. [windeurope.org/](http://windeurope.org/) (accessed July, 2023).